Optimal Design, Operation and Development of Oil Sands Upgrading Plants

by

Hossein Shahandeh

A thesis submitted in partial fulfillment of the requirements for the degree of

Doctor of Philosophy

in

Process Control

Department of Chemical and Materials Engineering
University of Alberta

Abstract

Canada has the third largest oil reserves in the world where 97% of these reserves are located in the oil sands, Alberta province. The product resulted from the extraction of oil sands reserves is called bitumen which can be diluted and shipped to the market or it can be proceeded and upgraded into a value-added product. The upgrading facilities mainly improve the quality of bitumen by rejecting carbon from it or adding hydrogen to it using operating units such as thermocracking or hydrocracking, respectively. Moreover, the upgrading process can be carried out through full or partial upgrading technologies. Note that the partial upgrading technology has not been commercialized yet. There is no doubt that upgrading bitumen would bring more social and economic benefits to the province; however, decision making at different levels of upgrading processes is a challenging task.

In this thesis, we attempt to address how to reach the optimal point of upgrading process at three different levels. The first level is the design problem in which the objective is selecting the most efficient units out of all possible options and finding the best arrangement among them for the full upgrading process. The second level is the operation problem, where there exists a hydrocracking-based full upgrading plant with determined operating units, and the goal is achieving the optimal operating conditions such as pressure and temperature. The third level is the development of upgrading plants in the future. In one study, the expansion planning of an existing thermocracking-based full upgrading plant is addressed. In a later study, the optimal planning of initial capacity and expansion of partial upgrading technologies is presented. It should be highlighted here that the objective functions of these works are economic terms such as net present value or profit, and the environmental impact is one of the constraints in our optimization problems. Furthermore, while the design and operation problems are modeled deterministically, different uncertainties are incorporated and stochastic models are considered for the development problems.

The major novelties and contributions of this thesis are threefold. Firstly, Augmented Lagrangian decomposition method is implemented to solve the design problem. The final optimization model of the design problem is a large–scale non–convex mixed integer nonlinear programming problem which commercial solvers are not able to find the optimal solution directly. Secondly, a multistage stochastic programming model is proposed for the development problem of full upgrading plant. An uncertainty set is defined for the synthetic crude oil price and carbon tax, and linear decision rule approximation is applied for the robust optimization of the developed mixed integer linear programming problem. Thirdly, a multistage stochastic programming model is proposed for the development problem of partial upgrading technologies. The developed model

cannot be handled with classical approaches (such as robust optimization or stochastic programming), and hence, two novel hybrid methods are introduced (to the best of our knowledge, one of them has not been studied in literature before). The hybrid methods are a combination of scenario–based and uncertainty set definitions for uncertainty.

Preface

This thesis is an original work by Hossein Shahandeh. The materials in this thesis are part of the research project under the supervision of Dr. Zukui Li, and are funded by Alberta Innovates Technology Futures (AITF).

Chapter 2 of this work has been published as H. Shahandeh, and Z. Li, "Design of Bitumen Upgrading and Utility Plant through Integrated Optimization," Industrial & Engineering Chemistry Research. 2017, 56, 2107–2126.

Chapter 3 of this work has been published as H. Shahandeh, and Z. Li, "Optimal Design of Bitumen Upgrading Facility with CO_2 Reduction," Computers & Chemical Engineering. 2017, 106, 106-121.

Chapter 4 of this work has been published as H. Shahandeh, and Z. Li, "Modeling and Optimization of the Upgrading and Blending Operations of Oil Sands Bitumen," Energy & Fuels. 2016, 30, 5202-5213.

Chapter 5 of this work has been published as H. Shahandeh, F. Motamed, and Z. Li, "Expansion Development Planning of Thermocracking–based Bitumen Upgrading Plant under Uncertainty," Computers & Chemical Engineering. 2018, 111, 225-240.

Chapter 6 of this work has been submitted as H. Shahandeh, F. Motamed, and Z. Li, "Capacity Planning of Partially Upgraded Bitumen Production with Multistage Stochastic Programming," Optimization and Engineering. 2018.

For all the materials listed above, I am responsible for the theory development, numerical simulation and analysis, as well as the manuscript composition. Dr. Zukui Li is the supervisory author and was involved with the guidance of concept formation and manuscript composition. And in Chapters 5 and 6, the publication is also completed with the help of Farough Motamed, who provides valuable advice to construct and improve the manuscript.

Acknowledgements

During the last four years, I have been given the privilege of studying at one of the best universities in Canada and had the opportunity to interact with some of the best researchers in Process System Engineering and Optimization. I would like to express my gratitude to those people who have assisted and accompanied me during my doctoral journey.

First and foremost, I would like to thank my supervisor, Dr. Zukui Li, for his patience, unconditional support, continuous encouragement, and dexterity to guide me through every step of my graduate studies. I am particularly grateful for the trust he put in me to work on optimization theories and application. Conducting my graduate studies under his supervision was challenging, based on real–world problems, purposeful, meaningful, and interesting. I also appreciate having weekly constructive discussions with him and knowing that his office door is always open.

I would like to thank the Alberta Innovates Technology Futures (AITF) for the financial support, and the Chemical and Materials Engineering Department and Faculty of Engineering at the University of Alberta for providing a pleasant environment to pursue my PhD.

I also want to express my gratitude to my true friends on Campus; Mehran, Farshad, Ali, Firouz, Mohammad, Atefeh, Nirwair, Alireza, Agustin, Seraphina, and Dave, for making my graduate student life a wonderful experience, both personally and professionally.

I want to express my gratitude to my great teammates; Farough and Said, from whom I gained a lot of help and advice. I am thankful for sharing their knowledge and expertise with me. I would also like to thank other members of the Computer Process Control (CPC) group who knowingly supported me during my studies.

Last but not the least, I owe my immense gratitude to my parents for their boundless love and support. I would like to extend my gratitude to my siblings for being my role models and the most influential characters in my life. I immensely thank them for their inspiration and for giving me confidence in my abilities.

Contents

List of Tables

List of Figures

List of Abbreviations

AD or ADU	Atmospheric distillation (unit)
ALR	Augmented Lagrangian relaxation
ALRP	Decomposition of ALR problem
ARMA	Auto regressive moving average
ASU	Air separation unit
ATB	Atmospheric tower bottom
bbl	Barrel
bpd	Barrel per day
CAPEX	Capital cost
CCR	Carbon capture ratio
CCS	Carbon capture and sequestration
CDU	Crude distillation unit
CLC	Chemical looping combustion
CSS	Cyclic steam stimulation
DilBit	Diluted bitumen
DP	Deterministic problem
DR or DRU	Diluent recovery (unit)
ECP	Effective cut point
FCC	Fluid catalytic cracking
FW	Freshwater
GHG	Greenhouse gas
GT	Gas turbine
GTC	Gas turbine combustor
HC	Hydrocracker
HDN	Hydrodenitrogenation
HDR	Husky Diluent Reduction
HDS	Hydrodesulfurization
HGO	Heavy gas oil
HGOHT	Heavy gas oil hydroTreater
HI–Q	High Quality
HP	High pressure
HRSG	Heat recovery steam generator
HT	Hydrotreater
IGCC	Integrated gasification combined cycle
LDR	Linear decision rule
LGO	Light gas oil
LGOHT	Light gas oil hydroTreater
LHSV	Liquid hourly space velocity
LHV	Low heat value
LP	Linear programming
MAINEX	Maintenance cost
MEA	MonoEthanolAmine
MILP	Mixed integer linear programming

MINLP	Mixed integer nonlinear programming
MMSCFD	Million standard cubic feet per day
MP	Medium Pressure
MSP	Multistage stochastic programming
MT	Mineral trapping
NG	Natural gas
NLP	Nonlinear programming
NPH	Naphtha
NPHHT	Naphtha hydroTreater
NPUP	National partial upgrading program
NPV	Net present value
OPEX	Operating cost
PSA	Pressure–swing adsorption
PU	Partial Upgrader
PUB	Partially upgraded blend
RO	Robust optimization
SAA	Sample average approximation
SAGD	Steam–assisted gravity drainage
scf	Standard cubic feet
SCGP	Shell coal gasification process
SCO	Synthetic crude oil
SGP	Shell gasification process
SMR	Steam methane reforming
SOR	Steam–to–oil ratios
SP	Stochastic programming
sthi	High–quality steam turbine
stlo	Low–quality steam turbine
SynBit	Mixture of sweet SCO and Bitumen
SynDilBit	Mixture of sweet SCO and DilBit
TC	Thermocracker
UCG	Underground coal gasification
VD or VDU	Vacuum distillation (unit)
VHP	Very high pressure
VTB	Vacuum tower bottom
WCS	Western Canadian select
WGS	Water gas shift
WTI	West Texas intermediate

Chapter 1

Introduction

1.1 Motivation

Crude oil is the global dominant energy source and the reliance of the world economy on it is expected to continue for a long time. It is estimated that the worldwide demand for crude oil will reach 111 million barrels per day (bpd) by 2040, and approximately 25% of it will be contributed by North America, including Canada and the United States [1]. Due to the increasing scarcity of conventional oil reserves, oil industries and governments are interested in unconventional oil resources. Note that oil reserves that cannot be accessed using conventional drilling techniques are referred to as unconventional oil. These reserves (e.g., tight oil, oil shale, and bitumen) need novel methods for extraction [2, 3]. Albertan oil sands has proven reserves equal to near 165.4 billion barrels (bbl) in three regions of Athabasca, Cold Lake and Peace River [4]. This ranks Canada as the third largest oil reserves in the world, after Venezuela and Saudi Arabia. Total crude bitumen production, including 46% of surface mining and 54% of in–situ, is about 2.8 million bpd in 2017 [4]. According to the latest forecast, the oil sands production is expected to increase by 3.67 million bpd in 2030 [5]. This means that there should be an investment in new infrastructures in order to be capable of handling the production increase.

About 20% of the bitumen reserves are extractable using surface mining methods. The rest 80% are more than 70 meters below the ground and are extractable using in–situ methods. Prominent in–situ methods currently used in the oil sands industry are the cyclic steam stimulation (CSS) and steam–assisted gravity drainage (SAGD), whereas SAGD accounts for the most widely used in–situ methods in Alberta. Nowadays, more than 16 SAGD projects are under operation in Alberta and many more are under development. Some examples of the prominent SAGD operations with significant bitumen production are MacKay River and Firebag operations of Suncor Energy, Foster Creek and Christina Lake operations of Cenovus Energy and Jackfish operations of Devon energy [6].

There are three major options to process the extracted bitumen; (1) transportation with a pipeline, (2) full upgrading, and (3) partial upgrading. Note that, about 45% or 1.1 million bpd of crude bitumen production was sent for full upgrading in Alberta and the rest was transported in 2015 (no partial upgrading). The first option, transportation, has the following challenges [7]. Firstly, the diluent is required to add to

unprocessed bitumen to have a flowing mixture as DilBit. Therefore, besides of pipeline capital cost, using diluent adds the cost to shippers of (i) paying tolls for the exported diluent, (ii) recovering diluent at the U.S. pipeline terminal, (iii) paying tolls for shipping back the recovered diluent. Secondly, such an act might raise concerns about the pipeline's possible environmental and economic impact at the provincial or federal level. For instance, the most recent dispute has been over the Trans Mountain pipeline expansion that would carry more Albertan bitumen to the British Columbia coast [8]. Hence, transportation of DilBit itself cannot be the solution.

As the second option, extracted bitumen can be further used for upgrading and then sold as a value–added product. During the upgrading, bitumen is processed into synthetic crude oil (SCO) making it usable in conventional refineries. Full upgrading can be achieved in two distinct ways: hydrocracking, which relies on hydrogen–addition or thermocracking, which is based on carbon–rejection. The resulting lighter compounds created through both these upgrading methods are mainly naphtha (NPH), light gas oil (LGO), and heavy gas oil (HGO). In hydrocracking, hydrogen is added to increase the mass fraction of hydrogen. This leads to the breakup of large hydrocarbon chains, forming lighter compounds. LC–Finning is the ongoing technique based on hydrocracking. In thermocracking, thermal energy is added to bitumen in order to break the large hydrocarbon chains into lighter ones. Delayed coking and fluid coking are the major running techniques based on thermocracking. Compared to hydrocracking, thermocracking has a lower conversion rate and produces coke which is an undesirable byproduct. Therefore, in Canada, hydrocracking technology is more favorable due to its capability of yielding high–quality distillates [9]. Full upgrading technologies have their own drawbacks as well. Not only would it require significant public investment by the province of Alberta, but also the final product, known as SCO, has a strong competitor in the market; light U.S. unconventional oil.

The third option, partial upgrading, has received a great amount of attention as the sustainable approach in the future [7]. Firstly, the final product of partially upgraded bitumen, partially upgraded blend (PUB), could be more favorable in the market compared to SCO. Although PUB is a higher–value product compared to bitumen, partial upgraders can only upgrade bitumen to a light crude similar to medium or heavy crude. Secondly, near one–third of the existing pipeline capacity would be free up for more transportation due to eliminating the need for diluent. Note that diluent is still required to transport bitumen from in–situ extraction facilities to partial upgraders; however, these two are supposed to be located close to each other. The main challenge with this option is that there has not any fully commercialized partial upgrader been developed so far. Therefore, there are many unknowns and uncertainties regarding technical issues, industrial–scale operation, and marketing of the final product.

The motivation of our research can be simply explained through the Figure 1.1. As it is shown, Athabasca bitumen is the heaviest crude oil stream being processed through U.S. refineries, and the average price for this commodity is the lowest among all different global crude oils being purchased. On the other hand, The operating cost of bitumen production is quite high. This is due to the demand of a variety of utilities during extraction and upgrading processes, including electricity, steam, hot water, freshwater (FW), natural gas

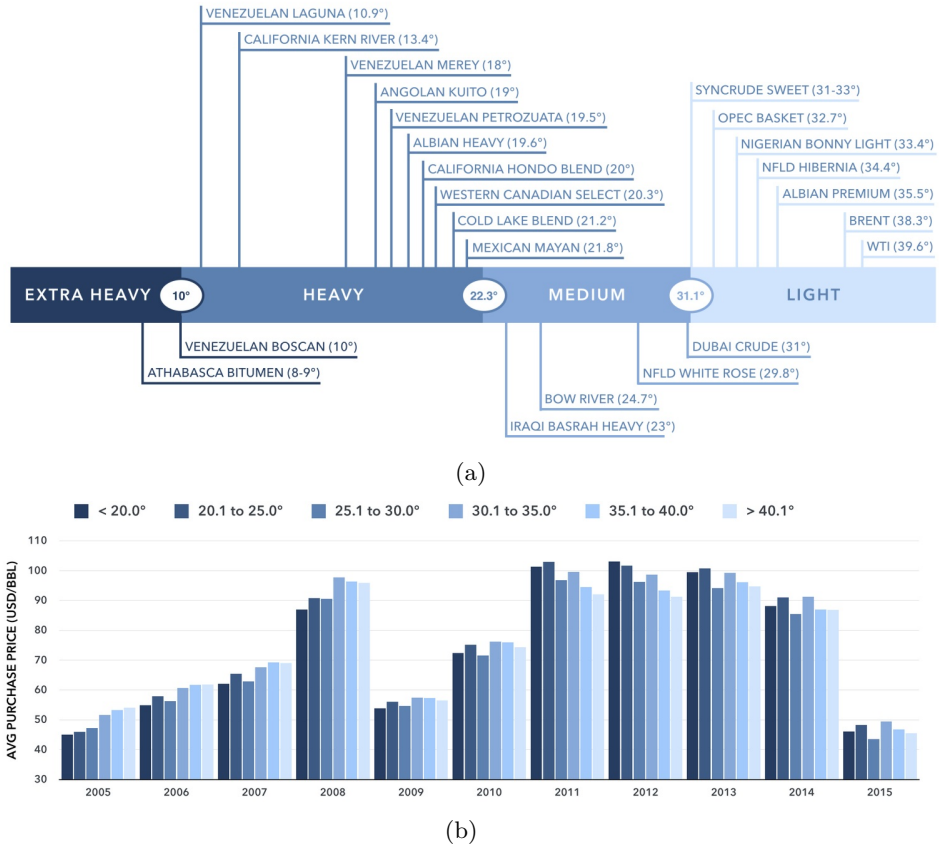

Figure 1.1: API–based comparison of (a) different crude oil streams processed through U.S. refineries, and (b) average U.S. refinery feedstock purchase price over the past 10 years [11]

(NG), and hydrogen. As a result profitability in the oil sands industry historically has been quite unstable and the fluctuating crude oil price affects the logistics of the government receiving advantages from these sources. For instance, the west Texas intermediate (WTI) price has been fluctuating between \$29.42/bbl and \$71.28/bbl just in the last three years. Nevertheless, despite the unstable market and low profitability, oil sands production is predicted to increase by 3.67 million bpd in 2030 [5]. Systematic operation optimization is necessary for different parts of the oil sands industry, especially the upgrading process. The focus of this thesis is on upgrading section as it was found that bitumen upgrading is the most cost– and energy–intensive section of SCO production [10]. Therefore, it is imperative to perform mathematical optimization for the bitumen upgrading process.

1.2 Literature review

The starting point for solving a problem is understanding it from top to bottom. In this section, different classifications for optimization are first introduced. Hierarchy of decision making, various types of optimization problems, and optimization under uncertainty are those discussed below. Finally, the previous studies in which mathematical programming was implemented to optimize a problem in the oil sands industry are

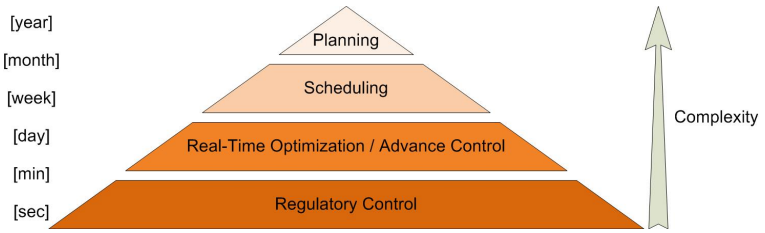

Figure 1.2: Hierarchy of decision making

reviewed.

1.2.1 Hierarchy of decision making

The first step of tackling an optimization problem is determining its level in the hierarchy of decision making (See Figure 1.2). Knowing the level of decision making in advance can help us to define the mathematical problem better. For example, solving a planning problem for a refinery can be very complex due to the presence of a large number of governing physical equation such as mass and energy balances. Because of the nature of this problem, it would be totally fine if the optimal solution is obtained even in a couple of days. However, on the other side of the spectrum, Real-Time Optimization sometimes requires to be as fast as hours. For example, after changing the feedstock of a reactor there is not that much time to find its optimal operating condition in order to maximize the yield. When the time step becomes less than hours, the facing problem can be categorized as process control problem rather than optimization one. Note that, optimization techniques would still be used in process control problems but at a simpler level. As a matter of fact, the hierarchy level forces the decision makers on how sophisticated a model can be.

1.2.2 Optimization problem classification

The optimization field has drastically expanded during the last decade. Many advance theories and algorithms have been proposed to solve engineering problems. In this section, major categories which mathematical problem can fall into are presented.

Different types of optimization method are discussed here first. The most complex optimization problem is the mixed integer nonlinear programming (MINLP) problem as stated below

$$
\begin{array}{ll}
\min & f(x,y) \\
\text{s.t.} & g_i(x,y) \leq 0 \quad i = 1,...,p_1 \\
& h_i(x,y) \leq 0 \quad i = 1,...,p_2 \\
& x \in X, y \in Y \\
& X = \{x | x \in \mathbb{R}^n, x^L \leq x \leq x^U, B \cdot x \leq b\} \\
& Y = \{y | y \in \{0,1\}^m, A \cdot y \leq a\}
\end{array}
$$

where there exist both nonlinear (g_i) and linear (h_i) constraints ($p_1, p_2 \geq 0$), and both continuous (x) and integer (y) variables ($m, n \geq 0$).

The optimization problem would reduce to the mixed integer linear programming (MILP) one if all the equations, including the objective function (f), are linear ($p_1 = 0, p_2 \geq 0$). Moreover, if the presented

problem does not have any integer variables ($n \geq 0, m = 0$), it would be a nonlinear programming (NLP) problem. Finally, the most simplest case is the linear programming (LP) in which there is neither integer ($n \geq 0, m = 0$) nor nonlinearity ($p_1 = 0, p_2 \geq 0$) in the model.

There are other classification categories which can be furtherer used for optimization problem:

- **Unconstrained versus constrained**. Whenever there is not any constraint on the variables in the formulation of a problem or we explicitly replace them all by a penalty term in the objective function, the problem is called unconstrained. Note that constraint optimization problem is more common, and the simplest way to define constraints are boundaries on the variables.

- **One or many objectives**. While having a single objective function is the case for the most optimization problems, it is possible to have multiple objective functions. Sometimes there are trade–offs between two or more desiring objectives. Finding an optimal solution to a problem with the highest profit (maximization) and lowest risk (minimization) is an example of this case. Such problems are handled by either forming a weighted combination of the conflicting objectives or by replacing all but one of the objectives with constraints.

- **Deterministic versus stochastic**. Once a model is formulated for a problem, values are supposed to be given to designing parameters. The efficiency of an operating unit, demand, commodity price are all examples of design parameters. If it is assumed that the parameters are known accurately for a given problem, the problem can be solved with Deterministic methods. Nevertheless, due to measurement error (applicable for the first given example) or representing information about the future (applicable for the last two examples) the parameters cannot be known with certainty. If the inherent uncertainty of a problem is incorporated into the model, the problem turns into a stochastic optimization problem which will be discussed in more details in the next section.

1.2.3 Optimization under uncertainty

There are two main alternative techniques to address optimization under uncertainty in a single period or in a multistage decision–making problem; robust optimization (RO) and stochastic programming (SP). The main criteria to determine which technique is more suitable to be implemented is whether there exist accurate probability distribution functions of the underlying stochastic parameters or not. The SP technique is more appropriate where such a probability distribution function can be found, while RO would be the better option when such information is unavailable or hard to obtain. These two techniques are discussed with more details below.

In order to explain the techniques better, the following mathematical expressions are used. The general deterministic LP problem of $\{\min_x\{c^T x : Ax \leq b\}\}$ with known parameters of (c, A, b) is selected for the sake of simplicity. Note that this problem can be easily expanded to a NLP one. Additionally, the same LP problem under uncertainty can be stated as $\{\min_x\{c^T x : Ax \leq b\} : (c, A, b) \in U\}$ with the data (c, A, b) varying in a given uncertainty set U.

Robust optimization technique. Instead of access to a complete stochastic description of the uncertainty, information with less detailed structure might be only available, for instance, upper and lower bounds on the magnitude of the uncertain quantities. Under this circumstance, the uncertainty can be described as a set which represents all possible realizations, the so-called "uncertainty set." The objective of the RO technique is to find the optimal solution ensuring that the constraints in the problem remain feasible for any possible realization. It can be said that the objective function would be optimized regarding the worst possible outcome and the solution as conservative as possible. According to this definition, the RO technique can be defined as

$$\min_{x}\left\{\max_{(c,A,b)\in U} c^T x : Ax \leq b \quad \forall (c,A,b) \in U\right\}.$$

Robust optimization was originally proposed as a linear programming problem with the incorporation of inexact data [12, 13]. As mentioned above, taking the worst case for each parameter is very conservative and RO was unsuccessful to be accepted by the operations research community.

However, recent studies by Ben–Tal [14, 15, 16, 17, 18], El–Ghaoui [19, 20], and Bertsimas [21, 22, 23] have tried to control the degree of conservatism since the 1990s. As a result, the new version of robust optimization is more general, and it is not limited to linear programming (quadratic, conic and semidefinite programs were also studied as other classes of convex optimization problem). Moreover, more complex uncertainty sets such as intersections of ellipsoidal uncertainty sets or uncertainty sets with budgets of uncertainty were taken into account. Defining controllable uncertainty sets was the major contribution of these articles. It means that the decision makers can select a level depending on how conservative they are. The other important analysis was the tractability of the robust counterpart. Robust optimization needs to be conducted through reformulating the original deterministic optimization problem, and hence, it is necessary to make sure the reformulated model is still convex and has finite dimension. Under these conditions, the problem would be called tractable which means the complexity of the resulting robust counterpart is not that expensive to be solved.

The RO concept was first proposed for optimization problem with parameters of unknown but fixed value, so–called static problems. Nevertheless, it has been widely used in (i) optimization problems with random parameters with unknown distributions and (ii) multistage decision–making where users can adjust their decisions with respect to the uncertainty observed over a time horizon.

Multistage robust optimization was also introduced for the very first time by Ben–Tal [24]. Applications of RO techniques on practical problems or theoretical works to improve the concepts have been widely implemented in various fields of study such as inventory management, facility location and transportation, scheduling, dynamic pricing and revenue management, project management, energy generation and distribution, or portfolio optimization. There are two review papers [25, 26] and one book [27] where the reader can refer to as well for a more thorough discussion and additional applications.

Stochastic programming technique. Despite the former section, the probability distributions of uncertainty might be known. This case is only possible where the ordering procedure repeats itself, and hence, a large and sufficient historical data can be used to estimate the distribution of uncertainty. For

example, if the uncertainty can be expressed as a cumulative distribution function, the objective function can be formulated as the expected value as below

$$\min_x \mathbb{E}\{c^T x : Ax \leq b\} : F(z) : = Prob((c, A, b) \leq z).$$

In most real cases, closed–form solutions for stochastic programming problems such as presented above are unavailable. Under these circumstances, a set of samples (1,...,k) can be selected with respective probabilities ($Pr_1, ..., Pr_k$) which is large enough to represent the whole range of uncertainty accurately. Hence, the stochastic program can be modeled as a deterministic optimization problem:

$$\min_x \sum_{k=1}^{K} \{Pr_k(c_k^T x_k) : A_k x_k \leq b_k\} : (c_k, A_k, b_k) \in K.$$

Questions that might arise at this point are how to construct the scenarios and how to measure the quality of obtained solutions. Different techniques were discussed by Heitsch and Römisch [28] and Pflug [29] to decrease the number of scenarios. Monte Carlo simulation is the most well–known approach that reduces the scenario set. This technique was offered by various authors under different names, but the one which has been used in the recent literature is the sample average approximation (SAA) method. The term "sample average approximation" method was first coined by Kleywegt et al [30]. Niederreiter studied rates of convergence for Monte Carlo and Quasi–Monte Carlo estimates of the expected values [31]. Two good works regarding statistical properties of the SAA method and complexity of two– and multi–stage stochastic programming were discussed by Ruszczynski and Shapiro [32] and Shapiro and Nemirovski [33], respectively.

Stochastic programming area was thoroughly studied with early developments by Dantzig [34], Beale [35], and Charnes and Cooper [36]. While the first two works presented the classic two–stage stochastic fixed recourse linear model, [34, 35], the former work introduced the concepts of chance constraints problems. The stochastic programming fundamentals have not been limited to either two–stage or linear problems, and there has been a significant improvement in theories and applications. One can start off by available books and monographs discussing the discipline of stochastic programming in a wide range of models and solution approaches [37, 32, 38]. For those who are interested in chance constraint optimization, the following references are suggested [39, 40].

1.2.4 Optimization application in oil sands industry

In this section, all the studies regarding the implementation of mathematical optimization in the oil sands industry are reviewed. The reviewing works are further divided into two groups of deterministic and stochastic problems.

Deterministic optimization problem. In one of the first attempts, the energy requirements for production of SCO and bitumen from oil sands were modeled and quantified [10]. Amounts of hot water, steam, power, hydrogen, diesel fuel, and process fuel were the estimated sources of energy. In addition to computing the energy demands of different bitumen extracting and upgrading methods, the greenhouse gas (GHG) emissions model was also incorporated. Moreover, the majority of GHG emissions (70–80%) resulted during the upgrading process [10]. In the following work, optimizing the energy production model for oil sands operations was presented [41]. Optimal combinations of power and hydrogen plants were determined

by the developed model satisfying the given energy demands of oil sands operations and CO_2 emissions constraint, at minimal cost [41]. In these two articles [10, 41], for given oil production demands, different schemes were proposed for SCO and DilBit productions. Moreover, it included different extraction methods (e.g., surface and in situ), upgrading technologies (such as fluid coking, delayed coking, and LC–fining), and energy producers with fixed capacities (such as boilers, hydrogen plants, and power plants).

In a more comprehensive study, the forecasted demands for electricity and hydrogen in oil sands operations were optimized under the CO_2 emissions constraints [42]. A MILP model was developed including varieties of hydrogen and power generation technologies (with and without CO_2 capture). By implementing the carbon capture in the hydrogen and power plants, 25% and 39% of CO_2 emissions reductions were achieved with respect to business–as–usual baselines in 2012 and 2030, respectively [42]. According to the results, the gasification (with and without capture) was an optimal technology for the hydrogen production, while the natural gas–based power production, particularly oxyfuel and combined cycle with CO_2 capture, showed great potential for power generation [42].

Later on, another energy model was introduced which optimized the energy infrastructure required to maintain oil production at minimum cost [43]. They proposed an integrated optimization model for simultaneous analysis of energy producers and production schemes. The novelty of this work was a simultaneous search for the most optimal configuration of oil production and its corresponding energy infrastructures meeting the total production demands and CO_2 emissions constraint [43]. Afterward, the integrated energy optimization model was investigated under various key environmental and operational factors [44]. CO_2 capture levels, natural gas prices, and steam–to–oil ratio (SOR) were the studied factors.

In the most recent work, a new energy optimization was modeled for the oil sands focusing on the upgrading operations [9]. The proposed model found the optimal configuration of upgraders while satisfying environmental regulations and product demands. Note here that in most of the mentioned works two distinct situations were investigated: (i) the current scenario which was based on existing technologies, and (ii) the future scenario which was based on projected targets in the future (e.g., 2030). In the work of [9], a model was presented for oil sands upgrading operations. This model determined the optimal scheme of upgrader at minimum cost with respect to environmental regulations and product demands. Furthermore, in this work, six existing upgraders were taken into account without proposing a general superstructure. When natural gas cost could change the optimal configuration drastically, it was found that the hydrocracking–based plant is more efficient [9]. In a more recent work, a multi–objective model was introduced for the same problem in which a five–stage upgrading superstructure was proposed [45]. Minimizations of both operating energy costs and associated CO_2 emissions were carried out. In the presented model, each unit had a set of operating modes, and each mode had a particular product yield and energy requirements. Applying the above assumption makes the model solvable with available commercial solvers; however, the optimal schemes of utility plant and associated carbon capture plant would be unknown.

Stochastic optimization problem. There have been few contributions on stochastic optimization in the oil sands industry. A single-period stochastic MINLP was formulated to address the Canadian oil sands

operations under environmental constraints on CO_2 emissions and water usage [46]. The uncertainties were analyzed separately, and the stochastic model led to a more economical solution than the deterministic one. Additionally, preference of the hydrocracking upgrader over thermocracking one, and not being able to meet the GHG emissions constraint for SORs higher than 2.48 are the two major findings of this work [46].

Later on, the uncertainties of natural gas and hydrogen prices, different productions demands, and yield of petroleum fractions were separately incorporated into a multi-scenario stochastic MINLP model [47]. A set of uncertain realizations was then defined to reach the optimal upgrading scheme, meeting different commodity specifications at minimum cost. Because the optimization was in the presence of worst–case realizations and uncertain economic and operational factors, it concluded that the proposed model could find the robust scheme. Although this model could find optimal infrastructure of the upgrading operations projected in year 2035, the objective function lacked many economic terms: capital, maintenance, and feed costs. It should be highlighted here, significant variations were observed in the optimal solutions under various uncertainty scenarios [47].

1.3 Thesis outline

In this thesis, Canadian bitumen upgrading problem at different levels of decision–making hierarchy is proposed. The optimal design, operation, and development are the three main problems which are addressed.

Chapter 2 proposes a new integrated model for simultaneous design optimization of upgrading plants in the oil sands industry and the associating utility plants. In the past, work has been mainly focused on the energy infrastructure of upgrading plants, and predesigned power and hydrogen plants were considered as utility plants. The novelty of this work is the incorporation of a detailed polygeneration energy system model with the bitumen upgrading plant model. In this way, optimal configurations can be found to meet the various energy requirements of upgrading plants in the oil sands industry. On the basis of the proposed optimization model, optimal configurations under different scenarios are discussed. Effects of upgrading plant capacity, being able to export power to the public grid, natural gas and electricity prices, and the margin between diluted bitumen and synthetic crude oil prices are studied.

CO_2 emissions from bitumen upgrading represent a major source of greenhouse gas emission in the oil sands industry of Canada. In Chapter 3, optimal design of bitumen upgrading plant is studied with the aim of CO_2 reduction. Various CO_2 capture techniques including oxyfuel combustion, pre–combustion and post–combustion are modeled and incorporated into an integrated optimization model for the simultaneous design of bitumen upgrading plant and the associated utility plant. To solve the resulting large–scale MINLP problem, augmented Lagrangian decomposition method is used. Optimal configurations under different scenarios (including plant capacity, natural gas, electricity and crude oil prices, and carbon tax) are discussed.

In Chapter 4, a general framework is proposed for the operation optimization of a bitumen upgrading plant in the oil sands industry. On the basis of simulation results from an upgrading plant in Aspen HYSYS environment, empirical models are developed through statistical analysis for different process units. Each generated correlation is a function of the relevant process unit operating conditions. All of the correlations

are further used to develop the upgrading plant optimization model, which is a non–convex NLP problem. The proposed model is tested on three examples in which different commodity demands are imposed as constraints: (i) no restriction for production, (ii) sweet SCO production, and (iii) mandatory multiple productions.

Expansion development of full upgrading plants is an important decision to make for the oil sands industry. In Chapter 5, we propose a multistage stochastic expansion development method to tackle uncertain SCO price and carbon tax. The linear decision rule–based technique is applied to solve the proposed stochastic optimization model. Various analyses are conducted based on optimization results: (i) effects of the uncertainty set size, (ii) comparison of solutions for selected pessimistic, realistic, and optimistic scenarios, (iii) effects of different operating modes for an upgrading plant, and (iv) cost distribution.

Partial upgrading technologies have received a great amount of attention as a promising and economic solution for Canadian oil sands bitumen processing. In Chapter 6, the optimal planning of initial capacity and expansion for the partial upgrading of bitumen is studied. We propose a multistage stochastic planning model, by considering various sources of uncertainties into the model. The main challenge of the stochastic model is the presence of terms in which an uncertain parameter is multiplied by an uncertain dynamic decision variable. To solve the problem, two hybrid methods are proposed: in method 1, the uncertain parameter is modeled with an uncertainty set and the dynamic variable is modeled as scenario dependent variables, and in method 2, the uncertain parameter is modeled with samples and the dynamic variable is modeled using the decision rule–based approximation. Finally, different criteria are defined and results obtained from both hybrid models are compared accordingly: (i) computational time, (ii) solution performance, and (iii) hybrid model solutions for representative scenarios.

1.4 Main contributions

The main contributions in this thesis can be summarized as follows:

- Developing a novel integrated optimization model for bitumen upgrading plant, utility facility, and carbon capture technologies.
- Implementing augmented Lagrangian decomposition algorithm for solving the large–scale MINLP problem.
- Proposing a general framework for the operation optimization of a bitumen upgrading plant in the oil sands industry.
- Proposing a multistage stochastic programming model for bitumen full upgrading plant capacity expansion planning and then solving the stochastic programming problem through linear decision rule–based method.
- Modeling a multistage stochastic planning problem for bitumen partial upgrading and presenting two hybrid methods (one of them is for the very first time) to solve the optimization problem.

Chapter 2

Design of Bitumen Upgrading and Utility Plant through Integrated Optimization[1]

2.1 Introduction

Utility plants of oil sands operations are required to be optimized simultaneously. As it is presented, there have been great contributions over oil sands operations optimization. However, all of the aforementioned studies considered the utility plant as a fixed source of energy. For instance, it was assumed that there are nine and six available power and hydrogen plants, respectively, from the literature [43]. Each plant has a fixed capacity, heating rate, capital, and operating cost. As a result, the only decision variables of these studies were type and number of power and hydrogen plants. A more detailed model is needed to achieve the optimal oil sands operations and their associated utility plants.

The most detailed model for utility plants has been proposed as a polygeneration energy system. Optimization of a polygeneration energy system was systematically addressed by Liu et al. [48, 49]. In his first paper, the design and planning of polygeneration infrastructure systems were formulated as a MILP problem [48]. The maximization of the net present value (NPV) over the planning time horizon was the objective of this study. The developed model was then applied for methanol and electricity productions in China in the period of 2010–2035 where 5 different feedstocks and 12 polygeneration technologies were included in the model. After carrying out result analysis, threshold analysis, and sensitivity analysis, it was concluded that the polygeneration technologies have more advantages than stand–alone technologies, and the polygeneration technologies that produce more electricity were more preferable due to the price of electricity. In the second paper, a MINLP model was formulated for the design optimization of polygeneration energy systems [49]. The presented model was basically based on the authors' previous work [48], and a general systematic approach was applied to make the model applicable for different technology, design, and operational requirements. While the earlier work carried out both design and planning optimization, the later one was just a design problem. To demonstrate the features and applicability of the suggested approach, a case study of a

[1] A version of this chapter was published in the *Industrial & Engineering Chemistry Research*, **2017**, *56*, 2107–2126

coal–based polygeneration plant producing electricity and methanol was then studied. Lately, Chen et al. proposed design and operational optimization of a polygeneration energy system under static [50] and flexible [51] conditions. In the first work, a superstructure was proposed for the polygeneration energy system in which power, liquid fuel (naphtha and diesel), and chemicals (methanol) can be produced from coal and biomass feedstocks [50]. To find the optimal design and operation of the explained superstructure, a mathematical model was presented being composed of mass and energy balances of all operating units, capital cost, and economic analyses. The solutions provided the optimal product distributions, NPVs, and CO_2 emissions under different scenarios for product prices and carbon taxes. Different production strategies such as carbon capture and sequestration (CCS) or biomass usage were also taken into account to demonstrate the effects of different carbon tax policies. Note here that the model was a NLP problem, and the objective function was NPV [50]. In the second work, despite their first attempt [50], varying market prices were considered for all products in daily and seasonal bases [51]. While the first work was called static design, the formulated model in here was more general, studying changes over the lifetime of the plant, namely, flexible. To do so, a number of scenarios were assumed with a certain frequency over the lifetime horizon. A two–stage programming framework was suggested in order to perform the design and operational optimizations at the same time. Different economic cases, including different oil prices and carbon taxes, were investigated [51].

In this Chapter, simultaneous optimization of the upgrading plant and the utility plant is addressed. The polygeneration energy system modeling is presented in Section 2.2. In Section 2.3, the model of upgrading plant for diluted bitumen is proposed. The nomenclature of presented model is available in Appendix A. Section 2.4 explains how the presented models in two previous sections can be integrated into each other. Section 2.5 reports the results obtained using the integrated model to find the optimal configuration of oil sands upgrading operators and their utility plants under different scenarios. Finally, concluding remarks are presented in section 2.6.

2.2 Utility plant

The proposed superstructure for the utility plant is shown in Figure 2.1. There are two process units for producing raw syngas: steam methane reforming (SMR) and gasifier. The SMR unit consumes natural gas and steam to produce sweet syngas. The gasifier unit uses heavy oil residue or coke to generate sour syngas. The sulfuric components are then processed and separated through the COS hydrolysis reactor and Selexol unit. The separated H_2S can be further processed in the Claus plant to produce elemental sulfur. The cleaned syngas is then passed through the water gas shift (WGS) and Selexol unit for converting the CO into CO_2. Afterward, pure hydrogen can be separated in the pressure–swing adsorption (PSA) unit. The tail gas exiting the PSA unit and two other streams withdrawn from the inlets of WGS and PSA units have a significant amount of CO which can be burned with air in gas turbine combustor–1 (GTC1). The exhaust gas resulting from the GTC1 is sent to gas turbine–1 (GT1) to generate power due to its high pressure and temperature. After GT1, the temperature of the outlet is still high and more energy can be recovered in the heat recovery steam generator–1 (HRSG1). Moreover, natural gas is another energy source which can

Table 2.1: Constant coefficients of enthalpy correlation (superheated)

Component	*ha*	*hb*	*hc*	*hd*
CO	-111.78	-0.0007	0.030	1.86E-06
H_2	-0.75	0.0009	0.028	1.54E-06
CO_2	-396.12	-0.0053	0.044	6.25E-06
H_2O	-243.71	-0.0129	0.035	5.18E-06
CH_4	-76.42	-0.0028	0.038	2.27E-05
Ar	-0.93	-0.0023	0.022	-6.08E-07
N_2	-1.09	-0.0006	0.030	1.65E-06
H_2S	-22.16	-0.0093	0.037	6.48E-06
COS	-141.82	-0.0125	0.051	3.69E-06
O_2	-1.23	-0.0025	0.032	2.02E-06
C_2H_6	-87.64	-0.0095	0.061	4.21E-05
C_3H_8	-112.87	-0.0179	0.110	4.13E-05
C_4H_{10}	-139.61	-0.0294	0.150	4.96E-05

be used for power and energy generation through GTC2, GT2, HRSG2 units. Boiler1 and Boiler2 units are employed to generate low– and high–quality duties by burning natural gas to meet the demands or produce additional amounts of duties. The extra duties are then sent to low– and high–quality steam turbines (stlo and sthi) in order to generate more power.

2.2.1 Thermodynamic model

In this section, the thermodynamic model of working fluids is presented for the proposed superstructure. Empirical models are generated for the enthalpy property. There are two sets of correlations for enthalpy estimation: superheated and saturated. According to operating pressure and temperature of units, most of the working fluids can be assumed to be at their superheated state. The only exception is saturated steam which is injected into a few units such as the gasifier and WGS. Therefore, two sets of empirical models are required for enthalpy calculation.

For the superheated case, the pressure and temperature are both effective on the enthalpy, but it is much more sensitive to the temperature. Enthalpies of pure components at different temperatures (in the range of -100 to 1500 $°C$) and pressures (in the range of 1 to 100 bar) are simulated with Aspen HYSYS, and correlations with accuracy higher than 0.999 of R–squared are generated with Design–Expert. The generated correlation model has the following general polynomial formulation.

$$H_j^{su} = ha_j + hb_j \cdot P + hc_j \cdot T + hd_j \cdot T^2 \quad \forall j \in J \tag{2.1}$$

where H_j^{su} is the enthalpy of j superheated component (GJ Mmol^{-1}), P is pressure (bar), T is temperature (°C), and ha, hb, hc, and hd are constant coefficients reported in Table 2.1.

For the saturated case, the pressure and temperature are both effective, but they are dependent on each other. Hence, the pressure is taken into account as the independent variable, while the temperature, liquid, and vapor enthalpies are calculated correspondingly. Note here, the saturated vapor enthalpy has a very nonlinear behavior, so an empirical model is generated for latent heat to calculate the saturated vapor

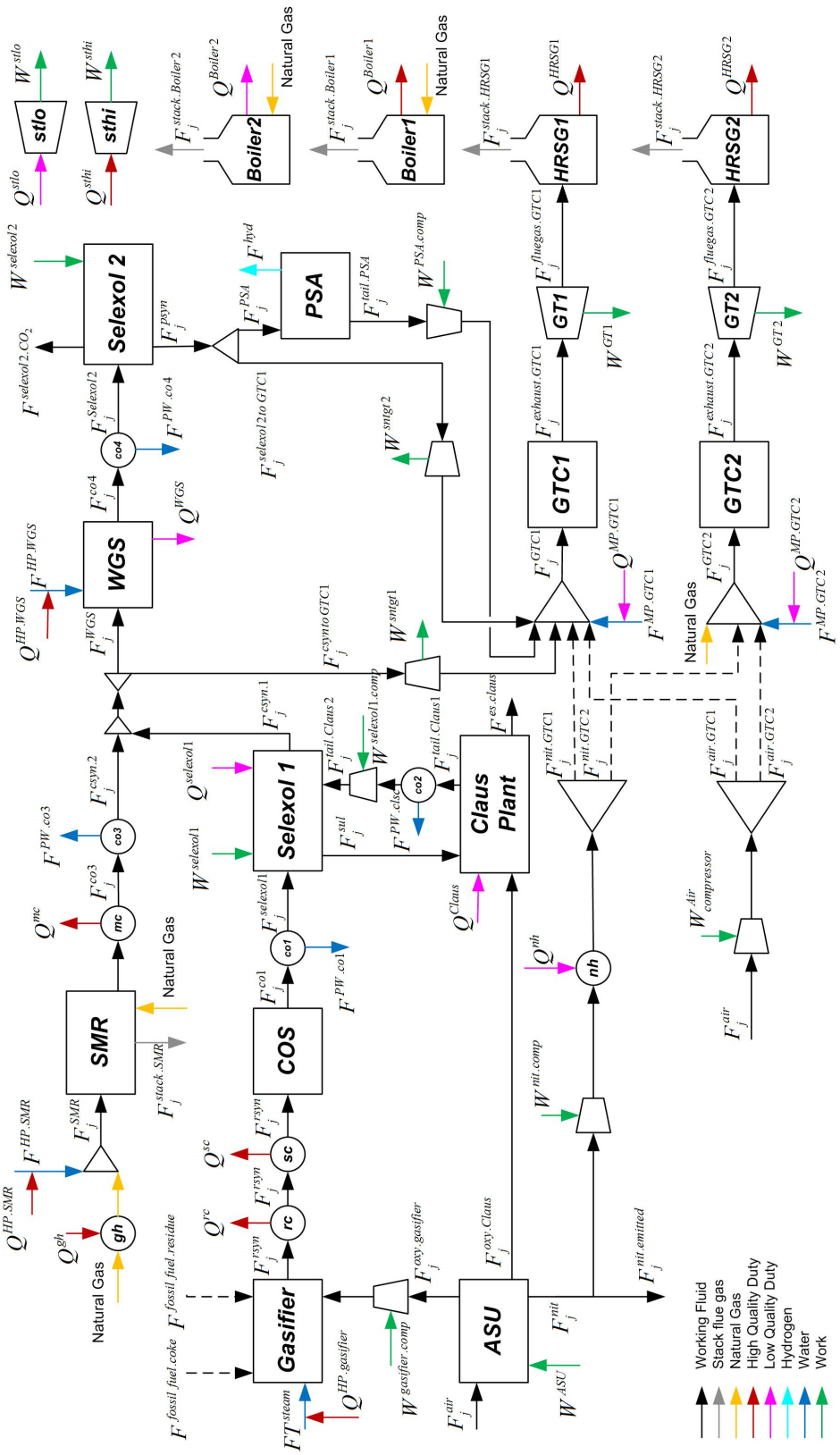

Figure 2.1: Superstructure of utility plant

Table 2.2: Constant coefficients of saturated enthalpy correlation

Index	T^{sat}	HL^{sat}	λ^{sat}
a	134.03	5.56	-1.60
b	0.21	0.33	0.52
c	-34.51	-285.60	42.14

Table 2.3: Operating temperature and pressure/pressure drop of working fluids [48, 50, 52, 53]

Stream	T (°C)	P or dP (bar)	Stream	T (°C)	P or dP (bar)
$rsyn(SCGP)$	1320	35	$tail.PSA$	187.5	18
$rsyn(SGP)$	1500	35	$hyd.PSA$	30	22
rc	593	-1.65	$selexol2.to.GTC1$	187.5	18
sc	205	-1.65	$csyn.to.GTC1$	187.5	18
sul	48.3	1.6	$exhaust.GTC1$	*	18
$oxy.Claus$	232.2	8.6	$fluegas.GTC1$	563.3	1
$tail.Claus1$	232.2	0.8	$stackgas.HRSG1$	131.9	1
$es.Claus$	178.0	1.2	$nit.GTC2$	196	26.8
gh	537.8	-1.0	$air.GTC2$	405	18
SMR	879.4	28.1	$exhaust.GTC2$	*	18
mc	448.9	-1.0	$NG.GTC2$	38	30
WGS	240	-4.6	$fluegas.GTC2$	563.3	1
$Selexol2$	232	-3.0	$stackgas.HRSG2$	131.9	1
$nit.GTC1$	196	26.8	$nit.ASU$	92.8	26.8
$air.GTC1$	405	18			

$*$ These operating conditions are variables with upper limit 1300 °C.

enthalpy indirectly. In this section, water is the only component. Enthalpies of pure water at different pressures (in the range of 1 to 100 bar) are simulated with Aspen HYSYS, and correlations with accuracy higher than 0.999 of R–squared are generated with Design–Expert. The following general polynomial models are developed.

$$T_{pl}^{sat} = T^{sat_a} \cdot P^{T^{sat_b}} + T^{sat_c} \quad \forall pl \in PL \tag{2.2}$$

$$HL_{pl}^{sat} = HL^{sat_a} \cdot P^{HL^{sat_b}} + HL^{sat_c} \quad \forall pl \in PL \tag{2.3}$$

$$\lambda_{pl}^{sat} = \lambda^{sat_a} \cdot P^{\lambda^{sat_b}} + \lambda^{sat_c} \quad \forall pl \in PL \tag{2.4}$$

$$HV_{pl}^{sat} = HL_{pl}^{sat} + \lambda_{pl}^{sat} \quad \forall pl \in PL \tag{2.5}$$

where $PL = \{LP, MP, HP, VHP\}$, T_{pl}^{sat} is saturated temperature (°C), HL_{pl}^{sat} is liquid saturated enthalpy (GJ Mmol^{-1}), λ_{pl}^{sat} is latent heat (GJ Mmol^{-1}), HV_{pl}^{sat} is vapor saturated enthalpy (GJ Mmol^{-1}), P is pressure (bar), T^{sat}, HL^{sat}, λ^{sat} are constant coefficients reported in Table 2.2.

Moreover, operating temperature and pressure/pressure drop of different units are provided in Table 2.3.

Table 2.4: Elemental compositions and water fraction in the feedstocks

Element	$xw_{i,gt}^{dry\ mass}$	
	SGP	$SCGP$
C	0.8437	0.883
H	0.0967	0.048
O	0.0023	0.000
N	0.0052	0.029
S	0.0501	0.037
$xw_{gt}^{\mathrm{H_2O}}$	0.0	0.015

Table 2.5: Steam to fuel and oxygen to fuel ratios in the gasifier

Parameter	SGP	SCGP
MR_{gt}^{steam} (tonne tonne^{-1})	0.23	0.23
MR_{gt}^{oxygen} (tonne tonne^{-1})	1.04	1.04

2.2.2 Process unit model

Gasifier unit. Instead of using complex chemical kinetic models, transport models, and thermodynamics models, the gasification process is modeled based on elemental mass balance and linear empirical energy balance. Five elements of C, H, O, N, and S (represented with index i) in the feedstock are converted to species of j (including CO, H_2, CO_2, H_2O, CH_4, Ar, N_2, H_2S, COS, O_2, C_2H_6, C_3H_8, C_4H_{10}) in order to produce raw syngas. Note here compositions of some species (O_2, C_2H_6, C_3H_8, C_4H_{10}) are fixed at zero since they are not produced during gasification. In this study, coke and residue withdrawn from thermocracking and hydrocracking are feedstock to be selected. For coke gasification and residue gasification, industrial technologies licensed by Shell, namely the Shell coal gasification process (SCGP) and the Shell gasification process (SGP) are employed, respectively. Fixed operating conditions are assumed. The gasifier type is shown with index gt in this Chapter. Note here, the feedstocks mass fractions of water ($xw_{gt}^{H_2O}$) and their dry mass compositions ($xw_{i,gt}^{dry\ mass}$) are all given (see Table 2.4). According to Table 2.5, the ratio of required steam and oxygen are also known. Furthermore, conversions of all elements ($CR_i^{gasifier}$) are assumed constant under unchanging operating conditions. They are all equal to 1 except the conversion rate of carbon which is 0.98.

The molar flow rates of all species in the raw syngas (F_j^{rsyn}) are related to the flow rates of steam inlet (M^{steam}) and oxygen inlet ($F^{oxy.gasifier}$) and mass flow rates of fossil fuels ($M_{gt}^{fossil\ fuel}$). The total mass balance can be formulated as

$$\begin{aligned}\sum_j n_{i,j}\cdot MW_i^{element}\cdot F_j^{rsyn} = \sum_{gt}\Big(b_{gt}^{gasifier}\cdot\Big[&CR_i^{gasifier}\cdot xw_{i,gt}^{dry\ mass}\cdot(1-xw_{gt}^{H_2O})\cdot M_{gt}^{fossil\ fuel}\\ &+xw_i^{element.H_2O}\cdot xw_{gt}^{H_2O}\cdot M_{gt}^{fossil\ fuel}+\tfrac{n_{i,H_2O}\cdot M^{steam}\cdot MW_i^{element}}{MW_{H_2O}^{specie}}\\ &+\textstyle\sum_j(n_{i,j}\cdot MW_i^{element}\cdot xm_{j,gt}^{oxy}\cdot FT^{oxy.gasifier})\Big]\Big)\quad\forall i\in I\end{aligned} \tag{2.6}$$

where $n_{i,j}$ is the number of atoms of element i in one molecule of species j, $xw_i^{element.H_2O}$ is mass fraction of element i in inlet water , $b_{gt}^{gasifier}$ is the binary variable to indicate fossil fuel inlet type between coke and

Table 2.6: Volumetric fractions of main species in the produced raw syngas

Component	$\alpha_{j,gt}^{rsyn}$	
	SGP	SCGP
CO	0.4962	0.6300
H_2	0.4505	0.3000
CO_2	0.0284	0.0200
H_2S	0.0076	0.0076

residue, and $xm_{j,gt}^{oxy}$ is mole fraction of species j in oxygen stream. Moreover, $MW_i^{element}$ and $MW_{H_2O}^{specie}$ are molecular weight of element i and specie j, respectively.

For elemental argon which is not involved in the chemical reaction, the inlet molar flow rate is equal to the outlet one:

$$F_j^{oxy.ASU} = F_j^{rsyn} \quad \forall j = \{\text{Ar}\} \tag{2.7}$$

Mass, molar, and volumetric flow rates can be related to each other with the following equations.

$$M_j^{rsyn} = F_j^{rsyn} \cdot MW_j^{specie} \quad \forall j \in J \tag{2.8}$$

$$M_j^{rsyn} = \sum_{gt}(b_{gt}^{gasifier} \cdot \rho_{j,gt} \cdot V_j^{rsyn}) \quad \forall j \in J \tag{2.9}$$

Note here, the temperature and pressure of the produced syngas with different gasification technologies are constant but they are not the same so distinctive densities of outlet species $\rho_{j,gt}$ are applied in above equations.

The mass flow rate ratio between fossil fuel and steam MR_{gt}^{steam} and oxygen MR_{gt}^{oxygen} inlets are also known from the reference. Total steam inlet to the gasifier is calculated as

$$M^{steam} = \sum_{gt}(b_{gt}^{gasifier} \cdot [\frac{MR_{gt}^{steam} \cdot M_{gt}^{fossil\ fuel}}{1 - xw_{gt}^{H_2O}}]) \tag{2.10}$$

To make sure that the volumetric fractions of produced raw syngas are in the acceptable range (see Table 2.6), following constraints are imposed for main species, CO, H_2, CO_2, and H_2S. The reference values are found from Shell industrial data [54].

$$V_j^{rsyn} = VT^{rsyn} \cdot xv_j^{rsyn} \quad \forall j \in J \tag{2.11}$$

$$\sum_j xv_j^{rsyn} = 1 \tag{2.12}$$

$$0.9 \cdot \sum_{gt}(b_{gt}^{gasifier} \cdot \alpha_{j,gt}^{rsyn}) \leq xv_j^{rsyn} \leq 1.1 \cdot \sum_{gt}(b_{gt}^{gasifier} \cdot \alpha_{j,gt}^{rsyn}) \quad \forall j \in \{\text{CO}, \text{H}_2, \text{CO}_2, \text{H}_2\text{S}\} \tag{2.13}$$

The following logical constraints are required to make sure that only one of the fossil fuel is sent into the gasifier unit and the capacity of gasification is not too small ($\underline{\Omega}^{gasifier}$) or too big ($\overline{\Omega}^{gasifier}$).

$$\sum_{gt} b_{gt}^{gasifier} = 1 \tag{2.14}$$

$$b_{gt}^{gasifier} \cdot \underline{\Omega}^{gasifier} \leq M_{gt}^{fossil\ fuel} \leq b_{gt}^{gasifier} \cdot \overline{\Omega}^{gasifier} \quad \forall gt \in GT \tag{2.15}$$

There are two heat exchangers after the gasifier, syngas radiant cooler (rc) and syngas convective cooler (sc). Both of them cool the produced raw syngas and generate high–pressure steam. The temperatures of syngas are 593 and 205 °C, respectively. Pressure drop of each heat exchanger is assumed to be 1.65 bar [48]. On the basis of the total energy balance, the released duty from a cooler can be calculated using the following equation, and this can be applied for both rc and sc.

$$Q = \sum_j F_j^{in} \cdot H_j^{su.in} - \sum_j F_j^{out} \cdot H_j^{su.out} \tag{2.16}$$

Moreover, steam is required in the gasifier. This amount of duty can be estimated according to the latent at the corresponding pressure.

$$Q = F^{water} \cdot \lambda^{sat} \tag{2.17}$$

The last part is a calculation of required works for compression of the oxygen inlet. Following the ratio equation is applied for electricity requirements (GW) of the corresponding compressor.

$$W^{gasifier.comp} = 0.001 \cdot \frac{FT^{oxy.gasifier} \cdot Eb^{gasifier.comp}}{Fb^{gasifier.comp}} \tag{2.18}$$

where $Eb^{gasifier.comp}$ and $Fb^{gasifier.comp}$ are electricity requirement and working flow rate of the base case equaling to 11.422 MW and 5.8975 Mmol h^{-1}, respectively. Note here, the coefficient 0.001 is for unit conversion of MW to GW.

COS unit. In the COS hydrolysis reactor, COS is converted to CO_2 and H_2S through the following reaction

$$\mathrm{COS} + \mathrm{H_2O} \longleftrightarrow \mathrm{CO_2} + \mathrm{H_2S} \tag{2.19}$$

The mass balance of this reactor can be formulated as below where the stoichiometric coefficient of species (Sto_j^{COS}) is based on the above reaction.

$$F_j^{co1} = F_j^{rsyn} + Sto_j^{\mathrm{COS}} \cdot F_{\mathrm{COS}}^{rsyn} \quad \forall j \in J \tag{2.20}$$

There is a cooler after the reactor which is used to condense and separate a major portion of produced water. The molar composition of water ($xm_{\mathrm{H_2O}}$) is reduced to 0.0016 after this unit. The mass balance of this unit can be stated as follows.

$$F_j^{in} = F_j^{out} \quad \forall j \in J/\{\mathrm{H_2O}\} \tag{2.21}$$

$$F_j^{in} = F^{PW} + F_j^{out} \quad \forall j \in J = \{\mathrm{H_2O}\} \tag{2.22}$$

$$xm_{\mathrm{H_2O}} = \frac{F_{\mathrm{H_2O}}^{out}}{\sum_j F_j^{out}} \tag{2.23}$$

Note that energy balance over this unit is neglected since the released duty from the hot stream does not have adequate quality for power generation. As a result, this source of energy is more appropriate for preheating.

Selexol unit. There are two sets of Selexol units in the proposed superstructure. The first one is for H_2S removal and it is integrated with the Claus plant. Syngas is then cooled and enters the second Selexol unit for removing CO_2. Part of the CO_2 can be compressed at this stage for carbon sequestration and the rest can be emitted. The mass and energy balance can be presented as follows.

For Selexol unit 1, the mass balance equations include

$$F_j^{csyn1} = S_j^{sel_1} \cdot (F_j^{selexol1} + F_j^{tail.claus2}) \quad \forall j \in J/\{\mathrm{CO_2}\} \tag{2.24}$$

$$F_j^{selexol1} + F_j^{tail.claus2} = F_j^{csyn1} + F_j^{sul} \quad \forall j \in J \tag{2.25}$$

$$F_{\mathrm{H_2S}}^{sul} = xm_{\mathrm{H_2S}}^{sul} \cdot (F_{\mathrm{H_2S}}^{sul} + F_{\mathrm{CO_2}}^{sul}) \tag{2.26}$$

where $S_j^{sel_1}$ is the split fraction of species j to the clean syngas in the Selexol Unit 1 (F_j^{csyn}), $xm_{\mathrm{H_2S}}^{sul}$ is the mole fraction of H_2S in the H_2S-rich stream (F^{sul}). Note here, $S_j^{sel_1}$ is a variable for CO_2, but it is set to $6 \cdot 10^{-7}$ for H_2S and fixed at 1 for the rest of the species, and $xm_{\mathrm{H_2S}}^{sul}$ is equal to 0.48 [50].

Heat and power consumptions of this unit also can be presented as the following equations.

$$Q^{selexol1} = 0.001 \cdot QC^{selexol1} \cdot FT^{selexol1} \tag{2.27}$$

$$W^{selexol1} = 0.001 \cdot EC^{selexol1} \cdot FT^{selexol1} \tag{2.28}$$

where $QC^{selexol1}$ and $EC^{selexol1}$ are regressed coefficients [50] for heat and power consumptions being 3849.6 MJ $\mathrm{kmol^{-1}}$ and 0.1061 Wh $\mathrm{mol^{-1}}$, respectively.

Additionally, the tail gas stream entering this unit from the Claus plant needs to be compressed. The power requirement of the compressor can then be estimated as follow.

$$W^{selexol1.comp} = 0.001 \cdot \frac{FT^{tail.claus2} \cdot Eb^{selexol1.comp}}{Fb^{selexol1.comp}} \tag{2.29}$$

where $Eb^{selexol1.comp}$ and $Fb^{selexol1.comp}$ are electricity requirement and working flow rate of base case equaling to 1.087 MW and 0.2931 Mmol $\mathrm{h^{-1}}$, respectively.

Note here, a portion of outlet from this unit can be directed to the gas turbine combustor ($F_j^{csyn.to.GTC1}$). To adjust the pressure, this stream is passed through a gas turbine which can generate electricity based on the following equation.

$$W^{sntgt1} = 0.001 \cdot \frac{FT^{csyn.to.GTC1} \cdot Eb^{sntgt1}}{Fb^{sntgt1}} \tag{2.30}$$

where Eb^{sntgt1} and Fb^{sntgt1} are electricity requirement and working flow rate of base case equaling to 8.1863 MW and 18.4207 Mmol $\mathrm{h^{-1}}$, respectively [50].

For the Selexol unit 2, the mass balance includes

$$F_j^{psyn} = S_j^{sel_2} \cdot F_j^{selexol2} \quad \forall j \in J \tag{2.31}$$

$$F_j^{selexol2} = F_j^{psyn} + F^{selexol2.\mathrm{CO_2}} \quad \forall j = \{\mathrm{CO_2}\} \tag{2.32}$$

$$F_j^{psyn} = F_j^{PSA} + F_j^{selexol2.to.GTC1} \quad \forall j \in J \tag{2.33}$$

where $F_j^{selexol2}$ and F_j^{psyn} are molar flow rates of the syngas inlet and outlet in the Selexol Unit 2, respectively, $F^{selexol2.\mathrm{CO_2}}$ is the total molar flow rate of CO_2 stream from the Selexol Unit 2, $S_j^{sel_2}$ is the split fraction of species c to the clean syngas in the Selexol Unit 2. Note here that $S_j^{sel_2}$ is set to be 1 for all species except CO_2 and 0.031 for CO_2 [50].

When there is no major heat consumption in this unit, the power consumption can be presented as the following equation.

$$W^{selexol2} = 0.001 \cdot EC^{selexol2} \cdot FT^{selexol2} \tag{2.34}$$

where $EC^{selexol2}$ is a regressed coefficient for power consumption being 1.6981 Wh mol^{-1}.

It should be noted that a portion of outlet from this unit can be directed to the gas turbine combustor ($F_j^{selexol2.to.GTC1}$). To adjust the pressure, this stream is passed through a gas turbine which can generate electricity (W^{sntgt2}) based on Equation 2.30 where the same parameters are still valid.

Claus plant. The H_2S–rich stream leaving the Selexol unit 1 is sent to the Claus plant, where it is converted to elemental sulfur as a product. This unit is based on the following reaction

$$\mathrm{H_2S} + \frac{1}{2}\mathrm{O_2} \longleftrightarrow \mathrm{H_2O} + \mathrm{S} \tag{2.35}$$

According to Figure 2.1 and the above equation, mass and energy balances of the Claus plant can be written as

$$F_j^{tail.claus1} = F_j^{oxy.claus} + F_j^{sul} + Sto_j^{claus} \cdot CR^{claus} \cdot F_{\mathrm{H_2S}}^{sul} \quad \forall j \in J \tag{2.36}$$

where Sto_j^{claus} is stoichiometric coefficient of elements from the above reaction equation and CR^{claus} is conversion rate of the Claus reaction. The conversion of H_2S in the Claus reaction is assumed to remain unchanged in all cases, which is 0.975.

The next equation calculates the oxygen requirement based on the conversion rate and stoichiometric coefficients of H_2S and oxygen.

$$F_{\mathrm{O_2}}^{oxy.claus} = \frac{1}{2} \cdot CR^{claus} \cdot F_{\mathrm{H_2S}}^{sul} \tag{2.37}$$

The following equations calculate the amount of sulfur production based on H_2S inlet and its conversion rate.

$$F^{es.claus} = CR^{claus} \cdot F_{\mathrm{H_2S}}^{sul} \tag{2.38}$$

$$M^{es.claus} = MW_s^{element} \cdot F^{es.claus} \tag{2.39}$$

Table 2.7: Compositions of oxygen and air streams

Component	Oxygen	Air
Ar	0.029	0.0205
N_2	0.016	0.7719
O_2	0.955	0.2076

There are heat production and work consumption associating with the Claus plant. By applying a total energy balance over this unit, the generated low quality heat can be calculated. To estimate the operating conditions of inlets and outlets, data from reference [52] are used. While the enthalpy of solid sulfur is calculated with Aspen HYSYS simulation, the enthalpies of the three remaining streams are calculated based on the developed correlation under superheated conditions.

$$\sum_j F_j^{sul} \cdot H_j^{su.sul} + \sum_j F_j^{oxy.claus} \cdot H_j^{su.oxy.claus} = Q^{claus} + \sum_j F_j^{tail.claus1} \cdot H_j^{su.tail.claus1} + F^{es.claus} \cdot H^{es.claus} \tag{2.40}$$

Note here, tail gas exiting this unit ($F_j^{tail.claus1}$) passes through a cooler followed with a compressor before entering the Selexol 1 unit. The cooler model is the same as the one discussed at the end of the COS Hydrolysis Reactor section. The power requirement is estimated according to the following equation.

$$W^{selexol1.comp} = 0.001 \cdot \frac{FT^{tail.claus2} \cdot Eb^{selexol1.comp}}{Fb^{selexol1.comp}} \tag{2.41}$$

where $Eb^{selexol1.comp}$ and $Fb^{selexol1.comp}$ are electricity requirement and working flow rate of base case equaling to 1.087 MW and 0.2931 Mmol h^{-1}, respectively.

Air separation unit (ASU). In the ASU, O_2 and N_2 are separated from each other. It is assumed that the mass fraction of O_2 and N_2 are given for both rich outlets [50]. Compositions of oxygen and air streams are reported in Table 2.7.

O_2 with over 95 mol % purity and a N_2 stream are produced by a cryogenic distillation process. Therefore, the mass balances would be expressed as below. Total oxygen requirements are summation of demands for the gasifier and Claus plant.

$$\sum_j F_j^{oxy} = \sum_j F_j^{oxy.gasifier} + \sum_j F_j^{oxy.claus} \tag{2.42}$$

Mass balance over the ASU unit can be stated as

$$F_j^{air} = F_j^{oxy} + F_j^{nit} \quad \forall j \in J \tag{2.43}$$

$$F_j^{oxy} = xm_j^{oxy} \cdot FT^{oxy} \quad \forall j \in J \tag{2.44}$$

$$F_j^{air} = xm_j^{air} \cdot FT^{air} \quad \forall j \in J \tag{2.45}$$

$$F_j^{oxy} = S_{O_2}^{ASU} \cdot F_j^{air} \quad \forall j = \{O_2\} \tag{2.46}$$

where $S_{O_2}^{ASU}$ is split fraction of O_2 (=0.94), xm is molar fraction (it is given for air and oxygen streams), and FT is total molar flow rate.

The next equation evaluates the electricity requirements (GW) of the ASU.

$$W^{ASU} = 0.001 \cdot \frac{FT^{air} \cdot Eb^{ASU}}{Fb^{ASU}} \tag{2.47}$$

where Eb^{ASU} and Fb^{ASU} are electricity requirement and working flow rate of base case equaling to 72.2496 MW and 29.138 Mmol h^{-1}, respectively.

SMR unit. In the proposed superstructure, SMR is considered an alternative method of hydrogen production. In this process, hydrocarbons, basically methane, are turned into hydrogen and carbon dioxide through the following reaction.

$$CH_4 + H_2O \longrightarrow CO + 3H_2 \tag{2.48}$$

This reaction takes place with the presence of HP steam. Mass flow rate of the steam is calculated according to the stoichiometric coefficient of the above reaction with 94% excess molar flow rate [53].

The mixture of steam and natural gas (F_j^{SMR}) is passed through the reactor and the products stream (F_j^{csyn2}) is sent to the WGS unit. The following equation models the mass balance for the SMR unit

$$F_j^{csyn2} = F_j^{SMR} + Sto_j^{SMR} \cdot CR^{SMR} \cdot F_j^{SMR} \quad \forall j \in J \tag{2.49}$$

where Sto_j^{SMR} is stoichiometric coefficients and CR^{SMR} is the conversion rate of SMR reaction and set as 76.9%.

The following logical constraints enforce that at least one of the two options (gasification and SMR) is selected for syngas production and the capacity of SMR is in a reasonable range.

$$1 \leq \sum_{gt} b_{gt}^{gasifier} + b^{SMR} \tag{2.50}$$

$$b^{SMR} \cdot \underline{\Omega}^{SMR} \leq VT^{NG.SMR} \leq b^{SMR} \cdot \overline{\Omega}^{SMR} \tag{2.51}$$

A preheater and a cooler exist before and after of the SMR units, respectively. The duties of these heat exchangers can be estimated with Equation 2.17 and the equations presented at the end of the COS Hydrolysis Reactor section. The corresponding pressure and temperature are provided in Table 2.3 for enthalpies calculations. Note here, these energy streams include high quality duties. Furthermore, natural gas is burned in the SMR to provide the required energy of reaction. To calculate the amount of required duty, the general energy balance Equation 2.16 should be used. Next, the mass flow rate of natural gas can be calculated as

$$M^{NG.SMR} = \frac{Q^{SMR}}{eff^{SMR} \cdot LHV^{NG}} \tag{2.52}$$

where $M^{NG.SMR}$ is mass flow rate (tonne h^{-1}) of natural gas and eff^{SMR} is the efficiency of natural gas conversion into heat duty. The efficiency is assumed to be 0.93 [55]. The Low heat value (LHV) of using natural gas is provided through simulation of natural gas in the Aspen HYSYS environment based on characteristics reported in Table 2.8. Consequently, the LHV is equal to 47.8417 GJ $tonne^{-1}$.

Table 2.8: Compositions of natural gas

Component	Composition
CO_2	0.010
CH_4	0.939
N_2	0.008
C_2H_6	0.032
C_3H_8	0.007
C_4H_{10}	0.004

WGS unit. This block is used for conversion of syngas into CO_2 and H_2, and then separation of tail gas (mainly CO_2) to obtain pure H_2. To do so, there are two units required: WGS reactors and PSA unit. Clean syngas first passes through three–stage WGS reactors in series, which include two high–temperature reactors and one low–temperature reactor, to convert part of the CO by the following exothermic reaction:

$$CO + H_2O \longleftrightarrow CO_2 + H_2 \tag{2.53}$$

Note here, the clean syngas inlet is a summation of clean syngas from both the gasifier and SMR units. The clean syngas streams come from the gasification (F_j^{csyn1}) and SMR (F_j^{csyn2}) units.

They get mixed first and then go through a splitter with two outlets: WGS feed (F_j^{WGS}) and GTC1 feed ($F_j^{csyn.to.GTC1}$).

$$F_j^{csyn1} + F_j^{csyn2} = F_j^{WGS} + F_j^{csyn.to.GTC1} \quad \forall j \in J \tag{2.54}$$

According to Figure 2.1, all the reactors can be modeled in a single unit. Since steam is an inlet stream in addition to clean syngas, the mass balance of water specie will be different with the other ones.

$$F_j^{co2} = F_j^{WGS} + Sto_j^{WGS} \cdot CR^{WGS} \cdot F_j^{WGS} \quad \forall j \in J/\{H_2O\} \tag{2.55}$$

$$F_j^{co2} = F_j^{WGS} + Sto_j^{WGS} \cdot CR^{WGS} \cdot F_j^{WGS} + F^{HP.WGS} \quad \forall j = \{H_2O\} \tag{2.56}$$

where F_j^{co2} is outlet mole flow rate for each specie, Sto_j^{WGS} is stoichiometric coefficient of elements from the above reaction equation and CR^{WGS} is the conversion rate of WGS reaction equal to 92%. Note here, the ratio of steam to molar flow rate to CO molar flow rate is fixed at 2.8.

Some low quality duty is generated during the WGS process. Its amount can be calculated with the general energy balance over the whole unit Equation 2.16. Moreover, there is a cooler with water separation after the WGS unit. It can be modeled as the equations discussed at the end of the COS Hydrolysis Reactor section.

PSA unit. In the PSA, only CO_2 is adsorbed and pure H_2 stream (F^{hyd}) is thus produced. The H_2 recovery is constant in this model because the operating conditions of PSA are specified for all cases. The split fraction of H_2 to the H_2 stream (S_{H2}^{PSA}) is 0.9. While the mass balance can be given as

$$F_j^{tail.PSA} = F_j^{PSA} \quad \forall j \in J/\{H_2\} \tag{2.57}$$

$$F_j^{tail.PSA} = (1 - S_{H2}^{PSA}) \cdot F_j^{PSA} \quad \forall j = \{\mathrm{H_2}\} \tag{2.58}$$

$$F^{hyd} = S_{H2}^{PSA} \cdot F_j^{PSA} \quad \forall j = \{\mathrm{H_2}\} \tag{2.59}$$

$$M^{hyd} = F^{hyd} \cdot MW_j^{specie} \quad \forall j = \{\mathrm{H_2}\} \tag{2.60}$$

Furthermore, a compressor is required to increase the pressure of the tail gas stream before it enters the gas turbine combustor. The following equation can be given for the work requirement.

$$W^{PSA.comp} = 0.001 \cdot \frac{FT^{tail.PSA} \cdot Eb^{PSA.comp}}{Fb^{PSA.comp}} \tag{2.61}$$

where $Eb^{PSA.comp}$ and $Fb^{PSA.comp}$ are electricity requirement and working flow rate of base case equaling to 2.1681 MW and 1.0 Mmol h^{-1}, respectively.

GT unit. Syngas or natural gas is combusted in the combustor of a gas turbine and high pressure and high temperature exhaust is produced. Power and high quality duty are generated by using the gas turbine and HRSG subsequently. Two sets of gas turbines are included in the proposed superstructure (see Figure 2.1); (i) gas turbine–1 with syngas feed, and (ii) gas turbine–2 with natural gas feed. While the first set is fixed, the second one is optional and a binary variable (b^{GTC2}) is used to take this issue into account. In the following combustion reactions, the first two represent the main reactions of gas turbine–1. All of them except the first one represent the major reactions of gas turbine–2. Natural gas compositions are provided in Table 2.8.

$$\mathrm{CO + H_2O \longrightarrow CO_2 + H_2} \tag{2.62}$$

$$\mathrm{H_2 + 0.5O_2 \longrightarrow H_2O} \tag{2.63}$$

$$\mathrm{CH_4 + 2O_2 \longrightarrow CO_2 + 2H_2O} \tag{2.64}$$

$$\mathrm{C_2H_6 + 3.5O_2 \longrightarrow 2CO_2 + 3H_2O} \tag{2.65}$$

$$\mathrm{C_3H_8 + 5O_2 \longrightarrow 3CO_2 + 4H_2O} \tag{2.66}$$

$$\mathrm{C_4H_{10} + 6.5O_2 \longrightarrow 4CO_2 + 5H_2O} \tag{2.67}$$

Air is required to be compressed to the combusting pressure in order to provide the required amount of oxygen for combustion. Moreover, a portion of the nitrogen stream, separated from the oxygen in the ASU, can be fed to this stage. The nitrogen stream acts as a diluent and it tries to control the exhaust

temperature not exceeding from a set point. Note here, it needs to be compressed and heated up before mixing with other inlets. Another option to control the temperature of the exhaust stream is injection of medium pressure steam, but it should not be more than one percent ($\underline{\Omega}^{GTC1}$ and $\overline{\Omega}^{GTC1}$) of total inlet. However, the flow rate of steam should be a small value constraints 2.70 and 2.73. The mass balance of mixer before entering the combustor can be expressed as the following:

For the mixer of the gas turbine–1:

$$F_j^{GTC1} = F_j^{nit.GTC1} + F_j^{air.GTC1} + F_j^{tail.PSA} + F_j^{selexol2.to.GTC1} + F_j^{csyn.to.GTC1} \quad \forall j \in J/\{\mathrm{H_2O}\} \tag{2.68}$$

$$F_j^{GTC1} = F_j^{nit.GTC1} + F_j^{air.GTC1} + F_j^{tail.PSA} + F_j^{selexol2.to.GTC1} + F_j^{csyn.to.GTC1} + F^{MP.GTC1} \quad \forall j = \{\mathrm{H_2O}\} \tag{2.69}$$

$$F^{MP.GTC1} \leq \overline{\Omega}^{GTC1} \cdot \sum_j F_j^{GTC1} \tag{2.70}$$

For the mixer of the gas turbine–2:

$$F_j^{GTC2} = F_j^{nit.GTC2} + F_j^{air.GTC2} + F_j^{NG.GTC2} \quad \forall j \in J/\{\mathrm{H_2O}\} \tag{2.71}$$

$$F_j^{GTC2} = F_j^{nit.GTC2} + F_j^{air.GTC2} + F_j^{NG.GTC2} + F^{MP.GTC2} \quad \forall j = \{\mathrm{H_2O}\} \tag{2.72}$$

$$F^{MP.GTC2} \leq \overline{\Omega}^{GTC2} \cdot \sum_j F_j^{GTC2} \tag{2.73}$$

The mass balances over the combustors are given as follows. For the combustor of the gas turbine–1:

$$F_j^{exhaust.GTC1} = F_j^{GTC1} + \sum_{r=1}^{2} (sto_{r,j}^{GTC1} \cdot F_j^{GTC1}) \quad \forall j \in J \tag{2.74}$$

$$F_j^{exhaust.GTC1} = R^{GTC1} \cdot F_j^{air.GTC1} \quad \forall j = \{\mathrm{O_2}\} \tag{2.75}$$

For the combustor of the gas turbine–2:

$$F_j^{exhaust.GTC2} = F_j^{GTC2} + \sum_{r=1}^{5} (sto_{r,j}^{GTC2} \cdot F_j^{GTC2}) \quad \forall j \in J \tag{2.76}$$

$$F_j^{exhaust.GTC2} = R^{GTC2} \cdot F_j^{air.GTC2} \quad \forall j = \{\mathrm{O_2}\} \tag{2.77}$$

where $sto_{r,j}^{GTC1}$ and $sto_{r,j}^{GTC2}$ are stoichiometric coefficients of reactions according to happening reactions in first and second gas turbines, respectively, R^{GTC1} and R^{GTC2} are excess oxygen molar flow equal to 0.647.

The energy balances of combustors are given as follows based on the following assumptions. First, the combustions happen under adiabatic condition. Second, while the temperature and pressure of inlets are known (see Table 2.3), only the pressure of the exhaust stream is given and its temperature is a variable. Third, there is an upper bound for the exhaust temperature.

For the combustor of the gas turbine–1:

$$\begin{aligned}\sum_j F_j^{exhaust.GTC1} \cdot H_j^{su.exhaust.GTC1} = &\sum_j F_j^{nit.GTC1} \cdot H_j^{su.nit.GTC1} + \sum_j F_j^{air.GTC1} \cdot H_j^{su.air.GTC1} \\ &+ \sum_j F_j^{tail.PSA} \cdot H_j^{su.tail.PSA} + \sum_j F_j^{selexol2.to.GTC1} \cdot H_j^{su.selexol2.to.GTC1} \\ &+ \sum_j F_j^{csyn.to.GTC1} \cdot H_j^{su.csyn.to.GTC1} + F^{MP.GTC1} \cdot H^{MP.GTC1}\end{aligned} \tag{2.78}$$

$$T^{exhaust.GTC1} \leq \overline{\Omega}^{exhaust.GTC1} \tag{2.79}$$

For the combustor of the gas turbine–2:

$$\begin{aligned}\sum_j F_j^{exhaust.GTC2} \cdot H_j^{su.exhaust.GTC2} = &\sum_j F_j^{nit.GTC2} \cdot H_j^{su.nit.GTC2} + \sum_j F_j^{air.GTC2} \cdot H_j^{su.air.GTC2} \\ &+ \sum_j F_j^{NG.GTC2} \cdot H_j^{su.NG.GTC2} + F^{MP.GTC2} \cdot H^{MP.GTC2}\end{aligned} \tag{2.80}$$

$$T^{exhaust.GTC2} \leq \overline{\Omega}^{exhaust.GTC2} \tag{2.81}$$

As mentioned before, air passes through a compressor for the pressure adjustment and the compressor work requirement is calculated as follow.

$$W^{air.comp} = 0.001 \cdot \frac{FT^{air} \cdot Eb^{air.comp}}{Fb^{air.comp}} \tag{2.82}$$

where $Eb^{air.comp}$ and $Fb^{air.comp}$ are electricity requirement and working flow rate of base case equaling to 35.7034 MW and 19.38 Mmol h^{-1}, respectively.

The preheating duty of nitrogen stream can be calculated as Equation 2.17 and its compression work can be given as follow.

$$W^{nit.comp} = 0.001 \cdot \frac{(FT^{nit.GTC1} + FT^{nit.GTC2}) \cdot Eb^{nit.comp}}{Fb^{nit.comp}} \tag{2.83}$$

where $Eb^{nit.comp}$ and $Fb^{nit.comp}$ are electricity requirement and working flow rate of base case equaling to 364.425 MW and 110.664 Mmol h^{-1}, respectively.

To estimate the work generation of gas turbines, the energy balance is applied according to the first line of equations for each gas turbine. The generated duty can be transformed into mechanical energy with the efficiency of 0.985 (the second line of equations for each gas turbine), eff^{GT1} and eff^{GT2}. On the basis of the reference work, there are upper and lower bounds for power generation through the gas turbines, the third line of equations for each gas turbine.

For the gas turbine–1 [56]:

$$\sum_j F_j^{exhaust.GTC1} \cdot H_j^{su.exhaust.GTC1} = \sum_j F_j^{fluegas.GTC1} \cdot H_j^{su.fluegas.GTC1} + Q^{GT1} \tag{2.84}$$

$$W^{GT1} = \frac{eff^{GT1} \cdot Q^{GT1}}{3600} \tag{2.85}$$

$$\underline{\Omega}^{GT1} \leq W^{GT1} \leq \overline{\Omega}^{GT1} \tag{2.86}$$

For the gas turbine–2 [56]:

$$\sum_j F_j^{exhaust.GTC2} \cdot H_j^{su.exhaust.GTC2} = \sum_j F_j^{fluegas.GTC2} \cdot H_j^{su.fluegas.GTC2} + Q^{GT2} \tag{2.87}$$

$$W^{GT2} = \frac{eff^{GT2} \cdot Q^{GT2}}{3600} \tag{2.88}$$

$$b^{GTC2} \cdot \underline{\Omega}^{GT2} \leq W^{GT2} \leq b^{GT2} \cdot \overline{\Omega}^{GTC2} \tag{2.89}$$

HRSG unit. The flue gas exiting the gas turbine is used to generate high quality duty since its temperature is still high. The amount of duty produced can be calculated with the following energy balance, where the enthalpies can be calculated according to the corresponding temperature and pressure reported in Table 2.3.

$$\sum_j F_j^{fluegas.GTC1} \cdot H_j^{su.fluegas.GTC1} = \sum_j F_j^{stack.GTC1} \cdot H_j^{su.stack.GTC1} + Q^{HRSG1} \tag{2.90}$$

$$\sum_j F_j^{fluegas.GTC2} \cdot H_j^{su.fluegas.GTC2} = \sum_j F_j^{stack.GTC2} \cdot H_j^{su.stack.GTC2} + Q^{HRSG2} \tag{2.91}$$

Boiler unit. In addition to gas turbines and HRSGs, high– and low–quality duties can also be produced from boilers consuming natural gas. To estimate the duty generation of boilers, LHV, and boilers efficiencies ($eff^{boiler.hi}$ and $eff^{boiler.lo}$) are required. As mentioned before, the LHV of using natural gas is equal to 47.8417 GJ tonne^{-1}. Moreover, the efficiencies are also assumed to be 0.93 [55].

$$M^{NG.boiler.hi} = \frac{Q^{boiler.hi}}{eff^{boiler.hi} \cdot LHV^{NG}} \tag{2.92}$$

$$M^{NG.boiler.lo} = \frac{Q^{boiler.lo}}{eff^{boiler.lo} \cdot LHV^{NG}} \tag{2.93}$$

where $M^{NG.boiler.hi}$ and $M^{NG.boiler.lo}$ are mass flow rate (tonne h^{-1}) of natural gas in boiler–hi and boiler–lo, respectively.

The existences of high– and low–quality boilers are optional. Binary variables thus are required to consider this state. Furthermore, capacities of boilers should be in acceptable ranges according to the following equations [56]

$$b^{boiler.hi} \cdot \underline{\Omega}^{boiler.hi} \leq M^{NG.boiler.hi} \leq b^{boiler.hi} \cdot \overline{\Omega}^{boiler.hi} \tag{2.94}$$

$$b^{boiler.lo} \cdot \underline{\Omega}^{boiler.lo} \leq M^{NG.boiler.lo} \leq b^{boiler.lo} \cdot \overline{\Omega}^{boiler.lo} \tag{2.95}$$

Steam turbine unit. The last sets of operating units are steam turbines which need to be modeled. There is a number of demands and supplies of high– and low–quality duties in the presented superstructure. The nets of production duties are positive values and it means that there are additional duties in the proposed

energy system. Note here, total energy and mass balances are discussed in the next section. One efficient way to recover these duties is installation of steam turbines to generate power. When Q^{sthi} and Q^{stlo} are the nets of high– and low–quality duties in the energy system, W^{sthi} and W^{stlo} (GW) powers can be generated with high– and low–steam turbines, respectively.

$$W^{sthi} = \frac{eff^{sthi} \cdot Q^{sthi}}{3600} \tag{2.96}$$

$$W^{stlo} = \frac{eff^{stlo} \cdot Q^{stlo}}{3600} \tag{2.97}$$

where eff^{sthi} and eff^{stlo} are efficiencies of high– and low–steam turbines equal to 0.4407 and 0.1542, respectively [50].

There are also upper and lower bounds for the total power generation with both sets of turbines as follows.

$$\underline{\Omega}^{st} \leq W^{sthi} + W^{stlo} \leq \overline{\Omega}^{st} \tag{2.98}$$

Total water, natural gas, steam, and power balance. There are two total mass balances (for water and natural gas) and three total energy balances (for high– and low–quality duties and power) over the whole presented superstructure. The nets of water and natural gas are positive meaning they are purchased from sources. On the other hand, the nets of duties can be zero or positive. The zero duty net implies not employing steam turbine to generate more power, and a positive value shows the vice versa. Moreover, the net of power can get a positive or negative value. When it is positive the energy system is able to sell electricity to the grid; otherwise, electricity is purchased for it.

$$\begin{aligned} MT^{FW} = {} & MT^{steam.HP} + MT^{HP.SMR} + MT^{HP.WGS} + MT^{MP.GTC1} + MT^{MP.GTC2} \\ & - MT^{PW.co1} - MT^{PW.clsc} - MT^{PW.co3} - MT^{PW.co4} \end{aligned} \tag{2.99}$$

$$MT^{NG} = MT^{NG.SMR} + M^{NG.SMR} + MT^{MG.GTC2} + MT^{boiler.hi} + MT^{boiler.lo} \tag{2.100}$$

$$\begin{aligned} Q^{sthi} = {} & Q^{rc} + Q^{sc} + Q^{mc} + Q^{HRSG1} + Q^{HRSG2} + Q^{boiler.hi} \\ & - Q^{HP.gasifier} - Q^{gh} - Q^{HP.SMR} - Q^{HP.WGS} \end{aligned} \tag{2.101}$$

$$\begin{aligned} Q^{stlo} = {} & Q^{Claus} + Q^{WGS} + Q^{boiler.lo} \\ & - Q^{selexol1} - Q^{nh} - Q^{MP.GTC1} - Q^{MP.GTC2} - Q^{demand} \end{aligned} \tag{2.102}$$

$$\begin{aligned} W^{net} = {} & W^{sntgt1} + W^{sntgt2} + W^{GT1} + W^{GT2} + W^{sthi} + W^{stlo} \\ & - W^{gasifier.comp} - W^{selexol.comp} - W^{selexol} - W^{ASU} - W^{selexol2} \\ & - W^{PSA.comp} - W^{nit.comp} - W^{air.comp} - W^{demand} \end{aligned} \tag{2.103}$$

2.2.3 Economic model

In this section, capital cost models of process units are presented. After finding operating flow rates, estimation of capital and operating costs of each individual unit would be required.

Table 2.9: Base case mass/molar flow rate or power consumption for capital costs [50]

Parameter		Unit	Value
Gasifier	Fb_{fdh}	tonne h^{-1}	226.97
	Fb_{fdp}	tonne h^{-1}	226.97
	Fb_{gas}	tonne h^{-1}	201.73
	Fb_{ash}	tonne h^{-1}	201.73
	Fb_{sr}	tonne h^{-1}	201.73
	Fb_{oth}	tonne h^{-1}	824.21
	Fb_{sco}	Mmol h^{-1}	30.7
COS reactor	Fb_{hy}	Mmol h^{-1}	27.34
Selexol1	Fb_{se1}	Mmol h^{-1}	19.77
Claus Plant	Fb_{cls}	Mmol h^{-1}	0.3878
AUS	Fb_{asu}	Mmol h^{-1}	29.18
WGS	Fb_{wgs}	Mmol h^{-1}	36.73
Selexol2	Fb_{se2tot}	Mmol h^{-1}	38.84
	Fb_{se2car}	Mmol h^{-1}	10.66
PSA	Fb_{psa}	Mmol h^{-1}	28.18
Gas Turbines	$Fb_{gt1},\ Fb_{gt2}$	MW	464.01
HRSGs	$Fb_{sg1},\ Fb_{sg2}$	MW	274.69
Steam Turbines	Fb_{st}	MW	274.69

Capital cost (CAPEX). For the most of units, except SMR and boilers, the capital cost models (C_l) and associating parameters are adopted from a reference [50]. This model can be generally stated as below.

$$C_l = Cb_l \cdot \left(\frac{F_l}{Fb_l}\right)^{sf_l} \tag{2.104}$$

where F_l and Fb_l are mass/molar flow rate or power consumption (depending on the type of process unit) of current process unit and base case l unit, respectively, sf_l and Cb_l are parameters reported in Tables 2.9, 2.10, and 2.11.

For the SMR unit, capital cost information is adopted from a reference [57]. The effective variable is volumetric flow rate of consuming natural gas in Million standard cubic feet per day (MMSCFD). The density of natural gas is simulated as 0.7212 kg m^{-3} with Aspen HYSYS.

$$C_{SMR} = Cb_{SMR} \cdot (VT^{NG.SMR})^{sf_{SMR}} \tag{2.105}$$

where Cb_{SMR} and sf_{SMR} are equal to \$1.759MM and 0.79, respectively [57].

For the boilers, a linear model is applied from a reference [56]. There are two influential factors: pressure, P^{bl} (bar), and mass flow rate of generated steam, $M^{steam.bl}$ (kg s^{-1}). Mass flow rate of steam can be calculated with Equation 2.17. Note here that the following equations are used twice, once for the low–quality duty boiler and another time for the high–quality duty boiler.

$$C^{bl} = (A^{bl} \cdot M^{steam.bl} + B^{bl})/1000 \tag{2.106}$$

$$A^{bl} = 0.249 \cdot P^{bl} + 47.19 \tag{2.107}$$

Table 2.10: Base case capital costs [50] ($MM)

Parameter		Value
Gasifier	Cb_{fdh}	36.35
	Cb_{fdp}	58.41
	Cb_{gas}	234.84
	Cb_{ash}	45.89
	Cb_{sr}	50.37
	Cb_{oth}	279.29
	Cb_{sco}	19.86
COS reactor	Cb_{hy}	7.86
Selexol1	Cb_{se1}	24.85
Claus Plant	Cb_{cls}	33.77
AUS	Cb_{asu}	195.69
WGS	Cb_{wgs}	15.66
Selexol2	Cb_{se2tot}	18.38
	Cb_{se2car}	36.38
PSA	Cb_{psa}	82.02
Gas Turbines	$Cb_{gt1},\ Cb_{gt2}$	136.37
HRSGs	$Cb_{sg1},\ Cb_{sg2}$	56.72
Steam Turbines	Cb_{st}	66.55

Table 2.11: Sizing factors for capital costs [50]

Parameter		Value
Gasifier	sf_{fdh}	0.85
	sf_{fdp}	0.81
	sf_{gas}	0.82
	sf_{ash}	0.93
	sf_{sr}	0.82
	sf_{oth}	0.67
	sf_{sco}	0.67
COS reactor	sf_{hy}	0.65
Selexol1	sf_{se1}	0.7
Claus Plant	sf_{cls}	0.67
AUS	sf_{asu}	0.75
WGS	sf_{wgs}	0.65
Selexol2	sf_{se2tot}	0.8
	sf_{se2car}	0.75
PSA	sf_{psa}	0.7
Gas Turbines	$sf_{gt1},\ sf_{gt2}$	0.76
HRSGs	$sf_{sg1},\ sf_{sg2}$	0.67
Steam Turbines	sf_{st}	0.7

$$B^{bl} = 3.29 \cdot P^{bl} + 624.6 \tag{2.108}$$

Total capital cost can be expressed as follows when its unit is $MM.

$$CAPEX^{polygeneration} = \sum_{l} C_l \tag{2.109}$$

It should be highlighted that the capital costs associated with operating units such as pumps, instrumentation, and piping are excluded from the economic model of utility plant. The reason is to avoid additional complexity into our model. For example, the piping system design requires exact locations of operating units, their distances from each other, materials used for the construction of pipelines, and pressure drop calculation. Consequently, the final calculated cost will be an underestimation of the actual value.

Operating cost (OPEX). Operating costs are expenses associated with the maintenance and administration of a process plant on a daily basis. To estimate the annual operational cost of a polygeneration energy system ($OPEX^{polygeneration}$), the following equation is given.

$$OPEX^{polygeneration} = OPEX^{polygeneration.fix} + OPEXb^{polygeneration.var} \cdot \frac{M_{gt}^{fossil\ fuel}}{Mb^{fossil\ fuel}} \tag{2.110}$$

where $OPEX^{polygeneration.fix}$, $Mb^{fossil\ fuel}$, and $OPEXb^{polygeneration.var}$ are fixed operating cost of polygeneration energy system, working flow rate of base case, and variable operating cost of polygeneration system of base case equaling to \$25.061MM yr^{-1}, 824.206 tonne h^{-1}, and \$207.295MM yr^{-1}, respectively.

2.3 Bitumen upgrading plant

In this section, the modeling of bitumen upgrading plant is explained. According to Figure 2.2, a general superstructure is presented first considering two alternatives of upgrading. A mathematical model is then formulated calculating product yields (including NPH, LGO, and HGO) and energy consumptions (being composed of natural gas, steam, power, and hydrogen). Blending rules are applied to meet the specifications of produced SCO. Finally, the economic analysis of upgrading plant is discussed. The purpose of this section is to provide a mathematical model for the energy requirement, economic analysis, and production rate calculation of bitumen upgrading plants.

2.3.1 Process unit model

Atmospheric distillation (AD) unit. In this unit, most of the diluent, which is just added to reduce the viscosity of bitumen and make it transportable in pipelines, is separated and sent back to the extraction unit. It is assumed that diluent is basically NPH, its recovery rate ($Yield_{NPH}^{AD}$) is 20.5%, and 90% of it is returned to the extraction unit ($RE_{NPH}^{extraction}$). On the basis of the available data from a reference [9], the yield of LGO ($Yield_{LGO}^{AD}$) can be varied between 12 and 17% and the yield of HGO ($Yield_{HGO}^{AD}$) is assumed to be zero. Therefore, the following mass balances can be expressed for the AD,

$$M_{NPH}^{out,AD} = M^{DBIT} \cdot Yield_{NPH}^{AD} \cdot (1 - RE_{NPH}^{extraction}) \tag{2.111}$$

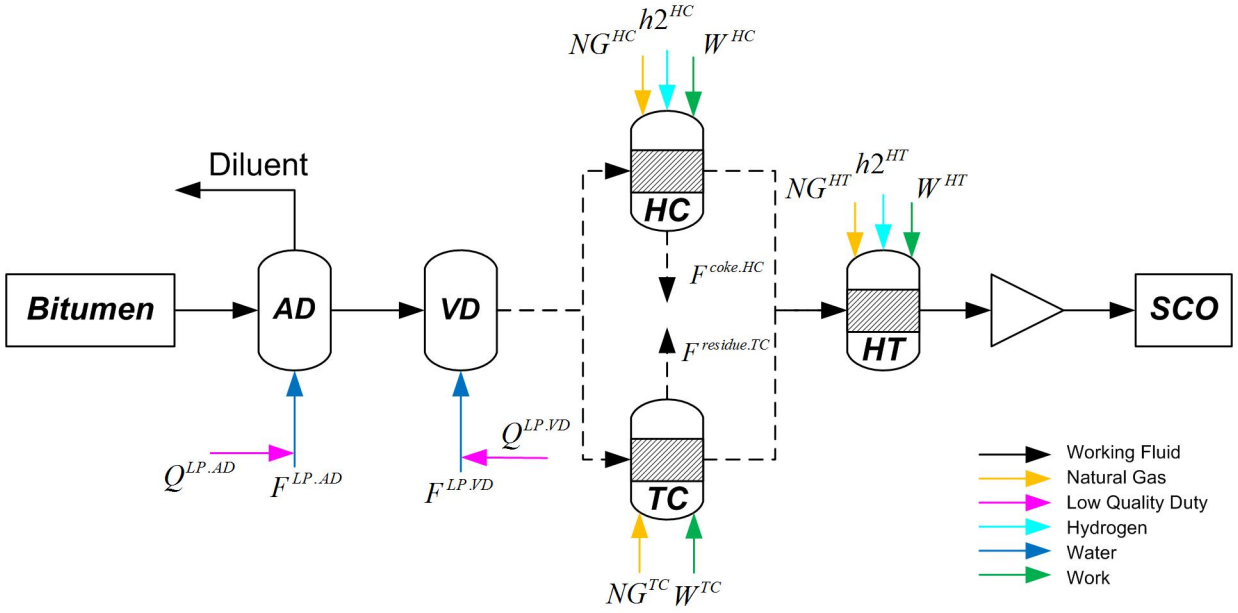

Figure 2.2: Superstructure of bitumen upgrading plant

$$M_{LGO}^{out,AD} = M^{DBIT} \cdot Yield_{LGO}^{AD} \tag{2.112}$$

$$M_{HGO}^{out,AD} = 0 \tag{2.113}$$

$$M^{ATB} = M^{DBIT} - \sum_{pd} M_{pd}^{out,AD} - M^{DBIT} \cdot Yield_{NPH}^{AD} \cdot RE_{NPH}^{extraction} \tag{2.114}$$

where M^{DBIT} is the inlet bitumen flow rate to the upgrading plant, and $M_{pd}^{out,AD}$ is the mass flow rate of pd product exiting from the AD.

For the energy balance, the only major energy consumption in the AD unit is steam. It can be estimated as

$$st^{AD} = M^{DBIT} \cdot SDRU \tag{2.115}$$

where $SDRU$ is 0.3 tonne of steam per tonne of diluted bitumen [43].

Vacuum distillation (VD) unit. In this unit, NPH, LGO, and HGO are separated from the atmospheric tower bottom (ATB) stream under vacuum conditions. The yields of these three products ($Yield_{pd}^{VD}$) try to be limited according to the following constraints. Note here that the constant values are adopted from a reference [58].

$$0.4 \leq Yield_{NPH}^{VD} \leq 1.3 \tag{2.116}$$

$$2.315 \leq \frac{Yield_{HGO}^{VD}}{Yield_{LGO}^{VD}} \leq 2.483 \tag{2.117}$$

$$27 \leq Yield_{LGO}^{VD} + Yield_{HGO}^{VD} \leq 44 \tag{2.118}$$

$$M_{pd}^{out,VD} = M^{ATB} \cdot Yield_{pd}^{VD} \quad \forall pd \in PD \tag{2.119}$$

$$M^{VTB} = M^{ATB} - \sum_{pd} M_{pd}^{out,VD} \tag{2.120}$$

where $M_{pd}^{out,VD}$ is the mass flow rate of pd product exiting from the VD, M^{ATB} is the inlet mass flow rate from the bottom of AD, and M^{VTB} is the outlet mass flow rate from the bottom of VD.

For the energy balance, the only major energy consumption in the VD unit is steam. It can be estimated as

$$st^{VAD} = M^{ATB} \cdot SVDU \tag{2.121}$$

where SVDU is 0.07 tonne of steam per tonne of ATB [43].

Hydrocracker (HC) unit. The next process unit can be hydrocracker or thermocracker. To produce more light products, the vacuum tower bottom (VTB) stream needs to undergo one of these units. Hence, there is a logical constraint to only let one of these two alternatives be active.

$$\sum_{cu} b_{cu}^{cracking} = 1 \tag{2.122}$$

On the basis of Table 2.12, the following yield–based mass balances can be used to model thhe hydrocracking unit.

$$\sum_{pd} Yield_{pd}^{HC} + Yield^{residue,HC} = 100 \tag{2.123}$$

$$M^{in,HC} = b_{HC}^{cracking} \cdot M^{VTB} \tag{2.124}$$

$$M_{pd}^{out,HC} = Yield_{pd}^{HC} \cdot (M^{in,HC} + h2^{HC}) \quad \forall pd \in PD \tag{2.125}$$

$$M^{residue} = Yield^{residue,HC} \cdot M^{in,HC} \tag{2.126}$$

$$\underline{\Omega}_{pd}^{HC} \leq Yield_{pd}^{HC} \leq \overline{\Omega}_{pd}^{HC} \quad \forall pd \in PD \tag{2.127}$$

$$\underline{\Omega}^{residue,HC} \leq Yield^{residue,HC} \leq \overline{\Omega}^{residue,HC} \tag{2.128}$$

For the energy correlation, hydrogen ($h2^{HC}$), electricity (el^{HC}), and heat (he^{HC}) are the main required sources of energy. They can be calculated as

$$h2^{HC} = \frac{M^{in,HC} \cdot HHF}{\rho^{h2}} \tag{2.129}$$

Table 2.12: upper and lower limits for HT yields [9]

Stream	$\underline{\Omega}^{HT}$	$\overline{\Omega}^{HT}$
NPH	6	12
LGO	18	38
HGO	30	39
Residue	20	37

Table 2.13: upper and lower limits for HC yields [9]

Stream	$\underline{\Omega}^{HC}$	$\overline{\Omega}^{HC}$
NPH	13	24
LGO	16	24
HGO	29	38
Coke	27	33

$$el^{HC} = b_{HC}^{cracking} \cdot \frac{PDDC \cdot M^{VTB}}{DVTB} \tag{2.130}$$

$$he^{HC} = b_{HC}^{cracking} \cdot \frac{FDDC \cdot M^{VTB}}{DVTB} \tag{2.131}$$

where HHF is the hydrogen requirement (= 8.464 standard cubic feet (scf) of H_2 per tonne of bitumen), and ρ^{h2} is the hydrogen density (equal to 423000 scf tonne^{-1}), PDDC defines the electricity requirement being equal to 3.9 kWh bbl^{-1}, FDDC represents the process fuel requirements being equal to 153 MJ bbl^{-1}, and DVTB is the density of VTB (DVTB = 0.16805 tonne bbl^{-1}) [43].

Thermocracker (TC) unit. On the basis of Table 2.13, the following yield–based mass balances can be used to model the thermocracking unit.

$$\sum_{pd} Yield_{pd}^{TC} + Yield^{coke,TC} = 100 \tag{2.132}$$

$$M^{in,TC} = b_{TC}^{cracking} \cdot M^{VTB} \tag{2.133}$$

$$M_{pd}^{out,TC} = Yield_{pd}^{TC} \cdot M^{in,TC} \quad \forall pd \in PD \tag{2.134}$$

$$M^{coke} = Yield^{coke,TC} \cdot M^{in,TC} \tag{2.135}$$

$$\underline{\Omega}_{pd}^{TC} \leq Yield_{pd}^{TC} \leq \overline{\Omega}_{pd}^{TC} \quad \forall pd \in PD \tag{2.136}$$

$$\underline{\Omega}^{coke,TC} \leq Yield^{coke,TC} \leq \overline{\Omega}^{coke,TC} \tag{2.137}$$

Table 2.14: upper and lower limits for HT yields [9]

Unit	$\underline{\Omega}^{HT}$	$\overline{\Omega}^{HT}$
NPH	95.8	98.3
LGO	97.4	98.2
HGO	89.5	94.5

For the energy correlation, electricity (el^{TC}) and heat (he^{TC}) are the main required sources of energy. They can be calculated as

$$el^{TC} = b_{TC}^{cracking} \cdot \frac{PDDC \cdot M^{VTB}}{DVTB} \tag{2.138}$$

$$he^{HC} = b_{TC}^{cracking} \cdot \frac{FDDC \cdot M^{VTB}}{DVTB} \tag{2.139}$$

where PDLF defines the electricity requirement being equal to 16.5 kWh bbl^{-1}, FDLCF represents the process fuel requirements being equal to 93.47 MJ bbl^{-1}, and DLF is the average density of inlet feed (DLF = 0.1654 tonne bbl^{-1}) [43].

Hydrotreater (HT) unit. The next processing units are hydrotreaters for NPH, LGO, and HGO. All the products from AD, VD, HC, and TC are mixed together in addition to hydrogen ($h2_{pd}^{HT}$) and then sent to catalytic hydrotreater reactors. According to Table 2.14, the yield–based mass balance of these units can be stated as

$$M_{pd}^{in,HT} = M_{pd}^{out,AD} + M_{pd}^{out,VD} + M_{pd}^{out,HC} + M_{pd}^{out,TC} \quad \forall pd \in PD \tag{2.140}$$

$$M_{pd}^{out,HT} = Yield_{pd}^{HT} \cdot (M_{pd}^{in,HT} + h2_{pd}^{HT}) \quad \forall pd \in PD \tag{2.141}$$

$$\underline{\Omega}_{pd}^{HT} \leq Yield_{pd}^{HT} \leq \overline{\Omega}_{pd}^{HT} \quad \forall pd \in PD \tag{2.142}$$

For the energy correlation, hydrogen is the main required source of energy. Note here that the power and energy requirements of hydrotreaters are already included in the hydrocracking and thermocracking units. hydrogen requirement can be calculated as

$$h2_{pd}^{HT} = \frac{M_{pd}^{in,HT} \cdot HHT_{pd}}{\rho_{pd}^{HT} \cdot \rho^{h2} \cdot UCF} \quad \forall pd \in PD \tag{2.143}$$

where HHT_{pd} are parameters that specify the hydrogen requirements in hydrotreaters equal to 930, 1150, and 1150 scf bbl^{-1} for NPH, LGO, and HGO, respectively, densities of NPH, LGO, and HGO are respectively 0.7440, 0.9125, and 0.9713 tonne m^{-3}, and UCF is a unit conversion factor, (UCF = 0.1589873 m^3 bbl^{-1}) [43].

Blending unit. After being hydrotreated, NPH, LGO, and HGO are blended together to produce the SCO. The mass fraction of each stream (xm_{pd}^{SCO}) should be higher than a lower bound reported in Table 2.15. Another important characteristic of our final product is its API gravity calculated through Equations 2.147

Table 2.15: lower limits for mass fractions of streams in SCO [9]

Stream	$\underline{\Omega}^{SCO}$
NPH	13.76
LGO	33.34
HGO	32.08

and 2.148. Note that, it is assumed that the sulfur and nitrogen contents, which are two other important specifications of the final SCO, are in acceptable ranges.

$$M^{SCO} = \sum M_{pd}^{out,HT} \tag{2.144}$$

$$xm_{pd}^{SCO} = \frac{M_{pd}^{out,HT}}{M^{SCO}} \quad \forall pd \in PD \tag{2.145}$$

$$\underline{\Omega}_{pd}^{SCO} \leq xm_{pd}^{SCO} \quad \forall pd \in PD \tag{2.146}$$

$$\rho^{SCO} = \frac{\sum_{pd} xm_{pd}^{SCO}/\rho_{pd}^{HT}}{\sum_{pd} xm_{pd}^{SCO}} \leq \overline{\Omega}^{\rho^{SCO}} \tag{2.147}$$

$$API^{SCO} = \frac{141.5}{\rho^{SCO}/\rho^{\mathrm{H_2O}}} - 131.5 \tag{2.148}$$

where $\overline{\Omega}^{\rho^{SCO}}$ is 0.8576 for the density of SCO.

2.3.2 Economic model

In this section, capital and operating cost modeling are presented for processing units. After finding operating flow rates, estimation of capital and operating costs of each individual unit would be required.

Capital cost. The capital cost of upgrading units are all adopted from a well–known textbook [57]. Capital cost (C_l) can be calculated based on the following general formula for each unit.

$$C_l = a_l \cdot V_l^{n_l} \quad \forall l \in L \tag{2.149}$$

$$CAPEX^{upgrading} = \sum_l C_l \tag{2.150}$$

where a_l and n_l are parameters for each unit (provided in Table 2.16), and V_l is the volumetric flow rate of inlet to each unit (bpd). To convert the inlet mass flow rates into volumetric ones, densities of streams are required. These values are assumed to be constant (see Table 2.17).

Note that the capital costs associated with operating units such as furnaces and pumps, instrumentation, and piping are excluded from the economic model of upgrading plant. Similar to the utility model, it is for the sake of simplicity, and hence, the capital cost estimations are underestimations of the actual values.

Table 2.16: economic terms of upgrading plant units [57]

Unit	a_l	n_l
AD	0.151	0.60
VD	0.151	0.60
HC	0.198	0.60
TC	0.109	0.68
TH	0.0532	0.68

Table 2.17: streams densities in upgrading plant [57]

Stream	Density (tonne m^{-3})
DBIT	0.9297
ATM	1.0217
VTB	1.0631
NPH	0.7165
LGO	0.8716
HGO	0.9365

Operating cost. Calculation of the operating cost $OPEX^{upgrading}$ is based on the reported value of CAN$6.7 per bbl of SCO in year 2008 [57]. Note here this number needs to be updated to U.S. dollar and year 2010 which most of the parameters are based on. Steam, hydrogen, heat, and electricity are the main utility demands. According to the energy correlations of each unit, the following equations can be used to estimate the total amount of energy requirements for a bitumen upgrading plant.

$$stT = st^{AD} + st^{VD} \tag{2.151}$$

$$h2T = h2^{HC} + \sum_{pd} h2^{HT}_{pd} \tag{2.152}$$

$$heT = he^{HC} + he^{TC} \tag{2.153}$$

$$elT = el^{HC} + el^{TC} \tag{2.154}$$

2.4 Integration of utility plant and bitumen upgrading plant

In this section, constraints that need be formulated into our model to couple the polygeneration energy system with bitumen upgrading plant are presented. As it is shown in Figure 2.3, the upgrading and utility plants need each other in order to operate properly. Diluted bitumen is processed into SCO through the upgrading plant. To do so, it demands hydrogen, low–quality duty, and power from the utility plant and natural gas from market. On the other hand, the upgrading plant can provide coke or heavy oil residue as a feedstock of the gasification unit in the utility plant. Moreover, the utility plant purchases the freshwater and natural gas from the market, and it is capable of supplying electricity for the market by being connected

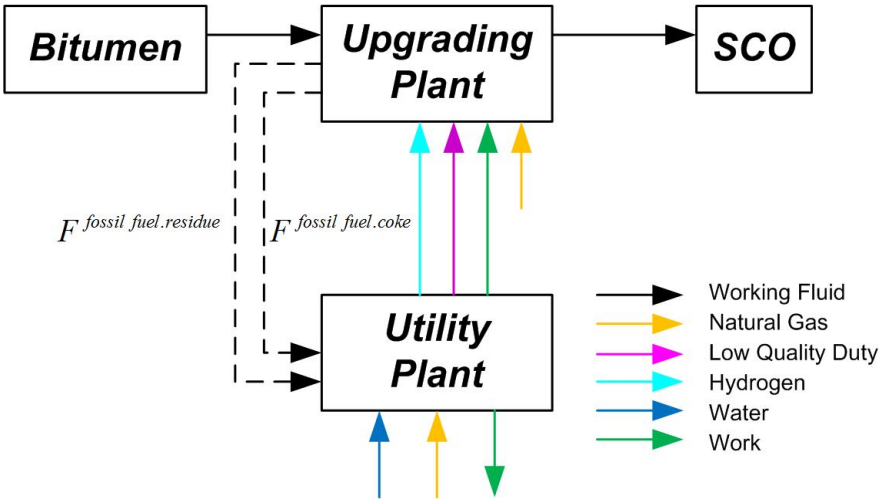

Figure 2.3: Superstructure of integrated polygeneration energy system and bitumen upgrading plant

to the grid. To consider the explained integration between these two plant, some constraints are required to be imposed which are presented in this section.

There are binary variables in both superstructures with the same meaning. $b_{gt}^{gasifier}$ in the polygeneration energy system and $b_{cu}^{cracking}$ in the upgrading plant represent the same variable. Note that, the associated sets are $cu \in \{TC, HC\}$ and $gt \in \{SCGP, SGP\}$ where (i) the first member of sets is for the thermocracker and its byproduct, and (ii) the second member of sets is for the hydrocracker and its byproduct, respectively. They are applied to determine whether the hydrocracking or the thermocracking unit is under operation. The following constraints are thus imposed.

$$b_{SCGP}^{gasifier} = b_{TC}^{cracking} \tag{2.155}$$

$$b_{SGP}^{gasifier} = b_{HC}^{cracking} \tag{2.156}$$

In the upgrading plant, coke or residue is a byproduct that can be used as a source of energy in the utility plant. However, the mass flow rate of consuming fossil fuel in the utility plant should not exceed its production mass flow rate in the upgrading plant.

$$M_{SGP}^{fossil\ fuel} \leq M^{residue} \tag{2.157}$$

$$M_{SCGP}^{fossil\ fuel} \leq M^{coke} \tag{2.158}$$

The next set of constraints is to make sure that different demands of the upgrading plant are met with the polygeneration energy system. Note here, some unit adjustments are necessary for the sake of unit uniformity. Moreover, it is assumed that required heat and steam of the upgrading plant is supplied with natural gas and low–quality duty, respectively.

$$h2T = M^{hyd} \tag{2.159}$$

Table 2.18: Purchasing costs [43, 59, 60]

Parameter	Unit	Value
CC^{NG}	\$ MJ^{-1}	0.00477
CC^{FW}	\$ $tonne^{-1}$	1.5
CC^{WTI}	\$ bbl^{-1}	33.51
WCS differential	%	42

Table 2.19: Commodities costs [59, 61, 62]

Parameter	Unit	Value
CC^{EL}	\$ kWh^{-1}	0.081
CC^{SU}	\$ $tonne^{-1}$	120
CC^{SCO}	\$ bbl^{-1}	33.77

$$elT = 10^6 \cdot W^{demand} \tag{2.160}$$

$$heT = 10^3 \cdot eff^{furnace} \cdot LHV^{NG} \cdot M^{NG.upgrading} \tag{2.161}$$

$$stT = \frac{Q^{demand} \cdot MW_{H2O}^{specie}}{\lambda_{MP}^{sat}} \tag{2.162}$$

2.4.1 Economic model

Each plant consumes different resources to operate properly and produce the required commodities. In this section, costs associated with purchasing feed and utilities and selling commodities are presented.

In the proposed superstructure, natural gas and freshwater are the major resources in addition to DilBit as the feed of upgrading plant. Purchasing cost ($Cost^{purchasing}$) can be estimated based on provided information in Table 2.18.

While SCO is the main product of the upgrading plant, power, hydrogen, sulfur element, and high– and low–quality duties are the generating commodities in the utility plant. In our case, it is assumed that hydrogen and duties are demanded for a chemical plant and power and sulfur are the only commodities are available for sale. Revenue cost ($Cost^{revenue}$) can then be calculated according to the selling costs of different commodities provided in Table 2.19.

The objective function of this study is NPV, which can be evaluated as

$$NPV = -CAPEX + Profit^{net} \cdot \frac{1}{r} \cdot \left(1 - \frac{1}{(1+r)^{t^{lf}}}\right) + \frac{R^{tax} \cdot CAPEX}{t^{dp}} \cdot \left(1 - \frac{1}{(1+r)^{t^{dp}}}\right) \tag{2.163}$$

where CAPEX is the total capital cost, $Profit^{net}$ is the net profit, r is the annual discount rate, t^{lf} is the lifetime of project, t^{dp} is the depreciation time of the project, and R^{tax} is the tax rate. These parameters are reported in Table 2.20.

$$CAPEX = CAPEX^{upgrading} + CAPEX^{polygeneration} \tag{2.164}$$

Table 2.20: economic terms [50]

Parameter	Unit	Value
R^{tax}		0.4
r		0.12
t^{lf}	yr	30
t^{dp}	yr	10
t^{op}	hr	7500

$$Profit^{net} = (1 - R^{tax}) \cdot (cost^{revenue} - [cost^{purchasing} + OPEX^{polygeneration} + OPEX^{upgrading}]) \quad (2.165)$$

2.5 Results and discussion

In this section, various scenarios are studied based on the proposed superstructure and the developed optimization model. The first factor under investigation is the capacity of upgrading plant. Here, we consider DilBit mass flow rate varying from 150 to 1500 tonne h^{-1} [63]. Second, we study the impact of whether or not to sell extra electricity to the public grid. The third part focuses on natural gas and electricity prices in the market. Finally, the margin between DilBit and SCO prices is investigated. The formulated integrated model is optimized under different scenarios and the results are discussed as follows.

There are number of nonlinear terms in the proposed optimization model, especially for the enthalpy calculation. There are some binary variables for selecting particular operating units. There are some bilinear terms resulted from energy or mass balance equations. All the mentioned terms lead to a non–convex MINLP problem. The global optimization solver BARON is used in GAMS for solving this problem. Two stopping criteria are used here: (1) computational time of 24 h, and (2) gap percent of 1% between the upper and lower bounds. Note here, the problem has 1105 variables as 8 of them are binary variables.

In Chapters 2 and 3, one point that is going to be noticed in the following results is an increase of computational time versus the upgrading plant capacity. This can be justified by the type of solver selected for the optimization in this Chapter. BARON is a global optimization solver, and hence, it searches the full feasible space of a problem to find the optimal solution. When the optimal design of an upgrading plant with higher capacity is studied, the feasible search will be larger as the upper bounds of variables exceeds. For example, the flow rates of outlets from the first distillation column cannot be larger than 150 and 500 (tonne h^{-1}) when the upgrading plant capacity is fixed at 150 and 500 (tonne h^{-1}), respectively. Therefore, a linear incremental trend can be seen for the computational time of optimization problems by increasing the upgrading plant capacity.

2.5.1 Effect of upgrading plant capacity when $W^{net} \neq 0$

In this section, optimization results under different capacities are presented with the possibility of being attached to the public grid for the importing/exporting of electricity. W^{net} can gain both positive and

Table 2.21: Effects of upgrading plant capacity (CC^{NG} = \$0.00477 MJ^{-1} and CC^{EL} = \$0.081 kWh^{-1})

	M^{DBIT} (tonne h^{-1})	150	500	850	1200	1500
	NPV (\$MM yr^{-1})	2785.56	2414.46	2137.1	1866.6	1646.99
	computational time (s)	908.51	2720.26	5222.63	9031.62	15195.22
	gap (%)	1	1	1	1	1
Decision variables	$b_{HC}^{cracking}$	1	0	0	0	0
	$b_{TC}^{cracking}$	0	1	1	1	1
	$b_{SGP}^{gasifier}$	1	0	0	0	0
	$b_{SCGP}^{gasifier}$	0	1	1	1	1
	b^{SMR}	0	1	1	1	1
	b^{GTC2}	1	1	1	1	1
	$b^{boiler.hi}$	0	0	0	0	0
	$b^{boiler.lo}$	1	1	1	1	1
SCO specifications	M^{SCO} (tonne h^{-1})	95.41	354.07	605.90	855.39	1069.15
	API^{SCO}	31.05	32.05	31.89	31.89	31.88
	xm_{NPH}^{SCO} (%)	0.14	0.16	0.16	0.16	0.16
	xm_{LGO}^{SCO} (%)	0.45	0.44	0.45	0.45	0.45
	xm_{HGO}^{SCO} (%)	0.41	0.40	0.39	0.39	0.39
Utilities consumptions	$\frac{M_{SGP}^{fossil\ fuel}}{M^{residue}}$	1.000				
	$\frac{M_{SCGP}^{fossil\ fuel}}{M^{coke}}$		1	1	0.999	0.991
	W^{net} (GW)	1.81	1.80	1.94	1.91	1.90
	$M^{total.NG}$ (tonne h^{-1})	180.8	194.1	234.5	232.3	235.3
Economic terms	$CAPEX$ (\$MM)	1087.8	1512.9	2023.9	2326.6	2579.6
	$OPEX$ (\$MM yr^{-1})	69.3	178.7	286.7	394.4	486.4
	purchases (\$MM yr^{-1})	457.5	826.2	1241.4	1583.1	1884.6
	commodities (\$MM yr^{-1})	1277.4	1746.8	2294.3	2736.3	3124.8

negative values. Positive values mean the capability of exporting electricity to the public grid and negative ones mean vice versa.

Results of optimal solutions are provided in Table 2.21. Figure 2.4 also shows the total natural gas consumptions of cases in the form of a stacked column chart. Distribution of natural gas consumption for each unit can be seen from this figure too. The following remarks can be concluded:

- Under the given price settings, increasing the upgrading plant capacity leads to less NPV. Since prices of DilBit and SCO are close, the profit gained from the upgrading operation is not significant. On the other side, the differences between electricity and natural gas prices are large. This results in a great amount of electricity generation in all the five scenarios. Even for the smallest upgrading plant, exportation of electricity is very large. In other words, most of the obtained benefits are resulted from the utility plant by selling electricity to the public grid rather than the upgrading plant itself.

- Except for the smallest capacity, the thermocracking process is more efficient for the upgrading plant. Moreover, coke and residue usage ratios are equal or very close to 1. This means that most of the available fossil fuel resources are consumed in the gasification unit. Hence, there will not be a stockpile of coke in the upgrading plant.

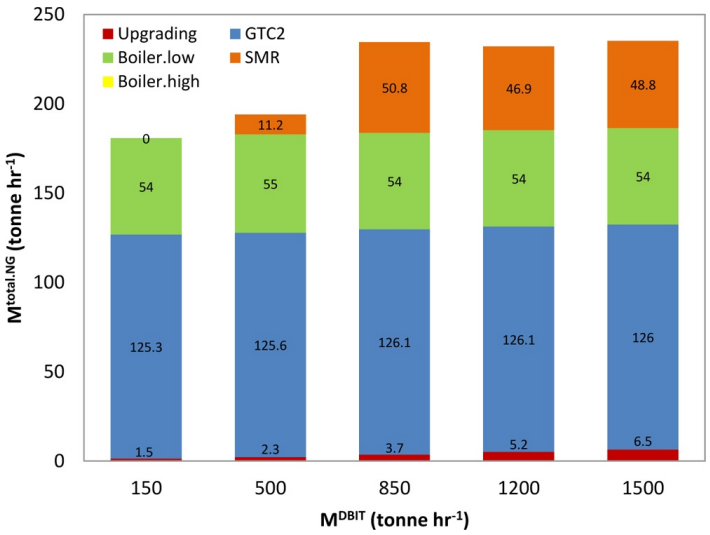

Figure 2.4: Comparison of total natural gas consumptions and their distributions for different upgrading plant capacities–being connected to public grid

- According to Figure 2.4, except for the smallest capacity, the SMR unit and the gasification unit are both used to generate syngas. The larger is the upgrading plant, the more hydrogen is demanded for hydrotreating. Therefore, the SMR unit is employed to compensate for the deficit of syngas for hydrogen production. In addition, extra produced syngas can be burnt in order to generate electricity in the gas turbine unit.

2.5.2 Effect of upgrading plant capacity when $W^{net} = 0$

In this section, optimizations at different capacities are presented without the possibility of being attached to the public grid for the importing/exporting of electricity. As a result W^{net} is forced to be zero here.

Results of optimal solutions are provided in Table 2.22. Figure 2.5 also shows the total natural gas consumptions of cases in the form of a stacked column chart. Distribution of natural gas consumption for each unit can be seen in this figure too. The following remarks can be concluded:

- Increasing the upgrading plant capacity still leads to less NPV. However, the optimal results in here are negative and much less compared to the previous section. The reason is that selling electricity to the public grid is not allowed here. Consequently, the utility plant supplies electricity as much as needed by the upgrading part. Moreover, as discussed in the previous section, upgrading itself is not the most efficient and profitable part of the process, so the optimal NPVs are all negative.

- The thermocracking process is selected in the upgrading plant under all operating capacities. Furthermore, coke usage ratios are equal or very close to 1 again too.

- According to Figure 2.5, because of being a self–sufficient plant, there is no need to invest in the SMR unit. an adequate amount of syngas can be produced through the gasification. In addition, gas

Table 2.22: Effects of upgrading plant capacity ($W^{net} = 0$, $CC^{NG} = \$0.00477$ MJ^{-1} and $CC^{EL} = \$0.081$ kWh^{-1})

	M^{DBIT} (tonne h^{-1})	150	500	850	1200	1500
	NPV (\$MM yr^{-1})	-1004.7	-1167.34	-1414.92	-1641.33	-1846.75
	computational time (s)	1049.36	1538.6	707.79	1099.13	999.83
	gap (%)	0.99	0.99	0.8	0.99	0.99
Decision variables	$b_{HC}^{cracking}$	0	0	0	0	0
	$b_{TC}^{cracking}$	1	1	1	1	1
	$b_{SGP}^{gasifier}$	0	0	0	0	0
	$b_{SCGP}^{gasifier}$	1	1	1	1	1
	b^{SMR}	0	0	0	0	0
	b^{GTC2}	0	0	0	1	1
	$b^{boiler.hi}$	0	0	0	0	0
	$b^{boiler.lo}$	1	1	1	1	1
SCO specifications	M^{SCO} (tonne h^{-1})	97.15	355.72	605.80	855.22	1069.24
	API^{SCO}	33.32	31.76	31.74	31.81	31.84
	xm_{NPH}^{SCO} (%)	0.19	0.16	0.15	0.15	0.15
	xm_{LGO}^{SCO} (%)	0.43	0.44	0.45	0.45	0.45
	xm_{HGO}^{SCO} (%)	0.38	0.41	0.40	0.40	0.39
Utilities consumptions	$\frac{M_{SGP}^{fossil\ fuel}}{M^{residue}}$					
	$\frac{M_{SCGP}^{fossil\ fuel}}{M^{coke}}$	1.000	0.85	0.861	0.862	0.872
	W^{net} (GW)	0.00	0.00	0.00	0.00	0.00
	$M^{total.NG}$ (tonne h^{-1})	54.9	56.2	58	59.7	63.3
Economic terms	$CAPEX$ (\$MM)	480.2	810.5	1161.9	1485.1	1753.3
	$OPEX$ (\$MM yr^{-1})	70	176.9	283.7	390.3	482.1
	$purchases$ (\$MM yr^{-1})	242.1	590	938.7	1287.2	1589.6
	$commodities$ (\$MM yr^{-1})	181	655.2	1115.7	1575.7	1970.4

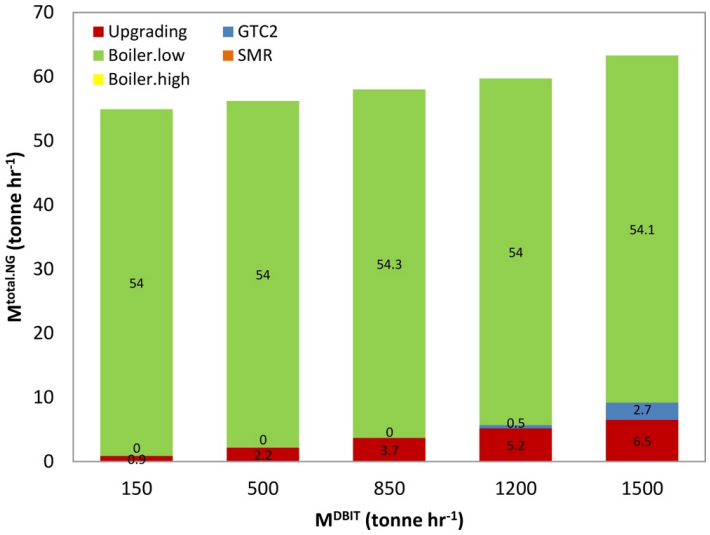

Figure 2.5: Comparison of total natural gas consumptions and their distributions for different upgrading plant capacities not being connected to public grid

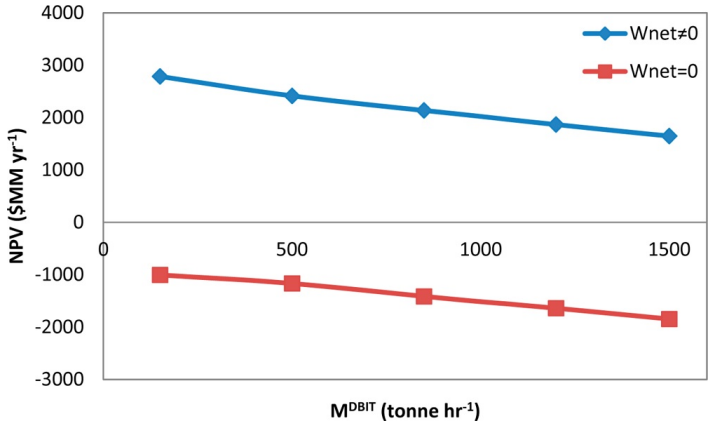

Figure 2.6: Comparison of optimal NPVs for different upgrading plant capacities and possibility of selling or not selling electricity

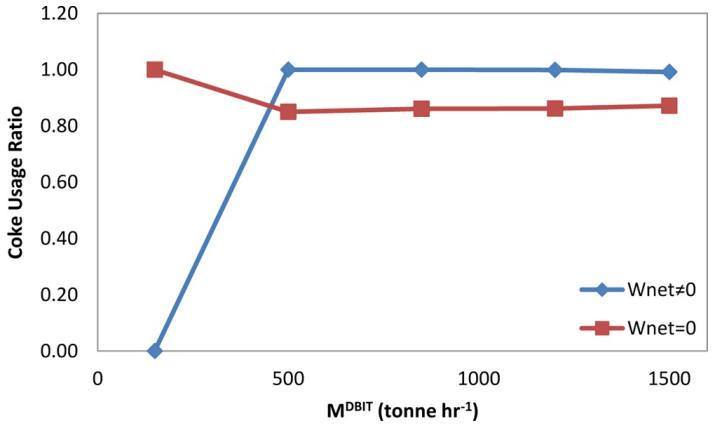

Figure 2.7: Comparison of optimal coke consumptions for different upgrading plant capacities and possibility of selling or not selling electricity (For the only point in which coke usage ratio is equal to zero, the heavy oil residue ratio is equal to 1).

turbine burning natural gas is only employed in the last two cases in order to compensate the deficit of electricity demands of the larger upgrading plants. Note here, in the previous section, this unit is under operation for all the five cases due to the advantage of generating additional electricity.

Figures 2.6 to 2.8 illustrate variations of optimal NPVs, coke usage ratios, and W^{net} for two explained scenarios of connecting to ($W^{net} \neq 0$) and disconnecting from ($W^{net} = 0$) the public grid. Exporting the electricity can be a significant and profitable option for a utility section of the upgrading plants.

2.5.3 Effects of natural gas and electricity prices

In this section, a study on the natural and electricity prices is presented when $W^{net} \neq 0$. The prices can be categorized in three levels (low, medium, and high). While low and high prices are the maximum and minimum of prices in a large historical period of time, the medium prices are the average of the available

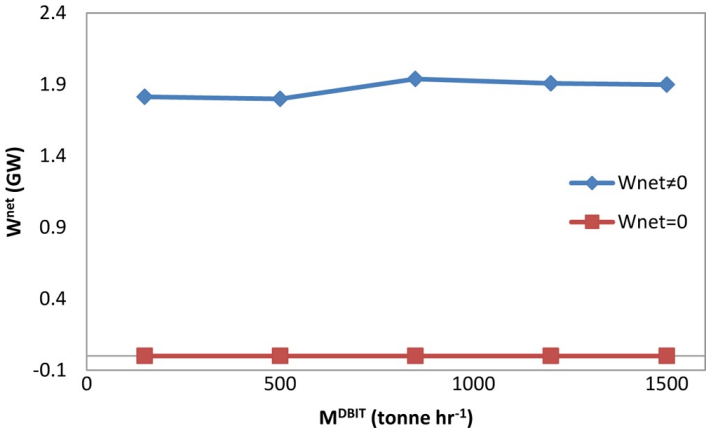

Figure 2.8: Comparison of optimal W^{net} for different upgrading plant capacities and possibility of selling or not selling electricity

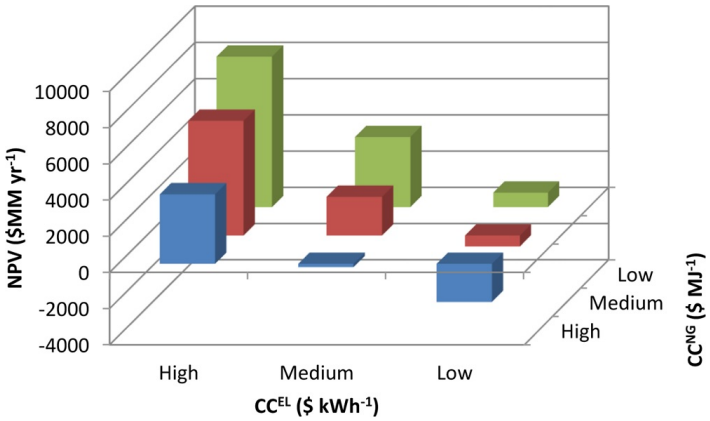

Figure 2.9: Comparison of optimal NPVs for different natural gas and electricity prices when $W^{net} \neq 0$

period of time. It should be highlighted here that the capacity of upgrading plant is assumed to be 850 tonne h^{-1}.

Results of optimal solutions are provided in Table 2.23. The following remarks can be concluded:

- The natural gas is required to be purchased and the electricity is a commodity to be sold. Therefore, the highest NPV is achieved with the low price of natural gas and high price of electricity (scenario 7). In addition, the lowest NPV is found when the natural gas price is high and the electricity price is low (scenario 3). Figure 2.9 presents the optimal NPVs at different prices.

- Except for scenario 1 where both prices are high, the thermocracking process is selected as the upgrading process. Moreover, coke and residue usage ratios are equal or very close to 1 only when the natural gas price is not low. When the natural gas price is low, there is less need for gasification and the SMR unit can be applied to operate simultaneously in order to produce required syngas.

- W^{net} is only found close to zero for scenario 3. As mentioned before, the natural gas price is high

Table 2.23: Effects of natural gas and electricity prices When $M^{DBIT} = 850$ tonne h^{-1} and $W^{net} \neq 0$

	scenario	1	2	3	4	5	6	7	8	9
	CC^{NG} (\$ MJ^{-1})	0.012	0.012	0.012	0.00477	0.00477	0.00477	0.00104	0.00104	0.00104
	CC^{EL} (\$ kWh^{-1})	0.141	0.081	0.037	0.141	0.081	0.037	0.141	0.081	0.037
	NPV (\$MM yr^{-1})	3844.86	-181.77	-2110.69	6333.01	2137.1	-602.87	8308.52	3871.59	801.48
	computational time (s)	838.01	1956.35	3349.15	3365.14	4692.21	4004.79	1829.43	2984.01	3775.98
	gap (%)	1	0.99	0.35	1	1	0.99	0.81	1	0.01
Decision variables	$b_{HC}^{cracking}$	1	0	0	0	0	0	0	0	0
	$b_{TC}^{cracking}$	0	1	1	1	1	1	1	1	1
	$b_{SGP}^{gasifier}$	1	0	0	0	0	0	0	0	0
	$b_{SCGP}^{gasifier}$	0	1	1	1	1	1	1	1	1
	b^{SMR}	0	0	0	1	1	0	1	1	1
	b^{GTC2}	1	1	0	1	1	1	1	1	1
	$b^{boiler.hi}$	0	0	0	0	0	0	0	0	1
	$b^{boiler.lo}$	1	1	1	1	1	1	1	1	1
SCO specifications	M^{SCO} (tonne h^{-1})	540.67	605.90	605.79	602.63	605.90	605.90	604.36	604.44	605.90
	API^{SCO}	31.05	31.89	31.89	32.03	31.89	31.89	31.99	31.85	31.89
	xm_{NPH}^{SCO} (%)	0.14	0.16	0.16	0.16	0.16	0.16	0.16	0.15	0.16
	xm_{LGO}^{SCO} (%)	0.45	0.45	0.45	0.45	0.45	0.45	0.45	0.45	0.45
	xm_{HGO}^{SCO} (%)	0.41	0.39	0.39	0.39	0.39	0.39	0.39	0.39	0.39
Utilities consumptions	$\frac{M_{SGP}^{fossil\ fuel}}{M^{residue}}$	0.824								
	$\frac{M_{SCGP}^{fossil\ fuel}}{M^{coke}}$		0.995	0.86	1	1	0.861	0.347	0.289	0.293
	W^{net} (GW)	1.94	1.72	0.02	1.94	1.94	1.69	2.06	2.02	1.86
	$M^{total.NG}$ (tonne h^{-1})	187.7	183	57.7	232.9	234.5	182.8	362.9	311.9	268.9
Economic terms	$CAPEX$ (\$MM)	2107.3	1791.6	1173.1	2041.7	2023.9	1712.6	2040	1925.1	1585.6
	$OPEX$ (\$MM yr^{-1})	269.6	286.6	283.9	286.4	286.7	283.9	273.5	272.1	272.7
	purchases (\$MM yr^{-1})	1647.5	1627.2	1087.7	1238.6	1241.4	1152.3	976	956.5	939.5
	commodities (\$MM yr^{-1})	3050.1	2163.1	1122.8	3162.3	2294.3	1585.7	3295.3	2337.9	1631.9

and the electricity price is low here, so generating additional electricity has no economic justification. Furthermore, the gas turbine unit consuming natural gas is not selected only for the scenario 3 for the same reason. Figure 2.10 presents the optimal W^{net} at different prices.

- Natural gas consumption decreases when its price increases and when the electricity price decreases. Figure 2.11 shows the optimal partial and total natural gas consumptions of operating units at different prices. Note here that the boiler.hi only operates for scenario 9. The reason is that less syngas is produced under these conditions, and hence, less syngas is burnt in the gas turbine–1 unit. Consequently, less high quality duty is generated in HRSG–1 unit, and the deficit of total high quality energy balance needs to be compensated by boiler.hi.

2.5.4 Effect of the margin between DilBit and SCO prices

In this section, the effect of the margin between DilBit and SCO prices is studied when $W^{net} \neq 0$. Moreover, three distinct capacities are also considered to have a better understanding about the studying system.

The prices of DilBit and SCO for the last eight years are shown in Figure 2.12. As it is shown, DilBit and SCO prices have been fluctuating significantly, while the margin between them has been more stable. Therefore, the margin is taken into account as the variable here. It is assumed that the SCO price is constant at its average value of \$80.32 bbl^{-1}. In addition, three levels of low, medium, and high are selected from historical data of the margin as 6.56, 17.44, and 32.98 (\$ bbl^{-1}), respectively. Note here that the low and high values are the maximum and minimum of data in the selected historical period of time, and the medium value is the average. Consequently, three levels of 73.76, 62.88, and 47.35 (\$ bbl^{-1}) are calculated for the

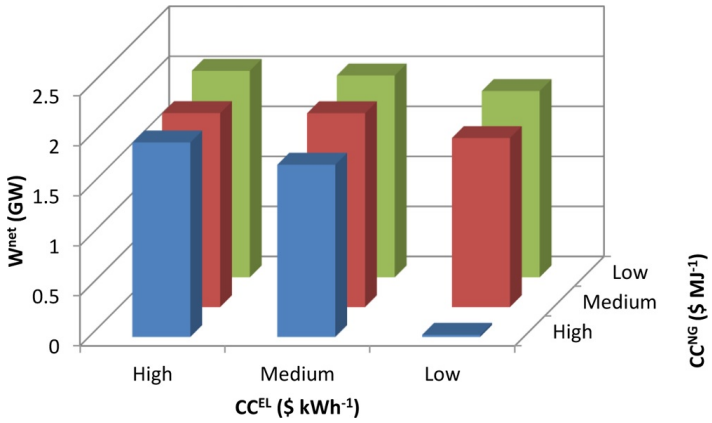

Figure 2.10: Comparison of optimal W^{net} for different natural gas and electricity prices when $W^{net} \neq 0$

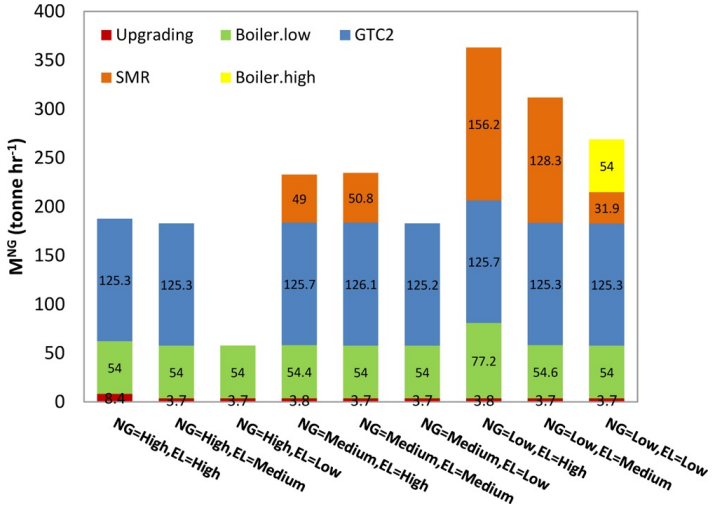

Figure 2.11: Comparison of total natural gas consumptions and their distributions for different natural gas and electricity prices when $W^{net} \neq 0$

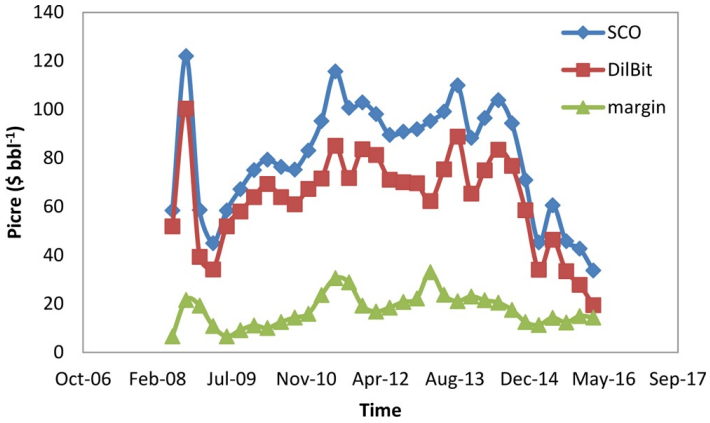

Figure 2.12: Historical data for the DilBit and SCO prices and the margin between them

DilBit price. Furthermore, the effect of the upgrading plant capacity is also studied (150, 850, and 1500 tonne h^{-1}).

Results of optimal solutions are provided in Table 2.24 6. The following remarks can be concluded:

- Although higher NPVs are achieved by the increase of margin, its trends are not consistent over capacity changes. When the margin is high, a larger upgrading plant is more economical to operate. However, this is exactly opposite for the low and medium margins, and smaller plants are more efficient. Figure 2.13 presents the optimal NPVs at different margins and DilBit flow rates.

- W^{net} values are very close to each other for all scenarios. When the size of the upgrading plant is small, the flow rate of syngas generated from the coke gasification is lower. Moreover, the SMR unit is not under operation for the scenarios 1–3. Therefore, the gas turbine consuming syngas produces less power under these operating conditions. Figure 2.14 shows the optimal Wnet at different margins and DilBit flow rates.

- Natural gas consumptions have the same trend as W^{net}. Figure 2.15 illustrates the optimal partial and total natural gas consumptions of operating units at different prices. Note here that the SMR operates for scenarios 4–9. For these scenarios, more syngas is generated resulting in larger W^{net}.

Table 2.24: Effects of margin between DilBit and SCO prices at distinct capacities when $W^{net} \neq 0$

	scenario	1	2	3	4	5	6	7	8	9
	CC^{SCO} (\$ bbl^{-1})	80.32	80.32	80.32	80.32	80.32	80.32	80.32	80.32	80.32
	CC^{DilBit} (\$ bbl^{-1})	73.76	62.88	47.35	73.76	62.88	47.35	73.76	62.88	47.35
	M^{DBIT} (tonne h^{-1})	150	150	150	850	850	850	1500	1500	1500
	NPV (\$MM yr^{-1})	1983.47	2371.24	2926.9	-1770.32	503.32	3740.68	-5240.34	-1233.7	4448.77
	computational time (s)	1962.53	1508.39	988.65	2641.87	4448.15	1655.49	3774.13	2580.13	4335.07
	gap (%)	0.01	0.53	1	0.99	1	1	0.37	0.99	1
Decision variables	$b_{HC}^{cracking}$	0	0	0	0	0	0	0	0	0
	$b_{TC}^{cracking}$	1	1	1	1	1	1	1	1	1
	$b_{SGP}^{gasifier}$	0	0	0	0	0	0	0	0	0
	$b_{SCGP}^{gasifier}$	1	1	1	1	1	1	1	1	1
	b^{SMR}	0	0	0	1	1	1	1	1	1
	b^{GTC2}	1	1	1	1	1	1	1	1	1
	$b^{boiler.hi}$	0	0	0	0	0	0	0	0	0
	$b^{boiler.lo}$	1	1	1	1	1	1	1	1	1
SCO specifications	M^{SCO} (tonne h^{-1})	97.90	97.91	97.93	605.69	605.88	605.79	1068.72	1068.93	1068.98
	API^{SCO}	34.07	33.93	33.57	31.90	31.89	31.89	31.89	31.88	31.82
	xm_{NPH}^{SCO} (%)	0.22	0.21	0.20	0.16	0.16	0.16	0.16	0.16	0.16
	xm_{LGO}^{SCO} (%)	0.39	0.39	0.41	0.45	0.45	0.45	0.45	0.45	0.45
	xm_{HGO}^{SCO} (%)	0.39	0.39	0.39	0.39	0.39	0.39	0.39	0.39	0.40
Utilities consumptions	$\frac{M_{SGP}^{fossil\ fuel}}{M^{residue}}$									
	$\frac{M_{SCGP}^{Fossil\ fuel}}{M^{coke}}$	1	1	1	1	1	1	1	1	0.983
	W^{net} (GW)	1.79	1.79	1.80	1.93	1.91	1.94	1.90	1.90	1.89
	$M^{total.NG}$ (tonne h^{-1})	181	181.6	186.4	232.7	228.6	234.3	234.4	233.6	235.3
Economic terms	$CAPEX$ (\$MM)	1057.9	1055.6	1059	2019.2	2003.9	2024.3	2586.5	2580.8	2570.5
	$OPEX$ (\$MM yr^{-1})	70.4	70.4	70.3	286.7	286.7	286.7	486.6	486.6	485.9
	$purchases$ (\$MM yr^{-1})	871.9	789.8	679.8	3581.4	3104.6	2445.1	6018	5188.5	4009.4
	$commodities$ (\$MM yr^{-1})	1522.1	1519.9	1525.3	3825.2	3816.4	3829.9	5834.6	5833.1	5827.4

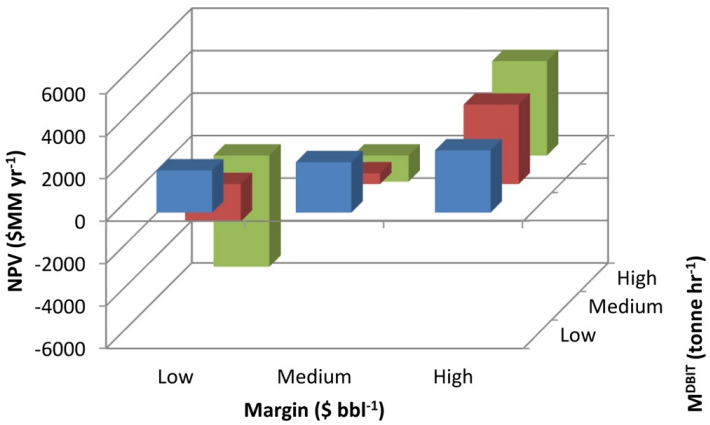

Figure 2.13: Comparison of optimal NPVs for different margins and capacities when $W^{net} \neq 0$

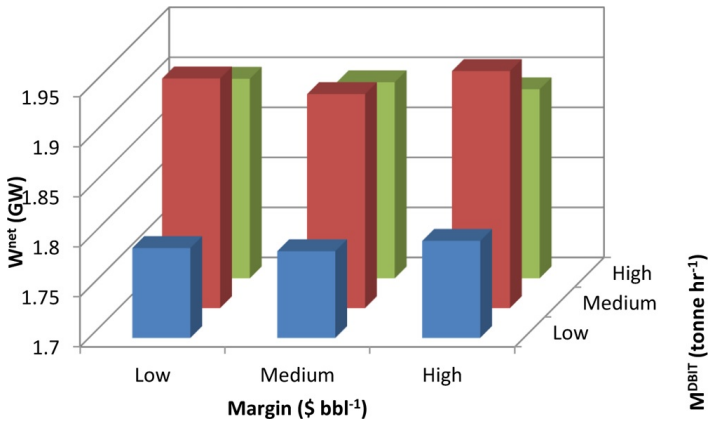

Figure 2.14: Comparison of optimal W^{net} for different margins and capacities when $W^{net} \neq 0$

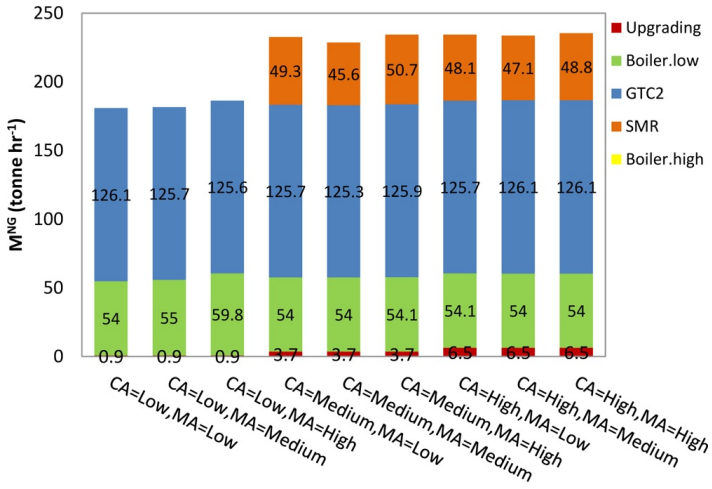

Figure 2.15: Comparison of total natural gas consumptions and their distributions for different margins and capacities when $W^{net} \neq 0$

2.6 Conclusion

According to the results, optimal configurations are different under distinct scenarios. First, it is observed that increasing the size of the upgrading plant is only beneficial when the margin between DilBit and SCO price is high. Otherwise, it is better to invest in a smaller plant. Second, the major profit is driven from selling additional electricity to the public grid due to the price of this commodity. While the NPVs of upgrading plants with connection to the public grid are large, they are negative when the power exports are equal to zero. Third, for most of the upgrading plant, thermocracking is chosen to process the vacuum distillation residue. The reason is that it requires less hydrogen for operation, and consequently, less fossil fuel or natural gas for gasification. Moreover, most of the coke or heavy oil residue withdrawn from the upgrading plant is consumed in the gasification unit to produce syngas. Fourth, being under operation of the SMR unit basically depends on the capacity of the upgrading plant, and it is selected for the upgrading plant with large capacity. Fifth, the gas turbine burning natural gas and the following HRSG units are only selected if selling extra electricity is an option. Sixth, the highest NPV is achieved with the low price of natural gas and high price of electricity, and the lowest NPV is found when the natural gas price is high and the electricity price is low. Furthermore, natural gas consumption decreases as its price increases and the electricity price decreases.

Chapter 3

Optimal Design of Bitumen Upgrading Facility with CO_2 Reduction[1]

3.1 Introduction

The large expansion of oil sands operations has a significant environmental impact too. Ordorica-Garcia et al. showed that SCO production is an energy intensive process, 1.5–2 (GJ bbl^{-1}) [10]. Large amount of energy is required in different forms (steam, hot water, hydrogen, power, process heat), but from the same source of fossil fuel leading to considerable CO_2 emissions [10]. In 2008, oil sands operations emitted one–third of the total emissions from all industrial sectors in Alberta, nearly 35 million tonnes of CO_2 [64]. As explained above, increasing the demands of SCO will be accompanied with upgrading more bitumen in oil sands. Such a growth rates will inevitably result in proportional increase in CO_2 emissions regarding to the high energy intensity of upgrading processes. Hence, there should be a way to mitigate the CO_2 emissions for better future and Canada's overall CO_2 mitigation plans.

Reducing the CO_2 emissions by CCS technology is the primary strategy to apply. Relatively large amounts of CO_2 are emitted through hydrogen and power plants integrated into the oil sands industry. These emissions can be captured through CCS; however, the urge to limit the associated costs with implementation of CCS is the major challenge. Finding the most efficient and economic technology has been thus very interesting. Note here, types of technology and fuel used for energy production, and the level and form of the energy demands in the oil sands industry are the important factors for the CCS costs [42].

Few studies have focused on carbon capture in Oil Sand industry. In the extraction sector, there are only two works investigating potential of CCS technologies in CO_2 emissions reduction in SAGD facilities [65]. Between post–combustion capture with amine scrubbing and oxyfuel combustion, the results showed better performance of the former one [66]. In the upgrading sector, there have been more attempts due to the fact that the upgrading processes demand ten times more hydrogen than conventional crude oils [67]. The more hydrogen it is required, the more fossil fuel should be consumed and consequently the higher the

[1] A version of this chapter was published in the *Computers & Chemical Engineering*, **2017**, *106*, 106-121

CO_2 emission rate. The large amounts of hydrogen demands can be met through steam reforming of natural gas or gasification of residue or coke where each of these processes uses its own specific feed.

Techno–economic assessments of upgrading facilities with different types of feeds were performed: natural gas [67], coke [68], underground coal [69], and residue [70]. The first work studied two different technologies: membrane separation process and the MonoEthanolAmine (MEA) absorption process and they both revealed comparable results in terms of energy penalty and CO_2 emissions reduction [67]. Integration of coke gasification with integrated gasification combined cycle (IGCC) plant was also studied in terms of performance and economic [68]. CO_2 physical absorption with the Selexol process and CO_2 mineral trapping (MT) were considered as carbon capture options, and the IGCC + Selexol process outperformed the IGCC + MT one. Techno–economic models were developed for the underground coal gasification (UCG) and SMR with and without CCS [69]. The costs of UCG hydrogen production were estimated to be \$1.78 kg^{-1} and \$2.11–\$2.70 kg^{-1} (depending on the distance of the sequestration site from the UCG plant of hydrogen) for without CCS and with CCS, respectively. The costs of SMR hydrogen production were estimated to be \$1.73 kg^{-1} and \$2.14–\$2.41 kg^{-1} for without CCS and with CCS, respectively [69]. Hydrogen production costs with CCS were reported in ranges since its cost depends on the distance of the sequestration site from the hydrogen generation plant. El Gemayel et al. investigated the feasibility of slurry hydrocracking, trickle–bed hydrotreating and residue gasification integration [70]. The integrated design was simulated with Aspen HYSYS simulator under different scenarios: (i) 90%, (ii) 65%, and no carbon capture with the MEA solvent [70].

In a more comprehensive study, the forecasted demands for electricity and hydrogen in oil sands operations were optimized under the CO_2 emissions constraints [42]. A MILP model was developed including varieties of hydrogen and power generation technologies (with and without CO_2 capture). By implementing the carbon capture in the hydrogen and power plants, 25% and 39% of CO_2 emissions reductions were achieved with respect to business–as–usual base–lines in 2012 and 2030, respectively [42]. According to the results, the gasification (with and without capture) was an optimal technology for the hydrogen production, while the natural gas–based power production, particularly oxyfuel and combined cycle with CO_2 capture, showed great potential for power generation [42]. Moreover, the stochastic modeling of the oil sands operations under the CO_2 emissions restrictions and water management was proposed [46]. The presented MINLP model accounted uncertainties in the natural gas price and SOR. Preference of the hydrocracking upgrader over thermocracking one, and not being able to meet the GHG emissions constraint for SORs higher than 2.48 are the two major findings of this work [46].

CO_2 infrastructure management has also been another field of study. An integrated framework was presented considering the economic and engineering aspects of the capture, transport, and storage of oil sands CO_2 emissions simultaneously [71]. Where various carbon prices were studies for the oil sands industry, substantial capture and storage were only occurred only above \$110 per tonne of CO_2 [71]. In another study, Bourne et al. focused on the Quest CCS Project [72]. Injecting over 1.08 million tonnes of CO_2 per year into a saline aquifer located in Alberta, this project will contribute to CO_2 emission reduction for 25 years.

A program was developed for the measurement, monitoring and verification of the storage performance for the sake of conformance and containment monitoring [72].

As mentioned above, finding the most appropriate CO_2 capture technology is very important. Comparison of CO_2 capture technologies can be carried out over different criteria. Comparative assessment of the PSA, physical absorption (Selexol), and chemical looping combustion (CLC) technologies was accomplished with respect to the energetic and exergetic efficiencies, and the level of CO_2 emissions [73]. For solely production of electricity, the overall CO_2 capture efficiency of the CLC, Selexol, and PSA processes were 99.9%, 93.5%, and 89.9%, respectively. For combined electricity and H_2 production, the overall CO_2 capture efficiency of the CLC, Selexol, and PSA processes were 59.4%, 59.1%, and 60.0%, respectively [73]. The three leading CO_2 capture technologies, oxyfuel combustion, pre–combustion and post–combustion, were compared in another study [74]. The techno–economic assessment of power plants was investigated under different scenarios that deliver different CO_2 product purities. Following remarks were reported: (i) for the oxyfuel combustion capture scenarios, wide variation in CO_2 product purity was seen, (ii) for the pre–combustion capture scenarios, wide cost variation was observed, and (iii) for the post–combustion capture plant, high CO_2 purity of 99.99 mol% was achieved with relative average cost [74].

To find the optimal scheme of bitumen upgrading plant, the focus has been on operating units of upgrading plant in which it is assumed that utilities such as hydrogen and electricity are purchased instead of being generated. Incorporating detailed models of utility and carbon capture plants into the existing upgrading model turns the problem into a non–convex MINLP. Various approaches have been applied to solve such problems. In [75], a linearization transformation technique was used as a linear underestimator of the original model, and a branch–and–refine algorithm was applied for global optimization. The advantage of the relaxed problem is utilized in an iterative procedure to solve the original hard problem. An alternative strategy is dividing the original problem into a master MILP problem and set of nonlinear subproblems of much smaller size [76]. Based on obtained dual information from the solution of the subproblems, optimality and feasibility cuts are continuously added to the master problem at each iteration. Another strategy is employing Lagrangian relaxation method firstly proposed by Guignard [77]. Cutting planes and subgradient are two classic approaches based on Lagrangian relaxation but they are not the most efficient ones. These methods cannot always solve the problems to their optimality and heuristic step should also be added to their solution algorithm. Moreover, Hybrid dual problems have been introduced to update the Lagrange multipliers by combining these concepts in order to improve the performance of former methods [78]. In addition, augmented Lagrangian relaxation (ALR) can be used, which is also based on Lagrangian relaxation but does not have the disadvantages of classic approaches and can reach the optimal solution [79]. In other words, the duality gap in classical Lagrangian relaxation can be overcome through using ALR. The reason is imposing a quadratic penalty term in the objective function compared to the classical Lagrangian relaxation methods.

Based on the discussed literature, the carbon capturing in oil sands operation has not been addressed comprehensively yet, where upgrading processes are the major CO_2 emitter part. Although there are com-

parative studies over different CCS technologies [73, 74], to the authors' knowledge, there is not any work regarding CO_2 reduction in upgrading facilities. There exist comprehensive optimization studies focusing on different hydrogen and power generations schemes [46, 42]. Nevertheless, these two works only considered carbon capture in a Boolean way: with CCS or without CCS. Therefore, an optimization problem needs to be addressed to find the optimal design of bitumen upgrading facility where different CCS technologies are also incorporated. To do so, our previous developed model for the design of optimal bitumen upgrading facility from Chapter 2 [80] has been updated by modeling the three major carbon capture approaches: pre–combustion, post–combustion, and oxyfuel combustion.

This Chapter is organized as follows: Section 3.2 states the problem of finding the optimal design of bitumen upgrading facility for CO_2 reduction. Section 3.3 presents the mathematical modeling of different carbon capture methods incorporated to our previous proposed model in Chapter 2. The nomenclature of presented model is available in Appendix A. The updated model could not be solved with available solvers, and hence, ALR method is introduced in Section 3.4. In Section 3.5, results from the optimization of different case studies are reported and discussed. Section 3.6 concludes the Chapter.

3.2 Problem statement

In this section, we present the main concepts for optimal design of bitumen upgrading plant and its integrated utility system with considering different technologies for the CCS. The problem is divided into four major sections: upgrading plant, gasification unit, utility system, and carbon capture unit. In the proposed modeling framework, the plant is divided into two major parts. Figure 3.1 shows the connections between these two parts. Note here that the only reason we split our problem this way is having two sections with nearly the same number of operating units and consequently close number of variables and constraints. Furthermore, there is no engineering advantage or disadvantage in splitting the four sections in a way we did.

In the Part A (see Figure 3.2), the major tasks are the bitumen upgrading and the resulted byproducts gasifying into syngas. To do so, the diluent is first separated with the diluent recovery unit (DRU), and the bottom of this tower is sent to the VDU in which products (including NPH, LGO, and HGO) are separated and pumped into the hydrotreaters. Afterwards, the residue of the VDU is cracked with either the hydrocracker or thermocracker unit. Note here, the dashed lines represent the possibility that a line might not exist in the final optimal configuration. The useful products of cracker units (NPH, LGO, and HGO) are separated and sent to the hydrotreaters, and the byproducts of these units need to be treated in an efficient way. In this study, it is assumed that the resulted residue from hydrocracking and the obtained coke from thermocracking are gasified in order to generate syngas and consequently produce hydrogen, power, and/or heat from this source of energy. The obtained NPH, LGO, and HGO from the VDU and cracking unit are passed through corresponding hydrotreaters and then mixed together as a single SCO product stream. The produced syngas from the gasification unit has a high value of sulfur which needs to be treated using the COS, Selexol–1, and Claus Plant units. Moreover, the clean syngas can also be generated with SMR unit

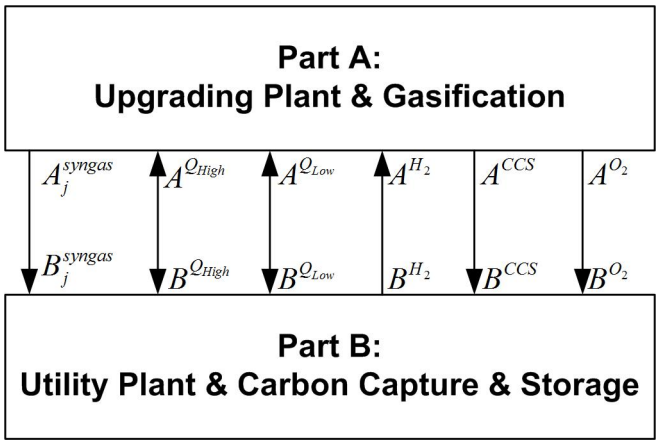

Figure 3.1: Interpretation of connection between the Parts A and B

and gasification of natural gas. Note here, operation of the SMR unit is optional. The obtained syngas streams from gasification of residues and natural gas are then mixed together.

In the Part B (see Figure 3.3), the major objectives are supplying required utilities for the whole plant, namely, hydrogen, heat, and power, and reducing CO_2 emissions using the CCS technologies. The syngas stream from the Part A is used to produce (i) hydrogen by passing through the PSA, or (ii) power and heat by going through the gas turbine–1 and HRSG–1. As an extra option, natural gas can be burned to generate power and heat using the gas turbine–2 and HRSG–2. There are steam turbines and boilers to supply more power and heat if they are required. For the carbon capture, three approaches are taken into account in this study: (1) pre–combustion method where CO compound in the syngas stream is converted into CO_2 in the WGS unit and a pure CO_2 stream is then separated in the Selexol–2 unit, (2) post–combustion method where different flue gas streams, which have low CO_2 concentration, are combined together and the mixed flow is then sent to the MEA unit, (3) oxyfuel combustion method where pure oxygen is applied instead of air for combustion of fossil sources. The operating units associated with the CCS technologies are colored green. For the gas turbine–1 and gas turbine–2, it is assumed that the syngas and natural gas are burned in the existence of air. The reason is that more power and heat would be generated this way. On the other hand, for the natural gas consumed in different units of upgrading, SMR, and boilers as the heat source, both options of combustion with air and pure oxygen are available. Note here, the ASU is employed in the Part B to generate the pure oxygen fluid demanded by the oxyfuel combustion (in the Part B) and the gasifier and Claus Plant (in the Part A).

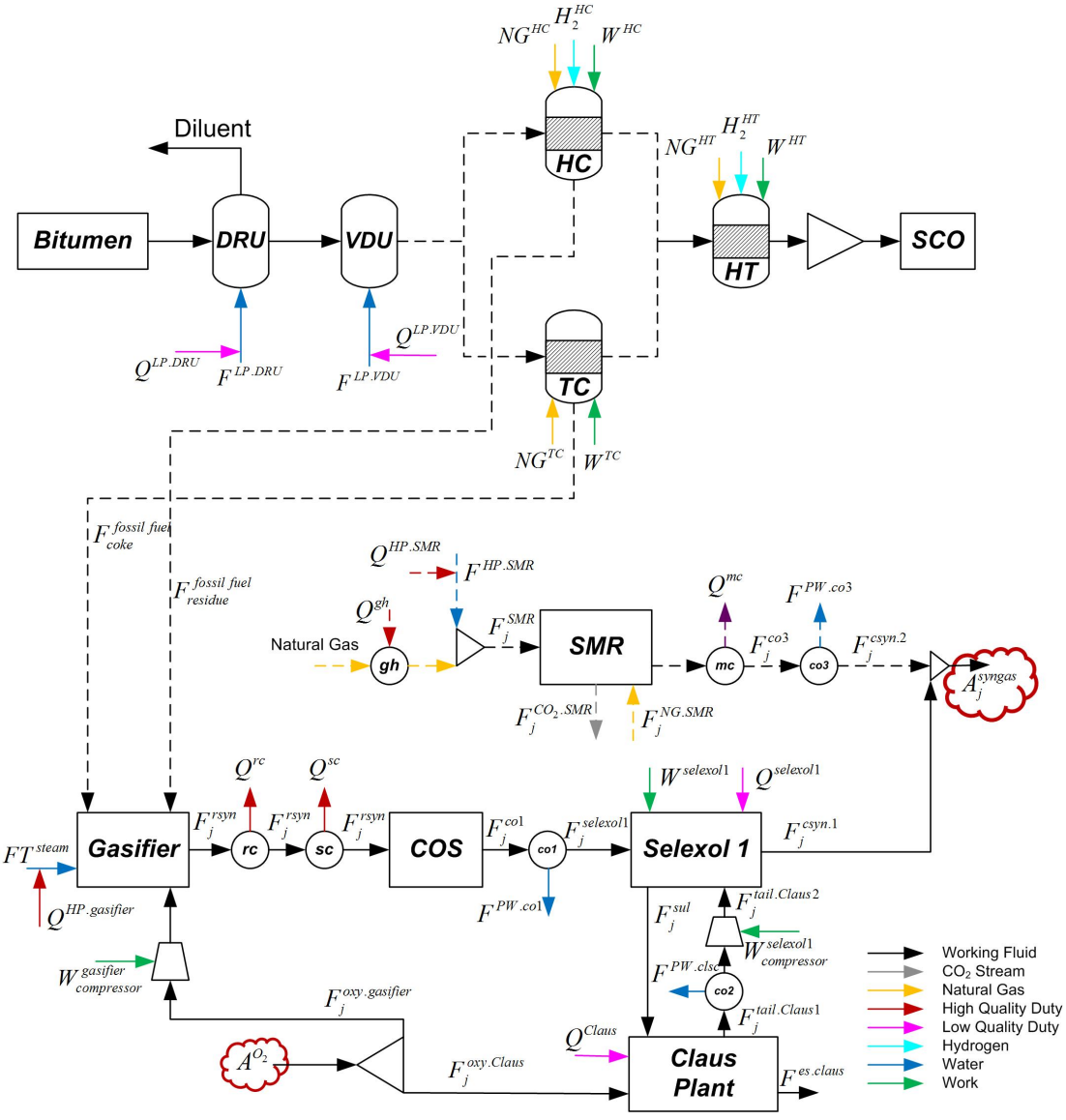

Figure 3.2: Proposed superstructure for the upgrading facility and gasification unit

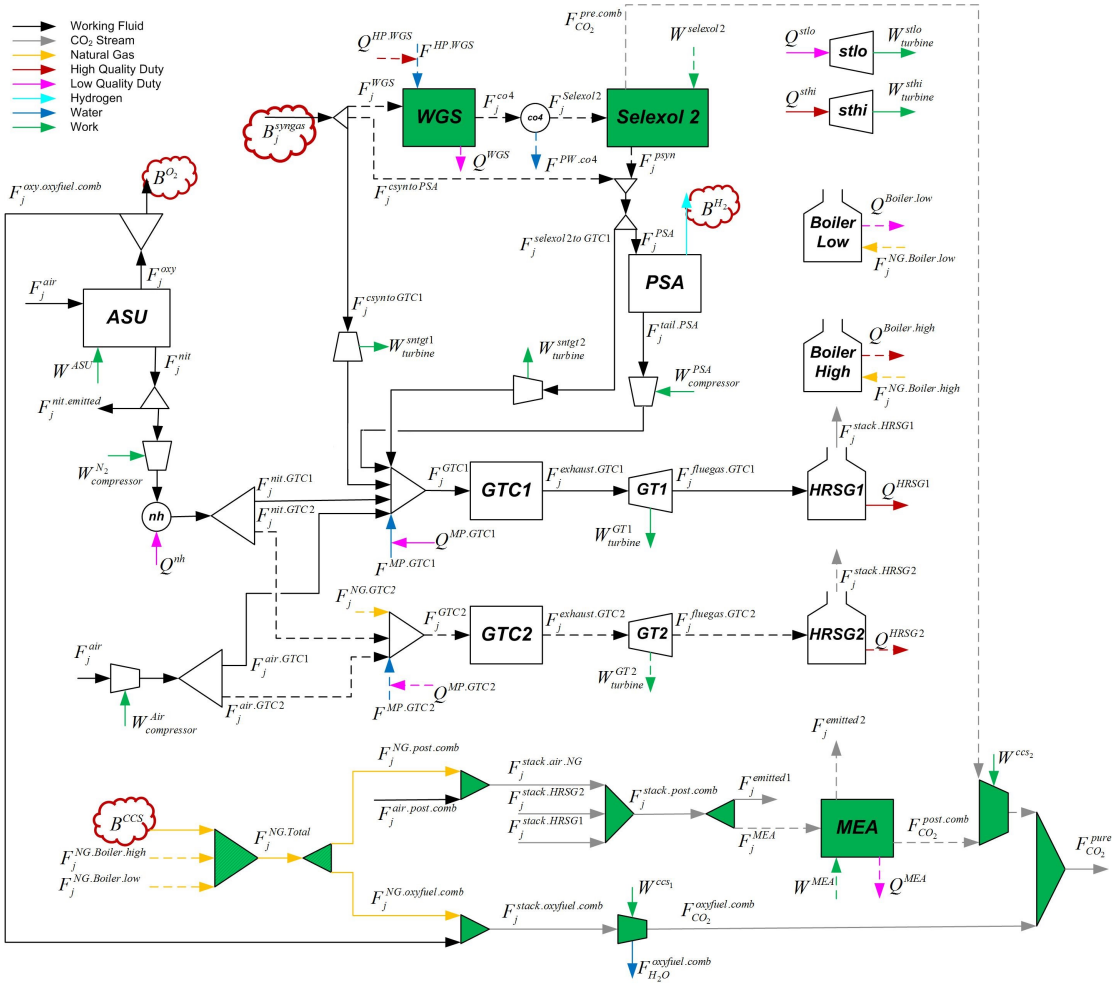

Figure 3.3: Proposed superstructure for the utility system and carbon capture

3.3 Mathematical modeling

In the previous Chapter, we modeled the same problem but without the carbon capture technologies. In this section, modeling that is incorporated into our previous model is discussed. There are also some small changes in other units modeling explained below as well.

3.3.1 Upgrading, gasification, and utility plant

Process modeling for the upgrading plant, gasification process, and utilities generation has been discussed in Chapter 2. Figure 3.4 shows the new superstructure of polygeneration energy system modified for CO_2 capturing. Compared to the superstructure in the previous Chapter, there are two additional stream lines for the utility system – showing with phosphoric thick lines in Figure 3.4. In the former attempt, it was assumed that the F_j^{WGS} passes through the WGS and Selexol–2 units in order to produce hydrogen in the PSA unit. However, these units are optional operating units here to capture CO_2 as a pre–combustion technique.

The new stream line ($F_j^{csyn.to.PSA}$) gives more flexibility to the system in the view of CO_2 capturing. Moreover, ASU unit generates more pure oxygen in the new superstructure to supply the required oxygen for the oxyfuel combustion ($F_j^{oxy.oxyfuel.comb}$). As a result, the Equations 2.42, needs to be modified as estated below:

$$\sum_j F_j^{oxy} = \sum_j F_j^{oxy.gasifier} + \sum_j F_j^{oxy.Claus} + \sum_j F_j^{oxy.oxyfuel.comb} \tag{3.1}$$

3.3.2 Carbon capture

Three different CO_2 capture technologies are incorporated in our process design problem. This section presents the energy and mass balances and economic model as well. A comprehensive superstructure is developed to study the CO_2 capture options. Figure 3.3 represents the proposed superstructure for the CO_2 capturing. There are five operating units consuming natural gas: upgrading plant, SMR, high– and low–quality boilers, and GTC–2. On the other side, GTC–1 is the only operating units burning the produced syngas in order to generate power and duty. All these six units need adequate amount of oxygen for the combustion as well. The required oxygen can be supplied as pure oxygen streams generated in the ASU unit or air streams. Burning the fossil fuel with the pure oxygen leads to a flue gas mainly being a mixture of CO_2 and H_2O, while applying air as the source of oxygen results in larger flow rate of flue gas being composed of CO_2, H_2O, and N_2. Since the major task of GTCs is generating power and heat, it is assumed that combustion next to the air stream is a better option for them. The reason is that the more flow rate passes through GTCs, the more power is generated and the more heat is recovered. Therefore, only post–combustion CO_2 capturing is considered for flue gas streams of two gas turbines ($FT^{stack.HRSG1}$ and $FT^{stack.HRSG2}$). For the other four streams, $FT^{NG.Upgrading}$, $FT^{NG.SMR.feed}$, $FT^{NG.Boiler.high}$ and $FT^{NG.Boiler.low}$, both options are taken into account. Hence, these four streams are mixed together first (shaded green mixer in Figure 3.3) and the mixed stream can go through the post–combustion, oxyfuel combustion, or combination of both (shaded green splitter in Figure 3.3).

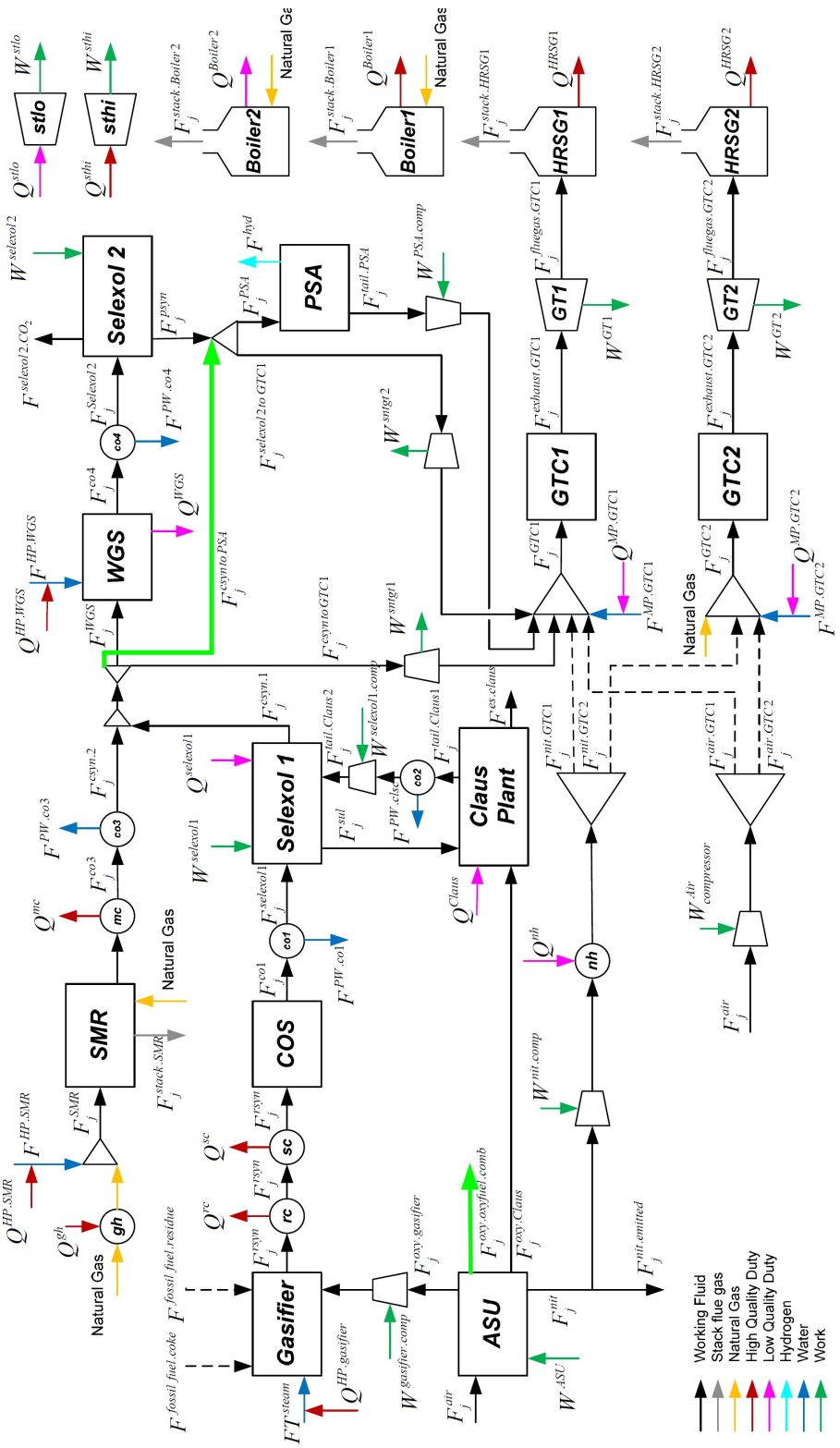

Figure 3.4: Modified superstructure of utility plant

Pre–combustion capture. Pre–combustion technology was already incorporated in the previous Chapter. However, it was not an optional unit. As a result, in this Chapter, a new binary variable (b^{WGS}) is introduced. Furthermore, modeling of some units needs to be modified according to the new proposed superstructure. In this section, those equations requiring revisions are discussed.

For the mixture before the WGS unit, there are three outlets now because of the new stream line ($F_j^{csyn.to.PSA}$). Hence, in addition to revising the total mass balance, a new ratio variable is defined to control ratios among the outlets.

$$F_j^{csyn1} + F_j^{csyn2} = F_j^{WGS} + F_j^{csyn.to.PSA} + F_j^{csyn.to.GTC1} \quad \forall j \in J \tag{3.2}$$

$$F_j^{WGS} = b^{WGS} \cdot (F_j^{csyn1} + F_j^{csyn2} - F_j^{csyn.to.GTC1}) \quad \forall j \in J \tag{3.3}$$

$$F_j^{csyn.to.PSA} = (1 - b^{WGS}) \cdot (F_j^{csyn1} + F_j^{csyn2} - F_j^{csyn.to.GTC1}) \quad \forall j \in J \tag{3.4}$$

Mass balance over the splitter after the Selexol–2 also requires to be modified. The associated mass balance can be presented as follow.

$$F_j^{psyn} + F_j^{csyn.to.PSA} = F_j^{PSA} + F_j^{selexol.to.GTC1} \quad \forall j \in J \tag{3.5}$$

$$F_j^{PSA} = R^{Se2} \cdot (F_j^{psyn} + F_j^{csyn.to.PSA}) \quad \forall j \in J \tag{3.6}$$

where R^{Se2} is the ratio of flow rate entering to the PSA unit.

Post–combustion capture. Post–combustion approach can be considered as follows. Assuming that 64.7% excess of oxygen is needed for the post–combustion CO_2 capturing, flow rates of air stream ($F_j^{air.post.comb}$) and flue gas ($F_j^{stack.air.NG}$) can be calculated. Afterwards, this flue gas is mixed with outlets of HRSGs to have the main stream of flue gas ($F_j^{stack.post.comb}$) for the post–combustion treatment. Note here, this stream is not necessarily sent to the capturing unit (F_j^{MEA}) and it can be emitted to the atmosphere ($F_j^{emitted1}$). CO_2 is captured in MEA unit ($F_{CO_2}^{post.comb}$) and then mixed with the capture CO_2 from the Selexol–2 unit ($F_{CO_2}^{pre.comb}$). The pure stream is then compressed and cooled in order to be ready for transportation and sequestration. The following equation can express the mass balances over the mixture and splitter:

$$FT^{NG.upgrading} + FT^{NG.SMR} + FT^{boiler.hi} + FT^{boiler.lo} = FT^{NG.total} \tag{3.7}$$

$$FT^{NG.total} = FT^{NG.post.comb} + FT^{NG.oxyfuel.comb} \tag{3.8}$$

The mass and energy balances of the MEA unit are explained here. According to a reference in which rigorous simulations of the MEA unit were carried out under different operating conditions, there are three

important factors to estimate the power, duty, and capital cost: (1) total mass flow rate of inlet stream (MT^{MEA}), (2) mass fraction of CO_2 in the inlet stream ($xm_{CO_2}^{MEA}$), and (3) Carbon Capture Ratio (CCR) [81, 82]. In order to calculate the mentioned variables, following equations can be applied for the mass balances over the MEA unit.

$$MT^{MEA} = \sum_j MW_j \cdot F_j^{MEA} \tag{3.9}$$

$$xm_{CO_2}^{MEA} = \frac{MW_{CO_2} \cdot F_{CO_2}^{MEA}}{MT^{MEA}} \tag{3.10}$$

$$F_j^{MEA} = F_j^{emitted2} \quad \forall j \in J/\{CO_2\} \tag{3.11}$$

$$F_j^{MEA} = F_j^{post.comb} + F_j^{emitted2} \quad \forall j = \{CO_2\} \tag{3.12}$$

$$F_j^{post.comb} = CCR \cdot F_j^{MEA} \quad \forall j = \{CO_2\} \tag{3.13}$$

The following logical constraint is also imposed to make sure that the capacity of MEA unit is in a feasible region.

$$b^{MEA} \cdot \underline{\Omega}^{MEA} \leq MT^{MEA} \leq b^{MEA} \cdot \overline{\Omega}^{MEA} \tag{3.14}$$

Estimations of required duty and power are the next step. Correlations with bilinear and trilinear terms in addition to quadratic and cubic ones were proposed in the reference [81, 82]. Nevertheless, the presented correlations are more complicated than all those which have been applied so far for the rest of our model in Chapters 2 and 3. Therefore, we simplified the complex correlations reported in the above references. The presented correlations were valid for following ranges: $500 \leq MT^{MEA}$ (tonne h^{-1}) ≤ 3000, $0.05 \leq xm_{CO_2}^{MEA} \leq 0.1$, and $0.5 \leq$ CCR ≤ 1. Firstly, 100 points were selected in the ranges and their corresponding energy terms were calculated using the reported correlations from [81]. Secondly, curve fittings were carried out employing the obtained results and linear correlations were found to replace with the complex ones. In other words, sample data were generated through calculating the available power, duties, and investment cost correlations first. Afterwards, new data analysis was performed and linear correlations were developed with R–squared accuracies higher than 0.95.

$$Q^{MEA} = b^{MEA} \cdot \left(277.20 - 441.76 \cdot CCR - 0.19 \cdot MT^{MEA} + 1275.02 \cdot xm_{CO_2}^{MEA}\right) \tag{3.15}$$

$$W^{MEA} = b^{MEA} \cdot \left(0.08 + 3.35 \cdot 10^{-5} \cdot CCR + 2.76 \cdot 10^{-8} \cdot MT^{MEA} + 1.26 \cdot 10^{-4} \cdot xm_{CO_2}^{MEA}\right) \tag{3.16}$$

where Q^{MEA} is produced duty and W^{MEA} is power requirement.

Oxyfuel combustion. Oxyfuel combustion approach can be expressed as follows. Assuming that 5% excesses of oxygen is appropriate for the combustion stage of the oxyfuel combustion, flow rates of air stream ($F_j^{oxy.oxyfuel.comb}$) and flue gas ($F_j^{stack.oxyfuel.comb}$) can be calculated. Afterwards, this flue gas is passed the multistage compression with inter cooling in order to liqudify and separate the water ($F_{H_2O}^{oxyfuel.comb}$) from the CO_2 ($F_{CO_2}^{oxyfuel.comb}$). The pure CO_2 stream is ready to be transported and sequestered.

Power requirement model of compressors for liquefaction of the captured CO_2 is presented below. For both compressors, ratio equations are applied for the estimation of electricity requirements (GW). Note here that cooling duties are neglected in this model.

$$W^{CCS_1} = 0.001 \cdot EC^{CCS_1} \cdot FT^{stack.oxyfuel.comb} \tag{3.17}$$

$$W^{CCS_2} = 0.001 \cdot EC^{CCS_2} \cdot (F_{CO_2}^{pre.comb} + F_{CO_2}^{post.comb}) \tag{3.18}$$

where EC^{ccs_1} and EC^{ccs_2} are the electricity requirement of base case equaling to 1.6981 (Wh mol^{-1}).

As it can be seen, in this Chapter, there are three new utility requirements (W^{CCS_1}, W^{CCS_2}, and W^{MEA}), and the overall balance of work consumption is thus updated as below:

$$\begin{aligned} W^{net} = {} & W^{sntgt1} + W^{sntgt2} + W^{GT1} + W^{GT2} + W^{sthi} + W^{stlo} \\ & - W^{gasifier.comp} - W^{selexol.comp} - W^{selexol} - W^{ASU} - W^{selexol2} \\ & - W^{PSA.comp} - W^{nit.comp} - W^{air.comp} - W^{demand} - W^{CCS_1} - W^{CCS_2} - W^{MEA} \end{aligned} \tag{3.19}$$

Economic model. In this section, capital cost models for the CO_2 capturing options are presented. After finding operating flow rates, estimation of the capital and operating costs of each individual unit would be required. The capital cost of the MEA unit is adopted from the afore–mentioned reference when a new linear correlation is developed for consistency of proposing model [81, 82].

$$C_{MEA} = b^{MEA} \cdot \left(-144.14 + 99.78 \cdot CCR + 0.08 \cdot MT^{MEA} + 407.84 \cdot xm_{CO_2}^{MEA} \right) \tag{3.20}$$

For the compressors, the capital cost model (C_{cc_1} and C_{cc_2}) and associated parameters are adopted from a reference [50]. This model can be stated as below:

$$C_{cc_1} = Cb_{cc_1} \cdot \left(\frac{M_{CO_2}^{oxyfuel.comb}}{Mb_{cc_1}} \right)^{sf_{cc_1}} \tag{3.21}$$

$$C_{cc_2} = Cb_{cc_2} \cdot \left(\frac{M_{CO_2}^{pre.comb} + M_{CO_2}^{post.comb}}{Mb_{cc_2}} \right)^{sf_{cc_2}} \tag{3.22}$$

where $M_{cc_1}^b$ and $M_{cc_2}^b$ are mass flow rate of the base case unit (=469.04 tonne h^{-1}), sf_{cc_1} and sf_{cc_2} (= 0.85), and $C_{cc_1}^b$ and $C_{cc_2}^b$ (= 38.69 \$MM) are parameters [50].

Total capital cost can be expressed as follows when its unit is (\$MM).

$$CAPEX^{CO_2.capturing} = C_{MEA} + C_{cc_1} + C_{cc_2} \tag{3.23}$$

Coupling constraints. There are several coupling constraints between the Part A and Part B. First, the syngas generated in the Part A is sent to the Part B:

$$A_j^{syngas} - B_j^{syngas} = 0 \quad \forall j = \{CO,\ H_2,\ CO_2,\ H_2O,\ CH_4,\ Ar,\ N_2\} \tag{3.24}$$

This equality is not required for the rest of components, including H_2S, COS, O_2, C_2H_6, C_3H_8, C_4H_{10}, due to the fact they are all zero.

There should be total energy balance for the whole system with respect to high– and low– quality duties between the Parts A and B:

$$A^{Q_{High}} - B^{Q_{High}} = 0 \tag{3.25}$$

$$A^{Q_{Low}} - B^{Q_{Low}} = 0 \tag{3.26}$$

where:

$$\begin{aligned}
A^{Q_{High}} &= Q^{rc} + Q^{sc} + Q^{mc} - Q^{HP.gasifier} - Q^{gh} - Q^{HP.SMR} \\
B^{Q_{High}} &= -Q^{HRSG1} - Q^{HRSG2} - Q^{boiler.hi} + Q^{HP.WGS} + Q^{sthi} \\
A^{Q_{Low}} &= -Q^{claus} - Q^{selexol1} - Q^{LP.DRU} - Q^{LP.DRU} \\
B^{Q_{Low}} &= -Q^{WGS} - Q^{boiler.lo} - Q^{MEA} + Q^{nh} + Q^{MP.GTC1} + Q^{MP.GTC2} + Q^{stlo}
\end{aligned}$$

The produced hydrogen in the Part B is sent to the Part A to be used in hydrocracker and hydrotreaters:

$$A^{H_2} - B^{H_2} = 0 \tag{3.27}$$

Except the natural gas streams that are assumed to be burned next to air and steam in the gas turbine–2 ($FT^{NG.GTC2}$) and SMR ($FT^{NG.SMR.feed}$) units, the rest of them (including (1) the natural gas demands by upgrading facility's units ($FT^{NG.Upgrading}$), (2) the natural gas burning in the SMR unit to provide heat (from the Part A), and (3) the natural gas consuming in high– and low– quality boilers ($FT^{NG.Boiler.high}$ and $FT^{NG.Boiler.low}$) from Part B) have the possibilities to be consumed with either air or oxygen. Therefore, the following total mass flow rate balance can be stated for the natural gas between the two parts:

$$A^{CCS} - B^{CCS} = 0 \tag{3.28}$$

where:

$$\begin{aligned}
A^{CCS} &= FT^{NG.upgrading} + FT^{NG.SMR} \\
B^{CCS} &= FT^{NG.total} - FT^{boiler.hi} - FT^{boiler.lo} \\
FT^{NG.upgrading} &= NG^{HC} + NG^{TC} + NG^{HT}
\end{aligned}$$

Part of the generated oxygen from the ASU unit is consumed in the Part B for the oxyfuel combustion and the rest is used in the Part A for the gasifier and Claus Plant units:

$$A^{O_2} - B^{O_2} = 0 \tag{3.29}$$

where:

$$A^{O_2} = FT^{oxy.gasifier} + FT^{oxy.claus}$$
$$B^{O_2} = FT^{oxy} - FT^{oxy.oxyfuel.comb}$$

There are 12 coupling constraints as seen in Equations 3.24-3.29. This set of equations is summarized as $A_c - B_c = 0 \quad \forall c \in C = \{1, ..., 12\}$.

Overall model. For the objective function, there are some modifications as well. The purchasing resources and selling commodities are the same as before. However, there is a new term for the capital cost ($CAPEX^{CO_2Capturing}$) due to the CO_2 capture. Also there must be a new term to count for the annual carbon tax emission, $Cost_{tax}^{CO_2}$.

$$CAPEX = CAPEX^{Upgrading} + CAPEX^{Polygeneration} + CAPEX^{CO_2Capturing} \tag{3.30}$$

$$Profit_{net} = (1 - R_{tax}) \cdot \Big(Cost^{Revenue} - [Cost^{Purchasing} + OPEX^{Upgrading} + OPEX^{Polygeneration} + Cost_{tax}^{CO_2}] \Big) \tag{3.31}$$

$Cost_{tax}^{CO_2}$ be stated as below:

$$Cost_{tax}^{CO_2} = P_{tax}^{CO_2} \cdot (M_{CO_2}^{emitted1} + M_{CO_2}^{emitted2}) \cdot t_{op} \tag{3.32}$$

where $P_{tax}^{CO_2}$ is the carbon tax per tonne of CO_2 emitted being equal to \$30 per tonne of CO_2.

The objective function of this study is still NPV, which is adopted from one of the main reference, can be denoted by:

$$NPV = -CAPEX + Profit_{net} \cdot \frac{1}{r} \cdot \left(1 - \frac{1}{(1+r)^{t_{lf}}}\right) + \frac{R_{tax} \cdot CAPEX}{t_{dp}} \cdot \frac{1}{r} \cdot \left(1 - \frac{1}{(1+r)^{t_{dp}}}\right) \tag{3.33}$$

Finally, the overall model can be summarized as

$$\begin{cases} \max & NPV \\ \text{s.t.} & \text{Equations 2.1 - 2.162 (except Equations 2.31, 2.33, 2.42, 2.54, and 2.103)} \\ & \text{Equations 3.1 - 3.32} \end{cases}$$

where Equations 2.1 – 2.162 include (1) the mass and energy balances, and economic model of the utility plant, and (2) the mass and energy balances, and economic model of the upgrading plant, and Equations

3.1 – 3.32 consist of (1) mass and energy balances, and economic model of the carbon capturing section, (2) coupling constraints between the Parts A and B, and (3) the overall objective function.

The full–space problem (P) is then can be simply stated as below

$$(P)\begin{cases} \max & NPV_A + NPV_B \\ \text{s.t.} & g_A \leq 0 \\ & h_A = 0 \\ & g_B \leq 0 \\ & h_B = 0 \\ & A_c - B_c = 0 \quad \forall c = \{1, ..., 12\} \end{cases}$$

where NPV_A and NPV_B are the objective functions, g_A and g_B are the nonlinear constrains, and h_A and h_B are the linear constrains of Part A and B, respectively. The remaining equations are those connect Parts A and B together as discussed above.

Note here, for the rest of the Chapter, the notation of ν(P) is applied to denote the optimal value of the objective function for problem(P).

3.4 Augmented Lagrangian decomposition method

The proposed full–space problem (P) presented in Section 3.3 is a large–scale MINLP, which contains some binary variables regarding process synthesis and design and many non–convex constraints mainly due to bilinear terms existing in component mass balance as an example. This means that standard MINLP solvers for convex optimization (such as DICOPT, KNITRO, or SBB) may perform poorly to reach the global optimality. Global MINLP solvers (e.g. BARON, SCIP, or COUENNE) have been thus developed to overcome this issue, but their computational time is substantially longer. Hence, a solution strategy needs to be implemented to find the optimal global point with reasonable computational time.

Decomposition is an efficient way for problem with a block–separable structure in the constraints and few coupling constrains. For the Lagrangian relaxation based decomposition methods, the optimum of primary problem is equal to the optimum of the dual problem if only all the constraints are convex and all the variables are continuous. However, our case study has integer variables and non–convex constrains, and hence, a duality gap will exist. In this study, we present a well–known technique to solve the relaxed version of full–space problem. ALR method is an approach to overcome existence of the mentioned gap by introducing a quadratic penalty term in the objective function of problem. The ALR function can then be stated as

$$(ALRP)\begin{cases} \min & -(NPV_A + NPV_B) + \sum_{c=1}^{12} \lambda_c \cdot (A_c - B_c) + \frac{\rho}{2} \cdot \sum_{c=1}^{12} (A_c - B_c)^2 \\ \text{s.t.} & g_A \leq 0 \\ & h_A = 0 \\ & g_B \leq 0 \\ & h_B = 0 \end{cases}$$

where λ represents the Lagrangian multipliers and $\rho \geq 0$ is a penalty parameter. As it can be seen, ALR is a combination of Lagrangian relaxation function and penalty function method. When the Lagrangian function is exact but not differentiable, the quadratic penalty function is smooth, but not exact. The ALR is both

smooth and exact. Note that another advantage of not having any duality gap is that the solution of the ALR method satisfies the full–space model, and hence, there is no need to have heuristic solutions for this method.

Although ALR implementation results in zero duality gap and no need to the heuristic solutions, the decomposition of ALR problem (ALRP) requires more effort since the quadratic penalty term makes the Parts A and B coupled again. Therefore, the variables of one part are optimized while holding the variables of other part fixed. For example, variables of the Part B are fixed (B_C^{fixed}) when the ALR problem of the Part A (ALRP_A) is solving and vice versa. Note that the fixed variables should be relaxed after each optimization at each iteration. Furthermore, to start this iterative procedure, a feasible solution from the full–space problem is required satisfying all the constraints. It can be provided by fixing binary variables and get a feasible solution to start with. The algorithm of ALR method is presented below in Figure 3.5. ALRP_A and ALRP_B can be expressed as follows

$$(ALRP_A)\begin{cases} \min & -NPV_A + \sum_{c=1}^{12} \lambda_c \cdot A_c + \dfrac{\rho}{2} \cdot \sum_{c=1}^{12} (A_c - B_c^{fixed})^2 \\ \text{s.t.} & g_A \leq 0 \\ & h_A = 0 \end{cases}$$

$$(ALRP_B)\begin{cases} \min & -NPV_B - \sum_{c=1}^{12} \lambda_c \cdot B_c + \dfrac{\rho}{2} \cdot \sum_{c=1}^{12} (A_c^{fixed} - B_c)^2 \\ \text{s.t.} & g_B \leq 0 \\ & h_B = 0 \end{cases}$$

After optimizing both parts, the multipliers and the penalty parameter still need to be updated iteratively. The following equations can be applied for this purpose.

$$\lambda^{(k+1)} = \lambda^{(k)} + s^{(k)} \tag{3.34}$$

$$\rho^{(k+1)} = 1.1 \cdot \rho^{(k)} \tag{3.35}$$

The initial values of ρ is set as 1 in this Chapter. As iteration goes on, this parameter is gradually increasing and a sufficiently large penalty parameter will make the augmented Lagrangian convex. However, when the penalty parameter becomes very large the sub–problem is difficult to solve. So the strategy used here is to start from small value and gradually increase until the solution converges.

The rest of this section focuses on the performance of the implemented decomposition method shown in Figures 3.6-3.8. Three criteria are analyzed: (i) convergence of a Lagrangian multiplier (λ), (ii) convergence of a subgradient (S), and (iii) convergence of the objective function. There are twelve multipliers and subgradients in the decomposed models, and the first Lagrangian multiplier (λ_1) and the first subgradient (S_1) are picked out as samples. Discussion in this section is based on the solution of scenario 4 presented in Table 3.1, Section 3.5.1.

All the proposed decomposed models were programmed in GAMS. All the problems are MINLP and the BARON solver was implemented for optimization. One hour computational time and relative optimality gap of 1% were set as the optimization stopping criteria. Furthermore, a desktop computer (single core of Intel®

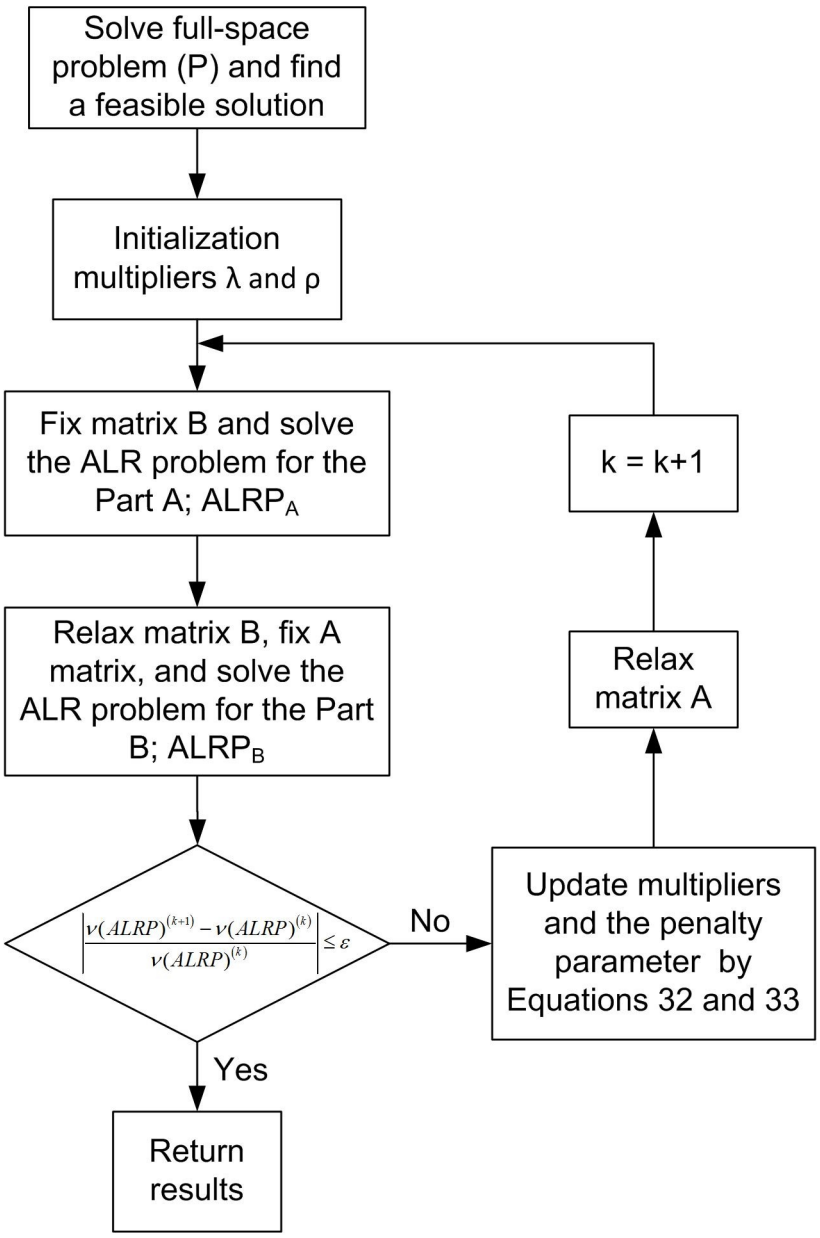

Figure 3.5: ALR decomposition algorithm

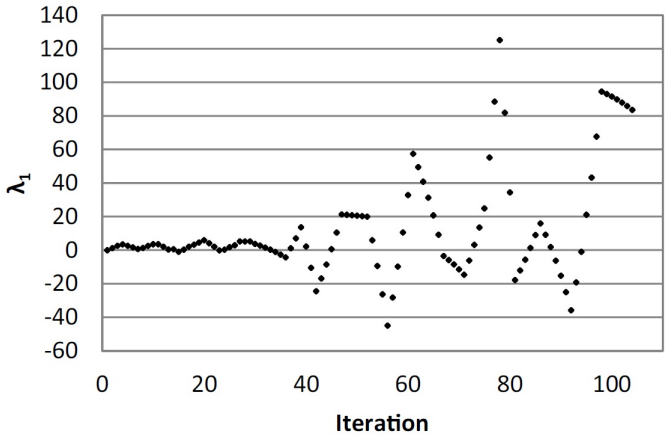

Figure 3.6: Convergence of the multiplier λ_1 for ALR method

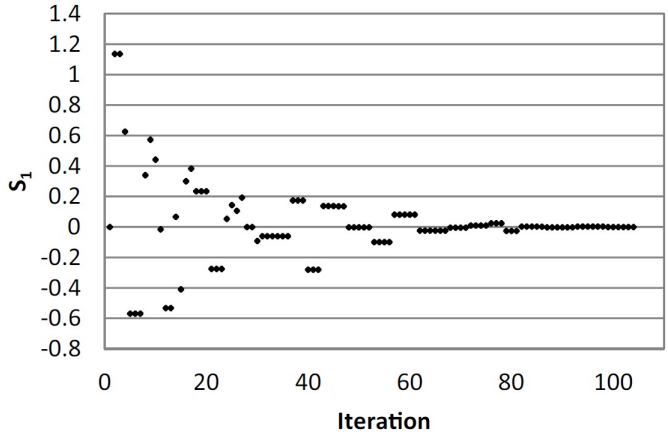

Figure 3.7: Convergence of the subgradient S_1 for ALR method

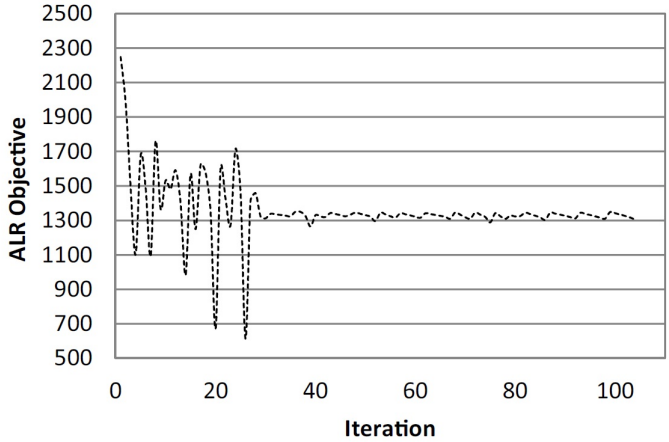

Figure 3.8: Convergence of the objective function for ALR method

Table 3.1: Effects of upgrading plant capacity (CC^{NG} = \$0.00477 MJ^{-1} and CC^{EL} = \$0.081 kWh^{-1})

	M^{DBIT} (tonne h^{-1})	150	500	850	1200	1500
	NPV (\$MM yr^{-1})	2294.3	1917.2	1610.00	1336.9	1105.7
Decision variables	$b_{SGP}^{gasifier}$	1	1	1	1	1
	$b_{SCGP}^{gasifier}$	0	0	0	0	0
	b^{SMR}	1	0	0	0	0
	b^{WGS}	1	1	1	1	1
	b^{GTC2}	1	1	1	1	1
	$b^{boiler.hi}$	0	0	0	0	0
	$b^{boiler.lo}$	0	1	1	1	1
	b^{MEA}	0	0	0	0	0
SCO specifications	M^{SCO} (tonne h^{-1})	98.0	359.1	610.5	862.0	1077.4
	API^{SCO}	31.0	31.0	31.0	31.0	31.0
	xm_{NPH}^{SCO} (%)	12.5	11.4	11.4	11.4	11.4
	xm_{LGO}^{SCO} (%)	49.9	54.5	54.5	54.5	54.5
	xm_{HGO}^{SCO} (%)	37.6	34.2	34.2	34.2	34.2
Utilities consumptions	W^{net} (GW)	1.86	01.78	1.78	1.79	1.79
	$M^{total.NG}$ (tonne h^{-1})	184.7	183.8	187.0	190.7	194.3
	$M^{total.FW}$ (tonne h^{-1})	154.1	215.2	371.5	540.5	650.4
Economic terms	$CAPEX$ (\$MM)	1299.6	1443.4	1816.8	2145	2405.6
	$OPEX$ (\$MM yr^{-1})	69.7	178.7	286.3	393.9	486.1
	$purchases$ (\$MM yr^{-1})	465.9	810.1	1162.6	1516.0	1819.3
	$commodities$ (\$MM yr^{-1})	1312.6	1737.7	2202.8	2669.0	3064.7
	$Carbon\ tax$ (\$MM yr^{-1})	94.2	121.0	129.9	139.0	145.3
CCS	$M^{CO2.emitter}$ (tonne h^{-1})	418.7	537.8	577.2	617.9	646.0
	$M^{CO2.captured}$ (tonne h^{-1})	147.4	89.6	152.4	215.1	276.9
	$\frac{M^{Oxyfuel}}{M^{Oxyfuel}+M^{Post.comb}}$ (%)	0.0	0.0	0.0	0.0	0.0

i5–4590 @ 3.30 GHz, 8 GB RAM) was used. The average computational time for ALR approach is 0.92 (h). Note that number of variables and constraints of the original problem (P) are 918 and 941, respectively. Furthermore, the number of nonlinear matrix entries in the model is 622 showing high–nonlinearity of the model.

According to Figure 3.6, the Lagrangian multiplier λ_1 of the ALR method converges nearly after hundred iterations. At the beginning, the penalty parameter is not large enough so the multiplier does not affected by it. Afterwards, the multiplier starts to oscillate when the penalty parameter is quite large and the subgradient value needs to be converged to zero. For the last iterations, the multiplier has robust behavior since it gets close to the optimal solution. For the subgradient S_1, ALR method could converge to the value of zero. According to Figure 3.7, ALR shows a robust performance regarding to convergence of S_1 to the zero value. Iteratively increasing the penalty parameter (ρ) forces the solver to find a solution in which the relaxed constraints are also satisfied in the relaxed problem. Notice that while the subgradients converge to zero and lead to feasible solution, the multipliers may not converge as shown in Figure 3.6. The reason is that the penalty parameter $\rho^{(k)}$ may be large, so based on Equation 3.32 the value of the multipliers may not converge while subgradient $s^{(k)}$ converges to 0.

One advantage of ALR method is that it does not require any heuristic solution, and this algorithm can find the optimal solution with very small number of iterations. The other feature of ALR method is that it has a robust performance for the convergence. Figure 3.8 demonstrates the convergence of the objective function for ALR method.

3.5 Results and discussion

3.5.1 Effects of capacity

Effects of different capacities on optimal design of the upgrading plant and integrated utility system are provided in this section. The upper and lower bounds of the capacity are based on existing operating plants. Furthermore, results from the previous Chapter are included wherever it seems to be necessary in order to (i) have better understanding of the problem and (ii) show effects of CCS.

Optimal solutions are reported in Table 3.1. The optimal NPVs and total natural gas consumptions at different capacities are compared in Figures 3.9 and 3.10. For the optimal solutions without CCS, associated results are adopted from the previous Chapter. In addition, Figure 3.11 shows distribution of natural gas consumption for each unit. The following remarks can be made:

- Regarding unit selection, the hydrocracking, WGS, and gasturbine–2 are selected for all the scenarios, while the thermocracking, high–quality boiler, and MEA units are not chosen at all. Moreover, the SMR and low–quality boiler are selected interchangeably. This means that the hydrocracking, WGS, and gasturbine–2 are more efficient for the upgrading, CCS, and power and heat generation, respectively.

- According to Figure 3.9, upgrading plants without CCS have higher NPVs due to not spending extra money and energy on the carbon capturing process.

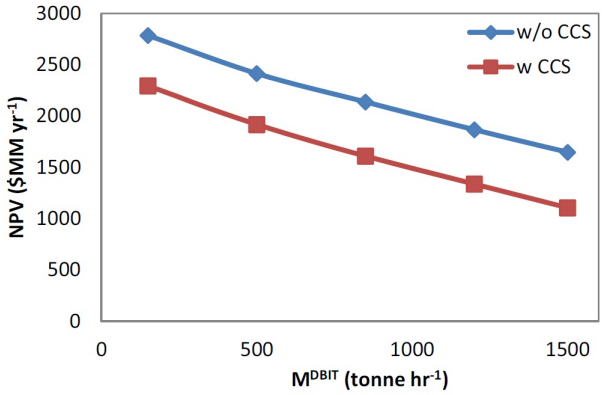

Figure 3.9: Comparison of optimal NPVs for different upgrading plant capacities

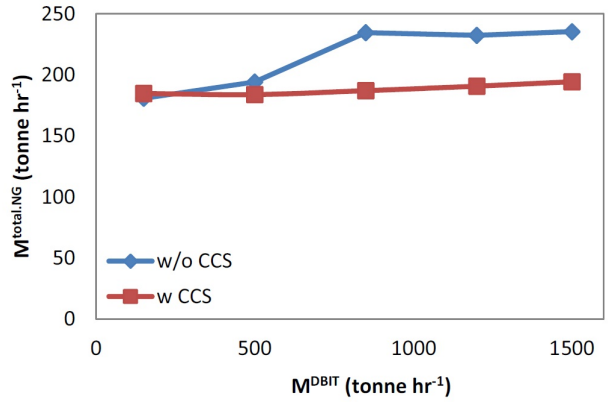

Figure 3.10: Comparison of total natural gas consumptions for different upgrading plant capacities

- The natural gas consumptions for the plants with and without CCS are different too. While a larger amount of natural gas is required for larger plants without CCS, the demands for natural gas are nearly constant for plants with CCS. It can be concluded that the carbon tax limits the consumption of the major source of CO_2 emissions.

- Alternative operation of SMR and low–quality boiler can be justified as follows. Other operating units require specific amount of low–quality duties, and this amount can be supplied with low–quality boiler easily. For the first case, there is no need to have a low–quality boiler due to small capacity of the upgrading plant, and the SMR has the chance to generate syngas leading to more electricity generation, consequently. Note that, although the major task of SMR in upgrading plants is hydrogen production from syngas, this task can also be taken care of by gasification of residue from hydrocracking.

- The only carbon capture technology that is used for all the scenarios is the pre–combustion one.

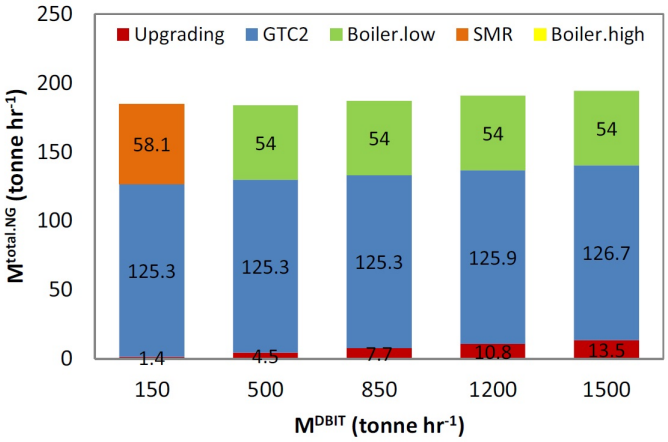

Figure 3.11: Comparison of total natural gas consumptions and their distributions with CCS

3.5.2 Effects of natural gas and electricity prices

In this section, effects of different natural and electricity prices on optimal design of the upgrading plant and integrated utility system are presented. The prices are categorized in three levels: low, medium, and high, where the low and high values are the maximum and minimum of prices in a large historical period of time and the medium values are the average of the available data. Note that, the capacity of upgrading plant is fixed at 850 tonne h^{-1} and the carbon tax is \$30 per tonne of CO_2.

Optimal solutions are reported in Table 3.2. Comparison of NPVs, natural gas consumptions and their distributions, and captured carbon are illustrated in Figures 3.12-3.14. We have the following remarks:

- For most of the scenarios, the hydrocracking, WGS, low–quality boiler, and gas turbine–2 are selected, while the thermocracking, high–quality boiler, and MEA units are not chosen. Moreover, the SMR is under operation when there is a large margin between electricity and natural gas prices (scenarios 4, 7, and 8). On the other hand, operation of the gas turbine–2 is not economic when the natural gas price is too expensive and the electricity is too low–cost. This means that the hydrocracking and WGS are more efficient for the upgrading and CCS, respectively, but operation of the SMR and gas turbine–2 are highly dependent on electricity and natural gas prices.

- According to Figure 3.12, the highest NPV belongs to the scenario 7 in which the price of natural gas is low and the price of electricity is high. The reason is that the natural gas is required to be purchased and the electricity is a commodity to be sold. Moreover, the lowest NPV belongs to the scenario 3 where the natural gas price is high and the electricity price is low.

- According to Figure 3.13, total natural gas consumptions are function of both prices. In the scenario 3, the price of electricity is too low and the price of natural gas is too high making the extra power generation uneconomical. Therefore, the gas turbine–2 is not chosen and selling power to the public grid is insignificant. In the scenarios 4, 7, and 8, the price of electricity is large enough and the price

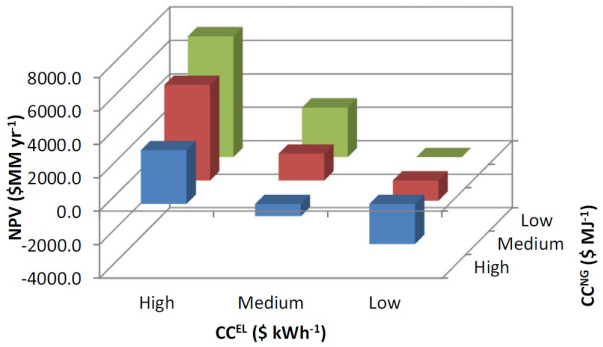

Figure 3.12: Comparison of optimal NPVs for different natural gas and electricity prices

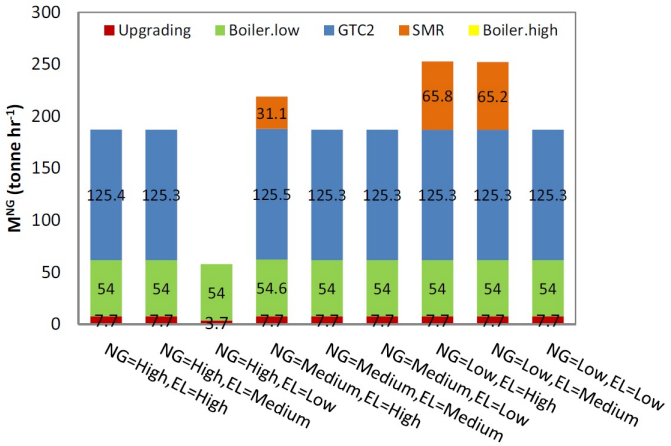

Figure 3.13: Comparison of natural gas consumptions for different natural gas and electricity prices

of natural gas is too low leading to power generation as much as possible. Hence, the SMR is selected to provide enough syngas to be consumed in the gas turbine–1.

- With respect to the carbon capturing, the post–combustion or oxyfuel combustion methods are not found efficient and WGS unit is determined to be under operation for eight of the scenarios (except the scenario 4). Figure 3.14 shows the mass flow rate of captured CO_2 for each scenario. Unfortunately, there is not any coherent trend in this Figure and a strong conclusion cannot be stated here.

3.5.3 Effects of margin between DilBit and SCO prices

Effects of different margins between DilBit and SCO prices on optimal design of the upgrading plant and integrated utility system are discussed in this section. Moreover, different capacities are taken into account for upgrading plant. According to the available historical data, the margins are categorized in three levels: low, medium, and high. Note that, the SCO price and the carbon tax are fixed at \$80.32 bbl^{-1} and \$30 per tonne of CO_2, respectively.

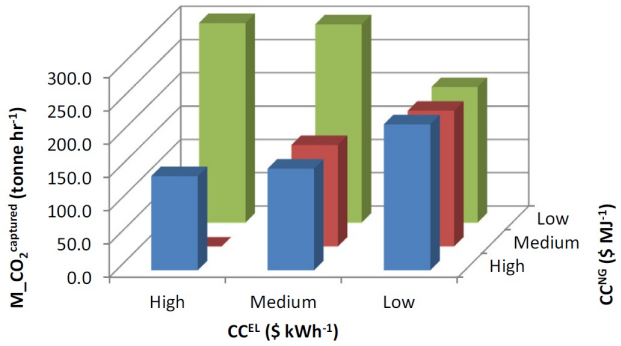

Figure 3.14: Comparison of captured carbon for different natural gas and electricity prices

Table 3.2: Effects of natural gas and electricity prices when $M^{DBIT} = 850$ tonne h^{-1} and carbon tax is \$30 per tonne of CO_2

	Scenario	1	2	3	4	5	6	7	8	9
	CC^{NG} (\$ MJ^{-1})	0.012	0.012	0.012	0.00477	0.00477	0.00477	0.00104	0.00104	0.00104
	CC^{EL} (\$ kWh^{-1})	0.141	0.081	0.037	0.141	0.081	0.037	0.141	0.081	0.037
	NPV (\$MM yr^{-1})	3214.7	-733.7	-2387.0	5717.5	1610.0	-1210.0	7223.1	2958.9	-0.7
Decision variables	$b^{gasifier}_{SGP}$	1	1	0	1	1	1	1	1	1
	$b^{gasifier}_{SCGP}$	0	0	1	0	0	0	0	0	0
	b^{SMR}	0	0	0	1	0	0	1	1	0
	b^{WGS}	1	1	1	0	1	1	1	1	1
	b^{GTC2}	1	1	0	1	1	1	1	1	1
	$b^{boiler.hi}$	0	0	0	0	0	0	0	0	0
	$b^{boiler.lo}$	1	1	1	1	1	1	1	1	1
	b^{MEA}	0	0	0	0	0	0	0	0	0
SCO specifications	M^{SCO} (tonne h^{-1})	566.5	610.5	605.9	610.5	610.5	610.5	610.5	610.5	610.5
	API^{SCO}	31.0	31.0	31.9	31.0	31.0	31.0	31.0	31.0	31.0
	xm^{SCO}_{NPH} (%)	12.2	11.4	15.6	11.4	11.4	11.4	11.4	11.4	11.4
	xm^{SCO}_{LGO} (%)	50.9	54.5	45.1	54.5	54.5	54.5	54.5	54.5	54.5
	xm^{SCO}_{HGO} (%)	36.8	34.2	34.2	34.2	34.2	34.2	34.2	34.2	34.2
Utilities consumptions	W^{net} (GW)	1.94	1.78	0.05	1.95	1.78	1.76	1.96	1.96	1.76
	$M^{total.NG}$ (tonne h^{-1})	187.1	187.0	57.7	218.9	187.0	187.0	252.7	252.2	187.0
	$M^{total.FW}$ (tonne h^{-1})	382.7	365.8	394.0	337.2	371.5	385.9	490.4	489.0	385.9
Economic terms	$CAPEX$ (\$MM)	2108.9	1816.7	1281.3	1946.5	1816.8	1822.4	2114.9	2112.7	1822.4
	$OPEX$ (\$MM yr^{-1})	279.8	286.3	286.7	286.3	286.3	286.3	286.3	286.3	286.3
	$Purchases$ (\$MM yr^{-1})	1648.1	1647.4	1091.2	1216.8	1162.6	1162.7	938.2	938.0	912.4
	$Commodities$ (\$MM yr^{-1})	3093.0	2202.7	1129.8	3181.3	2202.8	1608.8	3194.1	2311.4	1608.8
	$Carbon\ tax$ (\$MM yr^{-1})	162.2	129.8	40.6	183.4	129.9	118.3	136.4	136.6	118.3
CCS	$M^{CO2.emitter}$ (tonne h^{-1})	720.7	577.1	180.6	815.3	577.2	525.7	606.4	606.9	525.7
	$M^{CO2.captured}$ (tonne h^{-1})	141.3	152.4	219.2	0.0	152.4	203.8	299.8	297.9	203.8
	$\frac{M^{Oxyfuel}}{M^{Oxyfuel}+M^{Post.comb}}$ (%)	0.0	0.0	0.0	0.0	0.0	0.0	0.0	0.0	0.0

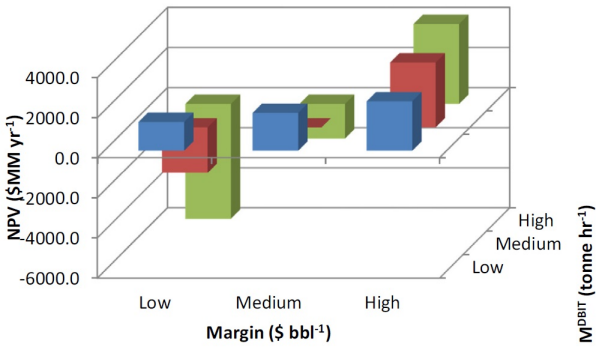

Figure 3.15: Comparison of optimal NPVs for different margins and capacities

Table 3.3 presents optimal solutions of this section. Like the previous section, NPVs, natural gas consumptions and their distributions, and captured carbon are compared with each other and demonstrated in Figures 3.15-3.17. The following observations are made:

- With respect to unit selection, the optimal solutions are very similar to Section 3.5.1. The WGS, and gas turbine–2 are selected for all the scenarios, while the high–quality boiler and MEA units are not chosen at all. The hydrocracker is more favorable except for only one case (scenario 3). The SMR and low–quality boiler are selected interchangeably as well. The results verify higher efficiency of the hydrocracking, WGS, and gas turbine–2 for the upgrading, CCS,and power and heat generation, respectively.

- The highest NPV of solutions occurs when the margin and capacity are both large (scenario 9) and the lowest NPV belongs to the small margin and large capacity (scenario 7). As it can be seen, the best and worst NPVs are both for the large capacity of upgrading plant (see Figure 3.15). Hence, it can be concluded that the large capacity upgrader is more dependent and vulnerable to the margin, and small capacity upgrader has less NPV changes over DilBit and SCO prices fluctuations.

- The natural gas consumptions for plants are nearly constant,and it seems that the carbon tax restrains consumption of the major source of CO_2 emissions. Additionally, the SMR and low–quality boiler are used alternatively, like Section 3.5.1. The reason behind this occurrence was discussed in Section 3.5.1.

- Concerning carbon capturing, the WGS unit is under operation for all the scenarios and post–combustion treatment is not selected like before. Moreover, for the first time, the oxyfuel combustion method is chosen for the carbon capture in the scenario 1, and 11.1% of natural gas is burned with pure oxygen. According to Figure 3.17, the margin between DilBit and SCO prices does not have any influence on the mass flow rate of captured CO_2. On the other hand, the higher the capacity, the larger the amount of CO_2 capturing.

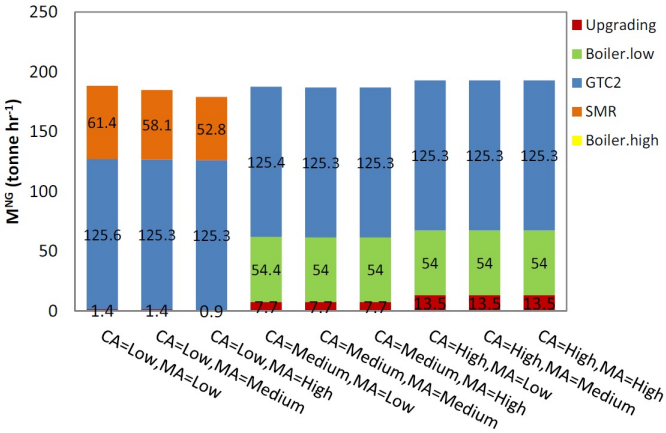

Figure 3.16: Comparison of natural gas consumptions for different margins and capacities

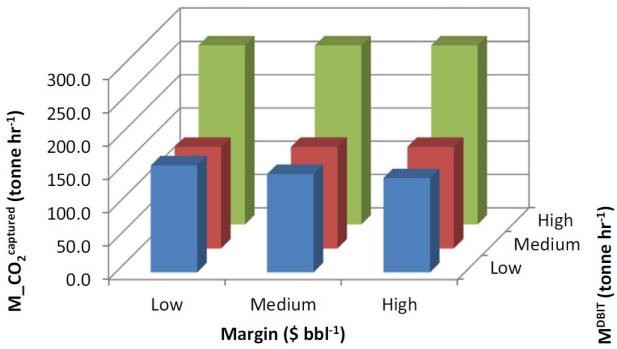

Figure 3.17: Comparison of captured carbon for different margins and capacities

Table 3.3: Effects of margin between DilBit and SCO prices for different upgrading plant capacities when carbon tax is \$30 per tonne of CO_2

	Scenario	1	2	3	4	5	6	7	8	9
	CC^{SCO} (\$ bbl^{-1})	80.32	80.32	80.32	80.32	80.32	80.32	80.32	80.32	80.32
	CC^{DilBit} (\$ bbl^{-1})	73.76	62.88	47.35	73.76	62.88	47.35	73.76	62.88	47.35
	M^{DBIT} (tonne h^{-1})	150	150	150	850	850	850	1500	1500	1500
	NPV (\$MM yr^{-1})	1439.3	1891.0	2468.2	-2275.8	-4.2	3233.3	-5728.8	-1726.2	3987.1
Decision variables	$b^{gasifier}_{SGP}$	1	1	0	1	1	1	1	1	1
	$b^{gasifier}_{SCGP}$	0	0	1	0	0	0	0	0	0
	b^{SMR}	1	1	1	0	0	0	0	0	0
	b^{WGS}	1	1	1	1	1	1	1	1	1
	b^{GTC2}	1	1	1	1	1	1	1	1	1
	$b^{boiler.hi}$	0	0	0	0	0	0	0	0	0
	$b^{boiler.lo}$	0	0	0	1	1	1	1	1	1
	b^{MEA}	0	0	0	0	0	0	0	0	0
SCO specifications	M^{SCO} (tonne h^{-1})	96.8	98	98	610.5	610.6	610.5	1077.4	1077.4	1077.4
	API^{SCO}	31.1	31.1	33.6	31	31	31	31	31	31
	xm^{SCO}_{NPH} (%)	12.8	12.6	20.0	11.4	11.4	11.4	11.4	11.4	11.4
	xm^{SCO}_{LGO} (%)	49.6	50.2	42.1	54.5	54.5	54.5	54.5	54.5	54.5
	xm^{SCO}_{HGO} (%)	37.6	37.2	37.8	34.2	34.2	34.2	34.2	34.2	34.2
Utilities consumptions	W^{net} (GW)	1.87	1.86	1.83	1.78	1.78	1.78	1.79	1.79	1.79
	$M^{total.NG}$ (tonne h^{-1})	188.3	184.8	179.0	187.5	187.0	187.0	192.8	192.8	192.8
	$M^{total.FW}$ (tonne h^{-1})	159.7	154.1	148.7	368.2	366.2	365.8	645.5	645.5	645.5
Economic terms	$CAPEX$ (\$MM)	1333.2	1300.1	1276.0	1817.1	1816.7	1816.7	2403.4	2403.4	2403.4
	$OPEX$ (\$MM yr^{-1})	69.6	69.8	70.4	286.3	286.3	286.3	486.1	486.1	486.1
	$Purchases$ (\$MM yr^{-1})	885.6	796.6	668.4	3506.5	3036.4	2366.5	5951.8	5123.6	3941.5
	$Commodities$ (\$MM yr^{-1})	1560.8	1560.0	1546.4	3743.2	3742.6	3742.6	5783.7	5783.7	5783.7
	$Carbon\ tax$ (\$MM yr^{-1})	94.3	94.2	92.6	130.2	129.8	129.8	146.3	146.3	146.3
CCS	$M^{CO2.emitter}$ (tonne h^{-1})	419.0	418.8	411.4	578.5	577.1	577.1	650.1	650.1	650.1
	$M^{CO2.captured}$ (tonne h^{-1})	160.3	147.4	141.5	152.4	152.4	152.4	268.9	268.9	268.9
	$\frac{M^{Oxyfuel}}{M^{Oxyfuel}+M^{Post.comb}}$ (%)	11.1	0.0	0.0	0.0	0.0	0.0	0.0	0.0	0.0

3.5.4 Effects of carbon tax

In this section, effects of different carbon taxes and capacities on optimal design of the upgrading plant and integrated utility system are presented. While the current set value for the carbon tax is \$30 per tonne of CO_2, \$10 and \$50 per tonne of CO_2 are also considered as low and high values for the carbon tax, respectively. In Alberta, carbon tax of \$15 per tonne of CO_2 was enacted in 2007 for the first time. To consider a little more extreme case, the lower value of carbon tax is set to \$10 per tonne of CO_2 in this Chapter [83]. The upper value of this parameter is unknown and it is dependent of future policies, and hence a value with the same difference between the current and lower values is set, \$50 per tonne of CO_2. The carbon tax is a cost–effective way to mitigate CO_2 emissions causing climate change. The higher the carbon tax, the more environmental friendly the plant would be. Note that, the capacity of upgrading plant is fixed at 850 tonne h^{-1}.

Table 3.4 reports optimal solutions of this section. Comparison of NPVs, natural gas consumptions and their distributions, and captured carbon are demonstrated in Figures 3.18-3.20. The following remarks can be concluded:

- The hydrocracking and gas turbine–2 are under operation for all the scenarios, while the thermocracking, high–quality boiler,and MEA units are not selected at all. Moreover, the SMR and low–quality boiler are employed alternatively (except the scenario 4 in which both of them are used). When the carbon taxis low and the capacity is low or medium, none of the capturing technologies is required

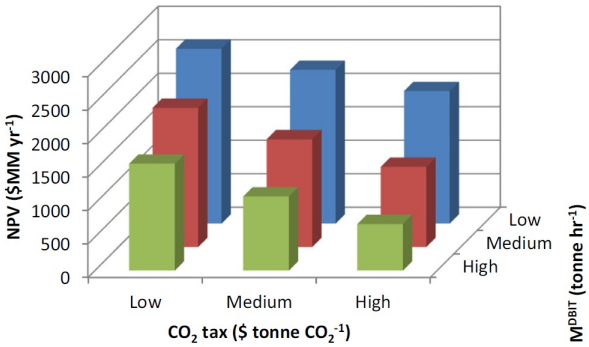

Figure 3.18: Comparison of optimal NPVs for different carbon taxes and capacities

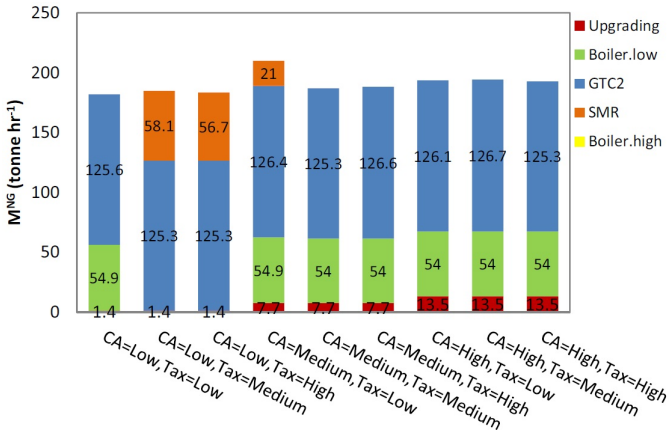

Figure 3.19: Comparison of total natural gas consumptions for different carbon taxes and capacities

to be used. Nevertheless, for large capacities or non–low carbon tax, only the WGS is chosen in the optimal schemes.

- According to Figure 3.17, the highest NPV belongs to the scenario 1 in which the carbon tax and upgrading plant are both low. Since all the scenarios are based on the current low margin between DilBit and SCO, the small capacity upgrader has more economic justification. Furthermore, carbon tax has a negative effect on the optimal NPVs.

- The optimal plants have approximately the same amount of total natural gas consumptions again. For all the scenarios (except scenario 4), the SMR and low–quality boiler are under operation alternatively.

- Regarding the carbon capturing, when the capacity is not large to produce massive amount of CO_2 and the carbon tax is low (scenarios 1 and 4), there is no need for any carbon capturing. For the rest of the scenarios, the WGS unit is found efficient like before. According to Figure 3.20, increasing the capacity of upgrading plant leads to more carbon capturing too.

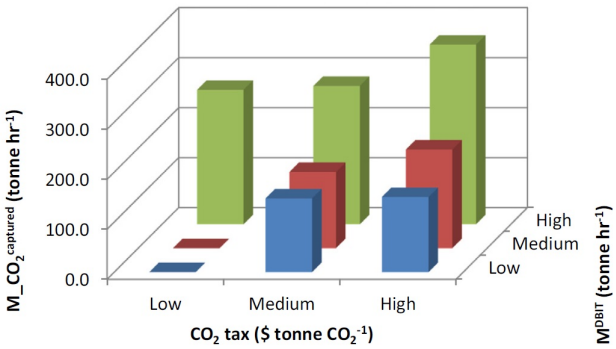

Figure 3.20: Comparison of captured carbon for different carbon taxes and capacities

Table 3.4: Effects of carbon tax for different upgrading plant capacities

	Scenario	1	2	3	4	5	6	7	8	9
	Carbon tax ($ tonne of CO_2^{-1})	10	30	50	10	30	50	10	30	50
	M^{DBIT} (tonne h^{-1})	150	150	150	850	850	850	1500	1500	1500
	NPV ($MM yr^{-1})	2612.9	2294.3	1978.3	2078.1	1609.98	1196.2	1594.7	1105.7	693.8
Decision variables	$b_{SGP}^{gasifier}$	1	1	1	1	1	1	1	1	1
	$b_{SCGP}^{gasifier}$	0	0	0	0	0	0	0	0	0
	b^{SMR}	0	1	1	1	0	0	0	0	0
	b^{WGS}	0	1	1	0	1	1	1	1	1
	b^{GTC2}	1	1	1	1	1	1	1	1	1
	$b^{boiler.hi}$	0	0	0	0	0	0	0	0	0
	$b^{boiler.lo}$	1	0	0	1	1	1	1	1	1
	b^{MEA}	0	0	0	0	0	0	0	0	0
SCO specifications	M^{SCO} (tonne h^{-1})	98.0	98.0	95.4	610.5	610.5	610.5	1077.4	1077.4	1077.4
	API^{SCO}	31.0	31.0	31.1	31.0	31.0	31.0	31.0	31.0	31.0
	xm_{NPH}^{SCO} (%)	12.5	12.5	12.7	11.4	11.4	11.4	11.4	11.4	11.4
	xm_{LGO}^{SCO} (%)	49.9	49.9	49.5	54.5	54.5	54.5	54.5	54.5	54.5
	xm_{HGO}^{SCO} (%)	37.6	37.6	37.8	34.2	34.2	34.2	34.2	34.2	34.2
Utilities consumptions	W^{net} (GW)	1.81	1.86	1.86	1.91	1.78	1.76	1.80	1.79	1.75
	$M^{total.NG}$ (tonne h^{-1})	181.8	184.7	183.3	210.0	187.0	188.3	193.6	194.3	192.8
	$M^{total.FW}$ (tonne h^{-1})	55.5	154.1	154.8	355.4	371.5	385.8	684.1	650.4	681.0
Economic terms	$CAPEX$ ($MM)	1063.8	1299.6	1308.3	1906.5	1816.8	1823.0	2403.5	2405.6	2412.1
	$OPEX$ ($MM yr^{-1})	69.7	69.7	69.2	286.3	286.3	286.3	486.1	486.1	486.1
	$Purchases$ ($MM yr^{-1})	459.7	465.9	463.4	1201.8	1162.6	1164.9	1818.5	1819.3	1817.1
	$Commodities$ ($MM yr^{-1})	1282.2	1312.6	1308.0	2282.8	2202.8	2191.6	3068.4	3064.7	3042.8
	$Carbon\ tax$ ($MM yr^{-1})	41.8	94.2	156.6	59.4	129.9	200.9	48.9	145.3	209.8
CCS	$M^{CO2.emitter}$ (tonne h^{-1})	558.0	418.7	417.5	791.5	577.2	535.7	652.2	646.0	559.4
	$M^{CO2.captured}$ (tonne h^{-1})	0.0	147.4	150.2	0.0	152.4	197.2	268.9	276.9	359.6
	$\frac{M^{Oxyfuel}}{M^{Oxyfuel}+M^{Post.comb}}$ (%)	0.0	0.0	0.0	0.0	0.0	0.0	0.0	0.0	0.0

Table 3.5: Input design parameter for the sensitivity analysis

Parameter	Minimum	Average	Maximum
CC^{EL} (\$ kWh^{-1})	0.037	0.081	0.141
$CC^{SCO} - CC^{DilBit}$ (\$ bbl^{-1})	6.56	17.44	32.97
CC^{NG} (\$ MJ^{-1})	0.00104	0.00477	0.012
M^{DBIT} (tonne h^{-1})	150	850	1500
Carbon tax (\$ tonne of CO_2)	10	30	50

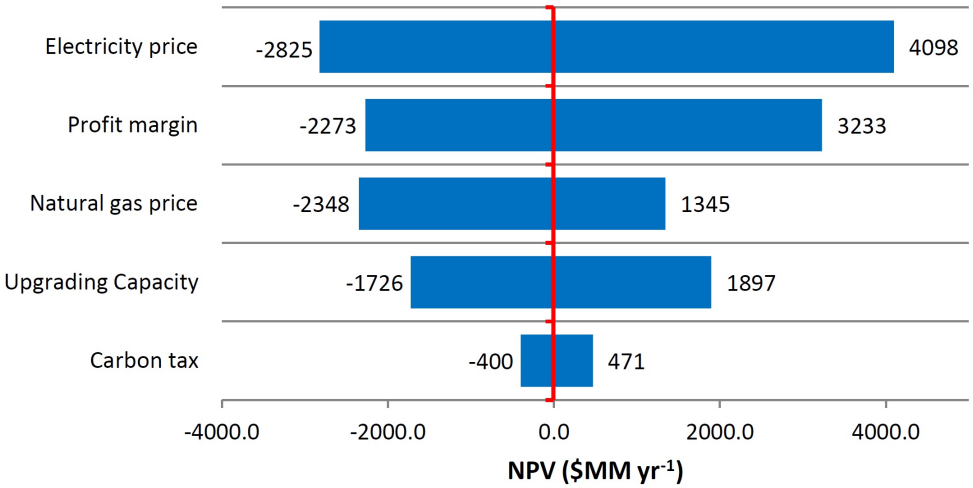

Figure 3.21: NPV sensitivity analysis based on tornado plot

3.5.5 NPV sensitivity analysis

In this section, a sensitivity analysis is presented. The studied design parameters are those that were presented in previous sections: (1) electricity price, (2) profit margin (the difference between SCO and DilBit price), (3) natural gas price, (4) upgrading plant capacity, and (5) carbon tax. The ranges of variations are provided in Table 3.5. A comparison among all these design parameters is provided here to demonstrate the sensitivity of NPV with respect to the variation of them.

Tornado plot is used to identify the inputs with the largest influence on the output uncertainty. According to Figure 3.21, electricity price is the main source of uncertainty due to its wide range and significant effect on NPV as a valuable selling commodity. Similarly, the profit margin has direct impacts on the NPV as the other selling commodity ranking it as the second source of uncertainty. The natural gas price and upgrading plant capacity are respectively the third and fourth effective design parameters with similar effects on the NPV. Lastly, the carbon tax is the least design parameter with an insignificant effect on the output uncertainty.

3.6 Conclusion

Based on the optimal solutions of different scenarios, the key findings of this study can be stated as followings. Firstly, Incorporating the carbon mitigation policy in the modeling led to less NPVs compared to the similar scenario without carbon capturing. Secondly, During the bitumen upgrading, the hydrocracking process was favored over thermocracking for most of the scenarios. Thirdly, Producing extra power with burning natural gas in a gas turbine was highly beneficial except one scenario in which the electricity price was low and the natural gas price was high. Moreover, the following HRSG unit after the gas turbine could generate enough high–quality duty and make the high–quality duty boiler unnecessary for all the scenarios. Fourthly, Among the CCS technologies, pre–combustion one was found the most efficient. In this approach, the produced syngas passes through the WGS and Selexol units. The MEA unit, which was the studied post–combustion approach, was not picked out for any of defined scenarios. The other option (oxyfuel combustion) was chosen only for one scenario in which natural gas was burned in the presence of pure oxygen. Fifthly, Two units of low–quality duty boiler and SMR were under operation alternatively for most of the scenarios. When the capacity was low, the SMR was preferred over the boiler. On the other hand, the low–quality duty boiler was found more beneficial for medium and high upgrading capacities. Note that, both of these units were selected when the margin between electricity and natural gas prices are large enough in order to generate more electricity. Sixthly, Since the margin between DilBit and SCO price is currently low,investing on large upgrading plant is not an economical decision. Large capacity upgraders may benefit more when the margin is adequately large. However, it was observed that they were more vulnerable to changes of the economic terms. On the other hand, small capacity upgrader was less beneficial but more robust to fluctuations of fossil fuels prices.

There is a contradiction between the optimal solutions of the previous two Chapters. In Chapter 2, it was found that the optimal upgrading technology is thermocracking; however, the results from Chapter 3 showed that the opposite technology is more efficient: hydrocracking. While there are widely used in industry (thermocracking has a higher share of 57%), they both have some advantages and disadvantages. Namely, thermocracking processes (i) have less capital cost as there is no need for hydrogen generation, (ii) have a lower production yield. Another important factor in the switching from thermocrackers into hydrocrackers can be the carbon capture. When the carbon tax was imposed, the pre–combustion technology was selected to reduce carbon emissions as well. The combination of pre–combustion and hydrogen production by means of syngas is a proven technique to increase the efficiency, and hence, this change in the optimal configuration is reasonable.

Chapter 4

Modeling and Optimization of the Upgrading and Blending Operations of Oil Sands Bitumen[1]

4.1 Introduction

The research on oil sands upgrading optimization is very limited. Nonetheless, a lot of attention has been paid to conventional refinery optimization. For instance, Leiras et al. reviewed refinery planning at different levels (strategic, tactical, or operational) and at different oil chain segments (upstream, midstream, or downstream) [84]. Key issues, advances, and future opportunities for scheduling, planning, and supply chain management of oil refinery operations were also discussed in another study [85]. Regardless of the optimization case study, formulating an appropriate and accurate model is the most essential step. Pinto and Moro modeled typical refinery process units [86] and presented a general modeling framework for the operational planning of petroleum supply chains, including processing unit, tank, and pipeline [87]. Later on, they extended their study to multiperiod and uncertain case for production planning of petroleum refineries [88]. It should be highlighted that it is difficult to apply a rigorous mechanistic model in refinery planning and operating optimization. The reason is that the mechanistic modeling makes the optimization problem too complex. Therefore, simplified models have been widely used, such as (i) empirical correlations for estimation of different product properties [89, 90, 91], (ii) swing cut approach for distillation units [89, 90, 92, 93], or (iii) artificial neural network [94, 95]. These types of equations can be expressed as linear or nonlinear equations.

An interesting research field has been on crude oil scheduling and allocation optimization. The scheduling part addresses unloading crude oils into storage tanks from ships or tankers, depending upon topology of the case study, arriving at different times. The allocation part focuses on sending feeds with various rates over time to the distillation columns. The crude oil unloading, storing, and processing in a marine–access refinery was studied by Reddy et al [96]. Simultaneous solving of oil quality, transfer quantity, tank allocation, and oil blending were addressed on the basis of a novel MILP solution algorithm. Mendez et al. proposed an integrated MILP–based approach to optimize off–line blending and scheduling of a refinery at the same

[1] A version of this chapter was published in the *Energy Fuels*, **2016**, *30*, 5202–5213

time [97]. To avoid a MINLP problem, an iterative procedure was presented that could be applied to both discrete and continuous time formulations. Numerical comparisons demonstrated that the proposed approach can converge to the same solutions but faster as a result of linearization. Li et al. worked on the gasoline blending recipe and scheduling decisions [98]. A slot–based continuous–time MILP formulation was developed for an integrated recipe, specification, blending, and storage problem. Several real–life operating features and policies were included in the model.

Refinery planning optimization has been another interesting subject in process system engineering. During planning optimization, finding the optimal flow rates of streams is the main purpose. These variables might be independently defined or might be specified as a function of operating conditions of associating units. Blending rules can also be incorporated into the model, wherever it is necessary. One of the first attempts in this area was carried out by Alhajri et al [89]. Their proposed model estimated product properties of crude distillation unit (CDU) and fluid catalytic cracking (FCC) unit when the independent variables were the cut–point temperatures and conversion, respectively. To meet the market specifications for commodities, some constraints and blending rules were imposed in addition to the product demands. Afterward, a robust optimization methodology was used [99]. When flow rates were independent variables in this study, uncertainties in costs, prices, commodity demands, and product yields were addressed. However, this approach was only implemented for a small case study, and its capability to solve real cases is unknown. Moreover, effects of operating variables, such as pressure and temperature, were not taken into account. In another work, Guerra et al. first developed nonlinear empirical models for CDU and FCC process units [90]. They then implemented those models in a NLP problem for a small case (with only the presence of CDUs) and a medium case (with the presence of CDUs and FCC) [100]. The empirical models related the properties, yield, flow rate, etc. of each unit outlet to the operating conditions.

The presented literature review reveals that studies have mainly focused on conventional refinery operation optimization and there have been limited contributions to oil sands operation optimization. Furthermore, the existing studies of oil sands operations have some limitations. First, the only commodity in these studies was assumed to be sweet SCO, and the other alternatives were neglected. Second, the operating conditions of process units were fixed, and hence, specification (such as nitrogen and sulfur contents) changes were not considered. To address these limitations, a new framework is proposed in this Chapter for simulation–based modeling and optimization of the upgrading plant with multiple bitumen blend and SCO product alternatives.

This Chapter is organized as follows: Section 4.2 describes the simulation of upgrading plants with Aspen HYSYS. Section 4.3 presents statistical analysis, which is used to generate correlations of different properties for each unit. Section 4.4 presents the formulation of operation optimization for upgrading plants being composed of the process models, commodity specification constraints, and objective function. The nomenclature of presented model is available in Appendix A. The solution strategy is also given in this section to explain how the global optimal point can be found. Three different examples are studied in section 4.5 to check the performance of proposed approach. Concluding remarks are given in the last section.

Table 4.1: General specifications for the simulated bitumen upgrading plant

Feed property[101, 102]		ADU[101, 58]		Cut point (°C) [101]		VDU[101, 58]	
temperature (°C)	67	top pressure (kPa)	120	NPH	40-180	top pressure (kPa)	2
pressure (kPa)	101.3	bottom pressure (kPa)	140	LGO	180-360	bottom pressure (kPa)	5
flow rate (kg h^{-1})	385500	NPH recovery (%)	90	HGO	360-540		

4.2 Process simulation

The upgrading process simulation with Aspen HYSYS is discussed in this section. In this Chapter, instead of using rigorous mechanistic models of bitumen upgrading units, empirical regression models are identified for operation optimization. Note here, R–squared is employed to measure the accuracy of the regression model. Deriving the correlations requires a large amount of sample data of each unit at different operating conditions. In this study, operating units are first simulated with Aspen HYSYS, version 8.4, and most of the parameters and assumptions are taken from references [101] and [102]. In the following paragraphs, the simulation procedure is discussed.

The first step of the simulation is defining the available components. There might be more than 1000 distinctive components in the bitumen mixture; therefore, finding the information for all of the existing components would be time–consuming. Another alternative for the simulation of bitumen has been applying hypothetical components. To do so, assay properties are imported from experimental results to the simulator, namely, specific gravity, viscosity, molecular weight, sulfur content, nitrogen content, etc [103]. Necessary experiments for data collection of western Canadian bitumen sample have also been carried out in two works [104, 105]. In the Aspen HYSYS environment, many assays have been predefined [106, 107]. In this study, Cold Lake blend–2011 (which represents a typical diluted bitumen product in Alberta) is used for the simulation of bitumen upgrading plant. As recommended by the software guideline, the Peng–Robinson thermodynamic package is also selected as the equation–of–state package [106].

The next step is adding operating units into the simulation environment and connecting them together. The simulating facility is for the sweet SCO production (see Figure 4.1) [101, 102, 58, 108]. The ADU is used first to separate the diluent from the feed. Afterward, a VDU is applied for separation of the original petroleum mixture into light ends, NPH, LGO, HGO, and vacuum residue. While separated, NPH, LGO, and HGO are then sent to their respective hydrotreaters and the vacuum residue undergoes the Canmet slurry hydrocracker, in which large molecules with high molecular weights are fractioned into smaller molecules with lower molecular weights and boiling points [101, 102]. Afterward, the hydrocracker lighter products are separated into NPH, LGO, and HGO again and hydrotreated. Moreover, the hydrocracker residue is recycled to the hydrocracker to reach higher efficiency (conversion rate). Auxiliary units, including pumps, heaters, and coolers, are also considered for pressure and temperature or phase changes.

To provide some perspective about the upgrading plant, feed operating conditions, specifications of atmospheric and vacuum distillation units, and cut point ranges of different intermediate products are reported in Table 4.1.

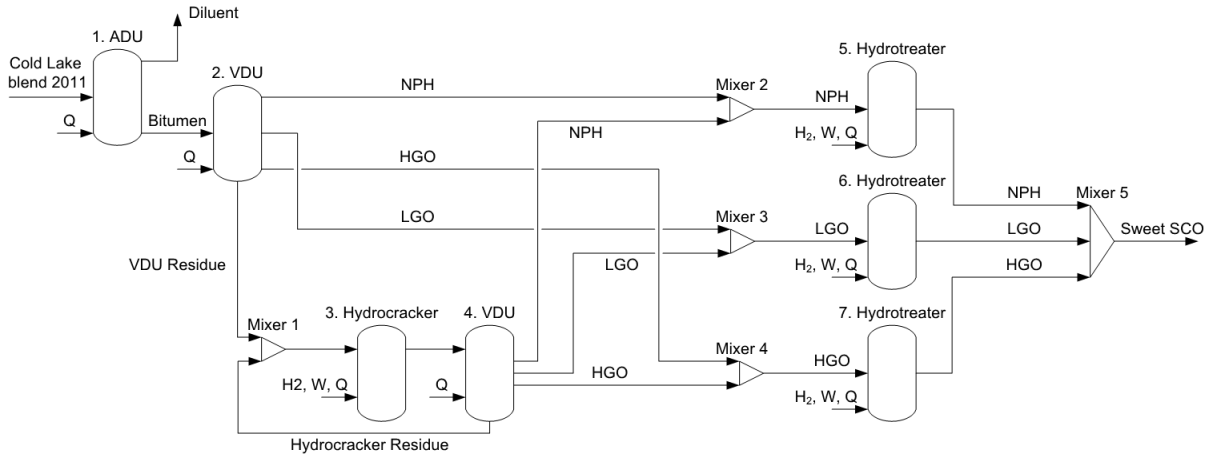

Figure 4.1: Process flow diagram of upgrading plant simulation

4.3 Correlation modeling

In this section, the procedure for generating the correlation models of process units is explained. Basically, the empirical models are developed to replace the rigorous mechanistic model, including kinetic and equilibrium relations and mass and energy balances. The correlations try to estimate the yield and properties of outlet streams based on operating conditions, such as the temperature, pressure, liquid hourly space velocity (LHSV), and cut point of NPH, LGO, and HGO. The important properties include the yield of products, specific gravity, viscosity, sulfur content, and nitrogen content of streams. Hence, five correlations should be determined for each outlet stream of each unit. The process units that need correlations are the separators (ADU and VDU) and reactors (hydrocracker and hydrotreaters).

For distillation units, the petroleum distillation column module is chosen for the simulation, in which the cut points of withdrawing streams are the independent operating variables. The pressure is assumed to be fixed for both ADU and VDU [101, 102]. The variables are known as effective cut point (ECP) in the Aspen HYSYS environment. It should be noted here, when there are p withdraws in P set, only the p and $(p+1)$ ECPs are effective on the properties of the pth withdraw. For example, the specific gravity of withdraws can be formulated as

$$SG_p = f(ECP_p, ECP_{p+1}) \quad \forall p \in P \tag{4.1}$$

where SG is the specific gravity and P is the set of VDU products, which includes NPH, LGO, and HGO. In addition, empirical equations were found from the literature [43] for steam requirement of ADU and VDU based on their inlet mass flow rate. The corresponding operating costs of separation units are incorporated into the optimization problem.

$$M_{ADU}^{steam} = 0.30 \cdot M_{in} \tag{4.2}$$

$$M_{VDU}^{steam} = 0.07 \cdot M_{in} \tag{4.3}$$

For the hydrocracking unit, petroleum shift reactor and petroleum distillation column modules are selected [101, 102]. These modules are incorporated with a spreadsheet to manually tune some outlet properties (i.e., yield and sulfur and nitrogen distributions) with available correlations from the literature. For example, the conversion rate of the residue in the hydrocracker, hydrodesulfurization (HDS), and hydrodenitrogenation (HDN) are given as follows:

$$CR_u^{residue} = 1 - \left[1 + k_A \cdot (P_{H_2})^{\beta} \cdot \frac{V \cdot (1-\epsilon)}{V_{AB_0}}\right]^{-1} \quad u = hydrocracker \tag{4.4}$$

$$CR_u^{HDS} = a + b \cdot CR_u^{residue} + c \cdot (CR_u^{residue})^2 \quad u = hydrocracker \tag{4.5}$$

$$CR_u^{HDN} = ratio^{HDN/HDS} \cdot CR_u^{HDS} \quad u = hydrocracker \tag{4.6}$$

where k_A, β, ϵ, a, b, c, and $ratio^{HDN/HDS}$ are all reported in references [101, 102].

Sulfur distribution in the outlets of the hydrocracker is expressed as

$$\gamma_p = a_p \cdot ln(CR_u^{residue} + d_p) + b_p \cdot CR_u^{residue} + c_p \cdot (CR_u^{residue})^2 \quad \forall p \in P, u = hydrocracker \tag{4.7}$$

where a_p, b_p, c_p, and d_p are available in the previous articles [100, 101]. The temperature, pressure, and LHSV are the variables for the hydrocracker, and ECPs are the variables for the VDU. During hydrocracking, breakup of large hydrocarbon chains into new lighter compounds is only taken place and there is no separation of lighter products at this stage. Therefore, we cannot develop desired correlations for each NPH, LGO, and HGO. Because these three products are separated through the following VDU, it would be better to present correlations of these two units as a single one. Note here that the simulations of these units are carried out separately, and it is just assumed that they are united during generation of empirical models. By this way, each property can be formulated on the basis of operating variables for each product; however, the number of variables is larger than a single unit

$$SG_{u,p} = f(T_u, P_u, LHSV_u, ECP_p, ECP_{p+1}) \quad \forall p \in P, u = hydrocracker \tag{4.8}$$

where the index of the hydrocracker for u represents the hydrocracker and its associated VDU.

For hydrotreaters, hydrodesulfurization and hydrodenitrogenation are the main reactions taking place with catalysts. Conversion rates of these two reactions were studied through experiments, and corresponding correlations were proposed for NPH–hydrotreater [109], LGO–hydrotreater [110], HGO–hydrotreater [111, 112]. The following empirical models are used for hydrodesulfurization and hydrodenitrogenation of NPH–hydrotreater, LGO–hydrotreater, and HGO–hydrotreater (given in Equations 4.9 and 4.10, Equations 4.11 and 4.12, and Equations 4.13 and 4.14, respectively).

$$CR_u^{HDS} = 1 - exp(k^{HDS} \cdot P^{\beta^{HDS}} / LHSV^{\alpha^{HDS}}) \quad u = NPH \tag{4.9}$$

$$CR_u^{HDN} = 1 - exp(k^{HDN} \cdot P^{\beta^{HDN}} / LHSV^{\alpha^{HDN}}) \quad u = NPH \tag{4.10}$$

$$\begin{aligned} CR_u^{HDS} =& 97.82 + 2.62 \cdot T_u - 0.87 \cdot P_u - 2.46 \cdot LHSV_u \\ & - 1.76 \cdot T_u^2 - 2.79 \cdot LHSV_u^2 + 1.53 \cdot T_u \cdot LHSV_u \quad u = LGO \end{aligned} \tag{4.11}$$

$$\begin{aligned} CR_u^{HDN} =& 97.63 + 4.45 \cdot T_u + 0.95 \cdot P_u - 5.87 \cdot LHSV_u - 4.57 \cdot T_u^2 \\ & - 2.08 \cdot P_u^2 - 4.44 \cdot LHSV_u^2 + 4.68 \cdot T_u \cdot LHSV_u \quad u = LGO \end{aligned} \tag{4.12}$$

$$\begin{aligned} CR_u^{HDS} =& 110.97 + 3.15 \cdot T_u - 31.04 \cdot LHSV_u - 3.09 \cdot P_u + 9.41 \cdot T_u \cdot LHSV_u \\ & 0.70 \cdot T_u \cdot P_u + 3.15 \cdot LHSV_u \cdot P_u - 2.87 \cdot T_u^2 + 8.01 \cdot LHSV_u^2 + 3.77 \cdot P_u^2 \quad u = HGO \end{aligned} \tag{4.13}$$

$$\begin{aligned} CR_u^{HDN} =& 124.14 + 37.04 \cdot T_u - 95.96 \cdot LHSV_u + 3.02 \cdot P_u - 6.13 \cdot T_u \cdot LHSV_u \\ & 6.25 \cdot T_u \cdot P_u + 4.77 \cdot LHSV_u \cdot P_u + 3.08 \cdot T_u^2 + 26.05 \cdot LHSV_u^2 + 2.55 \cdot P_u^2 \quad u = HGO \end{aligned} \tag{4.14}$$

For the hydrotreaters, the remaining properties are developed from the simulation results obtained from Aspen HYSYS. Note that here, correlations are based on changes of each term instead of the actual value.

$$\Delta SG_u = f(T_u, P_u, LHSV_u) \quad \forall u \in U \backslash \{hydrocracker\} \tag{4.15}$$

For the hydrocracker and each hydrotreater, hydrogen is also added and its flow rate was estimated in reference [101] (see Equations 4.16 and 4.17).

$$H_u = 2000 \cdot CR_u^{residue} \quad u = hydrocracker \tag{4.16}$$

$$H_u = f(F_u) \quad \forall u \in U \backslash \{hydrocracker\} \tag{4.17}$$

Furthermore, before the operating units, pumps and heaters are installed to adjust the temperature and pressure. The required work for a pump is mainly a function of the flow rate and pressure (Equation 4.18), and the required duty of a heater is dependent on the flow rate and temperature (Equation 4.19).

$$W_u = f(P_u, F_u) \quad \forall u \in U \tag{4.18}$$

$$Q_u = f(T_u, F_u) \quad \forall u \in U \tag{4.19}$$

where F is the mass flow rate and U is the process unit set, which includes the hydrocracker and NPH, LGO, and HGO hydrotreaters.

After identification of important properties and their related operating variables, simulations should be performed at different operating conditions to have enough samples for correlation generation. The first step is determining a valid range for each independent variable. Independent variables of each unit and their ranges (x_{min} and x_{max}) are provided in Table 4.2. For the ECPs, beginning and ending boiling point

Table 4.2: Operating variables to be optimized and the corresponding ranges

			Hydrotreater		
Variable	VDU [101]	Hydrocracker [101]	NPH [109]	LGO [57]	HGO [57]
temperature (°C)		420-480	260-280	330-350	350-370
pressure (MPa)		10-18	3-5	6.9-12.4	6.1-10.2
LHSV (h^{-1})		0.2-1	1-2	0.5-2	0.5-2
ECP_1 (°C)	30-50	30-50			
ECP_2 (°C)	170-190	170-190			
ECP_3 (°C)	250-370	250-370			
ECP_4 (°C)	530-550	530-550			

temperatures of each product are subtracted and added by 10 °C, respectively. The pressure, temperature, and LHSV ranges of reactors are adopted from the literature at which the obtained correlations are valid.

For the VDUs, three levels of variation are selected for each ECP. When each product is only dependent upon two consecutive ECPs, the total number of simulations is 9 (= 3 × 3) and the full factorial method is adopted for the design of simulations. For the NPH–hydrotreater, three levels of variation are selected for the pressure and LHSV and four levels of variation are assigned for the temperature as a result of its wider range. As a result, the total number of simulations is 36 (= 3 × 4 × 3) and the full factorial method is chosen again for the design of simulations. For the LGO–hydrotreater and HGO–hydrotreater, four levels of variation are selected for all variables, owing to their wider range of changes. The full factorial method is still the best choice for the design of simulations because the total number of simulations is still not too large (64 = 4 × 4 × 4).

For the hydrocracking part, as explained before, we integrate the hydrocracker and its separator into one unit for the correlation development. Hence, the number of variables for the estimation of each product property is five (temperature, pressure, LHSV, and two ECPs). Furthermore, five levels of variation are assumed for the temperature; four levels of variation are used for the pressure and LHSV; and three levels of variation are adopted for ECPs. A full factorial design leads to 720 (= 5 × 4 × 4 × 3 × 3) simulations, which is time–consuming. Therefore, the Latin hypercube sampling method is used to narrow the number of experiments to only 10% of actual ones. The existence of a recycle stream from the second VDU to the hydrocracker (see Figure 4.2) makes the developed correlations for this unit less accurate than others. Full factorial analysis was carried out for this unit first but with fewer levels for the ECPs. Nevertheless, the results were not more accurate. Therefore, where enhancing the accuracy of correlations was not feasible for this unit, the number of simulation runs is tried to be as less as possible to at least reduce the computational time.

After conducting the designed simulations at different operating conditions, the data are exported to Design–Expert software to generate the correlations. Since the orders of variable values are quite different, coded variables are calculated and used instead of the actual values according to the following equation [110]. Notice that the actual values are used for LHSVs (0.5–2) due to being close enough to the coded values (from

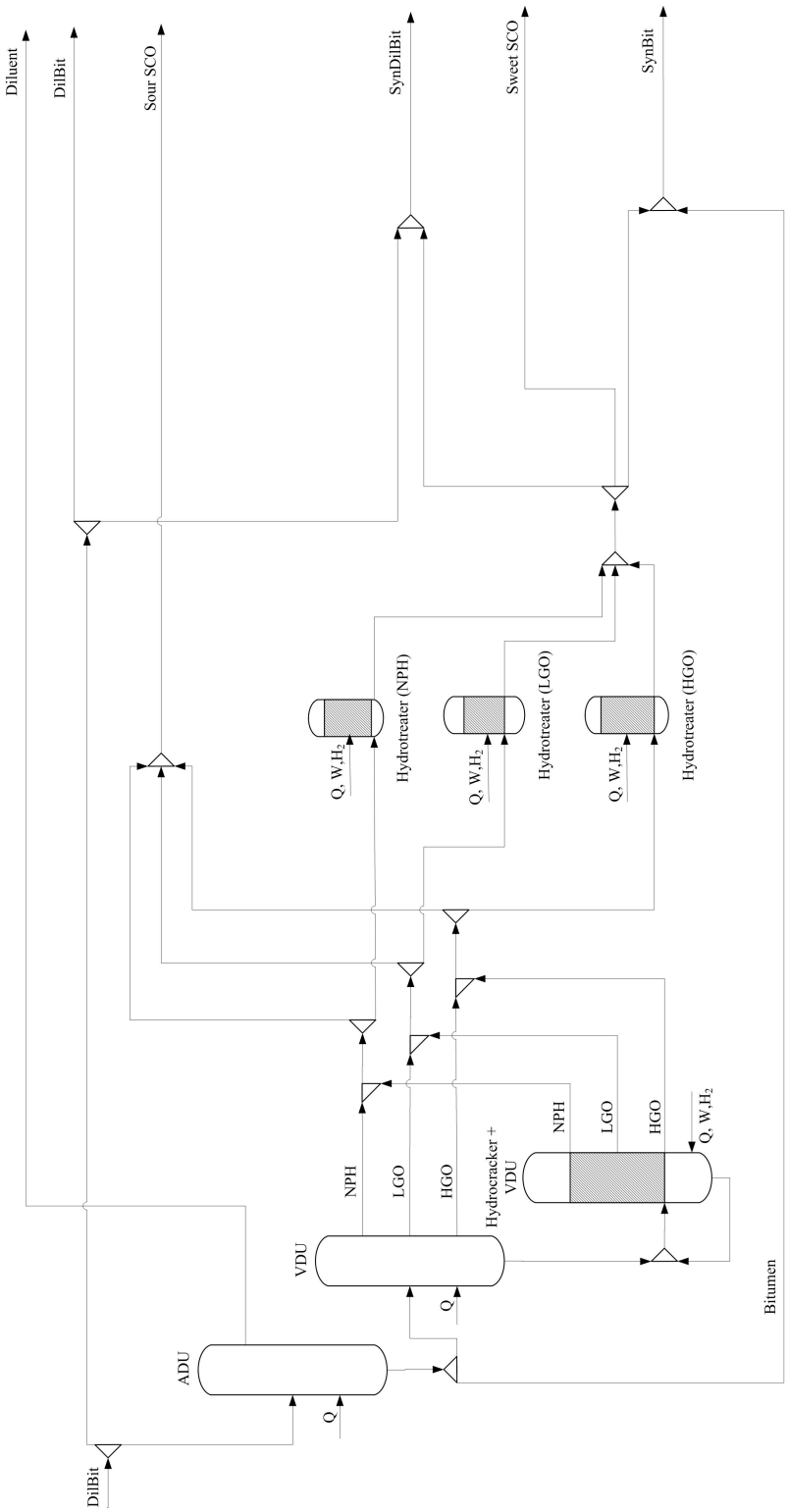

Figure 4.2: Multiproduct bitumen upgrading and blending plant

−1 to +1).

$$x_{coded} = \frac{2 \cdot x - (x_{max} + x_{min})}{x_{max} - x_{min}} \tag{4.20}$$

R–squared is taken into account to measure how close the simulation data are to the fitted regression curves. Wherever it is possible, linear correlations are chosen. Otherwise, quadratic terms are included to obtain higher accuracy. Regardless of the degree of generated polynomial, ineffective terms in each correlation are excluded to have simpler equations in the optimization model. R–squared of 0.99 or higher are achieved for all properties in different units, except the hydrocracker in which few properties could only obtain R–squared higher than 0.9. All of the correlation models are provided in the Appendix B.

4.4 Optimization

The optimization problem of upgrading plant operation can be stated as follows. The given information includes a fixed DilBit feed flow rate with known properties, a set of operating units, a set of correlations for each operating unit to estimate properties of products obtained from the previous section, a set of correlations for each operating unit to estimate the required work, duty, and hydrogen consumptions obtained from the previous section, demands for a set of commodities being composed of DilBit, sour SCO (mixture of untreated NPH, LGO, and HGO), sweet SCO (mixture of treated NPH, LGO, and HGO), SynDilBit (mixture of sweet SCO and DilBit), SynBit (mixture of sweet SCO and Bitumen), a set of specifications including viscosity, specific gravity, sulfur content, and nitrogen content for each commodity, and the costs of feed, commodities, and utilities. The objective is to determine the optimal operating conditions of processing units and flow rates to obtain the maximum profit.

4.4.1 Illustrative upgrading plant

As shown in Figure 4.2, a multiproduct upgrading plant is considered on the basis of hydrocracking technology. The optimization model is then formulated accordingly. DilBit feed can undergo the upgrading process, or it can be sold directly to the market. The separated diluent from ADU is sent back to the extraction plant. The SCO is a mixture of NPH, LGO, and HGO, and it might be produced as sour and/or sweet SCO(s). To produce SynDilBit or SynBit, sweet SCO is mixed with DilBit or bitumen, respectively. Several mixers and splitters are included in the plant to make the multiproduction possible. Depending on whether there is any demand for a specific commodity or not, some of the interconnections might be zero. Three intermediate products of NPH, LGO, and HGO are the main outlets from the VDU and hydrocracker. After mixing together, they can be sent to hydrotreaters for the sweet SCO production or directly used for the sour SCO production.

4.4.2 Mathematical optimization model

The model presented in this section is based on the following assumptions: the feed specifications are fixed, the arrangement of units is fixed, the hydrocracking technology is chosen for upgrading, and the generated correlations are valid in the range of operating conditions from Table 4.2. The proposed optimization model

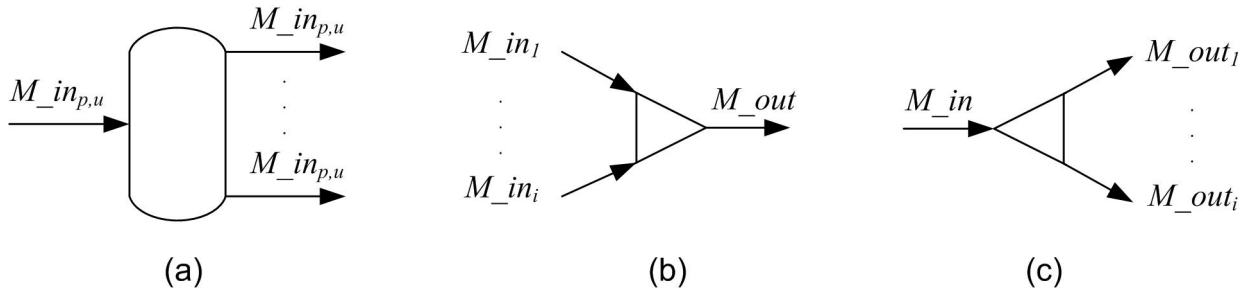

Figure 4.3: Schematics of units (a) process unit, (b) mixer, and (c) splitter

mainly consists of equality equations: (i) total mass balance for each unit, (ii) properties correlations of outlets from each operating unit, and (iii) blending rules after each mixer. Inequality equations are for products demand and their specifications. The formulated model is a non–convex NLP problem as a result of the nonlinearity appearing in correlation models and the blending rules. For instance, appearances of bilinear terms in the correlations are non–convex terms. A detailed model is presented in the following parts for the upgrading plant shown in Figure 4.2.

For each operating unit (Figure 4.3), there is one equation with respect to total mass balance. This equation is to estimate the outlet flow rates, which can be expressed through the yield.

$$M\_out_{p,u} = X_{p,yield} \cdot M\_in_{p,u} \quad \forall p \in P, u \in U \tag{4.21}$$

On the other hand, there are five correlations for each individual outlet from any operating units, namely, yield, specific gravity, viscosity, nitrogen content, and sulfur content. These correlations are a function of the operating conditions. A comprehensive list of correlation models can be found in the Appendix B. Notice that the variables in these equations are coded variables, as explained before. For example, the following correlations are used for the VDU (Equation 4.22), hydrocracker (Equation 4.23), and hydrotreaters (Equation 4.24), respectively.

$$X_{p,pr} = f(ECP_{p,s}, ECP_{p+1,s}) \quad \forall p \in P, pr \in PR, s = VDU_1 \tag{4.22}$$

$$X_{p,pr} = f(ECP_{p,s}, ECP_{p+1,s}, LHSV_u, T_u, P_u) \quad \forall p \in P, pr \in PR, u = hydrocracker, s = VDU_2 \tag{4.23}$$

$$X_{p,pr} = f(LHSV_u, T_u, P_u) \quad \forall p \in P, pr \in PR, u \in U \backslash \{hydrocracker\} \tag{4.24}$$

As an example, the yield of LGO withdrawing from VDU is

$$\begin{aligned} X_{LGO,yield} = 0.21387 - 4.13841 \cdot 10^{-3} \cdot ECP_{LGO,VDU} + 0.017477 \cdot ECP_{HGO,VDU} \\ -1.81078 \cdot 10^{-3} \cdot ECP_{LGO,VDU} \cdot ECP_{LGO,VDU} \\ +4.75853 \cdot 10^{-5} \cdot ECP_{HGO,VDU} \cdot ECP_{HGO,VDU} \end{aligned} \tag{4.25}$$

Table 4.3: Commodity specifications

Specification	Sour SCO	Sweet SCO	SynDilBit	SynBit
sulfur content (wt %)	3.180	0.180	2.510	3.150
nitrogen content (wt ppm)	1515.0	691.5	4456.4	2689.0
specific gravity	0.9396	0.8576	0.9377	0.9347
viscosity (cSt)	96.4	7.2	172	179

The mass balance for mixers are modeled as

$$M\_out = \sum_i M\_in_i \tag{4.26}$$

For nitrogen and sulfur contents, blending rules are based on the mass compositions [89]. The blending rule of specific gravity is based on the volumetric flow rate.

$$X_{pr}^{out} = \sum_i M\_in_i \cdot X_{pr,i}^{in} / M\_out \quad \forall pr \in \{nitrogen, sulfur\} \tag{4.27}$$

$$X_{SG}^{out} = \sum_i CV_i \cdot X_{SG,i}^{in} \tag{4.28}$$

The viscosity is converted to the blending index (Equation 4.29) and then blended using the volumetric fraction [113]. The blending index for the mixture is converted back to the viscosity (Equation 4.31).

$$BI_i = \frac{log(X_{viscosity,i}^{in})}{3 + log(X_{viscosity,i}^{in})} \tag{4.29}$$

$$BI_{blend} = \sum_i CV_i \cdot BI_i \tag{4.30}$$

$$X_{viscosity}^{out} = 10^{[3 \cdot BI_{blend}/(1-BI_{blend})]} \tag{4.31}$$

For splitters, only the mass balance needs to be modeled.

$$M\_in = \sum_i M\_out_i \tag{4.32}$$

For commodities, quality constraints should be imposed to meet the market quality requirements. Parameters for this part are adopted from the literature [114], and they are shown in Table 4.3.

$$X_{fp,pr} \leq spec_{fp,pr} \quad \forall fp \in FP, pr \in PR \tag{4.33}$$

To make sure that the volumetric blending ratio in each commodity is also in the valid range, lower and upper bounds are also imposed (see (Equation 4.34 and Table 4.4).

$$\theta_i \leq CV_i \leq \phi_i \quad \forall i \in I \tag{4.34}$$

Table 4.4: Lower and upper bounds for the volumetric blending ratio of commodities

Component	Sour SCO		Sweet SCO		SynDilBit		SynBit	
	θ_i	ϕ_i	θ_i	ϕ_i	θ_i	ϕ_i	θ_i	ϕ_i
NPH	0.05	0.30	0.05	0.30				
LGO	0.20	0.65	0.20	0.65				
HGO	0.20	0.65	0.20	0.65				
sweet SCO					0.51	0.77	0.53	0.80

Table 4.5: Price data

Parameter	Price
hydrogen ($ kg^{-1})	1.7 [9]
steam ($ tonne^{-1})	20.0 [115]
electricity ($ kWh^{-1})	0.076356 [9]
sour SCO ($ bbl^{-1})	40
sweet SCO ($ bbl^{-1})	60
SynDilBit ($ bbl^{-1})	50
SynBit ($ bbl^{-1})	45
DilBit ($ bbl^{-1})	10

The objective function of this study is profit and its economic parameters are reported in Table 4.5. The profit is calculated as the summation of incomes from selling different commodities minus energy and feed costs.

$$\begin{aligned} profit = \sum_{fp} V_{fp} \cdot price_{fp} - V_{feed} \cdot price_{feed} - \sum_{u} H_u \cdot price_{hydrogen} \\ - \sum_{u} W_u \cdot price_{electricity} - \sum_{u} Q_u \cdot price_{steam} \end{aligned} \tag{4.35}$$

4.4.3 Solution strategy

In this section, the solution strategy is explained. The optimization model presented in the previous section is a non–convex NLP. Therefore, it is possible to be trapped in a local optimum point by implementing a local optimization solver. To avoid this problem, global optimization is applied to search for the optimal solution within a predefined time limit. Specifically, the optimization problem is programmed in GAMS [116], and BARON [117] is used as the solver.

Introducing tight bounds for all variables of a model is very important to reach the global optimality of a non–convex optimization problem. This is due to use of these bounds in the convex envelopes for under– and overestimating the non–convex terms of the problem. First, lower bounds of mass and volume flow rates are zero, and their upper bounds are set equal to feed mass and volume flow rates. The reason is that none of the streams can have higher flow rates than the inlet feed. Second, some variables are based on percentage; therefore, their lower and upper bounds can be easily fixed at 0 and 100, respectively. Third, -1 and $+1$ are the lower and upper bounds of coded operating variables. Finally, for the rest of the variables, the objective function can be replaced by them. After performing optimization for each variable, safe bounds can be identified.

There are some points about the LHSV variables that should be clarified. This variable shows the ratio of liquid volume flow per hour to catalyst volume, and it can be calculated by dividing the inlet volumetric flow rate to the catalyst volume (see Equation 4.36). In this Chapter, hence, LHSVs can be concluded as a variable because the volumetric flow rate of the inlet can hold different values.

$$LHSV_u = \frac{V_u^{in}}{volume_u} \quad \forall u \in U \tag{4.36}$$

In this study, the inlet flow rate of reactors are variables, and thus, LHSVs are dependent variables in the adopted correlations for the conversion rates. However, there is no information about the catalyst volume of the reactors in previous studies. To resolve this issue, the following procedure is found applicable. First, after formulation of the optimization model in GAMS, the main objective function of profit is replaced with the inlet volumetric flow rate of each reactor. Notice here that the LHSVs are assumed independent variables at this step. Second, the maximum and minimum of inlet volumetric flow rates to the reactors are obtained by performing the maximization and minimization of the model. Third, the maximum and minimum of the catalyst volume can be calculated employing Equation 4.36, because the upper and lower bounds of LHSVs were reported for the each available correlation of the conversion rate (see Table 4.2). Fourth, the average of catalyst volumes found by minimization and maximization is assigned as the predesigned catalyst volume in reactors during the original optimization problem.

4.5 Case studies

Three different cases are presented in this section to illustrate the proposed optimization framework. They are all implemented in GAMS and solved with a desktop computer (single Intel Core i5–4590 at 3.30 GHz and 8 GB RAM). Furthermore, all of the solutions are found within a time limit of 10 hours or optimality gap of 1%. The decision variables in the proposed model are the operating conditions of the process units and mass and volume flow rates. Results of each example are interpreted accordingly.

4.5.1 Example 1

In this case, there is no demand on any specific commodity. Without any restriction on their flow rates, a combination of sour and sweet SCOs, SynDilBit, and SynBit, can be produced to achieve more benefits. After a global search, an optimal profit of \$51191.5 h^{-1} is found for this case. When there is no pre–specified demand for commodities, the SynDilBit is the only commodity that is produced under optimal conditions. According to Table 4.5, the SynDilBit is the second most expensive selling commodity. Production of sweet SCO is not the most economical alternative here, even though its selling price is the highest among the commodities. Note here that, when 1516.7 m^3 h^{-1} SynDilBit is produced, 37% feed (DilBit) should be sold directly to the market unprocessed. The blending ratio of sweet SCO and DilBit is also illustrated in Figure 4.4.

In Table 4.6, a comparison of current and required values for different specifications is reported for the SynDilBit. All four specifications are upper bounds, and the optimal values are all lower than them. In the

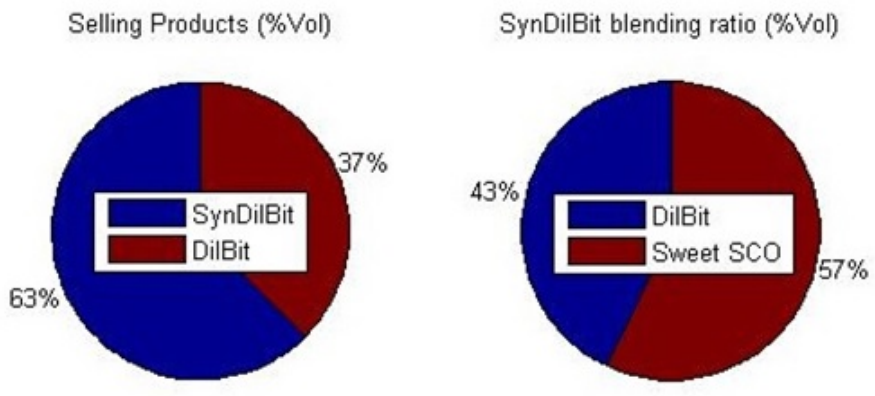

Figure 4.4: Optimal product composition and the blending ratio in example 1

Table 4.6: Comparison of product qualities and their specifications in Example 1

Vvariable	SynDilBit	
	Solution	Spec
viscosity (cSt)	14.7	172
nitrogen content (wt ppm)	1997.0	4456.4
sulfur content (wt %)	1.7	2.51
specific gravity	0.889	0.9377

sense of optimization, the nitrogen content of sweet SCO is the active constraint, because it is at the highest allowable value.

Before interpreting the solution results of operating conditions, the effects of the pressure, temperature, and LHSV on the process need to be clarified. The higher the pressure, temperature, and LHSV, the more conversion can be achieved for the desired reactions in the hydrocracker or hydrotreaters. Nevertheless, increasing the pressure and temperature leads to more electricity and steam costs, respectively. Moreover, a larger LHSV results in an increase of both electricity and steam costs simultaneously. Optimal operating conditions are reported in Table 4.7. Some points should be highlighted here by comparing the results in Table 4.7 with the operating ranges given in Table 4.2. Temperatures are the most effective variables, and they are set near or at their upper bounds for all units. The LHSVs are all approximately in the middle of the defined ranges. There is not a clear trend for the optimal pressures. The optimal pressure of NPH–hydrotreater is at the lower bound value. The reason is that the pressure was not an effective variable in the developed correlations [109]; therefore, the lowest value leads to the lowest electricity cost. When the optimal pressure is in the middle for the LGO–hydrotreater, they are at the highest extreme for the hydrocracker and HGO–hydrotreater. On the basis of optimal ECP values, one can understand that the NPH is separated in a wider range in the first VDU. This trend is vice versa for the HGO separation. For the withdrawn LGO, the ranges of cut points have nearly the same length but the LGO withdrawing from the second VDU is lighter.

Table 4.7: Optimal operating conditions of process units in Example 1

Variable	VDU_1	Hydrocracker and VDU_2	Hydrotreater		
			NPH	LGO	HGO
temperature (°C)		477.0	280	350	370
pressure (MPa)		18	3	8.4	10.2
LHSV (h^{-1})		0.48	1.15	1	0.86
ECP_1 (°C)	30	38.1			
ECP_2 (°C)	190	170			
ECP_3 (°C)	370	354.8			
ECP_4 (°C)	530	550			

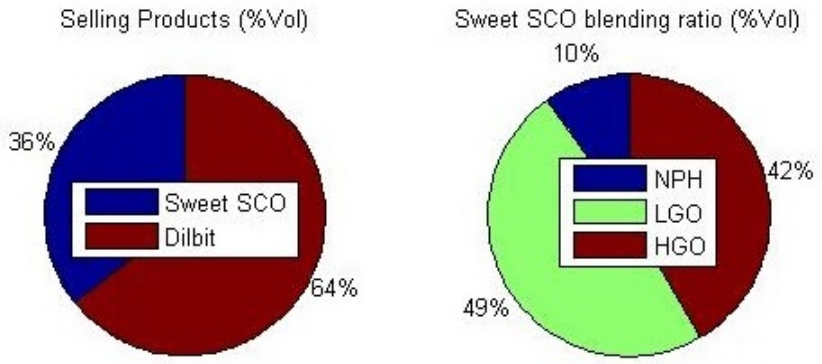

Figure 4.5: Optimal product composition and the blending ratio in example 2

4.5.2 Example 2

In the second case, the only option of production is the sweet SCO. The sour SCO, SynDilBit, and SynBit are not produced at all. The imposing constraint here is slightly different. The flow rates of sour SCO, SynDilBit, and SynBit are fixed at zero, because the flow rate of sweet SCO is greater than or equal to zero.

Global solution of \$33750.4 h^{-1} is found in this case, which is lower than the corresponding value in example 1. This is because of applying stricter constraints for final products. Because the sweet SCO is the only acceptable product in this case, a larger portion of feed is separated from the beginning of the process without undergoing any processing unit. Note here again that the sweet SCO is the most valuable commodity in this study. As a result of commodity specification constraints, it would be impossible to process the whole feed flow rate into just a single product. Hence, a large amount of DilBit is sent directly to the market. Production rates of 864.4 and 1562.1 m^3 h^{-1} are found for sweet SCO and DilBit, respectively. Figure 4.5 illustrates the blending ratios of selling products and sweet SCO. Four specification constraints are met, and nitrogen and sulfur contents of sweet SCO are the active constraints (see Table 4.8).

Table 4.9 includes the optimal operating conditions of example 2. Similar to the former case, the temperatures are the most effective variables in the process units. The optimal LHSVs are again all approximately in the middle of the defined range. The optimal pressures and ECPs also have the same trends as the previous case.

Table 4.8: Comparison of product qualities and their specifications in Example 2

Variable	Sweet SCO	
	Solution	Spec
viscosity (cSt)	7.0	7.2
nitrogen content (wt ppm)	691.5	691.5
sulfur content (wt %)	0.18	0.18
specific gravity	0.853	0.8576

Table 4.9: Optimal operating conditions of process units in Example 2

Variable	VDU_1	Hydrocracker and VDU_2	Hydrotreater		
			NPH	LGO	HGO
temperature (°C)		477.0	280	350	370
pressure (MPa)		17.58	3	8.38	10.2
LHSV (h^{-1})		0.48	1.15	1	0.86
ECP_1 (°C)	30	38.7			
ECP_2 (°C)	190	170			
ECP_3 (°C)	370	355.6			
ECP_4 (°C)	530	550			

4.5.3 Example 3

The third example is something between the first and second cases in terms of strictness for production demands. Here, small demands of 20 m^3 h^{-1} are assigned for all four commodities, namely, sweet and sour SCOs, SynDilBit, and SynBit. In the optimization model, volumetric flow rates of the mentioned streams are greater than or equal to 20.

Under these new circumstances, \$48593.1 h^{-1} is found as the best possible answer for the objective function through the global optimization. It is worth mentioning that the profit for this case is less than the first case, owing to the fact that selling the small amounts of all commodities is forced. Similar to examples 1 and 2, a portion of feed cannot be processed and is sold as DilBit. The optimal flow rates of sour and sweet SCOs, SynDilBit, SynBit, and DilBit are 20, 20, 1390.4, 20, and 975.8 m^3 h^{-1}, respectively. The volumetric blending ratios of selling products are demonstrated in Figure 4.6. Similar to the former cases, four specification constraints are met here. The viscosity and sulfur and nitrogen contents of sweet SCO and the nitrogen content of sour SCO are the active constraints here (see Table 4.10). The optimal operating conditions for this example are reported in Table 4.11. The same trends exist here for the optimal pressure, temperature, LHSV, and ECPs.

Table 4.10: Comparison of product current qualities and their specs in Example 3

Variable	Sweet SCO		Sour SCO		SynDilBit		SynBit	
	Solution	Spec	Solution	Spec	Solution	Spec	Solution	Spec
viscosity (cSt)	7.2	7.2	3.0	96.4	14.9	172	28.1	179
nitrogen content (wt ppm)	691.5	691.5	1515.0	1515.0	1996.1	4456.4	2192.2	2689.0
sulfur content (wt %)	0.18	0.18	1.26	3.18	1.72	2.51	1.90	3.15
specific gravity	0.854	0.8576	0.862	0.9396	0.889	0.9377	0.907	0.9347

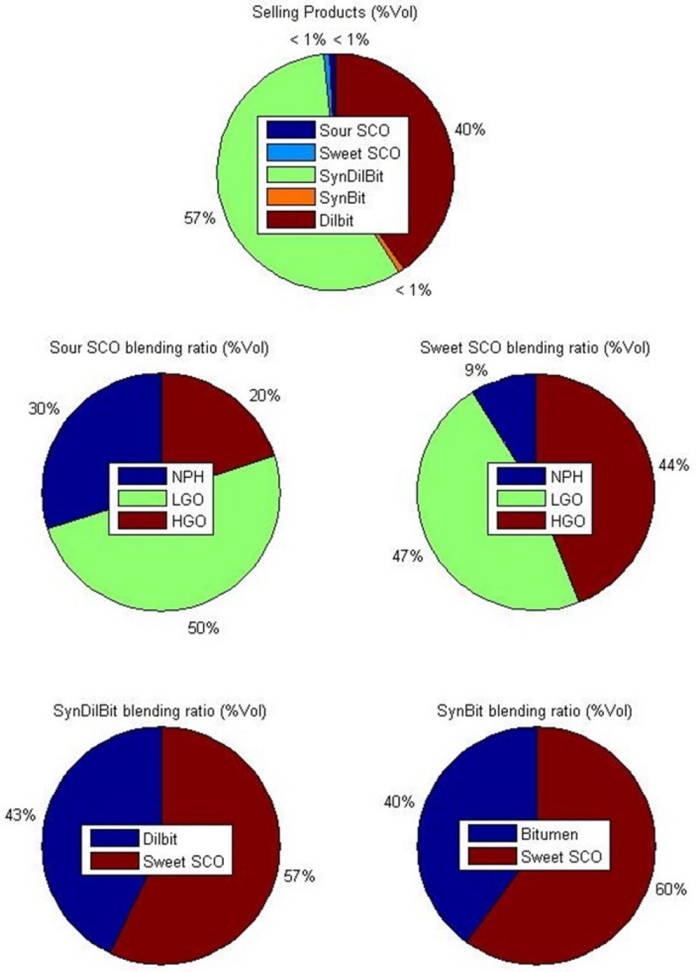

Figure 4.6: Optimal product composition and the blending ratio in example 3

Table 4.11: Optimal operating conditions of process units in Example 3

Variable	VDU_1	Hydrocracker and VDU_2	Hydrotreater		
			NPH	LGO	HGO
temperature (°C)		475.0	279.6	350	370
pressure (MPa)		18	3	8.67	10.2
LHSV (h^{-1})		0.47	1	0.92	0.87
ECP_1 (°C)	30	38.7			
ECP_2 (°C)	186.6	170			
ECP_3 (°C)	360.8	351.3			
ECP_4 (°C)	530	539.8			

Table 4.12: Comparison of the presented examples

Example	Optimality gap	CPU time (s)	Objective ($ h^{-1})
1	21.5	36000	51191.5
2	1.0	303	33750.4
3	19.8	36000	48593.1

Finally, problem size and computational time of examples are discussed here. The number of variables and equations are the same for the three examples (250 and 269, respectively), and the only difference between them is demand constraints. The computational times for the examples presented in the previous section are shown in Table 4.12. Even though the size of three cases are the same, the optimization can be carried out much faster in the second example compared to the other two using stricter constraints for the commodities demand.

4.5.4 Validation of optimization results

In this section, validation of the optimal solutions obtained by GAMS is presented. Because the empirical models are employed during the optimization, the optimal results need to be re–simulated in the Aspen HYSYS environment to make sure that the formulated model is accurate enough. To do so, the optimal solution of the third case is used, which is the most general case as a result of producing all of the commodities with minimum values. Independent variables, including ECPs, temperatures, pressures, and flow ratios of mixtures, are imported in the simulator, and LHSVs (as dependent variables) and commodity properties and volume flow rates are exported for the validation. A comparison of the simulation and optimization results is provided in Table 4.13. The average of errors between the simulation and optimization results is 5.1%. Accordingly, the simulation results are in agreement with those achieved through the optimization, and it can be concluded that the generated correlations are sufficiently precise to be applied in the optimization model.

One point that can be noticed from Table 4.13 is larger errors between GAMS optimization and Aspen HYSYS simulation results for the sweet SCO compared to the other products. This can be justified based on the following points. Firstly, comparing the sweet and sour SCOs, more operating units are required to process the sweet SCO (Hydrotreaters). Therefore, more errors are accumulated for the sweet SCO as empirical correlations are used to model the operating units. Secondly, 43% of SynDilBit is DilBit with zero error in properties estimation as they are fixed as feed specification. As a result, the specifications of SynDilBit are in a reasonable error range. Lastly, the specifications of SynBit have acceptable accuracy since 40% of SynBit is bitumen. Being separated at the very first operating unit (ADU), bitumen also has a very small amount of errors in properties estimation.

Table 4.13: Comparison of simulation and optimization results

	Commodity			
Property	Sour SCO	Sweet SCO	SynDilBit	SynBit
viscosity^a (cSt)	3.3	9.4	14.0	30.7
viscosity^b (cSt)	3.0	7.2	14.9	28.1
$\|error\|$ (%)	9.1	23.4	6.4	8.5
nitrogen content^a (wt ppm)	1555.5	646.5	1945.3	2149.0
nitrogen content^b (wt ppm)	1555.0	691.5	1996.1	2192.2
$\|error\|$ (%)	0.0	7.0	2.6	2.0
sulfur content^a (wt %)	1.23	0.16	1.67	1.86
sulfur content^b (wt %)	1.26	0.18	1.72	1.90
$\|error\|$ (%)	2.4	12.5	3.0	2.2
specific gravity^a	0.861	0.904	0.917	0.939
specific gravity^b	0.862	0.854	0.889	0.907
$\|error\|$ (%)	0.1	5.5	3.1	3.4
flow rate^a (bbl h^{-1})	21.0	19.6	1376.3	19.6
flow rate^b (bbl h^{-1})	20.0	20.0	1390.4	20.0
$\|error\|$ (%)	4.8	2.0	1.0	2.0
		hydrotreater		
dependent variable	hydrocracker	NPH	LGO	HGO
LHSV^a (h^{-1})	0.50	1.07	0.96	0.89
LHSV^b (h^{-1})	0.47	1.00	0.92	0.87
$\|error\|$ (%)	6.0	6.5	4.2	2.2

^{a} From Aspen HYSYS simulation. ^{b} From GAMS optimization.

4.6 Conclusion

In this Chapter, a novel optimization framework has been proposed for the bitumen upgrading plant. The hydrocracking–based upgrading plant is first simulated with Aspen HYSYS software. The process is then simulated under various operating conditions to obtain an adequate amount of data for correlation modeling. Afterward, empirical models are generated to estimate properties of outlet stream as a function of the operating conditions. According to the developed model, the proposed optimization problem is a non–convex NLP. For the global optimization, tight bounds on the variables are required, and they are defined by physical inspection of the plant configuration (global minimization and maximization with different variables as objective function) or basic mathematical logics (such as conversion rate or composition of contents, which should be in the range of 0–100 or 0–1, respectively). An upgrading plant that can produce multiple bitumen and SCO products is investigated. To show that the proposed model can be used for industrial purposes, three different cases are considered and the results show that the proposed approach is effective for the upgrading plant operation optimization.

Chapter 5

Expansion Development Planning of Thermocracking–based Bitumen Upgrading Plant under Uncertainty[1]

5.1 Introduction

Unconventional oil production in Canada is continuously increasing. The oil sands bitumen production in Alberta is projected to reach 3.8 million bpd by 2022, which will be two times the production as of 2012 [118]. While oil price fluctioation affects profitability of the oil sands industry, important issue is how to adjust production and expansion planning under an uncertain market environment. Another major concern for the continuous development of the oil sands industry is the environmental management. Sustainable development with minimum environmental conservation is a concern of Alberta provincial and Canadian federal governments. To follow the international agreements (the United Nations Framework and Kyoto protocol), Canada is committed to mitigating its GHG emissions. In Alberta, a carbon tax of $15 per tonne of CO_2 was enacted in 2007 for the first time [119]. Recently, it was increased to $20 and $30 per tonne of CO_2 in 2016 and 2017 [120, 121]. It is expected that the carbon tax rate will be increased; however, the exact future tax level is unknown. As it can be seen, the further development of the oil sands industry is accompanied with uncertainties in the both unpredictable oil price and changing environmental policies. Studying the development and expansion planning under uncertainties currently seems essential for the oil sands industry.

The uncertainty issue has received attention in various design and planning problems. The strategic planning of a bioethanol–sugar supply chain was studied under demand uncertainty [122]. A two–stage multi–scenario mixed–integer linear stochastic programming approach was proposed, and a decomposition technique was applied to solve it based on the sample average approximation technique. It was further shown that the stochastic model lead to more robust solution compared to the deterministic model. The strategic investment planning of a multi–product, multi–period supply chain problem was investigated [123]. To address the demand uncertainty, a two–stage mixed–integer linear stochastic programming model with risk consideration

[1] A version of this chapter was published in the *Computers & Chemical Engineering*, **2018**, *111*, 225–240

was taken into account to reduce the chances of very large objective function values during minimization. A two–stage mixed–integer linear stochastic programming was applied for the expansion planning of electricity generation plants [124]. Various power generation techniques (coal, combustion turbine, nuclear, combined cycle and wind generator) were considered. The load and wind availabilities were the uncertain parameters which were defined as independent and identically distributed random variables. Environmental regulations (including carbon tax and a renewable portfolio standard) were imposed on the model as well. This model was solved using the L–shaped method based on the Monte Carlo simulation. Comparing stochastic and deterministic solutions, policy assessments without considering uncertainties resulted in excessive expected costs. Later on, the same problem was addressed through a multistage mixed–integer linear stochastic programming model [125]. In another work [126], an optimization model was developed for produced water management during hydraulic fracturing operations. The uncertain parameters were defined in the form of fuzzy membership and probability density functions. This way the final model could express trade-off between the economic objective function and system reliability, such as meeting water treatment and disposal specifications. Nevertheless, the presented model was only applied to a hypothetical case.

In this Chapter, the focus is on the expansion planning of a single bitumen upgrading plant. We present a multistage expansion development model considering uncertainties in the SCO price and carbon tax. This Chapter is organized as follows: Section 5.2 states the general problem. A deterministic model of the expansion development is proposed in Section 5.3 for the thermocracking based upgrading plant. In Section 5.4, uncertainties are introduced and the multistage stochastic problem model is proposed. The nomenclature of presented model is available in Appendix A. As the solution method, Section 5.5 includes defining the uncertainty set, and the linear decision rule (LDR) approximation method. Section 5.6 discusses results obtained from the optimization of different models and case studies. Conclusions are made in Section 5.7.

5.2 Problem statement

The oil sands industry can be divided into extraction and upgrading sectors. The surface mining and in–situ extraction are the common extraction approaches, depending on an oil sands depth, while the thermocracking and hydrocracking are the well–known upgrading processes [9]. The bitumen upgrading plant studied in this Chapter is shown in Figure 5.1. A bitumen feed enters the plant from an extraction facility such as SAGD. Some LGO is separated at the first unit (DR), and the rest is sent to a thermocracker which is a delayed coker. The inlet of TC is then processed into three major products: NPH, LGO, and HGO. Single NPH and HGO streams go to their associated hydrotreaters: naphtha hydrotreater (NPHHT) and heavy gas oil hydrotreater (HGOHT), respectively. Furthermore, two LGO streams are mixed together and treated in their associated unit: light gas oil hydrotreater (LGOHT). Treated NPH, LGO, and HGO are blended together to make the final SCO product.

The problem addressed in this Chapter can be expressed as follows. We define a set of process units $p \in P$, a set of intermediate products $c \in C$, a set of time periods $t \in T$, and a set of utilities $u \in U$. Moreover, intermediate product yields of operating units, hydrogen and utilities requirement rates of process

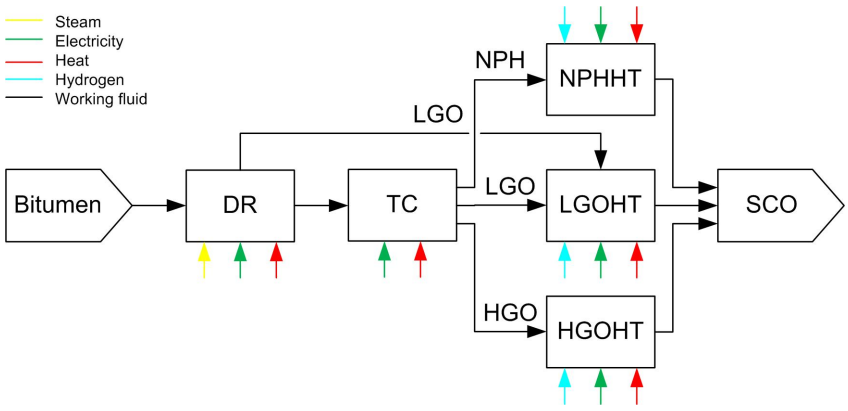

Figure 5.1: Superstructure of the thermocracking–based upgrading plant

units, CO_2 emission rates, and economic terms are known. Three modes of operation with various yield fractions and utility requirements (see Table 5.1 and Table 5.6) are available for the thermocracker unit adopted from literature. The associated information are derived from different upgrading configurations [9, 45]. Note that switching from one mode to another one is not an option here since each configuration is based on a licensed process, and each mode is under operation with a different company. The problem is to determine the best operating mode and expansion development of upgrading plant units to achieve the maximum NPV.

This Chapter is based on the following assumptions: (i) the planning horizon is 10 years and each time period is 2 years, (ii) coefficients associated with mass balances and utility requirements are assumed to be constant, (iii) the upgrading plant is under operation without capturing carbon dioxide, and (iv) there is no limitation on feed availability.

5.3 Deterministic optimization model

This section presents a deterministic optimization model for the expansion planning of the bitumen upgrading plant in the oil sands industry. The mathematical formulation of proposed problem is explained below.

Equation 5.1 sets an upper limit for the upgrading plant inlet ($\bar{\Omega}^M$). This value is set based on the highest capacity of current upgraders [127].

$$M^{in}_{DR,1} \leq \bar{\Omega}^M \tag{5.1}$$

Equation 5.2 expresses the outlet mass flow rates of three intermediate products from the first two units (DR and TC),

$$M^{out}_{p,c,t} = \alpha^{yield}_{p,c} \cdot M^{in}_{p,t} \quad \forall p \in SP, c \in C, t \in T \tag{5.2}$$

From the mass balance point of view, the DR and TC units are similar to splitters, while the hydrotreaters (NPHHT, LGOHT, and HGOHT) behave like mixers. This assumption simplifies the modeling when we define following subsets: $SP = \{DR, TC\}$, and $MP = \{NPHHT, LGOHT, HGOHT\}$.

Table 5.1: Intermediate product yields of DR and TC units ($\alpha_{p,c}^{yield}$)

Units	Mode	Product		
		NPH	LGO	HGO
DR	-	0.0	0.15	0.0
TC	1	0.17	0.24	0.32
TC	2	0.24	0.16	0.30
TC	3	0.13	0.16	0.38

Table 5.2: Hydrogen requirement rates (tonne m^{-3})

Parameter	NPHHT	LGOHT	HGOHT
$\alpha_p^{H_2}$	0.0123	0.0137	0.0312

Equation 5.3 is used to calculate the residue of the DR which is the inlet of the TC.

$$M_{TC,t}^{in} = (1 - \sum_{c} \alpha_{DR,c}^{yield}) \cdot M_{DR,t}^{in} \quad \forall t \in T \tag{5.3}$$

Equation 5.4 states that the inlets of the hydrotreaters come from the outlets of the first two units.

$$\sum_{p' \in SP} M_{p',c,t}^{out} = M_{p,t}^{in} \quad \forall (p,c) \in PC, t \in T \tag{5.4}$$

In addition, each intermediate product c is only treated in its associated hydrotreater. For example, the NPH product is only processed in the NPHHT. Thus, the paired set of $(p,c) \in PC$ is defined to consider this where $PC = \{NPHHT.NPH, LGOHT.LGO, HGOHT.HGO\}$.

The outlet mass flow rates of the hydrotreaters are calculated using equation 5.5. Note that the hydrogen streams are additional inlets.

$$M_{p,t}^{HTout} = \alpha_p^{HT} \cdot \left(M_{p,t}^{in} + M_{p,t}^{H2} \right) \quad \forall p \in MP, t \in T \tag{5.5}$$

The hydrogen requirement of each hydrotreater can be determined by equation 5.6.

$$M_{p,t}^{H2} = \frac{\alpha_p^{H_2} \cdot M_{p,t}^{in}}{\rho_p} \quad \forall p \in MP, t \in T \tag{5.6}$$

Equation 5.7 calculates mass flow rate of the SCO product. Tables 5.1-5.4 report the parameters associated to the discussed mass balance equations [45].

$$M_t^{SCO} = \sum_{p \in MP} M_{p,t}^{HTout} \quad \forall t \in T \tag{5.7}$$

Finally, to satisfy final product specification requirements, the SCO product has lower composition limits on NPH, LGO, and HGO components. Equation 5.8 imposes a constraint to produce SCO according to its

Table 5.3: Intermediate product yield of hydrotreaters

Parameter	NPHHT	LGOHT	HGOHT
α_p^{HT}	0.98	0.97	0.95

Table 5.4: Product densities (tonne m^{-3})

Parameter	DR	TC	NPHHT	LGOHT	HGOHT
ρ_p	0.93	1.02	0.74	0.89	0.97

Table 5.5: Upper and lower bounds

Parameter	$\underline{\Omega}_p^X$ (bpd)	$\bar{\Omega}_p^X$ (bpd)	$\underline{\Omega}_p^Q$ (%)	$\underline{\Omega}_p^{Spec}$ (%)	$\bar{\Omega}^M$ (tonne h^{-1})
DR	50000	150000	75		1500
TC	5000	60000	75		
NPHHT	5000	40000	75	13.76	
LGOHT	5000	40000	75	33.34	
HGOHT	5000	40000	75	32.08	

specifications (see Table 5.5).

$$\underline{\Omega}_p^{Spec} \leq \frac{M_{p,t}^{HTout}}{M_t^{SCO}} \quad \forall p \in MP, t \in T \tag{5.8}$$

In each time period (except the first one), unit expansion is possible. Equation 5.9 expresses that the expansion capacity at each period should be in an acceptable range (see Table 5.5),

$$\underline{\Omega}_p^X \cdot Y_{p,t} \leq X_{p,t} \leq \bar{\Omega}_p^X \cdot Y_{p,t} \quad \forall p \in P, t \in T \tag{5.9}$$

Equation 5.10 calculates the updated capacity of units after their expansions,

$$Q_{p,t} = Q_{p,t-1} + X_{p,t} \quad \forall p \in P, t \in T_{-1} \tag{5.10}$$

where, to simplify the mathematical representation, a subset of time period without its first element is denoted as T_{-1}.

Equation 5.11 enforces that volumetric inlet flow rates of the units are between 75%–100% of their capacities.

$$\underline{\Omega}_p^Q \cdot Q_{p,t} \leq \frac{UC_1 \cdot M_{p,t}^{in}}{\rho_p} \leq Q_{p,t} \quad \forall p \in P, t \in T \tag{5.11}$$

Different utilities are required for the upgrading process including steam, electricity and heat duty. While the steam is only consumed in the DR, all the units need the electricity and heat duty. Therefore, the utility set is defined as $U = \{st, el, ht\}$. Equation 5.12 calculates the total energy consumption of the upgrading plant. Table 5.6 reports the parameters associated with the utility requirements.

$$E_{u,t} = \sum_p \beta_{p,u} \cdot M_{p,t}^{in} \quad \forall u \in U, t \in T \tag{5.12}$$

Equations 5.13 and 5.14 define the capital cost of the first time period and the rest of time periods, respectively. Note that the intercept of the linearized correlations are multiplied by a binary variable ($Y_{p,t}$) in order to charge the capital cost if only there is an expansion. Table 5.7 reports the coefficients of the linear correlations for the capital cost estimation.

$$C_t^{CAPEX} = \sum_p (a_p \cdot Q_{p,t} + b_p) \quad \forall t \in \{1\} \tag{5.13}$$

Table 5.6: Energy requirements rates ($\beta_{p,u}$) [45]

Unit	Mode	Utility		
		$st(\frac{\text{tonne}}{\text{tonne}})$	$el(\frac{\text{kWh}}{\text{tonne}})$	$ht(\frac{\text{MJ}}{\text{tonne}})$
DR	-	0.0401	3.1	210
TC	1	0.0	20	880
TC	2	0.0	60	1120
TC	3	0.0	20	1570
NPHHT	-	0.0	13	100
LGOHT	-	0.0	13	750
HGOHT	-	0.0	13	320

Table 5.7: Capital cost coefficients [80, 128]

Unit	$a(\frac{\$\text{MM}}{\text{bpd}})$	b ($MM)
DR	0.000168	14.94
TC	0.001276	22.07
NPHHT	0.0002185	4.354
LGOHT	0.0004908	7.911
HGOHT	0.0004908	7.911

$$C_t^{CAPEX} = \sum_p (a_p \cdot X_{p,t} + b_p \cdot Y_{p,t}) \quad \forall t \in T_{-1} \tag{5.14}$$

Moreover, equation 5.15 states a budget ceiling on investment at each time period (see Table 5.5).

$$C_t^{CAPEX} \leq \bar{\Omega}_t^{Investment} \quad \forall t \in T \tag{5.15}$$

Note that $\bar{\Omega}_t^{Investment}$ is \$500MM for the first period and \$100MM for the following periods.

Equation 5.16 enforces the $M_{p,t}^{in}$ being nonnegative, and equation 5.17 expresses that $Y_{p,t}$ is a binary variable. Note that other continuous variables do not have to be limited with the nonnegativity constraint, since equation 5.16 automatically forces them to be.

$$M_{p,t}^{in} \geq 0 \quad \forall p \in P, t \in T \tag{5.16}$$

$$Y_{p,t} \in \{0,1\} \quad \forall p \in P, t \in T \tag{5.17}$$

Equation 5.18 defines NPV as the objective function which needs to be maximized. The NPV can be calculated from revenue, operating cost, capital cost, maintenance cost and carbon tax.

$$\begin{aligned}
\max \quad NPV = & \sum_{t\in T}\sum_{p\in MP} \frac{{}^{UC_1}/_{\rho_p} \cdot \gamma_t^{SCO} \cdot M_{p,t}^{HTout}}{(1+r)^t} - \sum_{t\in T} \frac{C_t^{CAPEX}}{(1+r)^t} \\
& - \sum_{t\in T} \frac{{}^{OT}/_{UC_2} \cdot (\sum_u \gamma_u^E \cdot E_{u,t} + \sum_{p\in MP} \gamma^{H_2} \cdot M_{p,t}^{H2})}{(1+r)^t} - \sum_{t\in T} \frac{\gamma^{MAINEX} \cdot \sum_{t'=1}^{t} C_{t'}^{CAPEX}}{(1+r)^t} \\
& - \sum_{t\in T} \frac{{}^{OT}/_{UC_2} \cdot \gamma_t^{CO_2} \cdot (\sum_u \delta_u^E \cdot E_{u,t} + \sum_{p\in MP} \delta^{H_2} \cdot M_{p,t}^{H2} + \delta^{SCO} \cdot M_t^{SCO})}{(1+r)^t} \\
& - \sum_{t\in T} \frac{{}^{UC_1}/_{\rho_{DR}} \cdot \gamma^{Bitumen} \cdot M_{DR,t}^{in}}{(1+r)^t}
\end{aligned} \tag{5.18}$$

Table 5.8: Supply cost [45]

Parameter	Utility			SCO	Bitumen	H_2	CO_2
	$st(\frac{\$}{\text{tonne}})$	$el(\frac{\$}{\text{kWh}})$	$ht(\frac{\$}{\text{MJ}})$	$(\frac{\$}{\text{bbl}})$	$(\frac{\$}{\text{bbl}})$	$(\frac{\$}{\text{tonne}})$	$(\frac{\$}{\text{tonne}})$
γ	17.72	0.073	0.00416	51.45	18.9	4200	30

Table 5.9: GHG emissions coefficients [45]

Parameter	Utility			SCO	H_2
	$st(\frac{\text{tonne of } CO_2}{\text{tonne}})$	$el(\frac{\text{tonne of } CO_2}{\text{kWh}})$	$ht(\frac{\text{tonne of } CO_2}{\text{MJ}})$	$(\frac{\text{tonne of } CO_2}{\text{tonne}})$	$(\frac{\text{tonne of } CO_2}{\text{tonne}})$
δ	0.1607	0.000367	0.000047	0.012	8.992

The first term is the revenue, which is calculated by assuming that the SCO price (γ_t^{SCO}) will be fixed at its current value of \$51.45 bbl^{-1} [129]. The second term is the total capital cost. The third term is the total operating cost with parameters provided in Table 5.8. The fourth term estimates the total maintenance cost. Note that, γ^{MAINEX} can be expressed as

$$\gamma^{MAINEX} = MAINEX \frac{(1+ir)^d - 1}{ir \cdot (1+ir)^d} \tag{5.19}$$

where MAINEX is the processing unit's annual maintenance cost percentage (3% in this work), ir is the annual real debt interest rate, and d is the depreciation time for the upgrading plant. The fifth term evaluates the carbon tax, and the corresponding parameters are available in Table 5.9. Finally, the last term is the feed cost, where it is assumed that the bitumen price ($\gamma^{Bitumen}$) is constant at \$18.9 bbl^{-1} [130]. This price is an average of different approaches for bitumen extraction techniques including mining, SAGD, CSS and cold production. Moreover, Table 5.10 reports some miscellaneous parameters associated with the economic analysis. Finally, the overall deterministic optimization model (DP) is given by equations 5.1–5.18, which is a MILP problem.

5.4 Stochastic optimization model

This section introduces a multistage stochastic model for the expansion development planning of upgrading plant in the oil sands industry. The multistage stochastic planning problem is solved through the decision rule–based approximation method, in which an uncertainty set is introduced to model perturbations of the uncertain parameters. Before presenting the stochastic model, the uncertain parameters are defined. Next, the uncertainty set construction is presented, followed by the decision rule–based counterpart model derivation.

Table 5.10: General key inputs [45]

Parameter	$UC_1(\frac{\text{bpd}}{\text{cmph}})$	$UC_2(\frac{\$\text{MM}}{\$})$	$OT(\frac{\text{h}}{\text{yr}})$	r (%)	i (%)	d (yr)
Values	150.97	10^6	7920	12	15	10

5.4.1 carbon tax uncertainty

The first uncertainty source considered here is related to the carbon tax. In Alberta, the carbon tax of \$15 per tonne of CO_2 was enacted in 2007 for the first time [119]. At 2017, this price was raised to \$30 per tonne of CO_2 [120]. In 2016, Canada signed on to the Paris climate agreement and the Canadian government announced that it will institute a pan–Canadian price floor for GHG emissions. That price floor will start in 2018 at \$30 per tonne of GHG emitted, rising to \$50 per tonne by 2022. The goal is to reduce Canadian GHG emissions by 30 percent from 2005 levels by 2030. In general, it is expected that the carbon tax will keep increasing in the next decade. Based on this understanding, the future carbon tax is modeled as following in this work:

$$\widetilde{\gamma}_t^{CO_2} = \gamma^{CO_2}(1 + \sum_{\tau=1}^{t} \zeta_\tau) \quad \forall t \in T \tag{5.20}$$

where γ^{CO_2} is the current tax price and ζ_t is a nonnegative uncertain parameter, which is assumed to be in the range of $[0, 1]$. Note that the above equation enforces an increasing trend for the future CO_2 price. Furthermore, to impose an upper bound on the future CO_2 price, the following equations can be incorporated:

$$\zeta_t \geq 0 \quad \forall t \in T \tag{5.21}$$

$$\sum_t \zeta_t \leq 1 \tag{5.22}$$

In equation 5.22, summation of the carbon tax changes over time periods is restricted to be less than one. In other words, it is assumed that the carbon tax can mostly be doubled till the end of planning horizon.

5.4.2 SCO price uncertainty

The second uncertainty source is the SCO product price. In this Chapter, a time series model trained from historical data (see Figure 5.2) is developed. auto regressive moving average (ARMA) type of model is used in this work:

$$\widetilde{\gamma}_t^{SCO} = \{\phi_1 \cdot \gamma_{t-1}^{SCO} + ... + \phi_p \cdot \gamma_{t-p}^{SCO}\} + \{\epsilon_t + \theta_1 \cdot \epsilon_{t-1} + ... + \theta_q \cdot \epsilon_{t-q}\} \tag{5.23}$$

where $\phi_1, ..., \phi_p, \theta_1, ..., \theta_q$ are parameters of the ARMA model, and they can be fitted using historical data. ϵ_t represents uncorrelated white noise (with zero mean).

ARMA model is a useful tool in analysis of the time series data. This model is based on stationary stochastic process depending on two polynomials: (a) autoregression, and (b) moving average. Regressing a variable on its own lagged values is carried out by the autoregression part. Modeling the error term is conducted by the moving average part. Note that the error term is a linear combination of error terms existing in the same period and at various times in the past. The order of the autoregressive and moving average parts is referred as p and q, respectively. In this Chapter, p and q are both set as 6 and the ARMA model is trained based on the history data. Figure 5.2 illustrates the historical data and its prediction by the trained model. Note that ϕs and θs are the trained parameters of the ARMA model. Equation 5.23 can be reformatted into a general form. For the sake of simplicity, an example case is discussed here for $p = 1$

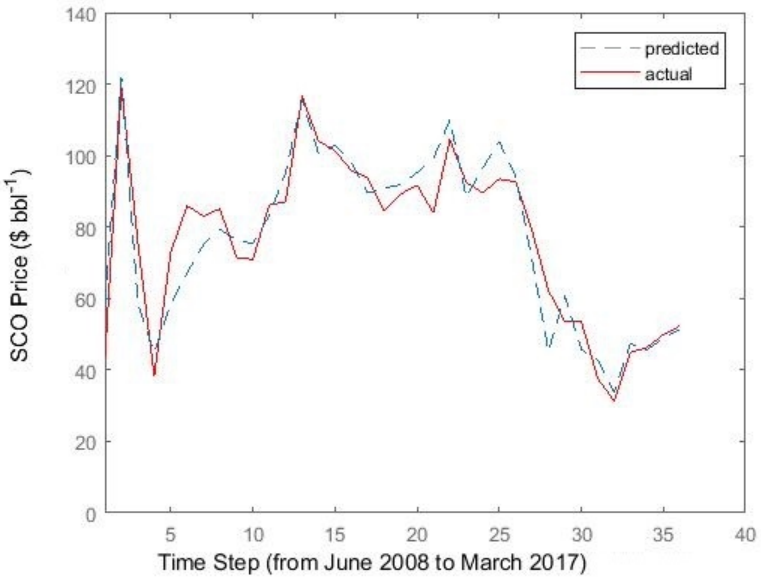

Figure 5.2: ARMA training based on the historical data

and $q = 1$. We demonstrate prediction of the two future steps (by assuming the process starts at time 0). The current and two future oil prices can be expressed as followings according to equation 5.23:

$$\gamma_0^{SCO} = \phi_1 \cdot \gamma_{-1}^{SCO} + \epsilon_0 + \theta_1 \cdot \epsilon_{-1} \tag{5.24}$$

$$\gamma_1^{SCO} = \phi_1 \cdot \gamma_0^{SCO} + \epsilon_1 + \theta_1 \cdot \epsilon_0 \tag{5.25}$$

$$\gamma_2^{SCO} = \phi_1 \cdot \gamma_1^{SCO} + \epsilon_2 + \theta_1 \cdot \epsilon_1 \tag{5.26}$$

As it can be seen, γ_0^{SCO} and γ_1^{SCO} on the right–hand side of above equations are required to be replaced in order to have a straight expression of the oil price at each time step. γ_0^{SCO} can also be stated according to equation 5.24, and then, it can be plugged in equation 5.25:

$$\begin{aligned} \gamma_1^{SCO} &= \phi_1 \cdot [\phi_1 \cdot \gamma_{-1}^{SCO} + \epsilon_0 + \theta_1 \cdot \epsilon_{-1}] + \epsilon_1 + \theta_1 \cdot \epsilon_0 \\ &= \phi_1^2 \cdot \gamma_{-1}^{SCO} + \phi_1 \cdot \theta_1 \cdot \epsilon_{-1} + (\phi_1 + \theta_1) \cdot \epsilon_0 + \epsilon_1 \end{aligned} \tag{5.27}$$

The above equation can now be used to reformulate γ_2^{SCO} in equation 5.26. By plugging equation 5.27 into equation 5.26, we get:

$$\begin{aligned} \gamma_2^{SCO} &= \phi_1 \cdot [\phi_1^2 \cdot \gamma_{-1}^{SCO} + \phi_1 \cdot \theta_1 \cdot \epsilon_{-1} + (\phi_1 + \theta_1) \cdot \epsilon_0 + \epsilon_1] + \epsilon_2 + \theta_1 \cdot \epsilon_1 \\ &= \phi_1^3 \cdot \gamma_{-1}^{SCO} + \phi_1^2 \cdot \theta_1 \cdot \epsilon_{-1} + \phi_1 \cdot (\phi_1 + \theta_1) \cdot \epsilon_0 + (\phi_1 + \theta_1) \cdot \epsilon_1 + \epsilon_2 \end{aligned} \tag{5.28}$$

On the right–hand sides of equations 5.27 and 5.28, ϵ_1 and ϵ_2 are the unknown uncertain parameters. Notice that ϵ_{-1} can be set as zero based on the zero mean assumption. Then, ϵ_0 can be calculated as following based on 5.24:

$$\epsilon_0 = \gamma_0^{SCO} - \phi_1 \cdot \gamma_{-1}^{SCO} \tag{5.29}$$

Equations 5.27 and 5.28 can be further compactly rewritten as below

$$\gamma_1^{SCO} = \begin{bmatrix} 1 & 0 \end{bmatrix} \begin{bmatrix} \epsilon_1 \\ \epsilon_2 \end{bmatrix} + \phi_1^2 \cdot \gamma_{-1}^{SCO} + \phi_1 \cdot \theta_1 \cdot \epsilon_{-1} + (\phi_1 + \theta_1) \cdot \epsilon_0 \tag{5.30}$$

$$\gamma_2^{SCO} = \begin{bmatrix} (\phi_1 + \theta_1) & 1 \end{bmatrix} \begin{bmatrix} \epsilon_1 \\ \epsilon_2 \end{bmatrix} + \phi_1^3 \cdot \gamma_{-1}^{SCO} + \phi_1^2 \cdot \theta_1 \cdot \epsilon_{-1} + \phi_1 \cdot (\phi_1 + \theta_1) \cdot \epsilon_0 \tag{5.31}$$

and they can be presented in a general format as equations 5.32, where the vector A_t^{SCO} and scalar B_t^{SCO} on the right–hand side are calculated based on known parameter values.

As a result, the SCO price in year t in the future can be estimated as

$$\widetilde{\gamma}_t^{SCO} = A_t^{SCO} \cdot \epsilon + B_t^{SCO} \quad \forall t \in T \tag{5.32}$$

where $\epsilon = [\epsilon_1, ..., \epsilon_{N_T}]^T$, with A_t^{SCO} and B_t^{SCO} being determined using the ARMA model parameters.

In addition to the ARMA model, in order to restrict the SCO price fluctuation, the following conditions are imposed on ϵ:

$$|\epsilon_t| \leq z_{1-\alpha} \quad \forall t \in T \tag{5.33}$$

$$\sum_t |\epsilon_t| \leq \Gamma^{SCO} \cdot z_{1-\alpha} \tag{5.34}$$

where $z_{1-\alpha}$ is $(1-\alpha)$ quantile of the standard normal distribution, Γ^{SCO} is a scalar to control size of the uncertainty set. In the proposed model, ϵ_t is assumed to follow the zero mean normal distribution with its variance determined from the ARMA model training. Parameter α is assumed to be 5% in this work, and hence, $[-z_{1-\alpha}, z_{1-\alpha}]$ corresponds to the 95% level confidence interval of ϵ_t. Γ^{SCO} is usually defined as an integer number in the range of one to maximum number of the time periods. For instance, if there are five time stages for t, $\Gamma^{SCO} = 5$ means that all five ϵ_t can reach their upper/lower bounds simultaneously. Consequently, since ϵ_t represents the SCO price, larger values of Γ^{SCO} lead to more oil price fluctuations.

Notice that equation 5.34 can be reformulated to eliminate the absolute term. Introducing new variable ϵ'_t to replace $|\epsilon_t|$, equations 5.33 and 5.34 can be equivalently rewritten as the following equations:

$$\epsilon'_t \leq z_{1-\alpha} \quad \forall t \in T \tag{5.35}$$

$$\sum_t \epsilon'_t \leq \Gamma^{SCO} \cdot z_{1-\alpha} \tag{5.36}$$

$$-\epsilon_t \leq \epsilon'_t \quad \forall t \in T \tag{5.37}$$

$$\epsilon_t \leq \epsilon'_t \quad \forall t \in T \tag{5.38}$$

Finally, we set a realistic lower bound for the SCO price. Based on the historical data, the SCO price has not been less than \$33.77 bbl^{-1} [80]. As a safe lower bound, we apply the following constraint to control minimum price of the SCO ($\underline{\Omega}^{SCO}$ = \$20 bbl^{-1}):

$$\underline{\Omega}^{SCO} \leq A_t^{SCO} \cdot \epsilon + B_t^{SCO} \tag{5.39}$$

Figure 5.3 illustrates samplings of $\tilde{\gamma}^{SCO}$ inside the corresponding uncertainty sets where Γ^{SCO} is 1 and 5, respectively. As it can be seen, both plots have the same trend, which were derived through the ARMA

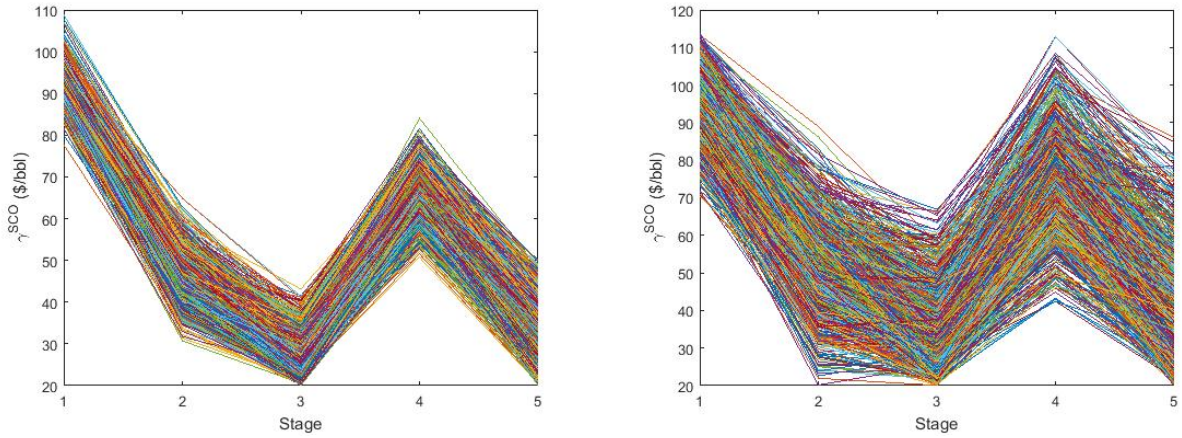

(a) (b)

Figure 5.3: Effect of Γ^{SCO} on γ^{SCO} prediction: (a) $\Gamma^{SCO} = 1$, and (b) $\Gamma^{SCO} = 5$

model. However, fluctuations of these two cases are quite distinctive. When Γ^{SCO} is small, SCO prices are limited to a smaller range (more conservative attitude). On the other hand, $\Gamma^{SCO} = 5$ increases the chance of oil price fluctuations (less conservative attitude). This parameter needs to be specified by the user, and it shows how conservative they are regarding the future oil price prediction.

5.4.3 Uncertainty set

The carbon tax and SCO price were defined as functions of the random variables of ζ and ϵ, respectively (See equation 5.20 and 5.32). For the sake of general formulation, the proposed uncertainties above and the corresponding constraints need to be combined together as a single uncertainty set. The uncertainties for the carbon tax (ζ_t), and SCO price (ϵ_t) can thus be organized in one uncertain vector as

$$\xi = [1, \zeta_1, ..., \zeta_{N_T}, \epsilon_1, ..., \epsilon_{N_T}] \tag{5.40}$$

Note that ϵ'_t is not included here since it is just an auxiliary set of variables which we introduce to remove the absolute term in equation 5.34. Appending these auxiliary variables to ξ leads to a vector with sixteen elements. Eventually, the uncertainty set is defined as

$$\Xi = \{\xi : \quad \text{Equations } 5.21, 5.22, 5.35, 5.36, 5.37, 5.38, 5.39\}$$

For simplicity in the following derivation, it is expressed as $\Xi = \{\xi : W \cdot \xi \geq h\}$, where W and h are a matrix and a vector of known coefficients from the mentioned equations in the uncertainty set, respectively.

After combining the carbon tax and SCO price uncertainties into an overall vector of ξ, the uncertain parameters can be modeled as equations 5.41 and 5.42. In order to retrieve original uncertainties (ζ_t and ϵ_t) from the vector (ξ), truncate matrices can be used. Defining truncate operators: (i) $P_t^{CO_2}$ to get ζ_t from the ξ, and (ii) P_t^{SCO} to get ϵ_t from ξ:

$$\widetilde{\gamma}_t^{CO_2}(\xi) = \gamma^{CO_2} \cdot (1 + P_t^{CO_2} \cdot \xi) \quad \forall t \in T \tag{5.41}$$

$$\widetilde{\gamma}_t^{SCO}(\xi) = A_t^{SCO} \cdot P_t^{SCO} \cdot \xi + B_t^{SCO} \quad \forall t \in T \tag{5.42}$$

5.4.4 Multistage stochastic model

Based on the developed DP model and the presented uncertainties, the following multistage stochastic optimization problem (SP) can be formulated.

$$\begin{aligned}
\max \quad & NPV = \mathbb{E}\Bigg[\sum_{t\in T} \sum_{p\in MP} \frac{{}^{UC_1}/_{\rho_p}}{(1+r)^t} \cdot \widetilde{\gamma}_t^{SCO}(\xi) \cdot M_{p,t}^{HTout}(\xi) - \sum_{t\in T} \frac{C_t^{CAPEX}(\xi)}{(1+r)^t} \\
& - \sum_{t\in T} \frac{{}^{OT}/_{UC_2}}{(1+r)^t} \cdot \Big(\sum_u \gamma_u^E \cdot E_{u,t}(\xi) + \sum_{p\in MP} \gamma^{H_2} \cdot M_{p,t}^{H2}(\xi)\Big) - \sum_{t\in T} \frac{\gamma^{MAINEX}}{(1+r)^t} \cdot \sum_{t'=1}^{t} C_{t'}^{CAPEX}(\xi) \\
& - \sum_{t\in T} \frac{{}^{OT}/_{UC_2}}{(1+r)^t} \cdot \widetilde{\gamma}_t^{CO_2}(\xi) \cdot \Bigg(\sum_u \delta_u^E \cdot E_{u,t}(\xi) + \sum_{p\in MP} \delta^{H_2} \cdot M_{p,t}^{H2}(\xi) + \delta^{SCO} \cdot M_t^{SCO}(\xi) \Bigg) \\
& - \sum_{t\in T} \frac{{}^{UC_1}/_{\rho_{DR}} \cdot \gamma^{Bitumen}}{(1+r)^t} \cdot M_{DR,t}^{in}(\xi) \Bigg] && \text{(5.43a)} \\
s.t. \quad & M_{DR,1}^{in}(\xi) \le \bar{\Omega}^M && \text{(5.43b)} \\
& M_{p,c,t}^{out}(\xi) = \alpha_{p,c}^{yield} \cdot M_{p,t}^{in}(\xi) \quad \forall p \in SP, c \in C, t \in T, \xi \in \Xi && \text{(5.43c)} \\
& M_{TC,t}^{in}(\xi) = (1 - \sum_c \alpha_{DR,c}^{yield}) \cdot M_{DR,t}^{in}(\xi) \quad \forall t \in T, \xi \in \Xi && \text{(5.43d)} \\
& \sum_{p'\in SP} M_{p',c,t}^{out}(\xi) = M_{p,t}^{in}(\xi) \quad \forall (p,c) \in PC, t \in T, \xi \in \Xi && \text{(5.43e)} \\
& M_{p,t}^{HTout}(\xi) = \alpha_p^{HT} \cdot \Big(M_{p,t}^{in}(\xi) + M_{p,t}^{H2}(\xi) \Big) \quad \forall p \in MP, t \in T, \xi \in \Xi && \text{(5.43f)} \\
& M_{p,t}^{H2}(\xi) = \frac{\alpha_p^{H_2} \cdot M_{p,t}^{in}(\xi)}{\rho_p} \quad \forall p \in MP, t \in T, \xi \in \Xi && \text{(5.43g)} \\
& M_t^{SCO}(\xi) = \sum_{p\in MP} M_{p,t}^{HTout}(\xi) \quad \forall t \in T, \xi \in \Xi && \text{(5.43h)} \\
& \underline{\Omega}_p^{Spec} \le \frac{M_{p,t}^{HTout}(\xi)}{M_t^{SCO}(\xi)} \quad \forall p \in MP, t \in T, \xi \in \Xi && \text{(5.43i)} \\
& \underline{\Omega}_p^X \cdot Y_{p,t} \le X_{p,t}(\xi) \le \bar{\Omega}_p^X \cdot Y_{p,t} \quad \forall p \in P, t \in T, \xi \in \Xi && \text{(5.43j)} \\
& Q_{p,t}(\xi) = Q_{p,t-1}(\xi) + X_{p,t}(\xi) \quad \forall p \in P, t \in T_{-1}, \xi \in \Xi && \text{(5.43k)} \\
& \underline{\Omega}_p^Q \cdot Q_{p,t}(\xi) \le \frac{UC_1 \cdot M_{p,t}^{in}(\xi)}{\rho_p} \le Q_{p,t}(\xi) \quad \forall p \in P, t \in T, \xi \in \Xi && \text{(5.43l)} \\
& E_{u,t}(\xi) = \sum_p \beta_{p,u} \cdot M_{p,t}^{in}(\xi) \quad \forall u \in U, t \in T, \xi \in \Xi && \text{(5.43m)} \\
& C_t^{CAPEX}(\xi) = \sum_p (a_p \cdot Q_{p,t}(\xi) + b_p) \quad \forall t = 1, \xi \in \Xi && \text{(5.43n)} \\
& C_t^{CAPEX}(\xi) = \sum_p (a_p \cdot X_{p,t}(\xi) + b_p \cdot Y_{p,t}) \quad \forall t \in T_{-1}, \xi \in \Xi && \text{(5.43o)} \\
& C_t^{CAPEX}(\xi) \le \bar{\Omega}_t^{Investment} \quad \forall t \in T, \xi \in \Xi && \text{(5.43p)} \\
& 0 \le M_{p,t}^{in}(\xi) \quad \forall p \in P, t \in T, \xi \in \Xi && \text{(5.43q)} \\
& Y_{p,t} \in \{0,1\} \quad \forall p \in P, t \in T && \text{(5.43r)}
\end{aligned}$$

In the above model, the carbon tax (γ^{CO_2}) and SCO price (γ^{SCO}) of the DP model are replaced with $\widetilde{\gamma}_t^{CO_2}$ and $\widetilde{\gamma}_t^{SCO}$, respectively. Furthermore, $\mathbb{E}[\cdot]$ is the expectation operator with respect to the uncertainty, and $\widetilde{\gamma}_t^{SCO}(\xi)$ and $\widetilde{\gamma}_t^{CO_2}(\xi)$ are the uncertain parameters, and Ξ is the uncertainty set defined for the uncertain parameters. Notice that in this proposed model, all the binary variables are cast as first stage decisions to reduce the complexity of the problem. As a trade–off, the solution will be suboptimal compared to the case of using adaptive binary decisions.

5.5 Solution method

While the stochastic optimization model SP is intractable, the LDR based solution method is used in this Chapter. Applying a LDR approximation, stochastic problems can be solved effectively under certain type of uncertainty sets [131]. The optimal solution resulted from the LDR approximation is a set of linear decision rules for decision variables rather than exact values. Accordingly, realized uncertainties till a decision stage are plugged into the linear decision rules, and then values for decision variables are determined for the next stage. Moreover, since the decision rules are linear, the problem size is a polynomial function of the number of stages. Therefore, this approach is a good candidate for multistage stochastic optimization problems. Although it was proposed a long time ago [132], the use of decision rules to solve problems under uncertainty has become popular recently [131, 133, 134, 135, 136]. Applications of this method have been found in reservoir operations [131], wind–storage systems [133], multiperiod plannings in generation facilities [134] and in general production plannings [135], and joint management of heat and power systems [136]. Furthermore, it is worth pointing out that the affine decision rule–based method received a lot of attention in multistage robust optimizations where the objective is based on the worst case performance over the uncertainty set. While in this work, the LDR method is applied to the multistage stochastic programming problem where the objective is based on the expected performance over the uncertainty set. Compared to traditional scenario tree–based multistage stochastic programming method, the proposed method seeks solution feasibility against an uncertainty set instead of finite number of scenarios, and the expected objective is evaluated based on all the realizations within the uncertainty set instead of the scenarios.

This section describes the LDR approximation method applied to solve the SP model. LDR is a technique which assumes a linear relationship between optimization variables and uncertain parameters. Consider a decision variable $A(\xi)$ depending on uncertainty, the LDR can be applied as: $A(\xi) = A \cdot \xi_{[t-1]}$, where $\xi_{[t-1]}$ means all the uncertainties which have been realized till the time t. $\xi_{[t-1]}$ can be explicitly modeled as the following using a truncate vector (P_t^{ξ}) based on ξ: $\xi_{[t-1]} = P_t^{\xi} \cdot \xi$. For instance, if there are three time periods, then $\xi = [1, \xi_1, \xi_2]^T$, and $P^{\xi} = [1\ 0\ 0\ ;1\ 1\ 0\ ;1\ 1\ 1]$. According to this formulation, $A(\xi)$ will be equal to A_1, $A_1 + A_2 \cdot \xi_1$, and $A_1 + A_2 \cdot \xi_1 + A_3 \cdot \xi_2$ for the first, second, and third time periods, respectively. Note that A_1, A_2, and A_3 are the optimization variables.

As an example on using the linear decision rule, counterpart of the constraint 5.43b ($M_{DR,1}^{in}(\xi) \leq$

$\bar{\Omega}^M,\ \forall \xi \in \Xi$) can be derived using the following steps: 1. Apply the LDR and factor $\xi_{[t-1]}$,

$$(M^{in}_{DR,1}) \cdot \xi_{[t-1]} \leq \bar{\Omega}^M \quad \forall \xi \in \Xi$$

2. Derive the robust counterpart and introduce the truncate operator P^{ξ}_1,

$$\left\{ \max_{\xi \in \Xi} \quad (M^{in}_{DR,1} \cdot P^{\xi}_1) \cdot \xi \right\} \leq \bar{\Omega}^M \quad \forall \xi \in \Xi$$

3. Use the uncertain set definition,

$$\left\{ \begin{array}{ll} \max & (M^{in}_{DR,1} \cdot P^{\xi}_1) \cdot \xi \\ s.t. & -W \cdot \xi \leq -h \end{array} \right\} \leq \bar{\Omega}^M$$

4. Introduce a dual variable Λ^b and apply duality to the inner LP problem,

$$\left\{ \begin{array}{c} \min \quad -h^T \cdot \Lambda^b \\ s.t. \quad -W^T \cdot \Lambda^b = (M^{in}_{DR,1} \cdot P^{\xi}_1)^T \\ \Lambda^b \geq 0 \end{array} \right\} \leq \bar{\Omega}^M$$

5. Drop the minimization operator,

$$\left\{ \begin{array}{l} -h^T \cdot \Lambda^b \leq \bar{\Omega}^M \\ -W^T \cdot \Lambda^b = (M^{in}_{DR,1} \cdot P^{\xi}_1)^T \\ \Lambda^b \geq 0 \end{array} \right.$$

For simplicity, derivations of the objective function and the remaining constraints for the SP model are included in the Appendix C. Finally, the overall LDR approximation of the SP model is summarized as following:

$$\begin{aligned}
\max \quad & NPV = \sum_{t \in T} \sum_{p \in MP} \frac{{}^{UC_1}/_{\rho_p}}{(1+r)^t} \cdot \Bigg[tr\Big((P^{SCO}_t)^T \cdot (A^{SCO}_t)^T \cdot M^{HTout}_{p,t} \cdot P^{\xi}_t \cdot \mathbb{E}_{\xi \in \Xi}[\xi \cdot \xi^T] \Big) \\
& + B^{SCO}_t \cdot M^{HTout}_{p,t} \cdot P^{\xi}_t \cdot \mathbb{E}_{\xi \in \Xi}[\xi] \Bigg] - \sum_{t \in T} \left[\frac{C^{CAPEX}_t}{(1+r)^t} \cdot P^{\xi}_t \cdot \mathbb{E}_{\xi \in \Xi}[\xi] \right] \\
& - \sum_{t \in T} \frac{{}^{OT}/_{UC_2}}{(1+r)^t} \cdot \left(\sum_u \gamma^E_u \cdot E_{u,t} + \sum_{p \in MP} \gamma^{H_2} \cdot M^{H2}_{p,t} \right) \cdot P^{\xi}_t \cdot \mathbb{E}_{\xi \in \Xi}[\xi] \\
& - \sum_{t \in T} \frac{\gamma^{MAINEX}}{(1+r)^t} \cdot \sum_{t'=1}^{t} C^{CAPEX}_{t'} \cdot P^{\xi}_{t'} \cdot \mathbb{E}_{\xi \in \Xi}[\xi] \\
& - \sum_{t \in T} \frac{{}^{OT}/_{UC_2}}{(1+r)^t} \cdot \gamma^{CO_2} \cdot \Bigg[\left(\sum_u \delta^E_u \cdot E_{u,t} + \sum_{p \in MP} \delta^{H_2} \cdot M^{H2}_{p,t} + \delta^{SCO} \cdot M^{SCO}_t \right) \cdot P^{\xi}_t \cdot \mathbb{E}_{\xi \in \Xi}[\xi] \\
& \qquad + tr\Big((P^{CO_2}_t)^T \cdot \left(\sum_u \delta^E_u \cdot E_{u,t} + \sum_{p \in MP} \delta^{H_2} \cdot M^{H2}_{p,t} + \delta^{SCO} \cdot M^{SCO}_t \right) \cdot P^{\xi}_t \cdot \mathbb{E}_{\xi \in \Xi}[\xi \cdot \xi^T] \Big) \Bigg] \\
& - \sum_{t \in T} \frac{{}^{UC_1}/_{\rho_{DR}} \cdot \gamma^{Bitumen}}{(1+r)^t} \cdot M^{in}_{DR,t} \cdot P^{\xi}_t \cdot \mathbb{E}_{\xi \in \Xi}[\xi] \qquad (5.44a) \\
s.t. \quad & -h^T \cdot \Lambda^b \leq \bar{\Omega}^M \qquad (5.44b) \\
& -W^T \cdot \Lambda^b = (M^{in}_{DR,1} \cdot P^{\xi}_1)^T \\
& \Lambda^b \geq 0
\end{aligned}$$

$$M_{p,c,t}^{out} = \alpha_{p,c}^{yield} \cdot M_{p,t}^{in} \quad \forall p \in SP, c \in C, t \in T \tag{5.44c}$$

$$M_{TC,t}^{in} = (1 - \sum_{c} \alpha_{DR,c}^{yield}) \cdot M_{DR,t}^{in} \quad \forall t \in T \tag{5.44d}$$

$$\sum_{p' \in SP} M_{p',c,t}^{out} = M_{p,t}^{in} \quad \forall (p,c) \in PC, t \in T \tag{5.44e}$$

$$M_{p,t}^{HTout} = \alpha_{p}^{HT} \cdot \left(M_{p,t}^{in} + M_{p,t}^{H2} \right) \quad \forall p \in MP, t \in T \tag{5.44f}$$

$$M_{p,t}^{H2} = \frac{\alpha_{p}^{H_2} \cdot M_{p,t}^{in}}{\rho_p} \quad \forall p \in MP, t \in T \tag{5.44g}$$

$$M_{t}^{SCO} = \sum_{p \in MP} M_{p,t}^{HTout} \quad \forall t \in T \tag{5.44h}$$

$$-h^T \cdot \Lambda_{p,t}^{i} \leq 0 \quad \forall p \in MP, t \in T \tag{5.44i}$$

$$-W^T \cdot \Lambda_{p,t}^{i} = \left(\left[\underline{\Omega}_{p}^{Spec} \cdot M_{t}^{SCO} - M_{p,t}^{HTout} \right] \cdot P_{t}^{\xi} \right)^T \quad \forall p \in MP, t \in T$$

$$\Lambda_{p,t}^{i} \geq 0 \quad \forall p \in MP, t \in T$$

$$-h^T \cdot \Lambda_{p,t}^{j_1} \leq -\underline{\Omega}_{p}^{X} \cdot Y_{p,t} \quad \forall p \in P, t \in T \tag{5.44j}$$

$$-W^T \cdot \Lambda_{p,t}^{j_1} = \left(-X_{p,t} \cdot P_{t}^{\xi} \right)^T \quad \forall p \in P, t \in T$$

$$\Lambda_{p,t}^{j_1} \geq 0 \quad \forall p \in P, t \in T$$

$$-h^T \cdot \Lambda_{p,t}^{j_2} \leq \bar{\Omega}_{p}^{X} \cdot Y_{p,t} \quad \forall p \in P, t \in T$$

$$-W^T \cdot \Lambda_{p,t}^{j_2} = \left(X_{p,t} \cdot P_{t}^{\xi} \right)^T \quad \forall p \in P, t \in T$$

$$\Lambda_{p,t}^{j_2} \geq 0 \quad \forall p \in P, t \in T$$

$$Q_{p,t} = Q_{p,t-1} + X_{p,t} \quad \forall p \in P, t \in T_{-1} \tag{5.44k}$$

$$-h^T \cdot \Lambda_{p,t}^{l_1} \leq 0 \quad \forall p \in P, t \in T \tag{5.44l}$$

$$-W^T \cdot \Lambda_{p,t}^{l_1} = \left(\left[\underline{\Omega}_{p}^{Q} \cdot Q_{p,t} - \frac{UC_1 \cdot M_{p,t}^{in}}{\rho_p} \right] \cdot P_{t}^{\xi} \right)^T \quad \forall p \in P, t \in T$$

$$\Lambda_{p,t}^{l_1} \geq 0 \quad \forall p \in P, t \in T$$

$$-h^T \cdot \Lambda_{p,t}^{l_2} \leq 0 \quad \forall p \in P, t \in T$$

$$-W^T \cdot \Lambda_{p,t}^{l_2} = \left(\left[\frac{UC_1 \cdot M_{p,t}^{in}}{\rho_p} - Q_{p,t} \right] \cdot P_{t}^{\xi} \right)^T \quad \forall p \in P, t \in T$$

$$\Lambda_{p,t}^{l_2} \geq 0 \quad \forall p \in P, t \in T$$

$$E_{u,t} = \sum_{p} \beta_{p,u} \cdot M_{p,t}^{in} \quad \forall u \in U, t \in T \tag{5.44m}$$

$$C_{t}^{CAPEX} = \sum_{p} \left(a_p \cdot Q_{p,t} + B_p \right) \quad \forall t = 1 \tag{5.44n}$$

$$C_{t}^{CAPEX} = \sum_{p} \left(a_p \cdot X_{p,t} + B_p \cdot Y_{p,t} \right) \quad \forall t \in T_{-1} \tag{5.44o}$$

$$-h^T \cdot \Lambda_{t}^{p} \leq \bar{\Omega}_{t}^{Investment} \quad \forall t \in T \tag{5.44p}$$

$$-W^T \cdot \Lambda_{t}^{p} = \left(C_{t}^{CAPEX} \cdot P_{t}^{\xi} \right)^T \quad \forall t \in T$$

$$\Lambda_{t}^{p} \geq 0 \quad \forall t \in T$$

Table 5.11: Expectation of uncertain parameters

$\mathbb{E}_{\xi\in\Xi}[\zeta]$		[0.1667, 0.1667, 0.1667, 0.1667, 0.1667]
$\mathbb{E}_{\xi\in\Xi}[\epsilon]$	$\Gamma^{SCO}=1$	[1.2530, 1.8525, 1.7973, 0.4994, 0.5290]
$\mathbb{E}_{\xi\in\Xi}[\epsilon]$	$\Gamma^{SCO}=2$	[2.9197, 4.0271, 3.6889, 1.2945, 1.2755]
$\mathbb{E}_{\xi\in\Xi}[\epsilon]$	$\Gamma^{SCO}=3$	[3.4491, 4.8414, 4.4043, 1.7453, 1.7138]
$\mathbb{E}_{\xi\in\Xi}[\epsilon]$	$\Gamma^{SCO}=4$	[3.4476, 4.8515, 4.4745, 1.8442, 1.7309]
$\mathbb{E}_{\xi\in\Xi}[\epsilon]$	$\Gamma^{SCO}=5$	[3.5758, 4.8785, 4.4844, 1.7951, 1.7624]

$$-h^T\cdot\Lambda^q_{p,t}\leq 0\quad\forall t\in T,p\in P \tag{5.44q}$$

$$-W^T\cdot\Lambda^q_{p,t}=\left(-M^{in}_{p,t}\cdot P^{\xi}_t\right)^T\quad\forall t\in T,p\in P$$

$$\Lambda^q_{p,t}\geq 0\quad\forall t\in T,p\in P$$

$$Y_{p,t}\in\{0,1\}\quad\forall p\in P,t\in T \tag{5.44r}$$

where P^{ξ}_t, P^{SCO}_t and $P^{CO_2}_t$ are the truncate vectors, Λ^b, $\Lambda^i_{p,t}$, $\Lambda^{j_1}_{p,t}$, $\Lambda^{j_2}_{p,t}$, $\Lambda^{l_1}_{p,t}$, $\Lambda^{l_2}_{p,t}$, Λ^p_t, and $\Lambda^q_{p,t}$ are new variable stemmed from the dual counterpart of all the inequality constraints, and $tr(\cdot)$ is the trace operator. Note that the expected values of the uncertain parameters are calculated as following. The uncertainty set associated with the carbon tax, ζ_t, is defined with equations 5.21 and 5.22. Furthermore, equations 5.33, 5.34, and 5.39 are used to determine a set for the SCO oil price uncertainty, ϵ_t. A sampling method is applied to compute the conditional expectation (see Table 5.11) within the uncertainty set. Specifically, 50,000 samples are generated inside the uncertainty sets (based on uniform distribution of ζ_t and normal distribution of ϵ_t). Afterwards, the means of samples in the sets are calculated and applied for the expectation estimation. Moreover, covariance matrices are evaluated using the same samples.

5.6 Results and discussion

In this section, results obtained from optimization of the deterministic and stochastic models are presented. First, the SP model solutions are validated using the DP model. Afterwards, the optimal solutions of two models are analyzed and compared. Before discussing the results, computational features of the models are reported here to have a better understanding of their complexities. Optimization problems of the DP and SP models are programmed in GAMS. The DP model is relatively small with 246 equations and 186 variables. On the other hand, the LDR approximation of the SP model includes 7,811 equations and 11,181 variables. As it can be seen, the SP model is quite large compared to its DP counterpart. Moreover, CPLEX solver with stopping criteria of one hour computational time and relative optimality gap of 0.1% are set. Using a desktop computer (single core of Intel® i5–4590 @ 3.30 GHz, 8 GB RAM), the optimal solutions are found in less than a second and five seconds for the DP and SP models, respectively.

5.6.1 Effects of uncertainty set size (Γ^{SCO})

In this part, effects of changing Γ^{SCO} are studied. The special case is when Γ^{SCO} is equal to zero. This can be used to validate the proposed SP model. Under this circumstance, if it is defined mathematically correct,

Table 5.12: Optimal NPV ($MM) of the SP models for different modes

Γ^{SCO}	Mode 1	Mode 2	Mode 3
5	8892.7	8444.8	6371.0
4	8841.3	8391.8	6321.9
3	8814.8	8365.4	6289.7
2	8121.2	7672.2	5650.7
1	6284.3	5868.1	4247.5

the SP model optimization leads to the same optimal solution as the DP model. Other values of Γ^{SCO}s are helpful to understand effects of the uncertainty set size on SP optimal solution. The bigger the Γ^{SCO}, the higher the chance of SCO price fluctuation. In other words, when Γ^{SCO} is smaller, the SCO price changes will be in a more conservative range. Note that the DP model does not vary with non–zero Γ^{SCO}.

$\Gamma^{SCO} = 0$. Here, we change the right–hand side of equation 5.22 as zero. Accordingly, ζ_t is forced to be zero as well based on equations 5.21 and 5.22. Moreover, we fix Γ^{SCO} as zero, and this results in $\epsilon_t = 0$ and $\epsilon'_t = 0$ based on equation 5.34. Under these circumstances, the uncertainty set of ξ is reduced to a singleton $[1, 0, ..., 0]^T$, and correspondingly, $\mathbb{E}_{\xi \in \Xi}[\xi]$ will be $[1, 0, ..., 0]^T$. Eventually, $\widetilde{\gamma}_t^{CO_2}(\xi)$ and $\widetilde{\gamma}_t^{SCO}(\xi)$ can be expressed as $[30, 30, 30, 30, 30]^T$ and B^{SCO}, respectively. Notice that the vector B^{SCO} is computed according to the ARMA model. As long as the decision parameters of this model (p and q) are fixed, the B^{SCO} vector will be unchanged regardless of Γ^{SCO} values. When Γ^{SCO} varies, the A^{SCO} matrix is the one which adjusts accordingly. For this study, the B^{SCO} vector is found as $[91.45, 44.40, 23.31, 62.81, 29.50]^T$.

If the above vectors of $\gamma_t^{CO_2}$ and γ_t^{SCO} are applied in the DP model, optimal solutions of the DP and SP models must be the same. Accordingly, $5217.2MM, $4904.6MM and $3560.7MM are the solutions for the modes 1, 2 and 3, respectively, where both DP and SP models converge to the same values. When the right–hand side of equation 5.22 and Γ^{SCO} are set as zero, having equal optimal values for the DP and SP models validates the developed SP model.

$\Gamma^{SCO} \neq 0$. Different Γ^{SCO}s, varying from 1 to 5, are selected to study effects of the uncertainty set size (see Table 5.12). while the current value of SCO ($51.45 bbl^{-1}) is applied for the DP models, the expected values of uncertain parameters are used for the corresponding SP model for each Γ^{SCO} value.

Obtained results from the DP model optimization are based on the SCO price and carbon tax fixed at $51.45 bbl^{-1} and $30 per tonne of CO_2, respectively. Accordingly, optimal solutions of the modes 1, 2 and 3, are found to be $5043.2MM, $4724.2MM and $3372.2MM, respectively. For the SP model, a higher Γ^{SCO} means a larger set for the uncertain parameters, and in our case, more SCO price fluctuations. According to Table 5.12, the NPVs increase when the uncertainty set is bigger. It means that considering less conservative case with a larger Γ^{SCO} is more favorable for the system. The reason is behind assumptions on which the uncertain SCO price is defined: (1) the studied upgrading plant is economical only when the SCO price is over $28.5 bbl^{-1} according to a sensitivity analysis of the DP model, (2) it is assumed that the lowest possible price ($\underline{\Omega}^{SCO}$) is $20 bbl^{-1}, and (3) there is no upper bound for the oil price. As it can be seen, the only range in which investing on the upgrading plant is not economical is below $28.5 bbl^{-1}. According to Figure 5.3, the oil price can vary from $20 to $115 bbl^{-1}. Consequently, the upgrading plant will be

Table 5.13: Comparison of mean values of the NPV ($MM) for the DP and SP models

Γ^{SCO}	Mode 1		Mode 2		Mode 3	
	SP	DP	SP	DP	SP	DP
5	8889.3	7653.6	8408.1	7277.1	6335.5	5760.1
4	8876.3	7643.1	8391.6	7269.8	6326.4	5753.9
3	8818.9	7614.0	8349.2	7243.5	6271.0	5719.7
2	8091.5	7157.8	7635.8	6803.5	5614.7	5315.6
1	6282.0	6000.5	5872.7	5672.8	4258.9	4258.9

profitable for most of the cases, except the range of [$20 to $28.5 bbl^{-1}].

5.6.2 Comparison of the deterministic and stochastic solution

In this section, advantages of the developed SP model are discussed. To do so, optimal solutions of the DP and SP models obtained from the previous section are applied and simulated for 50,000 random and feasible scenarios. This way, a fair comparison can be conducted between obtained solutions. Matlab and GAMS software are coupled together for this purpose. The DP and SP solutions are exported from GAMS to Matlab using a GDX file. Afterwards, the following steps are applied iteratively:

1. A sample set is generated inside the defined uncertainty set. Note that, in the uncertainty set definition, h and W matrices are both dependent on Γ^{SCO}.

2. A feasible sample set is applied into the optimal solution so as to calculate the objective function.

3. This procedure continues till the number of generated samples reaches 50,000.

Figure 5.4 illustrates NPV distribution of the DP and SP models, respectively, for mode 1 and $\Gamma^{SCO} = 1$. Moreover, Tables 5.13 and 5.14 summarize average and standard deviation values of the NPVs for the both DP and SP models, three modes, and five Γ^{SCO}s. There are two important points about the obtained results of this part:

- The mean values of the NPVs from the SP model simulations are very close to those from the previous part in which the NPVs were based on the expectation values. Minimum and maximum of differences between using sampling and expectation approaches are 0.002% and 0.637%.

- For all Γ^{SCO}s, mean values of the NPVs from the SP model simulations are larger than mean values of the NPVs from the DP model simulations. By increasing Γ^{SCO} from one to five, the SP model leads to more profits up to $1235.7MM compared to the DP model.

5.6.3 Scenario–based analysis

Four scenarios are manually defined, according to Table 5.15, in order to analyze the solution obtained from the stochastic model. These four scenarios can be taken into account as four extreme cases. For the CO_2 tax price, its values are assumed to be constant as its current value for the first three scenarios, and are

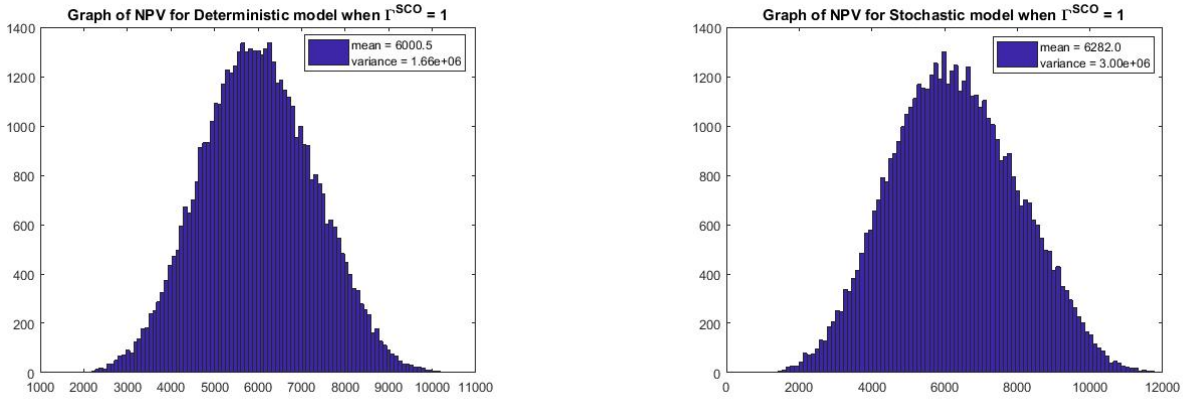

(a) (b)

Figure 5.4: Histogram presentations of the NPV estimation for 50,000 samples

Table 5.14: Comparison of standard deviation of the NPV for the DP and SP models

Γ^{SCO}	Mode 1		Mode 2		Mode 3	
	SP	DP	SP	DP	SP	DP
5	3759.0	2536.1	3759.0	2536.1	3784.6	2573.5
4	3739.5	2529.7	3739.5	2529.7	3788.0	2574.3
3	3678.6	2484.3	3678.6	2484.3	3709.6	2529.3
2	3096.2	2104.2	3096.2	2104.2	3106.5	2130.8
1	1701.9	1268.6	1701.9	1268.6	1731.4	1287.0

doubled for the last scenario. For the SCO price, three samples corresponding to the minimum, average, and maximum of the SCO price summation over the five stages are picked from Figure 5.3a for the first three scenarios. The last scenario has the same oil prices as the second one (the average oil prices prediction). Among the selected scenarios, scenario 1 has the most pessimistic SCO price forecast, and scenario 3 is the most optimistic case.

Analyses are carried out to see effects of the different scenarios and Γ^{SCO}s on optimal NPVs. Figure 5.5 shows solutions of the different scenarios under different modes when $\Gamma^{SCO} = 1$. The highest NPV is for the most optimistic one, scenario 3. On the other hand, the lowest NPV belongs to the most pessimistic one, scenario 1. Moreover, the carbon tax seems to have negligible consequences on the optimal solutions. Comparing scenarios S2 and S4, one can easily notice that the corresponding optimal NPVs are at the same orders. Hence, the SCO price is much more important on the optimal solution than the carbon tax.

A comprehensive comparison can also be carried out among efficiencies of different operation modes for the upgrading plant. As mentioned before, three modes are applied according to available information for thermocracking–based upgrading plants. Figure 5.5 demonstrates supremacy of mode 1 for all the considered scenarios. Moreover, for the same Γ^{SCO}, Table 5.13 reports excellence of mode 1 over the other two for the both DP and SP models. Mode 2 has the closest performance to mode 1, but still the smallest NPV differences between mode 1 and 2 is \$239.9MM according to Table 5.13. So, it can be concluded that mode 1 is the most efficient operating mode for the thermocracker. At mode 3, production rates of the NPH and

Table 5.15: Values of the uncertain parameters for each scenario

Parameter	Scenario			
	1	2	3	4
$\gamma_1^{CO_2}$ ($ tonne^{-1})	30	30	30	60
$\gamma_2^{CO_2}$ ($ tonne^{-1})	30	30	30	60
$\gamma_3^{CO_2}$ ($ tonne^{-1})	30	30	30	60
$\gamma_4^{CO_2}$ ($ tonne^{-1})	30	30	30	60
$\gamma_5^{CO_2}$ ($ tonne^{-1})	30	30	30	60
γ_1^{SCO} ($ bbl^{-1})	77.89	93.94	106.46	93.94
γ_2^{SCO} ($ bbl $^{-1}$)	33.00	47.14	64.00	47.14
γ_3^{SCO} ($ bbl $^{-1}$)	20.95	25.81	36.51	25.81
γ_4^{SCO} ($ bbl $^{-1}$)	55.74	66.12	77.83	66.12
γ_5^{SCO} ($ bbl $^{-1}$)	20.64	35.96	48.87	35.96

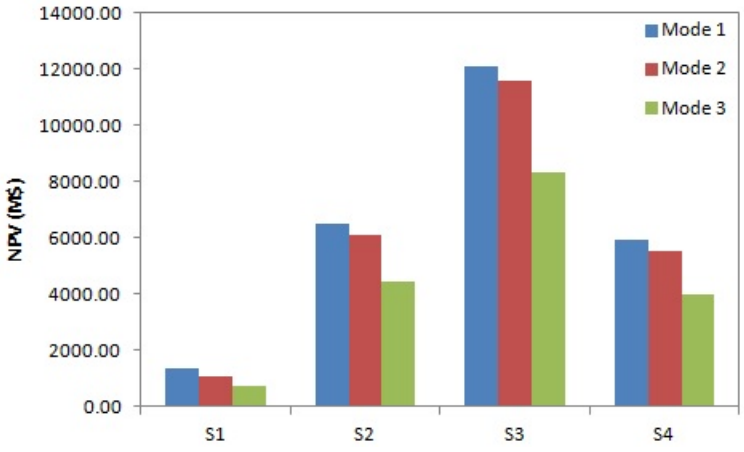

Figure 5.5: Optimal NPVs of considered sceneries when Γ^{SCO} is one

Table 5.16: The linear rules for $X_{p,t}$ (bpd) for $\Gamma^{SCO} = 1$ and mode 1

		t			
		2	3	4	5
p	DR	0	0	$60119.2 + 656.8 \cdot \xi_7 + 656.8 \cdot \xi_8$	0
	TC	60000.0	$31605.8 + 655.0 \cdot \xi_7 + 655.0 \cdot \xi_8$	$14986.6 - 146.0 \cdot \xi_7 - 146.0 \cdot \xi_8$	0
	NPHHT	0	0	$10917.7 + 119.3 \cdot \xi_7 + 119.3 \cdot \xi_8$	0
	LGOHT	0	$15085.5 + 312.6 \cdot \xi_7 + 312.6 \cdot \xi_8$	$7153.1 - 69.7 \cdot \xi_7 - 69.7 \cdot \xi_8$	0
	HGOHT	0	0	$15678.1 + 171.3 \cdot \xi_7 + 171.3 \cdot \xi_8$	0

Note: ξ_7 and ξ_8 correspond to the first year (ϵ_1) and second year (ϵ_2) of the SCO prices, respectively.

LGO are considerably less than the other two modes. Modes 1 and 2 produce nearly same portions of light products. However, larger electricity and heat demands of mode 2 make it less economical compared to mode 1.

Comparison among the expansion developments of different scenarios can also be found in Figure 5.6. As an example, capacity expansions of the process units over the time horizon are demonstrated in this Figure for mode 1 and $\Gamma^{SCO} = 1$. According to Figure 5.6, the deterministic solution results (yellow bars) are also shown in order to illustrate how different the DP solutions are from the SP ones. Furthermore, the linear decision rules corresponding to the expansion development variable ($X_{p,t}$) are also provided in Table 5.16.

The following points can be made from Figure 5.6:

- The deterministic solution results (yellow bars) have different trends for the expansion planning compared to the stochastic solution results. For the SP solution, the expansion developments mostly occur at the third and fourth time stages, while the major expansions in the DP solution occur at the third and fifth time stages.

- The difference in the expansion decisions of different scenarios shows flexibility of the SP model, in which we can change our decisions at each stage based on realized uncertainties of previous stages. The highest differences can be seen between the optimistic (cyan bars) and pessimistic (navy bars) scenarios. Moreover, the instinctive difference between S2 and S4 confirms triviality of the carbon tax again compared to the SCO price.

- Expansion capacities of the thermocracker unit at the second stage ($X_{TC,2}$) are all the same for the four scenarios. This is in agreement with the corresponding linear decision rule (see Table 5.16) in which there only exists an intercept. In other words, using the linear decision rule method does not necessarily mean that decision variables are dependent on uncertainty, and consequently scenarios.

5.6.4 Cost distribution

In this section, different cost elements included in the NPV are analyzed. These elements are revenue obtained from selling SCO, purchasing bitumen as feed, operating cost, capital cost, maintenance cost, and paying carbon tax.

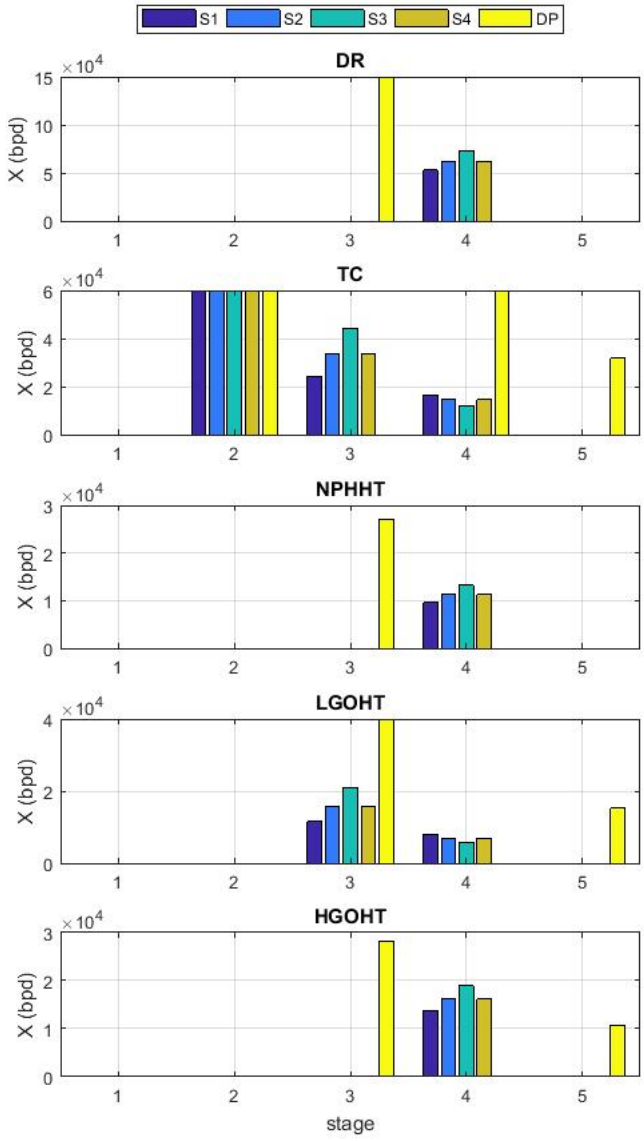

Figure 5.6: Expansion developments of process units when $\Gamma^{SCO} = 1$ (mode 1)

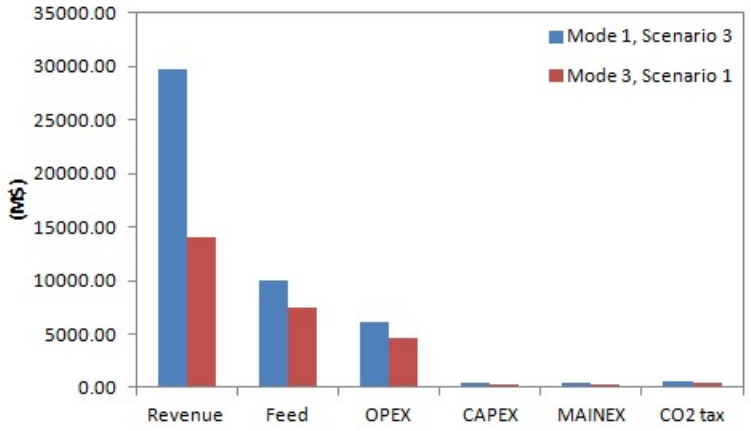

Figure 5.7: Costs distributions of the best and worst cases of Figure 5.5

For the sake of comparison, the best and worst cases from Figure 5.5 are selected, which are S3 of mode 1 and S1 of mode 3, respectively. The best case is scenario 3 at which the SCO price has relatively higher values, and the worst one corresponds to the lowest possible predicted oil prices, scenario 1. According to Figure 5.7, the major difference is between the revenue terms indicating importance of the SCO price. There is \$15,763.0MM more profits for the best case. Moreover, the feed and OPEX are the main costs compared to the other terms. Last but not least, ratios of the revenue to the carbon tax are near 30 and 53 for the worst and best cases, respectively. This explains why variations of carbon tax does not have significant impacts on optimal solutions of the previous sections. It also justifies independency of the decision rules from the carbon tax uncertainty. One can also notice that the linear rules are independent of the carbon tax as shown in Table 5.16.

5.7 Conclusion

According to the results, the following remarks can be concluded. First, the carbon tax has insignificant impacts on the optimal solution compared to the SCO price. After illustrating costs distributions of two extreme scenarios, it was noticed that the SCO price is the most dominant factor on NPVs while the carbon tax costs has a small impact on total NPVs. As a result, the obtained decision rules are independent of the carbon tax uncertainty. Second, LDR offers a flexible and robust solution depending on realized uncertainties. Rather than giving optimal solution values, LDR approach provides linear decision rules with coefficients found through optimization of an associated SP model. Solutions of the DP and SP models were compared through a sampling based evaluation, and they were further investigated through several representative scenarios. According to mean and standard deviation values of the solutions simulated by random samples, optimal solution of the SP models are all more economical and robust. Finally, it is worth mentioning that the uncertainty set size Γ^{SCO} affects the optimal solution. This parameter reflects the decision maker's perspective on the future uncertainty, and consequently, it may lead to distinctive solutions.

Chapter 6

Capacity Planning of Partially Upgraded Bitumen Production with Multistage Stochastic Programming[1]

6.1 Introduction

Alberta's oil sands has proven reserves of 165.4 billion bbl in three regions of Athabasca, Cold Lake and Peace River [4]. This ranks Canada as the third largest oil reserves in the world, after Venezuela and Saudi Arabia. Total crude bitumen production, including 46% of surface mining and 54% of in–situ, is about 2.8 million bpd in 2017 [4]. According to the latest forecast, the oil sands production is expected to increase to 3.67 million bpd in 2030 [5]. This means that there should be investment on new infrastructures in order to handle the production increase.

There are three major options to process this extra bitumen: (1) transportation with pipeline without upgrading, (2) full upgrading, and (3) partial upgrading. Note that, about 45% or 1.1 million bpd of crude bitumen production was sent for full upgrading in Alberta and the rest was transported in 2015 (without upgrading). The first option, transportation, does not appear to be the solution because of the following reasons [7]. Firstly, diluent is required to reduce the viscosity of unprocessed bitumen to have a flowing mixture known as DilBit. Therefore, besides of pipeline capital cost, using diluent adds the cost (i) paying tolls for the exported diluent, (ii) recovering diluent at the pipeline terminal, and (iii) paying tolls for shipping back the recovered diluent. Secondly, such act might raise concerns about the possible environmental and economic impact of pipeline transportation at provincial or federal level. For instance, the most recent dispute has been over the Trans Mountain pipeline expansion that would transport more Albertan bitumen to the British Columbia coast [8]. Hence, pipeline transportation of DilBit itself cannot solve the problem of bitumen production increase.

The second option, full upgrading, has even less chance than the first option. Not only would it require significant investment, but also the final product, known as SCO, has strong competitors in the market. For new full upgrading capacity building, Northwest Sturgeon Upgrader is the only ongoing project with large

[1] A version of this chapter was submitted in the *Optimization and Engineering*, **2018**

amount of public subsidies while Voyageur upgrader project was cancelled by Suncor in March 2012. The operation of CNOOC's upgrader has been suspended since July 2016 at the Long Lake in–situ project [7]. On the other hand, the dramatically expanding supply of light U.S. unconventional oil has made the SCO market smaller. Moreover, installation of full upgrading facilities next to the in–situ projects, which are the dominant technologies for the bitumen extraction, is neither practical nor economical. One of the reasons is the necessity of a pipeline system which takes us back to the cumbersome of the first option for bitumen processing. Therefore, investing on new full upgrading infrastructure is not a promissing option.

The third option, partial upgrading, is likely to be the sustainable approach in the future [7]. Firstly, the final product of partially upgraded bitumen, PUB, could be more favourable in the market compared to SCO. Although PUB is a higher–value product compared to bitumen, partial upgraders only upgrade bitumen to a light crude similar to medium or heavy crude. Secondly, near one third of the existing pipeline capacity would be free up for more transportation due to eliminating the need for diluent. Note that diluent is still required to transport bitumen from in–situ extraction facilities to partial upgraders; however, these two are supposed to be located close to each other. The only issue is that there is no fully commercialized partial upgrader being developed so far.

Scaling up the partial upgraders from a pilot plant to fully industrial production of PUB is the remaining challenge. To investigate this issue, a steering committee has been appointed as national partial upgrading program (NPUP), including Alberta Innovates, six industry partners, government of Saskatchewan, Alberta Energy, Alberta Economic Development and Trade, and Natural Resources Canada. The committee proposed an objective of partial upgrading of 20% of in–situ bitumen production by 2030. There have been a few studies which evaluate and compare partial upgrading technologies. The most recent one was a whitepaper reported by Jacobs Consultancy [137]. Previously, a similar project was studied in 2015 by Muse Stancil where only an executive summary version can be found [138]. Some representative partial upgrading technologies include: (i) High Quality (HI–Q) from MEG Energy [139, 140, 141], (ii) Bitumax from NEXEN [142, 143], (iii) Husky Diluent Reduction (HDR) from Husky Energy [144], and (iv) JetShear from Fractal Systems [145].

Another study was carried out in 2009 in which the author discussed the methods for delivering heavy oil and bitumen to the market and the promising partial upgrading technologies [146]. Later on, a more comprehensive review was conducted on the emerging technologies for upgrading of heavy crude oils [147]. The author concluded that there is not a unique solution for partial upgrading. Refineries can define their own technologies depending on the heavy oil feedstock. Two recent works focused on economic potential and environmental impact of partial upgraders [148], and their public–interest benefit [7].

In this study, we address the partial upgrading commercialization and its associated capacity planning according to the NPUP's target for 2030. This problem is modeled as a multistage stochastic programming (MSP) problem. Next, related references to this work are discussed below.

The problem that is addressed in this Chapter is MSP of bitumen partial upgrading. This problem is "multistage" since the decision variables are related to planning of an operation at multiple periods of time. Furthermore, planning for future without considering inherent uncertainties would not be robust and hence

trustworthy. While availability of feedstock is one of the unknowns in the future, partial upgraders have not been commercialized yet and there are also uncertainties regarding their efficiencies and costs. Therefore, the deterministic programming would not provide a robust solution for this problem. There are two approaches to deal with uncertainty in optimization: robust and stochastic optimization. Robust optimization assumes that the uncertain data resides in the uncertainty set. On the other hand, stochastic optimization is based on knowing the true probability distribution of uncertain parameters.

There are different methods for multistage stochastic programming, but the two popular ones are: (i) scenario tree, and (ii) decision rule approximation. The scenario tree is based on developing a set of scenarios with corresponding probability of occurrences. For example, the demand for production of an operation can be predicted to (1) increase by 10%, (2) not change, or (3) reduce by 10% in the preceding periods. Erbis et al. modeled a MSP to minimize the total production cost of carbon nanotube production capacity expansion planning [149]. Optimal timing of expansion, expansion size, process type, production volume, and also the occupational safety controls were determined through a MILP problem. Moreover, the effects of uncertainties on potential revenue were indicated through Monte Carlo simulations [149]. In another work, a two–stage stochastic integer programming model was presented for the optimal tactical semiconductor manufacturing capacity planning problem with demand and capacity uncertainty [150]. The "here–and–now" variables (variables which are made before realization of uncertainty) are the capacity procurement, and the "wait–and–see" variables (variables which are made after realization of uncertainty) are operational level variables such as production, inventory, and shipment. A large number of scenarios and integer decision variables were addressed by implementing a distributed parallel algorithm which solves a master and some scenario subproblems [150]. Golari et al. developed a multi–period, production–inventory planning model in a multi–plant manufacturing system powered with onsite and grid renewable energy [151]. To determine the optimal production quantity, the stock level, and the renewable energy supply in each period were the decision variables to minimize the aggregate production cost. After presenting the deterministic model, the stochastic one was introduced through a multistage, scenario tree of the power intermittency. A modified Benders decomposition algorithm was used to search for the optimal production schedule [151]. Later on, a multistage stochastic programming was applied for tactical planning of distribution problem of refined products [152]. Time series models were applied to represent oil price series and oil demand series, respectively. Then, as a link between the time series models and the stochastic model, these models were used within the scenario–based approach so as to define the joint realizations for such random parameters. Moreover, a scenario reduction approach was employed to improve the computational efficiency of problems [152].

The second popular method for multistage stochastic programming is decision rule–based approximation. In the LDR approach, dynamic decision variables are defined as affine functions of uncertainty, where the intercept and decision rule coefficients are the new optimization variables. The intercept represents the fixed value before realization of any uncertainty, while the decision rule coefficients is related to the real–time adjustment. Note that, at each time period, the adjustable decision variables only depend on the realized uncertainty. LDR has been implemented in many MSP applications. For example, Braaten applied LDR

approximation in the seasonal planning problem for a hydropower producer [153]. Decision variables were the amount to discharge for generation, pumping and spillage, and uncertainty was with inflow and price [153]. In another work, a deterministic model is proposed for multiperiod multiproduct planning problem with a third–party–logistics company [135]. The objective function was total cost subjected to raw materials, manufacturing capacity, and inventory constraints. By introducing demand uncertainty, robust counterpart and LDR approximation models were also developed and compared with the deterministic solution over different scenarios. It was shown that LDR approximation model outperform both deterministic and static robust counterpart models [135]. In our previous work, LDR method was applied for expansion development of full upgrading plants in oil sands industry [154]. We developed a MSP model under uncertainty in SCO and carbon tax. Studying different scenarios showed that (i) stochastic solution was more flexible, economical, and robust compared to the deterministic one, and (ii) final linear decision rules of variables were independent of carbon tax indicating its negligibility compared to SCO price [154].

The remainder of the Chapter is organized as follows. Section 6.2 states the problem, and Section 6.3 presents the MSP model. The nomenclature of presented model is available in Appendix A. Section 6.4 proposes two novel hybrid methods to address the challenge in solving the presented MSP model. Section 6.5 reports on numerical results and comparison of two hybrid models, and conclusions are drawn in Section 6.6.

6.2 Problem statement

The problem addressed in this Chapter can be expressed as follows. We define a set of partial upgrading technologies $i \in I$ and a set of time periods $t \in T$. Nominal values are reported for operating and capital cost coefficients (Table 6.1), processing bitumen target (Table 6.2), weighted score of each technology (Table 6.3), and periodical budget. In addition, bounds on capacity, and other parameters are given in Table 6.4. The problem is to determine the optimal capacity and operation plan at each period in order to achieve the lowest total cost during the whole time horizon of the operation. Note that, in this Chapter, parameters or variables which are independent on time period are expressed as static, while dynamic is used for those which are dependent on time periods.

For the processing bitumen target, the following assumptions were made. Firstly, the partial upgrading plant is assumed to be designed for a hypothetical in–situ facility with 180,000 bpd capacity (similar to the capacity of two existing in–situ facilities in Alberta: Foster Creek and Cold Lake [11]). Secondly, the production of the hypothetical in–situ facility will follow the same trend as the one predicted for in–situ production of bitumen for the province of Alberta (from 1.54 million bpd in 2016 to 2.16 million bpd in 2030 [5]). Therefore, the expected capacity for the hypothetical in–situ facility will be 250,000 bpd by 2030. To reach NPUP's goal (partial upgrading of 20% of in–situ bitumen produced by 2030), there is need for a partial upgrader with 50,000 bpd by 2030. By assuming that the initial capacity installation is around 30,000 bpd, the trend provided in the Table 6.2 can be applied.

The weighted score of each technology is required to take its commercialization potential into account.

Table 6.1: Operating and capital cost coefficients [138]

Partial upgrader	α_i (M$/bbl)	β_i (M$/bbl)
PU1	8.02e-6	22750e-6
PU2	8.02e-6	22750e-6
PU3	6.02e-6	6000e-6
PU4	3.06e-6	20000e-6
PU5	3.22e-6	14750e-6
PU6	10.02e-6	28250e-6

Table 6.2: In–situ bitumen partial upgrading target

Time period (t)	ν_t (bpd)
$2020 - 2022$	30,000
$2022 - 2024$	35,000
$2024 - 2026$	40,000
$2026 - 2028$	45,000
$2028 - 2030$	50,000

As it can be found in one of the reports in partial upgrading technology assessment [138], there are many factors that need to be considered such as methodology, technical viability, commercial applicability, costs and integration (See Table 6.3). There are some points needed to be clarified about this Table:

1. Each row represent the score from some sub–factors and associated sub–weights. For example, "costs" row is combination of (i) CAPEX and (ii) OPEX, and "Commercial Applicability" row includes (i) Refined Value Differential to Athabasca Dilbit, (ii) Financing Potential–Timing, (iii) Distillate Potential, (iv) Olefinicity, (v) Low Valued Product Sale/Disposal, (vi) Diluent Required.

2. The higher the score, the better the technology. The sub–factors were linearly transformed according to predefine ranges. For example, the OPEX sub–factor was defined in 2.5–10.5 ($/bbl) range, so a technology's score would be 10 if its OPEX is 2.5 ($/bbl).

3. In Muse Stancil's final report, the evaluation and comparison of technologies were based on the "Total Score" row [138].

In this Chapter, we present a more rigorous method for the sake of evaluation and comparison of technologies. To do so, we excluded the "Costs" row from Table 6.3, distributed its weight to other factors, and re–evaluated the total score as new parameter, ϕ_i. Accordingly, the new weight factors would be 8%, 38%, 46%, and 8% for Methodology, Technical Viability, Commercial Applicability, and Integration, respectively.

Finally, we assume that it takes two years (a time period) to construct a partial upgrader with specific capacity. Although the existing partial upgrading technologies are currently not ready for commercialization, we assumed that the first plant will start its operation by 2020. The last assumption is that there is a minimum amount of bitumen being processed through partial upgrading at time period t. It means that the optimal solution is supposed to process a minimum amount of feedstock or more.

Table 6.3: Commercialization factor [138]

Commercialization Factor	Partial Upgraders					
	PU1	PU2	PU3	PU4	PU5	PU6
Methodology (5%)	3.0	9.0	8.0	7.0	3.0	3.0
Technical Viability (25%)	3.4	4.8	7.2	7.2	5.2	3.2
Commercial Applicability (35%)	4.8	6.7	5.7	6.8	7.3	2.4
Costs (35%)	3.0	3.0	8.6	5.3	6.8	0.7
Integration (5%)	3.0	3.0	4.0	8.0	5.0	3.0
Total Score	**3.6**	**4.9**	**7.1**	**6.5**	**6.3**	**2.0**
ϕ_i	**4.0**	**5.9**	**6.3**	**7.1**	**6.0**	**2.8**

Table 6.4: Miscellaneous parameters of MDP model

Parameter	Value
γ	500 (M$)
δ	730 (day/year)
Φ	5.0
$\underline{\Omega}$	20,000 (bpd)
$\bar{\Omega}$	40,000 (bpd)
r	12 (%)

6.3 Multistage stochastic programming model

In this section, the MSP model is presented to address inherent uncertainties with the planning model. As mentioned in Introduction section, there is not any commercialized partial upgrading at the moment. There are many uncertainties regarding commercialization of existing technologies which need to be taken into account. By incorporating such uncertainties, we can find a more robust optimal solution than the deterministic model.

We incorporated uncertainties with all the associated parameters to each partial upgraders, being composed of the operating and capital costs (α_i and β_i) and commercialization factor (ϕ_i). Moreover, there is no guarantee in realization of assumed values for processing bitumen target (ν_t) and investment budget (γ) in the future, and hence, they were also considered as uncertain parameters. It is worth mentioning the properties of different uncertainties with respect to the time period. While the uncertainty associated with processing bitumen target is time–dependent, the rest of uncertainties can be assumed to be time–independent. Note that, in the MSP model, tilde symbol is used for uncertainty representation.

$$\min \quad Cost = \mathbb{E}\left[\sum_{t\in T}\sum_{i\in I}\frac{\delta\cdot\tilde{\alpha_i}\cdot O_{i,t}(\xi)}{(1+r)^{t+1}} + \sum_{i\in I}\frac{\tilde{\beta_i}\cdot C_i}{(1+r)} + \sum_{t\in T}\sum_{i\in I}\frac{\tilde{\beta_i}\cdot X_{i,t}(\xi)}{(1+r)^{t+1}}\right] \tag{6.1a}$$

$$s.t. \quad \tilde{\nu_t} \le \sum_i O_{i,t}(\xi) \quad \forall t\in T, \xi\in\Xi \tag{6.1b}$$

$$0.75\cdot(C_i + \sum_{t'\le t-1} X_{i,t'}(\xi)) \le O_{i,t}(\xi) \le (C_i + \sum_{t'\le t-1} X_{i,t'}(\xi)) \quad \forall i\in I, t\in T, \xi\in\Xi \tag{6.1c}$$

$$\sum_{i\in I}(\tilde{\beta_i}\cdot C_i) \le \tilde{\gamma} \quad \forall \xi\in\Xi \tag{6.1d}$$

$$\sum_{i \in I} \tilde{\beta}_i \cdot X_{i,t}(\xi) \leq \tilde{\gamma} \quad \forall t \in T, \xi \in \Xi \tag{6.1e}$$

$$\Phi \leq \frac{\sum_{i \in I} \tilde{\phi}_i \cdot (C_i + \sum_{t \in T} X_{i,t}(\xi))}{\sum_{i \in I} (C_i + \sum_{t \in T} X_{i,t}(\xi))} \tag{6.1f}$$

$$\underline{\Omega} \cdot Y_i^C \leq C_i \leq \bar{\Omega} \cdot Y_i^C \quad \forall i \in I \tag{6.1g}$$

$$\underline{\Omega} \cdot Y_{i,t}^X \leq X_{i,t}(\xi) \leq \bar{\Omega} \cdot Y_{i,t}^X \quad \forall i \in I, t \in T, \xi \in \Xi \tag{6.1h}$$

$$Y_i^C, Y_{i,t}^X \in \{0,1\} \quad \forall i \in I, t \in T \tag{6.1i}$$

The objective 6.1a is to minimize the overall cost which includes operating cost (first term), initial capacity installation cost (second term), and capacity expansion cost (third term). Equation 6.1b expresses that the overall operation of time period t is greater than or equal to the processing bitumen target in time period t. Equation 6.1c states that operation of technology i at time period t should be less than the available capacity (summation of initial capacity and expansion till $t-1$) and be greater than 75% of the available capacity. In other words, operation of a specific period is independent of the expansion decision of the same period due to two–years construction requirement. Equations 6.1d and 6.1e sets an upper limit (γ) on total investment for the initial capacity and expansion, respectively. Equation 6.1f is to make sure that the weight summation of score ϕ_i is larger than a threshold (Φ). For example, we do not want to choose a technology in which the operating and capital costs are low but there is not enough engineering facts supporting it. Equations 6.1g and 6.1h limit the capital and expansion capacities to be in reasonable ranges. Note that binary variables Y_i^C indicate whether an initial installation of technology i is made or not, and $Y_{i,t}^X$ indicate whether there is an expansion for technology i at time period t or not.

In the above model, all the uncertainties are summarized in vector ξ. Additionally, while C_i is a static decision variable, $O_{i,t}(\xi)$ and $X_{i,t}(\xi)$ are dependent on uncertainties. The reason can be better understood through visualization of uncertainties realization and decision making sequences (see Figure 6.1):

1. The static decisions are first made before the first period.
2. The time–dependent uncertainty is realized at the beginning of a time period.
3. The decision variables of t time period ($O_{i,t}(\xi)$ and $X_{i,t}(\xi)$) are made with respect to realization of uncertainties in t and previous time periods.

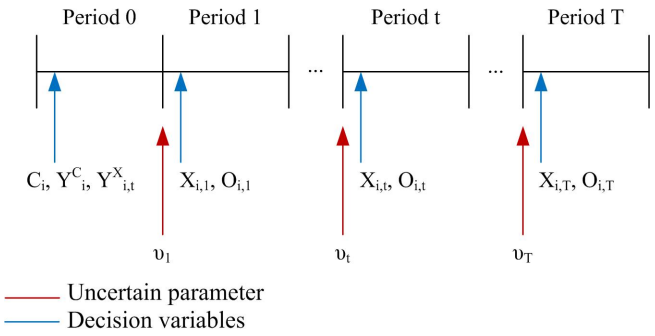

Figure 6.1: Timetable of uncertainty realization and decision making

6.4 Hybrid model

For the presented MSP model, there are two terms causing solution difficulties: $\tilde{\beta}_i \cdot X_{i,t}(\xi)$ from Equation 6.1e and $\tilde{\phi}_i \cdot X_{i,t}(\xi)$ from Equation 6.1f. In these terms, we have multiplication of a static uncertain parameter and an adjustable variable dependent on dynamic uncertainty. Under this circumstance, applying strong duality theorem from linear programming is impossible and another approach needs to be considered.

The method presented in this Chapter is a hybrid multistage stochastic programming–robust optimization model. When we have two sources of uncertainties multiplying by each other, one term can be treated with a scenario–based representation and the other one can be handled with uncertainty set. Since each term can be modeled with either of the two approaches, we propose the following hybrid models:

1. **Hybrid model 1 (H1)**. This model applies uncertainty set for the static uncertain parameter (robust optimization) and scenario tree for the adjustable variable (stochastic programming). To the best of our knowledge, there has been only two studies addressing such a problem [155, 156] by presenting a hybrid model. In Shabani and Sowlati work [155], the dynamic uncertainty was the monthly available feedstock defined through a scenario tree, and the static uncertainty was the feed quality presented as a polyhedral uncertainty sets. In the other work [156], the transportation cost was the dynamic uncertainty defined by stochastic scenarios, and the demand and return in each period and for each retailer were the static uncertainty presented as a polyhedral uncertainty sets.

2. **Hybrid model 2 (H2)**. This model uses an uncertainty set for the dynamic uncertainty (robust optimization) and a number of samples for the static uncertain parameter (stochastic programming). To the best of the authors' knowledge, there has not been any attempt with similar idea.

6.4.1 Hybrid model 1

In this section, hybrid model 1 is introduced. A scenario tree is built for the dynamic uncertain parameter (ν_t), and a node index ($s \in S$) is applied. As a result, the adjustable variables have fixed values at each node. On the other hand, the static uncertain parameters are modeled using uncertainty sets. The uncertainty set defined for four parameters (α_i, β_i, ϕ_i, and γ), and the scenario tree developed for the only dynamic

parameter (ν_s) are discussed below.

Uncertainty set. Uncertain parameters are assumed to be uniform within the range of perturbation ϵ:

$$\tilde{\alpha}_i = \bar{\alpha}_i \cdot (1 + \xi^{\alpha_i}) \quad \forall i \in I \tag{6.2a}$$

$$|\xi^{\alpha_i}| \leq \epsilon \quad \forall i \in I \tag{6.2b}$$

$$\tilde{\beta}_i = \bar{\beta}_i \cdot (1 + \xi^{\beta_i}) \quad \forall i \in I \tag{6.2c}$$

$$|\xi^{\beta_i}| \leq \epsilon \quad \forall i \in I \tag{6.2d}$$

$$\tilde{\phi}_i = \bar{\phi}_i \cdot (1 + \xi^{\phi_i}) \quad \forall i \in I \tag{6.2e}$$

$$|\xi^{\phi_i}| \leq \epsilon \quad \forall i \in I \tag{6.2f}$$

$$\tilde{\gamma} = \bar{\gamma} \cdot (1 + \xi^{\gamma}) \tag{6.2g}$$

$$|\xi^{\gamma}| \leq \epsilon \tag{6.2h}$$

Finally, all the static uncertainties can be aggregated as an uncertainty vector $\xi = [\xi^{\alpha_1}$ ... $\xi^{\alpha_6}, \xi^{\beta_1}$ ... $\xi^{\beta_6}, \xi^{\phi_1}$ ... $\xi^{\phi_6}, \xi^{\gamma}]$, and all the constraints in (6.2) can be summarized into uncertainty set $\Xi = \{\xi : W \cdot \xi \geq h\}$.

Scenario tree. The scenario tree for uncertainty in processing bitumen target is demonstrated in Figure 6.2). The number shown on each arch represent the increase in processing target for partial upgrading from previous node. Note that, [20,000 30,000 40,000] (bpd) are assumed for the first stage, and [0 5,000 10,000] (bpd) are applied for the rest of the time horizon. The scenario tree has six stages, including years of 2018, 2020, ... , 2026, and 2028.

The proposed hybrid model 1 is:

$$\min \quad Cost = \mathbb{E}\left[\sum_{s\in S}\sum_{i\in I} \frac{\delta \cdot \bar{\alpha}_i \cdot (1 + \xi^{\alpha_i}) \cdot O_{i,s}}{(1+r)^{\tau_s+1}} + \sum_{i\in I} \frac{\bar{\beta}_i \cdot (1 + \xi^{\beta_i}) \cdot C_i}{(1+r)} + \sum_{s\in S}\sum_{i\in I} \frac{\bar{\beta}_i \cdot (1 + \xi^{\beta_i}) \cdot X_{i,s}}{(1+r)^{\tau_s+1}}\right] \tag{6.3a}$$

$$s.t. \quad \tilde{\nu_s} \leq \sum_i O_{i,s} \quad \forall s \in S \tag{6.3b}$$

$$0.75 \cdot (C_i + \sum_{s'\in A(s)} X_{i,s'}) \leq O_{i,s} \leq (C_i + \sum_{s'\in A(s)} X_{i,s'}) \quad \forall i \in I, s \in S \tag{6.3c}$$

$$\sum_{i\in I} \bar{\beta}_i \cdot (1 + \xi_i^{\beta}) \cdot C_i \leq \bar{\gamma} \cdot (1 + \xi^{\gamma}) \quad \forall \xi \in \Xi \tag{6.3d}$$

$$\sum_{i\in I} \bar{\beta}_i \cdot (1 + \xi_i^{\beta}) \cdot X_{i,s} \leq \bar{\gamma} \cdot (1 + \xi^{\gamma}) \quad \forall s \in S_{-1}, \xi \in \Xi \tag{6.3e}$$

$$\Phi \leq \frac{\sum_{i\in I} \bar{\phi}_i \cdot (1 + \xi^{\phi_i}) \cdot (C_i + \sum_{s'\in P(s)} X_{i,s'})}{\sum_{i\in I} (C_i + \sum_{s'\in P(s)} X_{i,s'})} \quad \forall s \in L, \xi \in \Xi \tag{6.3f}$$

$$\underline{\Omega} \cdot Y_i^C \leq C_i \leq \bar{\Omega} \cdot Y_i^C \quad \forall i \in I \tag{6.3g}$$

$$\underline{\Omega} \cdot Y_{i,s}^X \leq X_{i,s} \leq \bar{\Omega} \cdot Y_{i,s}^X \quad \forall i \in I, s \in S, \xi \in \Xi \tag{6.3h}$$

$$Y_i^C, Y_{i,s}^X \in \{0, 1\} \quad \forall i \in I, s \in S \tag{6.3i}$$

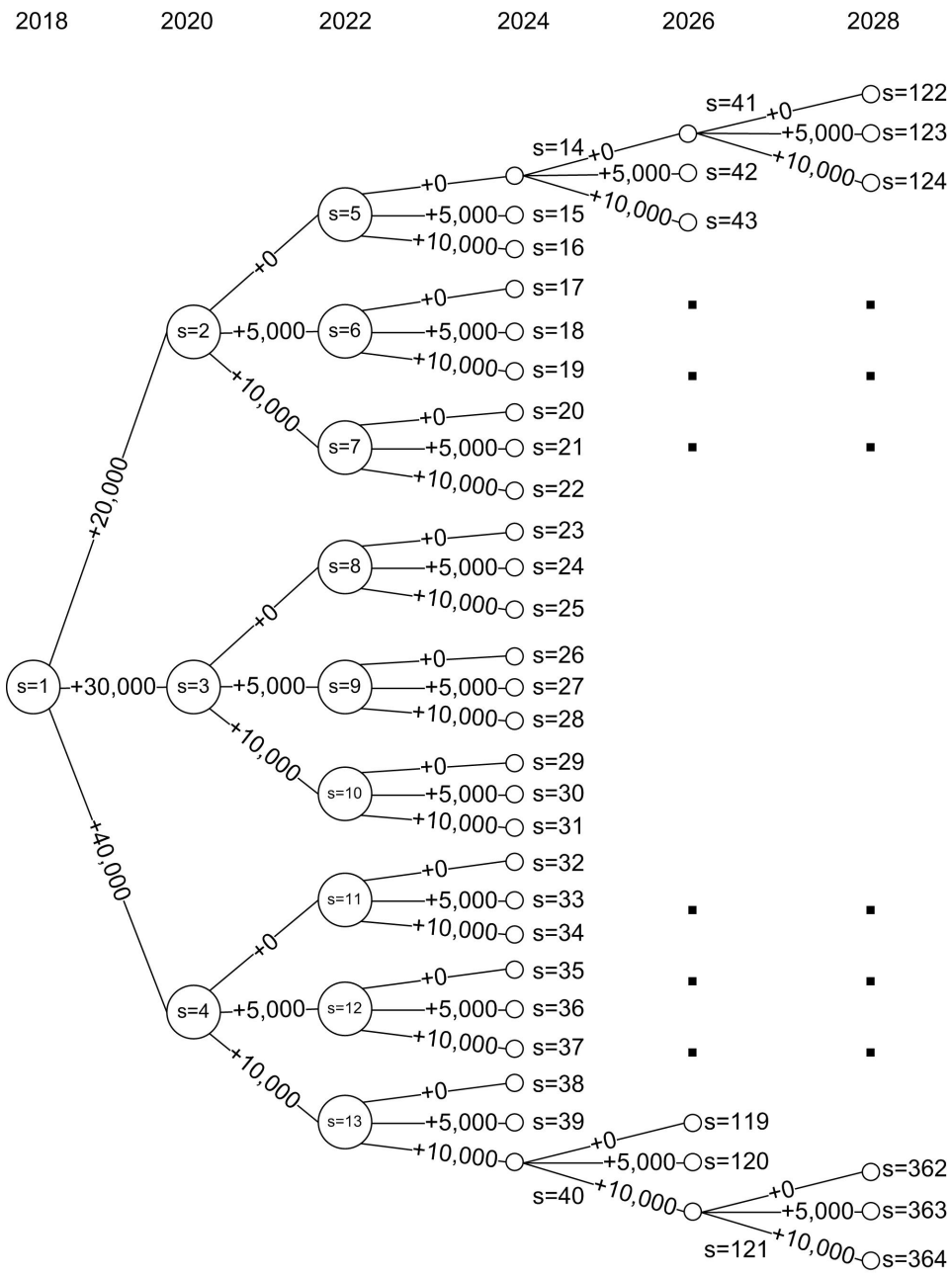

Figure 6.2: The scenario tree for uncertainty in processing bitumen target

Consequently, the robust counterpart of the MSP model can be developed as

$$\min \quad Cost = \sum_{i\in I} \bar{\alpha_i} \cdot \sum_s \frac{\delta \cdot Pr_s \cdot O_{i,s}}{(1+r)^{\tau_s+1}} + \sum_{i\in I} \frac{\bar{\beta_i} \cdot C_i}{(1+r)} + \sum_{i\in I} \bar{\beta_i} \cdot \sum_s \frac{Pr_s \cdot X_{i,s}}{(1+r)^{\tau_s+1}} \tag{6.4a}$$

$$s.t. \quad \nu_s \leq \sum_i O_{i,s} \quad \forall s \in S \tag{6.4b}$$

$$0.75 \cdot (C_i + \sum_{s'\in A(s)} X_{i,s'}) \leq O_{i,s} \leq (C_i + \sum_{s'\in A(s)} X_{i,s'}) \quad \forall i \in I, s \in S \tag{6.4c}$$

$$-h^T \cdot \Lambda^d \leq \left[\bar{\gamma} - \sum_{i\in I} \bar{\beta_i} \cdot C_i\right] \tag{6.4d}$$

$$-W^T \cdot \Lambda^d = \left[\sum_{i\in I} \bar{\beta_i} \cdot P^{\beta_i} \cdot C_i - \bar{\gamma} \cdot P^{\gamma}\right]^T$$

$$-h^T \cdot \Lambda^e_s \leq \left[\bar{\gamma} - \sum_{i\in I} \bar{\beta_i} \cdot X_{i,s}\right] \quad \forall s \in S_{-1} \tag{6.4e}$$

$$-W^T \cdot \Lambda^e_s = \left[\sum_{i\in I} \bar{\beta_i} \cdot P^{\beta_i} \cdot X_{i,s} - \bar{\gamma} \cdot P^{\gamma}\right]^T \quad \forall s \in S_{-1}$$

$$-h^T \cdot \Lambda^f_s \leq \left[\sum_{i\in I} \left(\bar{\phi_i} \cdot (C_i + \sum_{s'\in P(s)} X_{i,s'}) - \Phi \cdot (C_i + \sum_{s'\in P(s)} X_{i,s'})\right)\right] \quad \forall s \in L \tag{6.4f}$$

$$-W^T \cdot \Lambda^f_s = \left[-\sum_{i\in I} \bar{\phi_i} \cdot P^{\phi_i} \cdot (C_i + \sum_{s'\in P(s)} X_{i,s'})\right]^T \quad \forall s \in L$$

$$\underline{\Omega} \cdot Y^C_i \leq C_{i,s} \leq \bar{\Omega} \cdot Y^C_i \quad \forall i \in I \tag{6.4g}$$

$$\underline{\Omega} \cdot Y^X_{i,s} \leq X_{i,s} \leq \bar{\Omega} \cdot Y^X_{i,s} \quad \forall i \in I, s \in S \tag{6.4h}$$

$$0 \leq \Lambda^d, \Lambda^e_s, \Lambda^f_{s'} \quad \forall s \in S_{-1}, s' \in L \tag{6.4i}$$

$$Y^C_{i,s}, Y^X_{i,s} \in \{0,1\} \quad \forall i \in I, s \in S \tag{6.4j}$$

6.4.2 Hybrid model 2

In this section, hybrid model 2 is introduced. For the stochastic optimization part, $|K|$ number of samples were generated for the static uncertain parameters (α_i, β_i, ϕ_i, γ_i). On the other hand, an uncertainty set was designed for the dynamic uncertain parameter (ν_t), and the dynamic decision variables were approximated using LDR. Uncertainty set defined for the only adjustable parameter (ν_t) is discussed below.

Uncertainty set. Uncertain parameter is assumed to be uniform but with different ranges at each time period. For the first period, the uncertain variable can be varied in a large range of 20,000–40,000 bpd, and its variations are limited between 0 and 10,000 bpd for the rest of time periods.

$$\tilde{\nu_t} = \sum_t \xi^{\nu_t} \quad \forall t \in T \tag{6.5a}$$

$$20000 \leq \xi^{\nu_t} \leq 40000 \quad \forall t \in \{t = 1\} \tag{6.5b}$$

$$0 \leq \xi^{\nu_t} \leq 10000 \quad \forall t \in T^{-1} \tag{6.5c}$$

Finally, all the dynamic uncertainties can be aggregated as an uncertainty vector as $\xi = [1, \xi^{\nu_1}, ..., \xi^{\nu_T}]$, and all the constraints (6.5) can be summarized into uncertainty set $\Xi = \{\xi : M \cdot \xi \geq l\}$.

The size of K set is determined as follows. When the size of this set is small, the optimal solution would miss some possible occurrence of events, and hence, it cannot represent a robust solution. A large set of samples, on the other hand, would cause higher computational cost which is always a cumbersome. To solve this issue, firstly, the samples were generated by implementing Latin hypercube sampling method to have a more well–distributed multidimensional set. Secondly, a sensitivity analysis was carried out to indicate a specific number of samples after which the objective function of H2 model will not change significantly. It was found that 1000 samples would be sufficient for our problem. The proposed hybrid model 2 is:

$$\min \quad Cost = \mathbb{E}\left[\sum_{t\in T}\sum_{i\in I}\sum_{k\in K}\frac{\alpha_{i,k}\cdot\delta\cdot O_{i,t}\cdot\xi_{[t]}}{K\cdot(1+r)^{t+1}} + \sum_{i\in I}\sum_{k\in K}\frac{\beta_{i,k}\cdot C_i}{K\cdot(1+r)} + \sum_{t\in T}\sum_{i\in I}\sum_{k\in K}\frac{\beta_{i,k}\cdot X_{i,t}\cdot\xi_{[t]}}{K\cdot(1+r)^{t+1}}\right] \tag{6.6a}$$

$$s.t. \quad \sum_t \xi^{\nu_t} \le \sum_i O_{i,t}\cdot\xi_{[t]} \quad \forall t\in T, \xi\in\Xi \tag{6.6b}$$

$$0.75\cdot(C_i + \sum_{t'\le t-1} X_{i,t'}\cdot\xi_{[t']}) \le O_{i,t}\cdot\xi_{[t]} \le C_i + \sum_{t'\le t-1} X_{i,t'}\cdot\xi_{[t']} \qquad \forall i\in I, t\in T, \xi\in\Xi \tag{6.6c}$$

$$\sum_{i\in I}\beta_{i,k}\cdot C_i \le \gamma_k \quad \forall k\in K \tag{6.6d}$$

$$\sum_{i\in I}\beta_{i,k}\cdot X_{i,t}\cdot\xi_{[t]} \le \gamma_k \quad \forall k\in K, t\in T, \xi\in\Xi \tag{6.6e}$$

$$\Phi \le \frac{\sum_{i\in I}\phi_{i,k}\cdot(C_i+\sum_{t\in T}X_{i,t}\cdot\xi_{[t]})}{\sum_{i\in I}(C_i+\sum_{t\in T}X_{i,t}\cdot\xi_{[t]})} \quad \forall k\in K, \xi\in\Xi \tag{6.6f}$$

$$\underline{\Omega}\cdot Y_i^C \le C_i \le \bar{\Omega}\cdot Y_i^C \quad \forall i\in I \tag{6.6g}$$

$$\underline{\Omega}\cdot Y_{i,t}^X \le X_{i,t}\cdot\xi_{[t]} \le \bar{\Omega}\cdot Y_{i,t}^X \quad \forall i\in I, t\in T, \xi\in\Xi \tag{6.6h}$$

$$Y_i^C, Y_{i,t}^X \in \{0,1\} \quad \forall i\in I, t\in T \tag{6.6i}$$

Consequently, the robust counterpart of the MSP model can be developed as

$$\min \quad Cost = \sum_{i\in I}\sum_{k\in K}\left(\sum_{t\in T}\frac{\alpha_{i,k}\cdot\delta\cdot O_{i,t}\cdot P_t\cdot\mathbb{E}_{\xi\in\Xi}[\xi]}{K\cdot(1+r)^{t+1}} + \frac{\beta_{i,k}\cdot C_i}{K\cdot(1+r)} + \sum_{t\in T}\frac{\beta_{i,k}\cdot X_{i,t}\cdot P_t\cdot\mathbb{E}_{\xi\in\Xi}[\xi]}{K\cdot(1+r)^{t+1}}\right) \tag{6.7a}$$

$$s.t. \quad -l^T\cdot\Pi_t^b \le 0 \quad \forall t\in T \tag{6.7b}$$

$$-M^T\cdot\Pi_t^b = \left[P_t^\nu - \sum_i O_{i,t}\cdot P_t\right]^T \quad \forall t\in T$$

$$-l^T\cdot\Pi_{i,t}^{c_1} \le -0.75\cdot C_i \quad \forall i\in I, t\in T \tag{6.7c}$$

$$-M^T\cdot\Pi_{i,t}^{c_1} = \left[0.75\cdot\sum_{t'\le t-1}(X_{i,t'}\cdot P_{t'}) - O_{i,t}\cdot P_t\right]^T \quad \forall i\in I, t\in T$$

$$-l^T\cdot\Pi_{i,t}^{c_2} \le C_i \quad \forall i\in I, t\in T$$

$$-M^T\cdot\Pi_{i,t}^{c_2} = \left[O_{i,t}\cdot P_t - \sum_{t'\le t-1}X_{i,t'}\cdot P_{t'}\right]^T \quad \forall i\in I, t\in T$$

$$\sum_{i\in I}\beta_{i,k}\cdot C_i \le \gamma_k \quad \forall k\in K \tag{6.7d}$$

$$-l^T\cdot\Pi_{k,t}^e \le \gamma_k \quad \forall k\in K, t\in T \tag{6.7e}$$

$$-M^T\cdot\Pi_{k,t}^e = \left[\sum_{i\in I}\beta_{i,k}\cdot X_{i,t}\cdot P_t\right]^T \quad \forall t\in T$$

$$-l^T \cdot \Pi_k^f \leq \sum_{i\in I} \phi_{i,k} \cdot C_i - \Phi \cdot \sum_{i\in I} C_i \quad \forall k \in K \tag{6.7f}$$

$$-M^T \cdot \Pi_k^f = \left[\Phi \cdot \sum_{i\in I}\sum_{t\in T} X_{i,t} \cdot P_t - \sum_{i\in I} \phi_{i,k} \cdot \sum_{t\in T} X_{i,t} \cdot P_t\right]^T \quad \forall k \in K$$

$$\underline{\Omega} \cdot Y_i^C \leq C_i \leq \bar{\Omega} \cdot Y_i^C \quad \forall i \in I \tag{6.7g}$$

$$-l^T \cdot \Pi_{i,t}^{h_1} \leq -\underline{\Omega} \cdot Y_{i,t}^X \quad \forall i \in I, t \in T \tag{6.7h}$$

$$-M^T \cdot \Pi_{i,t}^{h_1} = \left[-X_{i,t} \cdot P_t\right]^T \quad \forall i \in I, t \in T$$

$$-l^T \cdot \Pi_{i,t}^{h_2} \leq \bar{\Omega} \cdot Y_{i,t}^X \quad \forall i \in I, t \in T$$

$$-M^T \cdot \Pi_{i,t}^{h_2} = \left[X_{i,t} \cdot P_t\right]^T \quad \forall i \in I, t \in T$$

$$Y_i^C, Y_{i,t}^X \in \{0,1\} \quad \forall i \in I, t \in T \tag{6.7i}$$

$$0 \leq \Pi_t^b, \Pi_{i,t}^{c_1}, \Pi_{i,t}^{c_2}, \Pi_{k,t}^e, \Pi_{k,t}^f, \Pi_{i,t}^{h_1}, \Pi_{i,t}^{h_2} \quad \forall i \in I, k \in K, t \in T \tag{6.7j}$$

6.5 Results and discussion

In this section, results obtained from different cases are provided to compare the two proposed models. Note that all the experiments were conducted in GAMS platform on a desktop computer (single core of Intel® i5–4590 @ 3.30 GHz, 8 GB RAM). All the problems were MILP and the CPLEX solver was used for optimization. Furthermore, one hour computational time limit and relative optimality gap of 1% were set as the stopping criteria of optimization runs.

6.5.1 Computational time

One of the most important factors used in comparing different optimization models is the computational cost. In this part, both H1 and H2 models are analyzed with regard to their computational time, number of variables, and the optimal objective value. While the original stated problem has six time periods between 2018 and 2030, a range of four to eight time periods are studied for the comparison.

Figure 6.3a illustrates the computational time comparison for H1 and H2 models. For both models, the computational time is very small except the last case with eight time periods. In addition, the H1 model is more sensitive to the number of time periods, and hence, this model is not efficient for a large number of stages. The reason can also be explained by Figure 6.3b showing the number of variables. For H2 model, the number of variables has a linear trend versus the number of time periods, while the H1 model shows an exponential trend.

Effects of number of time periods on each model is discussed here. For H1 model, adding one time period would increase the number of possible scenarios with the power of three, as we defined three possible scenario at each node. For example, by increasing the number of time periods from 4 to 5, the number of scenarios will grow from 121 to 364 (near 200% increase). On the other hand, adding one time period in H2 model only leads to a new decision rule coefficient variable to each decision variables.

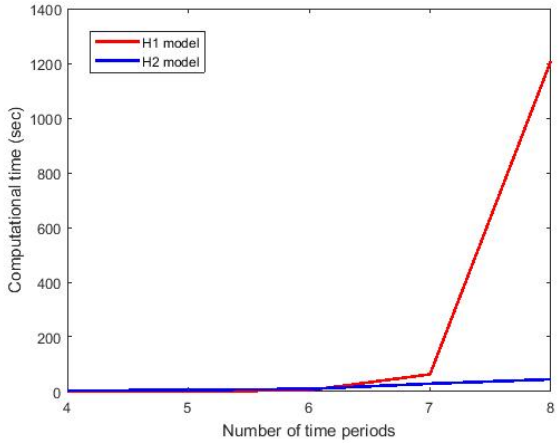

(a)

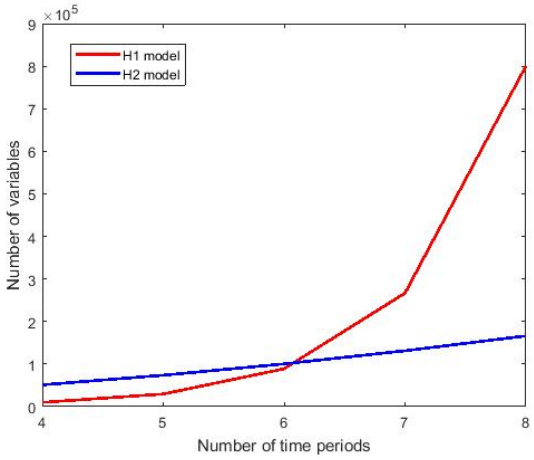

(b)

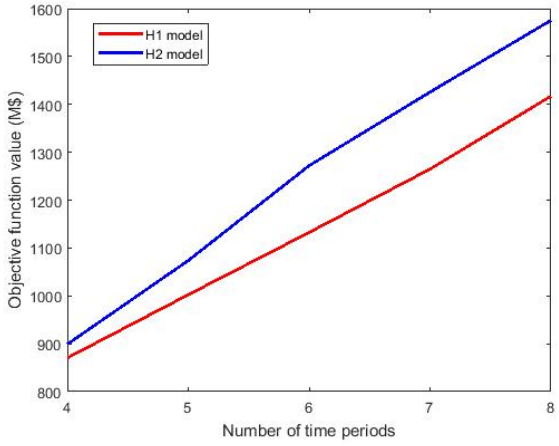

(c)

Figure 6.3: Computational time, number of variables, and objective function value comparison of H1 and H2

Table 6.5: The decision rules for expansion and operation of $PU3$ technology

t	$O_{'PU3',t}$	$X_{'PU3',t}$
1	$20,000 + 0.50 \cdot \xi_1$	$1.00 \cdot \xi_1$
2	$30,000 + 0.75 \cdot \xi_1$	0
3	$30,000 + 0.75 \cdot \xi_1$	0
4	$30,000 + 0.75 \cdot \xi_1 + 1.00 \cdot \xi_2$	0
5	$25,000 + 1.00 \cdot \xi_1 + 0.50 \cdot \xi_4 + 1.00 \cdot \xi_5$	0

6.5.2 Solution performance

In this section, the optimal solutions of H1 and H2 models are compared for the case where number of time periods is 6. To have a fair comparison, we evaluate the solution performance over a set of different scenarios. The set of scenarios used is the one that initially developed for the H1 model, because this is the set that H1 optimal solution is based on and also all of them are inside the defined uncertainty set of H2 model.

For each scenario in H1 model, the objective function value were extracted from GAMS solution for all the 243 possible scenarios. For H2 model, the procedure is explained below:

1. The optimal solution was imported from GAMS into MATLAB through a GDX file. According to Table 6.5, only one technology was chosen and the other technologies were not used.

2. A set of ξ generated according to the scenario tree used in H1 model. For example, based on Figure 6.2, when the scenario of ν_t is $[20,000 \quad 20,000 \quad 20,000 \quad 20,000 \quad 20,000]$, the corresponding ξ would be $[20,000 \quad 0 \quad 0 \quad 0 \quad 0]$ according to Equation 6.5.

3. Finally, applying the 243 scenarios in the decision rules and then calculating the objective function.

Figure 6.4 illustrates the distribution of objective values for both H1 and H2 models. It shows that H1 model leads to lower costs on average. This is consistent with the trend in Figure 6.3c. Nevertheless, H2 model is not limited to these scenarios as there is a defined set in which these scenarios belong to. Although the H1 solution is better, the H2 solution is more robust and can handle a larger set of uncertainty in the future. H1 solution might be infeasible for some unseen scenarios.

6.5.3 H1 and H2 solutions for three representative scenarios

In this section, solutions for three representative scenarios are discussed. These scenarios are (1) ν_t with the lowest possible trend which is $[20,000 \quad 20,000 \quad 20,000 \quad 20,000 \quad 20,000]$, (2) ν_t with the average possible trend which is $[30,000 \quad 35,000 \quad 40,000 \quad 45,000 \quad 50,000]$, and (3) ν_t with the highest possible trend which is $[40,000 \quad 50,000 \quad 60,000 \quad 70,000 \quad 80,000]$. Figure 6.5 shows the capacity (dark bars) and operation level (light bars) of best technology, which is $PU3$, from 2018 till 2030. All the decision variables for other technologies are zero. Solid black line represents the minimum amount of processing bitumen target which needs to be processed though partial upgrading (ν_t). The following points can be concluded from this Figure.

The sequence of decision making is the first point to mention. At the beginning of each period, we make two major decisions till the next stage: capacity expansion and operation level. These two have different

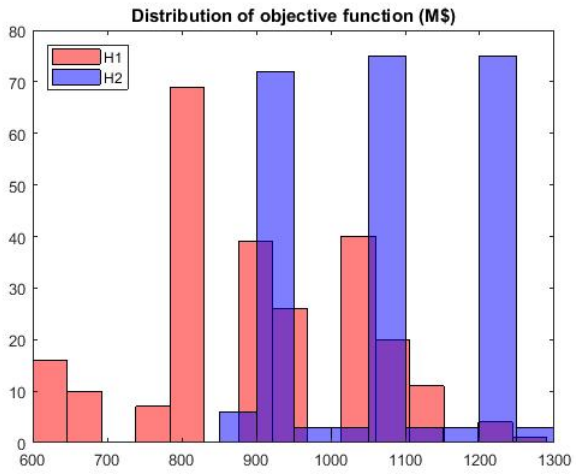

Figure 6.4: Histogram presentations of the objective function estimation for 243 scenarios from scenario tree

time orders. The capacity expansion is the decision we make at the beginning of a time period, but we are only able to take that capacity under operation starting from the following time step since it takes some time to build an operating unit. On the other hand, operation volume is selected at each period and can be executed for the same time period. For example, according to Figure 6.5a, it is decided to expand the capacity from 40,000 to 60,000 bpd for H2 model at 2020, and this expansion is under construction during 2020–2022, and finally it is available for operation from 2022. Furthermore, the operation of each time period is something between 75–100% of the available capacity at the same time period.

One can notice that the optimal decisions are all the same for the time period of 2020–2022. This is because the decisions of the first time period of 2018–2020 are independent of uncertainty. For the first time period, instead of expansion variable ($X_{i,t}$), we used another variable for installation capacity as C_i which is independent of defined uncertainty. Moreover, since there is no existing capacity for the first time period, corresponding operation is automatically equal to zero at the time period of 2018–2020.

Operation level is always greater than or equal to ν_t. As shown in Equation 5.43b, there is only a lower bound for amount of processed bitumen. As mentioned earlier, the target of NPUP is partial upgrading of 20% of in–situ bitumen production at 2030. This is treated as a minimum amount, and there is definitely a higher chance for operation of partial upgraders if they could operate under commercial scale in the near future. The only point that needs to be explained here is why there is higher processing than a specific lower bound when the objective function is minimization of costs. The reason is behind another constraint that we defined, Equation 5.43h. This constraint forces the expansion volume to be in a reasonable range; therefore, small expansion of capacity is not an option. As a result, when we have gradual increases in ν_t, the optimal solution has to prepare for that growth one step ahead. For example, in Figure 6.5c, capacity of H1 model is expanded at time periods of 2022–2024 and 2026–2028 when the actual demands for corresponding capacities are at time periods of 2024–2026 and 2028–2030.

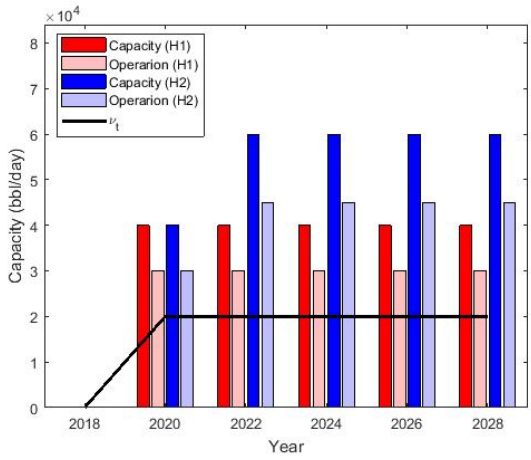

(a)

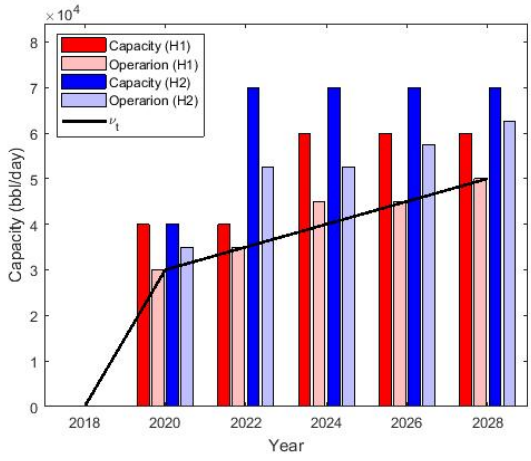

(b)

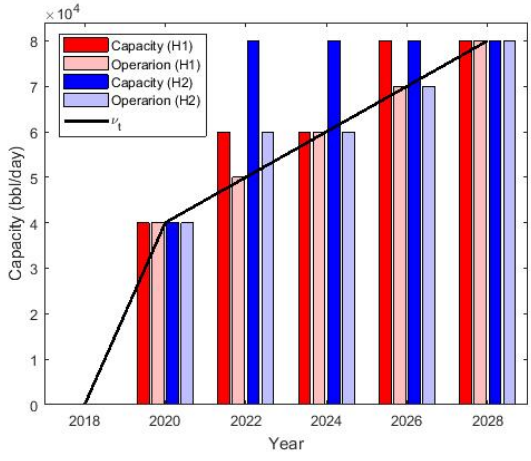

(c)

Figure 6.5: Installation, expansion, and operation comparison of three extreme scenarios for $PU3$ technology

6.6 Conclusion

Multistage stochastic programming model was presented in this Chapter for the optimal planning of initial capacity and expansion of bitumen partial upgrading. The case study was the NPUP's target for partial upgrading of 20% Canadian bitumen produced by in–situ approach. Incorporation of different uncertainty led to a complex stochastic optimization problem. Two hybrid models were developed to solve the problem in which static uncertain parameters were modeled with either uncertainty set (H1 model) or scenario (H2 model) and the dynamic uncertain parameters were modeled with either scenario tree (H1 model) or uncertainty set (H2 model), respectively.

Two proposed models were compared to each other. Firstly, computational time of the two models were studied. Time periods varying from four to eight were analyzed for this part. The H2 model was found computationally more efficient. Applying linear decision rule approximation to the adjustable decision variables made this model tractable with polynomial behavior of computational time versus the increase of time periods. Therefore, the exponential growth of scenario tree in the H1 model would be an issue for cases with large number of time periods. Secondly, performance of the solutions obtained from the two models were studied for the case with six periods. The scenario tree generated for H1 model was used to evaluate the performance of H2 model solution. Objective values resulted from H1 model were lower on average which was expected. The solution of H2 model is more robust as it was obtained from a large uncertainty set, while the solution of H1 model is only feasible for the scenario tree. Finally, three favorite scenarios were selected in order to discuss the optimal solutions in more details. The lowest, average, and highest possible trends of ν_t were taken into account for this purpose.

Chapter 7

Concluding Remarks and Future Works

This chapter briefly concludes and summarizes the key findings of the previous chapters of the thesis. Moreover, some recommendations are provided to further improve the methods applied in this thesis.

7.1 Concluding remarks

A comprehensive optimization model, which integrates the upgrading plant in the oil sands industry and the associated utility system, was presented in Chapter 2. The developed model maximizes the NPV when all the utility requirements of the upgrading plant are met by the polygeneration energy system. This is different from the literature work in which predesigned power and hydrogen plants with fixed operating conditions were used. Different upgrading plant capacities, being connected or disconnected to the public grid, various natural gas and electricity prices, and distinct margins between DilBit and SCO prices were the investigated factors. The results showed that the model can be a powerful tool for process design of the upgrading plant in the oil sands industry.

The key findings of this Chapter can be summarized as (1) increasing the size of the upgrading plant was only beneficial when the margin between DilBit and SCO price was high. Otherwise, it was better to invest in a smaller plant. (2) Selling additional electricity to the public grid was the major profit due to the price of this commodity. (3) In the upgrading plant, thermocracking was chosen to process the vacuum distillation residue for most of the scenarios. (4) Operation of SMR unit depended on the capacity of the upgrading plant, and it would be only selected for the upgrading plant with large capacity. (5) The gas turbine burning natural gas and the following HRSG units were only selected if selling extra electricity was an option. (6) While the highest NPV was achieved at a low natural gas price and high electricity price, the lowest NPV was found when the natural gas price was high and the electricity price was low.

To complete the model proposed in Chapter 2, a comprehensive optimization model was presented in Chapter 3 which includes bitumen upgrading facility, associated utility system, and the carbon capture process. The objective was finding the optimal design with the maximum of NPV when environmental concerns were also taken into account. The studied scenarios were based on different upgrading plant

capacities, natural gas and electricity prices, margins between diluted bitumen and SCO prices, and carbon taxes. The developed model was a large–scale non–convex MINLP problem which commercial solvers were incapable of finding its optimal solution directly. As a result, a robust decomposition algorithm was proposed after dividing the full–space model into two parts. Augmented Lagrangian decomposition method was applied for different scenarios.

The key findings of this Chapter can be summarized as (1) incorporating the carbon mitigation policy in the modeling led to lower NPVs compared to the similar scenario of Chapter 2 without carbon capture. (2) Despite Chapter 2, the hydrocracking process was favored over thermocracking for most of the scenarios in the upgrading plant. (3) Producing extra power from natural gas combustion in a gas turbine was highly beneficial except for one scenario (low electricity price and high natural gas price). (4) Pre–combustion was found as the most efficient CCS technology. The post–combustion and oxyfuel combustion technologies were barely chosen. (5) Low–quality duty boiler and SMR units were under operation alternatively for most of the scenarios. The SMR was preferred for smaller upgrading capacities, and low–quality duty boiler was found more beneficial for medium and high upgrading capacities. (6) Investing in a large upgrading plant was not an economical decision when the margin between DilBit and SCO price was small. Although large capacity upgraders were more profitable when the margin was adequately large, they were more vulnerable to fluctuations of fossil fuels prices.

In Chapter 4, it was assumed that a hydrocracking–based upgrading plant existed and determining its optimal operating conditions was the problem to be addressed. To do so, a novel optimization framework was proposed. Different properties of working fluids were empirically modeled as functions of units operating conditions. The correlations were developed according to the statistical analysis and data–driven from Aspen HYSYS simulation software. The proposed optimization problem was a non–convex NLP, and tight bounds on the variables were imposed to reach global optimality.

The key findings of this Chapter can be summarized as: (1) the SynDilBit was found as the economic commodity that was produced under optimal conditions when there was no pre–specified demand for commodities. (2) The most effective operating variables were temperatures, and their optimal values were at their defined upper bounds. The LHSVs were nearly in the middle of the defined bounds, and the trend for pressures was not clear. (3) The cutting points of different intermediate products were different in the first and second vacuum distillation columns. For the first column, the NPH was separated in a wider range, and the cutting points were in a smaller range for the HGO separation. Furthermore, the LGO was withdrawn with approximately similar ranges of cut points in both columns.

Starting with Chapter 5, the optimization problems were studied under uncertainty. Chapter 5 addressed the problem of expansion development of an existing thermocracking-based full upgrading plant. A stochastic multistage expansion development model was proposed considering the SCO price and carbon tax uncertainties. The solution of the presented stochastic model was obtained through the linear decision rule–based method. Effects of the uncertainty set size, comparison of solutions for selected pessimistic, realistic, and optimistic scenarios, effects of different operating modes for an upgrading plant, and cost distribution

analyses were conducted. The final solution was able to demonstrate the flexibility, robustness, and economic advantages of the stochastic solution rather than the deterministic one.

The key findings of this Chapter can be summarized as: (1) the optimal solution was mainly under the influence of the SCO price, and the carbon tax was an insignificant factor. In the costs distributions illustration, it was shown that the SCO price was the most important portion of NPVs while the carbon tax costs had a small share in total NPVs. Consequently, the decision rules were only dependent on the SCO price in the optimal stochastic solution. (2) Applying the linear decision rule offered a more flexible and robust solution. Deterministic and stochastic solutions were evaluated and compared through a large set of random samples. The solutions were also analyzed with several representative scenarios. Optimal solutions of the stochastic models were all more economical based on the mean and standard deviation values of the simulated solutions. (3) The uncertainty set size, which reflects the decision maker's perspective on the future uncertainty, was an effective parameter on the optimal solution. Distinctive solutions can be achieved depending on the value chosen for this parameter.

While there are currently some full upgrading plants under operation, the main focus of the private and public sectors is on developing new technologies as partial upgrading. NPUP has set a target to partially upgrade 20% of Canadian bitumen extracted by in–situ approaches. Chapter 6 of this thesis addressed the optimal planning of initial capacity and expansion of bitumen partial upgrading with the presence of uncertainty. The developed model was a multistage stochastic planning problem which had a unique feature: multiplication of uncertain parameters by uncertain dynamic decision variables. Two hybrid models were developed to tackle the problem in which different approaches were selected to define the uncertainty set. The static uncertain parameters can be modeled with either uncertainty set or scenario, and the dynamic uncertain parameters can be modeled with either scenario tree or uncertainty set. Consequently, in the hybrid model 1, the uncertain parameter was modeled with an uncertainty set and the dynamic variable was modeled as scenario dependent variables. In hybrid model 2, the uncertain parameter was modeled with samples and the dynamic variable was modeled using the decision rule–based approximation. Finally, results obtained from both hybrid models were compared to each other based on (i) computational time, (ii) solution performance, and (iii) hybrid model solutions for representative scenarios.

The key findings of this Chapter can be summarized as: (1) The H2 model was found computationally more efficient in the range of four to eight time periods. Applying H1 model was along with developing scenario tree which normally results in exponential growth of scenarios versus time periods increase. On the other hand, the H2 model was based on the linear decision rule approximation which its model tractability has been proved before, and hence, had a linear trend versus time periods increase. (2) Objective values resulted from the H1 model were lower on average where the scenario tree generated for the H1 model was used with six time periods. While the solution of the H1 model was only feasible for the scenario tree, the solution of the H2 model was more robust as it was obtained from a large uncertainty set. Therefore, having poor performance was expected for the H2 model solution comparing to the H1 model.

7.2 Future works

7.2.1 Optimal design and operation under uncertainty

In Chapters 2 and 3, the optimal design of full upgrading plant and its integrated utility plant was proposed. Moreover, in Chapters 4, we presented the optimal operation of a nominal full upgrading plant. Note that the optimization model for these Chapters was deterministic–based optimization problems. An important finding of these three Chapter was that their optimal solutions were highly dependent on efficiencies operating units, purchasing and selling prices, environmental regulations, demands, or availability of feedstock. In future works, optimization under uncertainties can be carried out by incorporating uncertainties into the developed deterministic models. By conducting optimization under uncertainty, the final solution will be more robust to different possible scenarios in the future.

7.2.2 Relaxing the binary variables as adjustable variables

The proposed model in Chapters 5 and 6 can even be further robust by relaxing the binary variables. In this thesis, the binary variables were assumed to be first–stage decision variables. It means that the user cannot change them after observation of uncertainties. Dividing the uncertainty set into partitions and presenting multiple binary solutions would be great to be considered as the next step for future work. Depending on uncertainty maps on which partition of the uncertainty set, a different set of binary variables will be picked as the solution. Consequently, the optimal solution would be more flexible and robust.

7.2.3 Optimal design and operation of partial upgrading facilities

The main focus of this thesis was on full upgrading plants at different levels of decision–making hierarchy. The partial upgrading technologies were not fully covered in our study since there was very limited public information regarding partial upgrading when we started our research four years ago. Nevertheless, partial upgrading technologies have successfully passed the pilot plant operation and are ready for the demonstration phase. Therefore, it would be the best time to put some effort on optimal design and operation of partial upgraders (similar to Chapters 2–4) as there might not be any further social or economic interest on a new full upgrading infrastructure.

Bibliography

[1] "World oil outlook," http://www.opec.org/opecweb/staticfilesproject/media/downloads/publications/WOO2014.pdf, Organization of the Petroleum Exporting Countries, Report, 2014 (accessed August 2016).

[2] A. Demirbas, A. Bafail, M.-M. Zytoon, and N. Sayed, "Unconventional energy sources: Safety impacts, opportunities, and economic challenges," *Energy Sources, Part B: Economics, Planning and Policy*, vol. 12, pp. 387–393, 2017.

[3] H. Wang, F. Ma, X. Tong, Z. Liu, X. Zhang, Z. Wu, D. Li, B. Wang, Y. Xie, and L. Yang, "Assessment of global unconventional oil and gas resources," *Petroleum Exploration and Development*, vol. 43, pp. 925–940, 2016.

[4] "Government of alberta's facts and stats," https://www.alberta.ca/index.aspx, accessed: 2018-03.

[5] "Crude oil forecast, markets and transportation," https://www.capp.ca/publications-and-statistics/publications/303440, Canadian Association of Petroleum Producers (CAPP), Report, 2017 (accessed May 2018).

[6] M. Teare, R. Cruickshank, S. Miller, S. Overland, and R. Marsh, "Alberta's energy reserves 2013 and supply/demand outlook 2014–2023," https://www.aer.ca/data-and-publications/statistical-reports/st98, Report, 2013.

[7] G. Fellows, R. Mansell, R. Schlenker, and J. Winter, "Public-interest benefit evaluation of partial-upgrading technology," The School of Public Policy Research Papers, University of Calgary. Vol. 10, Issue 1, January, Report, 2017.

[8] "CBC news," http://www.cbc.ca/news, 2016 (accessed September 2016).

[9] J. Charry-Sanchez, A. Betancourt-Torcat, and L. Ricardez-Sandoval, "An optimization energy model for the upgrading processes of canadian unconventional oil," *Energy*, vol. 68, pp. 629–643, 2014.

[10] G. Ordorica-Garcia, E. Croiset, P. Douglas, A. Elkamel, and M. Gupta, "Modeling the energy demands and greenhouse gas emissions of the canadian oil sands industry," *Energy & Fuels*, vol. 21, no. 4, pp. 2098–2111, 2007.

[11] "Oil sands magazine," http://www.oilsandsmagazine.com, 2015 (accessed August 2018).

[12] J. E. Falk, "Exact solutions of inexact linear programs," *Operations Research*, vol. 24, no. 4, pp. 783–787, 1976.

[13] A. L. Soyster, "Convex programming with set-inclusive constraints and applications to inexact linear programming," *Operations research*, vol. 21, no. 5, pp. 1154–1157, 1973.

[14] A. Ben-Tal and A. Nemirovski, "Robust convex optimization," *Mathematics of operations research*, vol. 23, no. 4, pp. 769–805, 1998.

[15] ——, "Robust solutions of uncertain linear programs," *Operations research letters*, vol. 25, no. 1, pp. 1–13, 1999.

[16] ——, "Robust solutions of linear programming problems contaminated with uncertain data," *Mathematical programming*, vol. 88, no. 3, pp. 411–424, 2000.

[17] ——, "Robust optimization–methodology and applications," *Mathematical Programming*, vol. 92, no. 3, pp. 453–480, 2002.

[18] A. Ben-Tal, A. Nemirovski, and C. Roos, "Robust solutions of uncertain quadratic and conic-quadratic problems," *SIAM Journal on Optimization*, vol. 13, no. 2, pp. 535–560, 2002.

[19] L. El Ghaoui and H. Lebret, "Robust solutions to least-squares problems with uncertain data," *SIAM Journal on matrix analysis and applications*, vol. 18, no. 4, pp. 1035–1064, 1997.

[20] L. El Ghaoui, F. Oustry, and H. Lebret, "Robust solutions to uncertain semidefinite programs," *SIAM Journal on Optimization*, vol. 9, no. 1, pp. 33–52, 1998.

[21] D. Bertsimas and M. Sim, "Robust discrete optimization and network flows," *Mathematical programming*, vol. 98, no. 1-3, pp. 49–71, 2003.

[22] ——, "The price of robustness," *Operations research*, vol. 52, no. 1, pp. 35–53, 2004.

[23] D. Bertsimas, D. Pachamanova, and M. Sim, "Robust linear optimization under general norms," *Operations Research Letters*, vol. 32, no. 6, pp. 510–516, 2004.

[24] A. Ben-Tal, A. Goryashko, E. Guslitzer, and A. Nemirovski, "Adjustable robust solutions of uncertain linear programs," *Mathematical Programming*, vol. 99, no. 2, pp. 351–376, 2004.

[25] D. Bertsimas, D. B. Brown, and C. Caramanis, "Theory and applications of robust optimization," *SIAM review*, vol. 53, no. 3, pp. 464–501, 2011.

[26] V. Gabrel, C. Murat, and A. Thiele, "Recent advances in robust optimization an robustness," Technical report, Universite Paris-Dauphine, Tech. Rep., 2012.

[27] A. Ben-Tal, L. El Ghaoui, and A. Nemirovski, *Robust optimization*. Princeton University Press, 2009.

[28] H. Heitsch and W. Römisch, "Scenario reduction algorithms in stochastic programming," *Computational optimization and applications*, vol. 24, no. 2-3, pp. 187–206, 2003.

[29] G. C. Pflug, "Scenario tree generation for multiperiod financial optimization by optimal discretization," *Mathematical programming*, vol. 89, no. 2, pp. 251–271, 2001.

[30] A. J. Kleywegt, A. Shapiro, and T. Homem-de Mello, "The sample average approximation method for stochastic discrete optimization," *SIAM Journal on Optimization*, vol. 12, no. 2, pp. 479–502, 2002.

[31] H. Niederreiter, *Random number generation and quasi-Monte Carlo methods*. SIAM, 1992, vol. 63.

[32] A. Ruszczynski and A. Shapiro, "Stochastic programming, volume 10 of handbooks in operations research and management science," 2003.

[33] A. Shapiro and A. Nemirovski, "On complexity of stochastic programming problems," in *Continuous optimization*. Springer, 2005, pp. 111–146.

[34] G. B. Dantzig, "Linear programming under uncertainty," 1955, vol. 1, pp. 197–206.

[35] E. M. Beale, "On minimizing a convex function subject to linear inequalities," *Journal of the Royal Statistical Society. Series B (Methodological)*, pp. 173–184, 1955.

[36] A. Charnes and W. W. Cooper, "Chance-constrained programming," *Management science*, vol. 6, no. 1, pp. 73–79, 1959.

[37] J. R. Birge and F. Louveaux, *Introduction to stochastic programming*. Springer Science & Business Media, 2011.

[38] S. W. Wallace and W. T. Ziemba, *Applications of stochastic programming.* SIAM, 2005.

[39] R. Henrion, "Introduction to chance-constrained programming," *Tutorial paper for the Stochastic Programming Community home page*, 2004.

[40] A. Prékopa, *Stochastic programming.* Springer Science & Business Media, 2013, vol. 324.

[41] G. Ordorica-Garcia, A. Elkamel, P. L. Douglas, E. Croiset, and M. Gupta, "Energy optimization model with CO_2-emission constraints for the canadian oil sands industry," *Energy and Fuels*, vol. 22, no. 4, pp. 2660–2670, 2008.

[42] G. Ordorica-Garcia, A. Elkamel, P. Douglas, and E. Croiset, "Optimal implementation of CO_2 capture technology in power and hydrogen production for oil sands operations," *Canadian Journal of Chemical Engineering*, vol. 88, no. 5, pp. 881–888, 2010.

[43] A. Betancourt-Torcat, G. Gutierrez, A. Elkamel, and L. Ricardez-Sandoval, "Integrated energy optimization model for oil sands operations," *Industrial & Engineering Chemistry Research*, vol. 50, no. 22, pp. 12 641–12 663, 2011.

[44] A. Betancourt-Torcat, A. Elkamel, and L. Ricardez-Sandoval, "A modeling study of the effect of carbon dioxide mitigation strategies, natural gas prices and steam consumption on the canadian oil sands operations," *Energy*, vol. 45, no. 1, pp. 1018–1033, 2012.

[45] J. Charry-Sanchez, A. Betancourt-Torcat, and A. Almansoori, "Environmental and economics trade-offs for the optimal design of a bitumen upgrading plant," *Industrial and Engineering Chemistry Research*, vol. 46, pp. 11 996–12 013, 2016.

[46] A. Betancourt-Torcat, A. Almansoori, A. Elkamel, and L. Ricardez-Sandoval, "Stochastic modeling of the oil sands operations under greenhouse gas emission restrictions and water management," *Energy & Fuels*, vol. 27, no. 9, pp. 5559–5578, 2013.

[47] U. Gomes, B. Patil, A. Betancourt-Torcat, and L. Ricardez-Sandoval, "Optimal infrastructure of the upgrading operations in the oil sands under uncertainty: A multiscenario MINLP approach," *Industrial & Engineering Chemistry Research*, vol. 53, no. 42, pp. 16 406–16 424, 2014.

[48] P. Liu, D. I. Gerogiorgis, and E. N. Pistikopoulos, "Modeling and optimization of polygeneration energy systems," *Catalysis Today*, vol. 127, no. 1-4, pp. 347–359, 2007.

[49] P. Liu, E. N. Pistikopoulos, and Z. Li, "A mixed-integer optimization approach for polygeneration energy systems design," *Computers & Chemical Engineering*, vol. 33, no. 3, pp. 759–768, 2009.

[50] Y. Chen, T. A. Adams, and P. I. Barton, "Optimal design and operation of static energy polygeneration systems," *Industrial & Engineering Chemistry Research*, vol. 50, no. 9, pp. 5099–5113, 2011.

[51] ——, "Optimal design and operation of flexible energy polygeneration systems," *Industrial & Engineering Chemistry Research*, vol. 50, no. 8, pp. 4553–4566, 2011.

[52] J. L. Haslbeck, N. J. Kuehn, E. G. Lewis, L. L. Pinkerton, J. Simpson, M. J. Turner, E. Varghese, and M. C. Woods, "Cost and performance baseline for fossil energy plants volume 1: Bituminous coal and natural gas to electricity," Report DOE/NETL-2010/1397, Revision 2a, 2013.

[53] "Equipment design and cost estimation for small modular biomass systems, synthesis gas cleanup, and oxygen separation equipment; task 1: Cost estimates of small modular systems," Report NREL/SR-510-39943, 2006.

[54] J. Wolff and J. Jones, "Shell gasification technology: Generating profit from the bottom of the barrel," Report, 2013.

[55] C.-L. Chen, C.-Y. Lin, and J.-Y. Lee, "Retrofit of steam power plants in a petroleum refinery," *Applied Thermal Engineering*, vol. 61, no. 1, pp. 7–16, 2013.

[56] O. Aguilar, S. J. Perry, J. K. Kim, and R. Smith, "Design and optimization of flexible utility systems subject to variable conditions: Part 1: Modelling framework," *Chemical Engineering Research and Design*, vol. 85, no. 8, pp. 1136–1148, 2007.

[57] M. R. Gray, *Upgrading Oilsands Bitumen and Heavy Oil*. Edmonton, Alberta, Canada: The University of Alberta Press, 2015.

[58] J. Chen and M. Munteanu, "Optimizing bitumen upgrading scheme - modeling and simulation approach," in *12AIChE - 2012 AIChE Spring Meeting and 8th Global Congress on Process Safety, Conference Proceedings*, Conference Proceedings.

[59] "Canadian Natural Resources Limited announces 2016 first quarter results," Canadian Natural Resources Limited, Report, 2016.

[60] "Market prices by Gas Alberta Inc." http://www.gasalberta.com/, 2016 (accessed September 2016).

[61] http://www.auc.ab.ca, 2016 (accessed August 2016).

[62] "Sulfur pricing," ICIS Pricing, Report, 2014.

[63] "Alberta oil sands industry: quarterly update," Government of Alberta, Report, Fall, 2015.

[64] "Alberta environment: Report on 2008 greenhouse gas emissions," Alberta Environment, Report, April 2010.

[65] R. Hill, S. Scott, D. Butler, S. P. Sit, D. Burt, R. Narayanan, T. Cole, C. Li, V. Lightbown, and Z. John Zhou, "Application of molten carbonate fuel cell for CO_2 capture in thermal in situ oil sands facilities," *International Journal of Greenhouse Gas Control*, vol. 41, pp. 276–284, 2015.

[66] I. Bolea, A. A. Checa, and L. M. Romeo, "Assessment of the integration of CO_2 capture technology into oil–sand extraction operations," *International Journal of Energy and Environmental Engineering*, vol. 5, no. 4, pp. 323–332, 2014.

[67] C. B. Tarun, E. Croiset, P. L. Douglas, M. Gupta, and M. H. M. Chowdhury, "Techno-economic study of CO_2 capture from natural gas based hydrogen plants," *International Journal of Greenhouse Gas Control*, vol. 1, no. 1, pp. 55–61, 2007.

[68] S. Nourouzi-Lavasani, F. Larachi, and M. Benali, "Energy and hydrogen coproduction from (Athabasca bitumen) coke gasification with CO_2 capture," *Industrial and Engineering Chemistry Research*, vol. 47, no. 18, pp. 7118–7129, 2008.

[69] B. Olateju and A. Kumar, "Techno-economic assessment of hydrogen production from underground coal gasification (UCG) in Western Canada with carbon capture and sequestration (CCS) for upgrading bitumen from oil sands," *Applied Energy*, vol. 111, pp. 428–440, 2013.

[70] J. E. Gemayel, A. Macchi, R. Hughes, and E. J. Anthony, "Simulation of the integration of a bitumen upgrading facility and an IGCC process with carbon capture," *Fuel*, vol. 117, pp. 1288–1297, 2014.

[71] R. S. Middleton and A. R. Brandt, "Using infrastructure optimization to reduce greenhouse gas emissions from oil sands extraction and processing," *Environmental Science & Technology*, vol. 47, pp. 1735–1744, 2013.

[72] S. Bourne, S. Crouch, and M. Smith, "A risk-based framework for measurement, monitoring and verification of the quest ccs project, Alberta, Canada," *International Journal of Greenhouse Gas Control*, vol. 26, pp. 109–126, 2014.

[73] S. Mukherjee, P. Kumar, A. Hosseini, A. Yang, and P. Fennell, "Comparative assessment of gasification based coal power plants with various CO_2 capture technologies producing electricity and hydrogen," *Energy & Fuels*, vol. 28, no. 2, pp. 1028–1040, 2014.

[74] R. T. J. Porter, M. Fairweather, C. Kolster, N. Mac Dowell, N. Shah, and R. M. Woolley, "Cost and performance of some carbon capture technology options for producing different quality CO_2 product streams," *International Journal of Greenhouse Gas Control*, vol. 57, pp. 185–195, 2017.

[75] J. Gong and F. You, "Optimal design and synthesis of algal biorefinery processesfor biological carbon sequestration and utilization with zero direct greenhousegas emissions: MINLP model and global optimization algorithm," *Ind. Eng.Chem. Res.*, vol. 53, pp. 1563–1579, 2014.

[76] P. Liu, E. N. Pistikopoulos, and Z. Li, "Decomposition based stochasticprogramming approach for polygeneration energy systems design underuncertainty," *Industrial & Engineering Chemistry Research*, vol. 49, pp. 3295–3305, 2010.

[77] M. Guignard, "Lagrangean relaxation," *Top*, vol. 11, no. 2, pp. 151–200, 2003.

[78] S. Mouret, I. E. Grossmann, and P. Pestiaux, "A new Lagrangian decomposition approach applied to the integration of refinery planning and crude-oil scheduling," *Computers and Chemical Engineering*, vol. 35, no. 12, pp. 2750–2766, 2011.

[79] Z. Li and M. Ierapetritou, "Production planning and scheduling integrationthrough augmented Lagrangian optimization," *Comput. Chem. Eng.*, vol. 34, pp. 996–1006, 2010.

[80] H. Shahandeh and Z. Li, "Design of bitumen upgrading and utility plant through integrated optimization," *Industrial & Engineering Chemistry Research*, 2017.

[81] L. Tock, "Thermo-environomic optimisation of fuel decarbonisation alternative processes for hydrogen and power production," Thesis, 2013.

[82] L. Tock and F. Maréchal, "Process design optimization strategy to develop energy and cost correlations of CO_2 capture processes," *Computers & Chemical Engineering*, vol. 61, pp. 51–58, 2014.

[83] "2008–11 fiscal plan – complete volume (Alberta budget 2008)," Minister of Finance and Enterprise, Report, 2008.

[84] A. Leiras, G. Ribas, S. Hamacher, and A. Elkamel, "Literature review of oil refineries planning under uncertainty," *Int. J. Oil, Gas and Coal Technology*, vol. 4, no. 2, 2011.

[85] N. K. Shah, Z. Li, and M. G. Ierapetritou, "Petroleum refining operations: Key issues, advances, and opportunities," *Industrial and Engineering Chemistry Research*, vol. 50, no. 3, pp. 1161–1170, 2011.

[86] J. M. Pinto, M. Joly, and L. F. L. Moro, "Planning and scheduling models for refinery operations," *Computers & Chemical Engineering*, vol. 24, no. 9-10, pp. 2259–2276, 2000.

[87] S. M. S. Neiro and J. M. Pinto, "A general modeling framework for the operational planning of petroleum supply chains," *Computers and Chemical Engineering*, vol. 28, no. 6-7, pp. 871–896, 2004.

[88] ——, "Multiperiod optimization for production planning of petroleum refineries," *Chemical Engineering Communications*, vol. 192, no. 1-3, pp. 62–88, 2005.

[89] I. Alhajri, A. Elkamel, T. Albahri, and P. Douglas, "A nonlinear programming model for refinery planning and optimisation with rigorous process models and product quality specifications," *Int. J. of Oil, Gas and Coal Technology*, vol. 1, no. 3, pp. 283–307, 2008.

[90] O. J. Guerra and G. A. C. Le Roux, "Improvements in petroleum refinery planning: 1. formulation of process models," *Industrial & Engineering Chemistry Research*, vol. 50, no. 23, pp. 13 403–13 418, 2011.

[91] J. Muñoz, R. Aguilar, L. Castañeda, and J. Ancheyta, "Comparison of correlations for estimating product yields from delayed coking," *Energy & Fuels*, vol. 27, no. 11, pp. 7179–7190, 2013.

[92] A. M. Alattas, I. E. Grossmann, and I. Palou-Rivera, "Integration of nonlinear crude distillation unit models in refinery planning optimization," *Industrial and Engineering Chemistry Research*, vol. 50, no. 11, pp. 6860–6870, 2011.

[93] B. C. Menezes, J. D. Kelly, and I. E. Grossmann, "Improved swing-cut modeling for planning and scheduling of oil-refinery distillation units," *Industrial and Engineering Chemistry Research*, vol. 52, no. 51, pp. 18 324–18 333, 2013.

[94] T. Gueddar and V. Dua, "Disaggregation-aggregation based model reduction for refinery-wide optimization," *Computers and Chemical Engineering*, vol. 35, no. 9, pp. 1838–1856, 2011.

[95] ——, "Novel model reduction techniques for refinery-wide energy optimisation," *Applied Energy*, vol. 89, no. 1, pp. 117–126, 2012.

[96] P. C. P. Reddy, I. A. Karimi, and R. Srinivasan, "Novel solution approach for optimizing crude oil operations," *AIChE Journal*, vol. 50, no. 6, pp. 1177–1197, 2004.

[97] C. A. Mendez, I. E. Grossmann, I. Harjunkoski, and P. Kaboré, "A simultaneous optimization approach for off-line blending and scheduling of oil-refinery operations," *Computers and Chemical Engineering*, vol. 30, no. 4, pp. 614–634, 2006.

[98] J. Li, I. A. Karimi, and R. Srinivasan, "Recipe determination and scheduling of gasoline blending operations," *AIChE Journal*, vol. 56, no. 2, pp. 441–465, 2010.

[99] A. Leiras, S. Hamacher, and A. Elkamel, "Petroleum refinery operational planning using robust optimization," *Engineering Optimization*, vol. 42, no. 12, pp. 1119–1131, 2010.

[100] O. J. Guerra and G. A. C. Le Roux, "Improvements in petroleum refinery planning: 2. case studies," *Industrial & Engineering Chemistry Research*, vol. 50, no. 23, pp. 13 419–13 426, 2011.

[101] J. Gemayel, "Integration and simulation of a bitumen upgrading facility and an IGCC process with carbon capture," Thesis, 2012.

[102] A. Frandsen, D. Hogan, and S. McCuskey, "In situ bitumen hydrocarbon extraction and upgrading," Chemical Engineering Department, Report, 2015.

[103] *HYSYS® 2004.2: Tutorials & Applications*, Aspen Technology, Inc.: Cambridge, USA, 2005.

[104] O. Castellanos Díaz, M. Sanchez-Lemus, F. Schoeggl, M. Satyro, S. Taylor, and H. Yarranton, "Deep-vacuum fractionation of heavy oil and bitumen, part i: Apparatus and standardized procedure," *Energy & Fuels*, vol. 28, no. 5, pp. 2857–2865, 2014.

[105] M. Sánchez-Lemus, F. Schoeggl, S. Taylor, K. Růžička, M. Fulem, and H. Yarranton, "Deep-vacuum fractionation of heavy oil and bitumen, part ii: Interconversion method," *Energy & Fuels*, vol. 28, no. 5, pp. 2866–2873, 2014.

[106] *FAQ: Modeling Heavy Oils Using Aspen HYSYS®*, Aspen Technology, Inc.: Burlington, Ontario, Canada, 2010.

[107] *Jump Start: Assay Management in Aspen HYSYS® Petroleum Refining*, Aspen Technology, Inc.: Burlington, Ontario, Canada, 2015.

[108] A. Alvarez-Majmutov, J. Chen, and M. Munteanu, "Simulation of bitumen upgrading processes," *Petroleum Technology Quarterly*, vol. 18, no. 2, pp. 39–43, 2013.

[109] S. Yui and E. Chan, *Hydrogenation of Coker Naphtha with NiMo Catalyst.* Elsevier, 1992, vol. Volume 73, pp. 59–66.

[110] A. Owusu-Boakye, A. K. Dalai, D. Ferdous, and J. Adjaye, "Maximizing aromatic hydrogenation of bitumen-derived light gas oil: Statistical approach and kinetic studies," *Energy & Fuels*, vol. 19, no. 5, pp. 1763–1773, 2005.

[111] D. Ferdous, A. K. Dalai, and J. Adjaye, "Hydrodenitrogenation and hydrodesulphurization of heavy gas oil using $NiMo/Al_2O_3$ catalyst containing phosphorus: Experimental and kinetic studies," *The Canadian Journal of Chemical Engineering*, vol. 83, no. 5, pp. 855–864, 2005.

[112] ——, "Hydrodenitrogenation and hydrodesulfurization of heavy gas oil using $NiMo/Al_2O_3$ catalyst containing boron: Experimental and kinetic studies," *Industrial & Engineering Chemistry Research*, vol. 45, no. 2, pp. 544–552, 2006.

[113] G. Centeno, G. Sánchez-Reyna, J. Ancheyta, J. A. Muñoz, and N. Cardona, "Testing various mixing rules for calculation of viscosity of petroleum blends," *Fuel*, vol. 90, no. 12, pp. 3561–3570, 2011.

[114] "crudemonitor.ca: maintained by crude quality inc, canadian association of petroleum producers (CAPP) and small explorers and producers association of Canada (SEPAC) as stakeholders," http://www.crudemonitor.ca/home.php, accessed: 2015-09.

[115] A. Costa, B. Bakhtiari, S. Schuster, and J. Paris, "Integration of absorption heat pumps in a kraft pulp process for enhanced energy efficiency," *Energy*, vol. 34, no. 3, pp. 254–260, 2009.

[116] A. Brooke, D. Kendrick, A. Meeraus, and R. Raman, *GAMS: A user's guide, release 2.50*. GAMS Development Corporation, 1988.

[117] N. Sahinidis, "BARON: A general purpose global optimization software package," *Journal of Global Optimization*, vol. 8, no. 2, pp. 201–205, 1996.

[118] E. Lazzaroni, M. Elsholkami, I. Arbiv, E. Martelli, A. Elkamel, and M. Fowler, "Energy infrastructure modeling for the oil sands industry: Current situation," *Applied Energy*, vol. 181, pp. 435–445, 2016.

[119] "Fact sheet: Carbon pricing around the world (2012)," http://www.eesi.org/papers/view/fact-sheet-carbon-pricing-around-the-world.

[120] "Carbon levy and rebates," https://www.alberta.ca/climate-carbon-pricing.aspx, 2017.

[121] "Alberta boosts carbon tax to $20 a tonne starting in 2016 as part of climate change plan," https://business.financialpost.com/, 2016 (accessed September 2016).

[122] A. Kostin, G. Guillén-Gosálbez, F. Mele, M. Bagajewicz, and L. Jiménez, "Design and planning of infrastructures for bioethanol and sugar production under demand uncertainty," *Chemical Engineering Research and Design*, vol. 90, pp. 359–376, 2012.

[123] F. Oliveira, V. Gupta, S. Hamacher, and I. E. Grossmann, "A Lagrangean decomposition approach for oil supply chain investment planning under uncertainty with risk considerations," *Computers & Chemical Engineering*, vol. 50, pp. 184–195, 2013.

[124] H. Park and R. Baldick, "Stochastic generation capacity expansion planning reducing greenhouse gas emissions," *IEEE Transactions on Power Systems*, vol. 30, pp. 1026–1034, 2015.

[125] ——, "Multi-year stochastic generation capacity expansion planning under environmental energy policy," *Applied Energy*, vol. 183, pp. 737–745, 2016.

[126] X. Zhang, A. Y. Sun, and I. J. Duncan, "Shale gas wastewater management under uncertainty," *Journal of Environmental Management*, vol. 165, pp. 188–198, 2016.

[127] "Alberta oil sands industry: quarterly update," http://www.albertacanada.com/files/albertacanada/AOSID-QuarterlyUpdate-Fall2015.pdf, Government of Alberta, Report, 2015 (accessed September 2016).

[128] H. Shahandeh and Z. Li, "Optimal design of bitumen upgrading facility with CO_2 reduction," *Computers & Chemical Engineering*, vol. 106, pp. 106–121, 2017.

[129] "Canadian natural resources limited announces 2017 first quarter results," https://www.cnrl.com/upload/media-element/1084/04/0504-q1-17-front-end.pdf, Canadian Natural Resources Limited, Report, 2014 (accessed May 2017).

[130] "Canada's oil sands - opportunities and challenges to 2015: an update," https://www.neb-one.gc.ca/nrg/sttstc/crdlndptrlmprdct/rprt/archive/pprtntsndchllngs20152006/pprtntsndchllngs20152006-eng.pdf, National Energy Board (NEB), Report, 2006 (accessed May 2017).

[131] L. Pan, M. Housh, P. Liu, X. Cai, and X. Chen, "Robust stochastic optimization for reservoir operation," *Water Resources Research*, vol. 51, pp. 409–429, 2015.

[132] C. C. Holt, F. Modigliani, and J. F. Muth, "Derivation of a linear decision rule for production and employment," *Management Science*, vol. 2, pp. 159–177, 1956.

[133] H. Ding, P. Pinson, Z. Hu, and Y. Song, "Optimal offering and operating strategies for wind-storage systems with linear decision rules," *IEEE Transactions on Power Systems*, vol. 31, pp. 4755–4764, 2016.

[134] R. Domınguez, A. J. Conejo, and M. Carrión, "Investing in generation capacity: A multi-stage linear-decision-rule approach," *IEEE Transactions on Power Systems*, vol. 31, pp. 4784–4794, 2016.

[135] B. S. Kim and B. D. Chung, "Affinely adjustable robust model for multiperiod production planning under uncertainty," *IEEE Transactions on Engineering Management*, vol. 64, pp. 505–514, 2017.

[136] M. Zugno, J. M. Morales, and H. Madsen, "Commitment and dispatch of heat and power units via affinely adjustable robust optimization," *Computers & Operations Research*, vol. 75, pp. 191–201, 2016.

[137] B. Keesom and J. Gieseman, "Bitumen Partial Upgrading 2018 Whitepaper," Jacobs Consultancy Inc., Tech. Rep., March 2018.

[138] "Canadian heavy oil crude competitiveness study phase 2," http://www.ai-ees.ca/wpcontent/uploads/2016/04/canadian_heavy_crude_oil_competitiveness_study_executive_summary_final.pdf, Muse Stancil, Report, 2015.

[139] T. Corscadden, J. Kearns, G. Diduch, D. Hocking, and D. Remesat, "Separation of solid asphaltenes from heavy liquid hydrocarbons using novel apparatus and process," Patent 20 140 246 357, September, 2014.

[140] T. Corscadden, G. Diduch, D. Hocking, D. Remesat, and J. Kearns, "Solvent de-asphalting with cyclonic separation," Patent 9 150 794, October, 2015.

[141] ——, "Low complexity, high yield conversion of heavy hydrocarbons," Patent 9 200 211, December, 2015.

[142] A. De Klerk, N. G. Zerpa Reques, Y. Xia, and A. A. Omer, "Integrated central processing facility (CPF) in oil field upgrading (OFU)," Patent 20 140 138 287, May, 2014.

[143] P. Pereira Almao, G. L. Trujillo, E. Peluso, C. Galarraga, C. Sosa, C. Scott Algara, F. Lopez-linares, L. A. Carbognani Ortega, and N. G. Zerpa Reques, "Systems and methods for catalytic steam cracking of non-asphaltene containing heavy hydrocarbons," Patent 9 562 199, February, 2017.

[144] R. F. Bernar and L. Jia, "Partial upgrading system and method for heavy hydrocarbons," Patent 20 160 145 505, May, 2016.

[145] M. Chornet, C. Chronopoulos, and S. Dehkissia, "Treatment of heavy oils to reduce olefin content," Patent 9 745 525, August, 2017.

[146] J. Colyar, "Has the time for partial upgrading of heavy oil and bitumen arrived?" *Digital Refining*, pp. 43–56, Q4 2009.

[147] L. C. Castaneda, J. A. Munoz, and J. Ancheyta, "Current situation of emerging technologies for upgrading of heavy oils," *Catalysis Today*, vol. 220, pp. 248–273, 2014.

[148] E. Nduagu, A. Sow, E. Umeozor, and D. Millington, "Economic potentials and efficiencies of oil sands operations: Processes and technologies," Canadian Energy Research Institute, Study No. 164, March, Report, 2017.

[149] S. Erbis, S. Kamarthi, T. P. Cullinane, and J. A. Isaacs, "Multistage stochastic programming (MSP) model for carbon nanotube production capacity expansion planning," *ACS Sustainable Chemistry & Engineering*, vol. 7, pp. 1633–1641, 2014.

[150] R. J. Zhou and L. J. Li, "Tactical capacity planning for semiconductor manufacturing: MILP models and scalable distributed parallel algorithms," *AIChE Journal*, vol. 62, pp. 3930–3946, 2016.

[151] M. Golari, N. Fan, and T. Jin, "Multistage stochastic optimization for production-inventory planning with intermittent renewable energy," *Production and Operations Management*, vol. 26, pp. 409–425, 2017.

[152] C. Lima, S. Relvas, and A. Barbosa-Povoa, "Stochastic programming approach for the optimal tactical planning of the downstream oil supply chain," *Computers & Chemical Engineering*, vol. 108, pp. 314–336, 2018.

[153] S. V. Braaten, O. Gjønnes, K. Hjertvik, and S.-E. Fleten, "Linear decision rules for seasonal hydropower planning: Modelling considerations," *Energy Procedia*, vol. 87, pp. 28–35, 2016.

[154] H. Shahandeh, F. Motamed, and Z. Li, "Expansion development planning of thermocracking-based bitumen upgrading plant under uncertainty," *Computers & Chemical Engineering*, vol. 111, pp. 225–240, 2018.

[155] N. Shabani and T. Sowlati, "A hybrid multi-stage stochastic programming-robust optimization model for maximizing the supply chain of a forest-based biomass power plant considering uncertainties," *Journal of Cleaner Production*, vol. 112, pp. 3285–3293, 2016.

[156] E. Keyvanshokooh, S. M. Ryan, and E. Kabir, "Hybrid robust and stochastic optimization for closed-loop supply chain network design using accelerated benders decomposition," *European Journal of Operational Research*, vol. 249, pp. 76–92, 2016.

Appendix A

Nomenclature for different Chapters

A.1 Nomenclature for Chapter 2

Indices and sets

$cu \in CU$	Set of cracking type
$gt \in GT$	Set of gasification type
$i \in I$	Set of element
$j \in J$	Set of species
$l \in L$	Set of operating unit
$pd \in PD$	Set of upgrader products
$pl \in PL$	Set of pressure level
$r \in R$	Set of natural gas combustion reaction

Binary variable

b	Binary variable

Continuous variable

el	Electricity consumption
elT	Total electricity consumption
F	Molar flowrate
FT	Total molar flowrate
H	Enthalpy
$h2$	Hydrogen mass flowrate
$h2T$	Total hydrogen mass flowrate
he	Heat duty
heT	Total heat duty
HL	Saturated liquid enthalpy
HV	Saturated vapor enthalpy
M	Mass flowrate
P	Pressure
Q	Heat duty
st	Steam flowrate
stT	Total steam flowrate
T	Temperature
V	Volumetric flowrate

VT	Total volumetric flowrate
W	Power
xm	Mole fraction
xw	Volume fraction
xv	Mass fraction
$Yield$	Yield

Parameters

α	Volumetric fractions of main species in the produced raw syngas
γ	Latent heat
γ^{sat_a}, γ^{sat_b}, γ^{sat_c}	Water latent heat regressed coefficients
ρ	Density
$\overline{\Omega}$, $\underline{\Omega}$	Upper and lower bounds
A, B, C	Capital cost estimation regressed coefficients for boilers
A, n	Capital cost estimation regressed coefficients for upgrader units
Cb, Fb, sf	Capital cost estimation regressed coefficients for polygeneration units
CR	Conversion rate
DLF	Average density of inlet feed of thermocracker
$DVTB$	Density of VTB
Eb	Electricity of base case
EC and QC	Regressed coefficients for heat and power consumptions
eff	Efficiency
Fb	Molar flowrate of base case
$FDDC$	Process fuel requirements of hydrocracker
$FDLCF$	Process fuel requirements of thermocracker
ha, hb, hc, hd	Pure enthalpy regressed coefficients
HFF	Hydrogen requirement of hydrocracker
HHT	Hydrogen requirements of hydrotreaters
HL^{sat_a}, Hl^{sat_b}, Hl^{sat_c}	Saturated liquid water enthalpy regressed coefficients
LHV	Low heat value
Mb	Mass flowrate of base case
MR	Mass flowrate ratio
MW	Molecular weight
n	Number of atoms
$OPEXb$	Operating cost of base case
$PDDC$	Electricity requirement of hydrocracker
$PDLF$	Electricity requirement of thermocracker
R	Excess ratio of oxygen molar flow
RE	Return ratio
S	Split fraction
$SDRU$	Steam requirement of atmospheric distillation unit
Sto	Stoichiometric coefficient
T^{sat_a}, T^{sat_b}, T^{sat_c}	Saturated water temperature regressed coefficients
UCF	Unit conversion factor

Uppercase letters

AD	Atmospheric distillation unit
ASU	Air separation unit
ATB	Atmospheric tower bottom
bl	Boiler
$CAPEX$	Capital cost

CCR	Carbon capture ratio
CCS	Carbon capture and storage
co	Cooler unit
$comp$	Compressor
COS	COS hydrolysis reactor unit
$csyn$	Clean syngas
$DBIT$	DilBit
es	Element of sulfur
fix	Fixed
FW	Fresh water
gh	Natural gas heater
GT	Gas turbine
GTC	Gas turbine combustion unit
HC	Hydrocracking unit
hi	High
HP	High pressure
$HRSG$	Heat recovery steam generator
HT	Hydrotreating unit
hyd	Hydrogen
in	Inlet
lo	Low
mc	SMR cooler
MP	Medium pressure
NG	Natural gas
nh	Nitrogen heater
nit	Nitrogen
$OPEX$	Operation cost
out	Outlet
oxy	Oxygen
PSA	Pressure swing adsorption
$psyn$	Pure syngas
PW	Pure water
rc	Syngas radiant cooler
$rsyn$	Raw syngas
sat	Saturated
sc	Syngas convective cooler
SCO	Synthetic crude oil
sel	Selexol unit
SMR	Steam methane reforming
$sntgt$	Syngas turbine
st	Steam turbine
$stack$	Stack gas
$sthi$	High quality steam turbine
$stlo$	Low quality steam turbine
su	Super heat
sul	Sulfur
$SVDU$	Tonne of steam per tonne of ATB
TC	Thermocracking unit
var	Variable
VD	Vacuum distillation unit
VTB	Vacuum tower bottom
WGS	Water gas shift unit

A.2 Nomenclature for Chapter 3

Indices and sets

$c \in C$	Set of coupling constraint
$cu \in CU$	Set of cracking type
$gt \in GT$	Set of gasification type
$i \in I$	Set of element
$j \in J$	Set of species
$l \in L$	Set of operating unit
$pd \in PD$	Set of upgrader products
$pl \in PL$	Set of pressure level
$r \in R$	Set of natural gas combustion reaction

Binary variable

b	Binary variable

Continuous variable

A	Variable from Part A appearing in coupling constraints
B	Variable from Part B appearing in coupling constraints
el	Electricity consumption
elT	Total electricity consumption
F	Molar flowrate
FT	Total molar flowrate
H	Enthalpy
$h2$	Hydrogen mass flowrate
$h2T$	Total hydrogen mass flowrate
he	Heat duty
heT	Total heat duty
HL	Saturated liquid enthalpy
HV	Saturated vapor enthalpy
M	Mass flowrate
P	Pressure
Q	Heat duty
st	Steam flowrate
stT	Total steam flowrate
T	Temperature
V	Volumetric flowrate
VT	Total volumetric flowrate
W	Power
xm	Mole fraction
xw	Volume fraction
xv	Mass fraction
$Yield$	Yield

Parameters

α	Volumetric fractions of main species in the produced raw syngas
γ	Latent heat
γ^{sat_a}, γ^{sat_b}, γ^{sat_c}	Water latent heat regressed coefficients

ρ	Density
$\overline{\Omega}$, $\underline{\Omega}$	Upper and lower bounds
A, B, C	Capital cost estimation regressed coefficients for boilers
A, n	Capital cost estimation regressed coefficients for upgrader units
Cb, Fb, sf	Capital cost estimation regressed coefficients for polygeneration units
CR	Conversion rate
DLF	Average density of inlet feed of thermocracker
$DVTB$	Density of VTB
Eb	Electricity of base case
EC and QC	Regressed coefficients for heat and power consumptions
eff	Efficiency
Fb	Molar flowrate of base case
$FDDC$	Process fuel requirements of hydrocracker
$FDLCF$	Process fuel requirements of thermocracker
ha, hb, hc, hd	Pure enthalpy regressed coefficients
HFF	Hydrogen requirement of hydrocracker
HHT	Hydrogen requirements of hydrotreaters
HL^{sat_a}, Hl^{sat_b}, Hl^{sat_c}	Saturated liquid water enthalpy regressed coefficients
LHV	Low heat value
Mb	Mass flowrate of base case
MR	Mass flowrate ratio
MW	Molecular weight
n	Number of atoms
$OPEXb$	Operating cost of base case
$PDDC$	Electricity requirement of hydrocracker
$PDLF$	Electricity requirement of thermocracker
R	Excess ratio of oxygen molar flow
RE	Return ratio
S	Split fraction
$SDRU$	Steam requirement of atmospheric distillation unit
Sto	Stoichiometric coefficient
T^{sat_a}, T^{sat_b}, T^{sat_c}	Saturated water temperature regressed coefficients
UCF	Unit conversion factor

Uppercase letters

AD	Atmospheric distillation unit
ASU	Air separation unit
ATB	Atmospheric tower bottom
bl	Boiler
$CAPEX$	Capital cost
CCR	Carbon capture ratio
CCS	Carbon capture and storage
co	Cooler unit
$comp$	Compressor
COS	COS hydrolysis reactor unit
$csyn$	Clean syngas
$DBIT$	DilBit
$emitted$	Emitted gas
es	Element of sulfur
fix	Fixed
FW	Fresh water
gh	Natural gas heater

GT	Gas turbine
GTC	Gas turbine combustion unit
HC	Hydrocracking unit
hi	High
HP	High pressure
$HRSG$	Heat recovery steam generator
HT	Hydrotreating unit
hyd	Hydrogen
in	Inlet
lo	Low
mc	SMR cooler
MEA	Monoethanolamine unit
MP	Medium pressure
NG	Natural gas
nh	Nitrogen heater
nit	Nitrogen
$OPEX$	Operation cost
out	Outlet
oxy	Oxygen
$Oxyfuel$	Oxyfuel combustion
$Post.comb$	Post–combustion CCS technology
$Pre.comb$	Pre–combustion CCS technology
PSA	Pressure swing adsorption
$psyn$	Pure syngas
PW	Pure water
rc	Syngas radiant cooler
$rsyn$	Raw syngas
sat	Saturated
sc	Syngas convective cooler
SCO	Synthetic crude oil
sel	Selexol unit
SMR	Steam methane reforming
$sntgt$	Syngas turbine
st	Steam turbine
$stack$	Stack gas
$sthi$	High quality steam turbine
$stlo$	Low quality steam turbine
su	Super heat
sul	Sulfur
$SVDU$	Tonne of steam per tonne of ATB
TC	Thermocracking unit
var	Variable
VD	Vacuum distillation unit
VTB	Vacuum tower bottom
WGS	Water gas shift unit

A.3 Nomenclature for Chapter 4

Indices and sets

$fp \in P$	Set of final product
$i \in U$	Set of stream (used in blender, mixers, splitters)
$p \in T$	Set of intermediate product
$pr \in C$	Set of property
$s \in U$	Set of separation unit
$u \in T$	Set of reaction unit
$ut \in C$	Set of utility

Parameters

α, β, k	Kinetic coefficients for HDN and HDS conversions
θ, ϕ	Lower and upper bounds for volumetric blending ratio
γ	Sulfur distribution in the hydrocracker outlets
a_p, b_p, c_p	Kinetic coefficients for sulfur conversion in the hydrocracker
a, b, c, d	Regressed coefficients of sulfur distribution in hydrocracker outlet
$Feed_{pr}$	Feed specifications
$Price_{ut}$	Utility price
$Price_{fp}$	Final product price
$Volume$	Catalyst volume
$Spec_{fp,pr}$	Final products specifications
$Ratio$	Conversion ratio of HDN to HDS

Variables

BI	Blending index
CR	Conversion rate
CV_i	Volume composition
$ECP_{s,p}$	Cut point range
H_u	Hydrogen requirement
$LHSV_u$	LHSV of operating unit
M_{fp}	Final products mass flow rate
$M\_in_{p,u}$	Inlet mass flow rate
$M\_out_{p,u}$	Outlet mass flow rate
P_u	Pressure of operating unit
Q_u	Duty requirement
T_u	Temperature of operating unit
V_{fp}	Final products volume flow rate
$V\_in_{p,u}$	Inlet volume flow rate
$V\_out_{p,u}$	Outlet volume flow rate
W_u	Work requirement
$X^{in}_{pr,i}$, X^{out}_{pr}	Steam properties

A.4 Nomenclature for Chapter 5

Indices and sets

$p \in P$	Set of operating units
$u \in U$	Set of utilities
$t \in T$	Set of time periods
$c \in C$	Set of products
MP	Subset of mixer-type units ($NPHHT$, $LGOHT$, $HGOHT$)
SP	Subset of splitter-type units (DR, TC)
PC	Subset of matching between product and associated hydrotreater

Parameters

α	Significance level
$\alpha_{p,c}^{yield}$	Yield coefficient of splitter-type units
$\alpha_p^{H_2}$	Hydrogen requirement coefficients ($\frac{tonne}{m^3}$)
α_p^{HT}	Yield coefficient of mixers
$\beta_{p,u}$	Energy requirements coefficient ($\frac{energy}{tonne}$)
γ^{CO_2}	Carbon tax economic coefficient ($\frac{\$}{tonne\ CO_2}$)
$\gamma^{Bitumen}$	Bitumen price ($\frac{\$}{bbl}$)
γ_u^E	Energy requirements economic coefficients ($\frac{\$}{energy}$)
γ^{H_2}	Hydrogen requirement economic coefficients ($\frac{\$}{tonne}$)
γ^{MAINEX}	Maintenance economic coefficient
γ^{SCO}	SCO price ($\frac{\$}{bbl}$)
Γ	A scalar to control the uncertainty set size
δ_u^E	GHG emission coefficient of Energy sources ($\frac{tonne\ CO_2}{energy}$)
δ^{H_2}	GHG emission coefficient of Hydrogen ($\frac{tonne\ CO_2}{tonne}$)
δ^{SCO}	GHG emission coefficient of SCO production ($\frac{tonne\ CO_2}{tonne}$)
ϵ_t	Uncertainties for SCO price
ζ_t	Uncertainties for CO_2 tax price
θ_q	$ARMA$ ARMA model coefficients
ρ_p	Density ($\frac{tonne}{m^3}$)
ϕ_p	$ARMA$ ARMA model coefficients
$\bar{\Omega}_t^{Investment}$	Capital investment limitation corresponding to period t ($M\$$)
$\underline{\Omega}^M$	Upper bound for the inlet to the upgrading plant ($\frac{tonne}{hr}$)
$\underline{\Omega}_p^Q$	Lower bound for percentile of capacity usage (%)
$\underline{\Omega}_p^{spec}$	Lower bound for percentile of each product in final blend (%)
$\underline{\Omega}_p^X, \bar{\Omega}_p^X$	Lower and upper bounds for expansion capacity (bpd)
a_p	Gradient of linear capital cost equation
A_t^{SCO}	Constant coefficients vector of reformulated $ARMA$ model at year t
b_p	Intercept of linear capital cost equation ($M\$$)
B_t^{SCO}	Constant coefficients scalar of reformulated $ARMA$ model at year t
d	Depreciation time (yr)
h	The coefficients vector of general uncertainty set
ir	Annual real debt interest rate (%)
OT	Operating time (hr)
P_t	Truncate matrix at year t
r	Discount rate (%)
UC_1	Unit conversion from cubic meter per hour into barrel per day ($\frac{bpd}{\frac{m^3}{hr}}$)
UC_2	Unit conversion from \$ to M\$ ($\frac{M\$}{\$}$)
W	Coefficient matrix of general uncertainty set

$z_{1-\alpha}$	$1-\alpha$ quantile of standard normal distribution

Decision variables

Λ	Variable stemmed from dual counterpart of inequality constraint
C_t^{CAPEX}	Capital cost investment of year t ($M\$$)
$Y_{p,t}$	Binary capacity expansion decision for process p in the year t
$M_{p,t}^{H2}$	Mass flow rate of hydrogen in hydrotreater p at year t ($\frac{tonne}{hr}$)
$M_{p,c,t}^{out}$	Mass flow rate of outlet product c from splitter p at year t ($\frac{tonne}{hr}$)
$M_{p,t}^{in}$	Mass flow rate of inlet to splitter p at year t ($\frac{tonne}{hr}$)
$M_{p,t}^{HTout}$	Mass flow rate of outlet from hydrotreater p at year t ($\frac{tonne}{hr}$)
$M_{p,t}^{H2}$	Mass flow rate of hydrogen in hydrotreater p at year t ($\frac{tonne}{hr}$)
M_t^{SCO}	Total mass flow rate of SCO at year t ($\frac{tonne}{hr}$)
$E_{u,t}$	Energy consumption of utility u at year t ($\frac{energy}{hr}$)
$X_{p,t}$	Capacity expansion of process p to be installed in period t (bpd)
$Q_{p,t}$	Total capacity of process p in period t (bpd)

A.5 Nomenclature for Chapter 6

Indices and sets

$i \in I$	Set of technologies for partial upgrading
$t \in T$	Set of time periods
$\xi \in \Xi$	Set of uncertainties
$s, s' \in S$	Set of notes on the scenario tree in H1 model
$k \in S$	Set of samples in H2 model
S_{-1}	Subset of notes on the scenario tree except the $s = 1$
L	Subset of leaf (all the nodes on the last stage of scenario tree)
$A(s)$	Subset of node s's ancestors (excluding itself)
$P(s)$	Subset of node s's path (including itself)

Parameters

α_i	Operating cost coefficient for each technology (M$/bbl)
β_i	Capital cost coefficient for each technology (M$/bbl)
δ	Operating days per time period (day/year)
γ	Investment budget (M)
r	Interest rate (%)
ν_t	Processing bitumen target (bpd)
ϕ_i	Commercialization factor
$\underline{\Omega}$, $\bar{\Omega}$	lower and upper bounds for capacity (bpd)
Φ	Commercialization threshold
Pr_s	Probability of node s on the scenario tree
τ_s	Time period order of node s on the scenario tree
ϵ	Perturbation of uncertainties (%)
h	Coefficient vector of uncertainty set for H1 model
W	Coefficient matrix of uncertainty set for H1 model
l	Coefficient vector of uncertainty set for H2 model
M	Coefficient matrix of uncertainty set for H1 model

Decision variables

Λ^d, Λ^e_s, Λ^f_s	Variables stemmed from dual counterpart of inequality constraints 5.43d, 5.43e, and 5.43f in H1 model
Π^b_t, $\Pi^{c_1}_{i,t}$, $\Pi^{c_2}_{i,t}$, $\Pi^e_{k,t}$, Π^f_k, $\Pi^{h_1}_{i,t}$, $\Pi^{h_2}_{i,t}$	Variables stemmed from dual counterpart of inequality constraints 5.43b, 5.43c, 5.43e, 5.43f, and 5.43h in H2 model
Y^C_i	Binary variables for capital installation of a technology
$Y^X_{i,t}$	Binary variables for expansion installation of a technology
C_i	Capital capacity of a technology (bpd)
$X_{i,t}$	Expansion capacity of a technology at a time period (bpd)
$O_{i,t}$	Operating capacity of a technology at a time period (bpd)

Appendix B

The Correlation Models for Chapter 4

ADU:

$$M_{ADU}^{steam} = 0.3 \cdot M_{in} \tag{B.1}$$

VDU:

$$M_{VDU}^{steam} = 0.07 \cdot M_{in} \tag{B.2a}$$

$$Nitrogen_{NPH} = -1.1E-08 \cdot ECP_2 \cdot ECP_2 - 4.7E-08 \cdot ECP_2 + 2.15E-07 \tag{B.2b}$$

$$Sulfur_{NPH} = 0.02763 \cdot ECP_2 \cdot ECP_2 + 0.07862 \cdot ECP_2 + 0.1807 \tag{B.2c}$$

$$Mhu_{NPH} = 0.02707 \cdot ECP_2 \cdot ECP_2 + 0.07024 \cdot ECP_2 + 0.4502 \tag{B.2d}$$

$$SG_{NPH} = 0.004779 \cdot ECP_2 \cdot ECP_2 + 0.01774 \cdot ECP_2 + 0.7329 \tag{B.2e}$$

$$Yield_{NPH} = 0.0018 \cdot ECP_2 \cdot ECP_2 + 0.0041 \cdot ECP_2 + 0.016 \tag{B.2f}$$

$$Nitrogen_{LGO} = +147.18432 + 2.86069 \cdot ECP_2 + 30.40266 \cdot ECP_3 \tag{B.2g}$$

$$Sulfur_{LGO} = +1.75363 + 0.023791 \cdot ECP_2 + 0.062843 \cdot ECP_3 + 0.010058 \cdot ECP_2 \cdot ECP_2 \tag{B.2h}$$

$$Mhu_{LGO} = +4.74345 + 0.17567 \cdot ECP_2 + 0.56310 \cdot ECP_3 + 0.068909 \cdot ECP_2 \cdot ECP_2 \tag{B.2i}$$

$$\begin{aligned} SG_{LGO} = {} & +0.88689 + 1.37358E-03 \cdot ECP_2 + 3.33672E-03 \cdot ECP_3 \\ & + 5.88416E-04 \cdot ECP_2 \cdot ECP_2 \end{aligned} \tag{B.2j}$$

$$\begin{aligned} Yield_{LGO} = {} & +0.21387 - 4.13841E-03 \cdot ECP_2 + 0.017477 \cdot ECP_3 \\ & - 1.81078E-03 \cdot ECP_2 \cdot ECP_2 + 4.75853E-05 \cdot ECP_3 \cdot ECP_3 \end{aligned} \tag{B.2k}$$

$$Nitrogen_{HGO} = +1891.27966 + 71.97267 \cdot ECP_3 + 126.07138 \cdot ECP_4 + 30.42418 \cdot ECP_4 \cdot ECP_4 \tag{B.2l}$$

$$Sulfur_{HGO} = +3.41270 + 0.046276 \cdot ECP_3 + 0.050067 \cdot ECP_4 + 0.011876 \cdot ECP_4 \cdot ECP_4 \tag{B.2m}$$

$$\begin{aligned} Mhu_{HGO} = {} & +289.22703 + 66.55369 \cdot ECP_3 + 52.46940 \cdot ECP_4 + 13.55374 \cdot ECP_3 \cdot ECP_4 \\ & + 16.23277 \cdot ECP_4 \cdot ECP_4 \end{aligned} \tag{B.2n}$$

$$\begin{aligned} SG_{HGO} = {} & +0.96901 + 2.12806E-03 \cdot ECP_3 + 2.03606E-03 \cdot ECP_4 \\ & + 4.71796E-04 \cdot ECP_4 \cdot ECP_4 \end{aligned} \tag{B.2o}$$

$$Yield_{HGO} = +0.33598 - 0.017477 \cdot ECP_3 + 0.018338 \cdot ECP_4 - 4.75853E-05 \cdot ECP_3 \cdot ECP_3$$

$$+ 3.42919E-03 \cdot ECP_4 \cdot ECP_4 \tag{B.2p}$$

$$Nitrogen_{Residue} = 26.34 \cdot ECP_4 \cdot ECP_4 + 161.5 \cdot ECP_4 + 8015 \tag{B.2q}$$

$$Sulfur_{Residue} = 0.01214 \cdot ECP_4 \cdot ECP_4 + 0.07081 \cdot ECP_4 + 6 \tag{B.2r}$$

$$Mhu_{Residue} = 8.699e+10 \cdot ECP_4 \cdot ECP_4 + 1.402e+11 \cdot ECP_4 + 9.181e+10 \tag{B.2s}$$

$$SG_{Residue} = 0.0005244 \cdot ECP_4 \cdot ECP_4 + 0.003078 \cdot ECP_4 + 1.076 \tag{B.2t}$$

$$Yield_{Residue} = -0.003429 \cdot ECP_4 \cdot ECP_4 - 0.01834 \cdot ECP_4 + 0.4336 \tag{B.2u}$$

Hydrocracker + VDU:

$$\begin{aligned} Nitrogen_{NPH} = &+ 5.56934E-03 - 3.41717E-03 \cdot T + 2.75696E-04 \cdot P + 0.016030 \cdot LHSV \\ &- 0.060022 \cdot ECP_1 + 0.013143 \cdot ECP_2 + 1.09939E-03 \cdot T \cdot P - 0.013272 \cdot T \cdot LHSV \\ &+ 0.020090 \cdot T \cdot ECP_1 + 5.30326E-03 \cdot T \cdot ECP_2 - 2.11108E-03 \cdot P \cdot LHSV \\ &+ 4.98978E-04 \cdot P \cdot ECP_1 + 1.41042E-04 \cdot P \cdot ECP_2 - 0.025826 \cdot LHSV \cdot ECP_1 \\ &- 2.73547E-03 \cdot LHSV \cdot ECP_2 + 7.84411E-03 \cdot ECP_1 \cdot ECP_2 + 0.012479 \cdot T \cdot T \\ &+ 1.88504E-04 \cdot P \cdot P - 1.14387E-03 \cdot LHSV \cdot LHSV + 0.058537 \cdot ECP_1 \cdot ECP_1 \\ &+ 0.018957 \cdot ECP_2 \cdot ECP_2 \end{aligned} \tag{B.3a}$$

$$\begin{aligned} Sulfur_{NPH} = &+ 0.017031 + 0.044737 \cdot T + 2.94935E-03 \cdot P - 0.025501 \cdot LHSV \\ &+ 4.85641E-03 \cdot ECP_1 + 5.06177E-04 \cdot ECP_2 - 1.16075E-03 \cdot T \cdot P \\ &- 0.045826 \cdot T \cdot LHSV + 3.47623E-03 \cdot T \cdot ECP_1 - 8.18866E-04 \cdot T \cdot ECP_2 \\ &- 1.52838E-03 \cdot P \cdot LHSV - 1.35538E-03 \cdot P \cdot ECP_1 - 2.85293E-03 \cdot P \cdot ECP_2 \\ &- 7.36624E-03 \cdot LHSV \cdot ECP_1 - 1.07984E-03 \cdot LHSV \cdot ECP_2 \\ &- 2.49490E-03 \cdot ECP_1 \cdot ECP_2 + 0.019296 \cdot T \cdot T - 2.32262E-03 \cdot P \cdot P \\ &+ 1.77364E-03 \cdot LHSV \cdot LHSV + 1.77461E-03 \cdot ECP_1 \cdot ECP_1 \\ &+ 1.62665E-03 \cdot ECP_2 \cdot ECP_2 \end{aligned} \tag{B.3b}$$

$$\begin{aligned} Mhu_{NPH} = &+ 0.46196 + 1.70029E-06 \cdot T + 5.71080E-07 \cdot P - 8.66296E-06 \cdot LHSV \\ &+ 6.24085E-05 \cdot ECP_1 + 6.51610E-05 \cdot ECP_2 + 7.32833E-08 \cdot T \cdot P \\ &- 4.17125E-06 \cdot T \cdot LHSV + 1.93883E-06 \cdot T \cdot ECP_1 + 1.51126E-06 \cdot T \cdot ECP_2 \\ &- 6.26342E-07 \cdot P \cdot LHSV - 2.68602E-07 \cdot P \cdot ECP_1 + 7.48383E-07 \cdot P \cdot ECP_2 \\ &- 2.52620E-06 \cdot LHSV \cdot ECP_1 - 2.71313E-06 \cdot LHSV \cdot ECP_2 \\ &+ 2.09744E-06 \cdot ECP_1 \cdot ECP_2 + 2.89361E-06 \cdot T \cdot T - 4.61306E-07 \cdot P \cdot P \\ &+ 7.65316E-06 \cdot LHSV \cdot LHSV - 4.65518E-05 \cdot ECP_1 \cdot ECP_1 \\ &- 4.42299E-05 \cdot ECP_2 \cdot ECP_2 \end{aligned} \tag{B.3c}$$

$$\begin{aligned} SG_{NPH} = &+ 0.75933 + 5.70415E-07 \cdot T + 1.76151E-07 \cdot P - 2.46676E-06 \cdot LHSV \\ &+ 1.98527E-05 \cdot ECP_1 + 1.57850E-05 \cdot ECP_2 + 5.30961E-08 \cdot T \cdot P \end{aligned}$$

$$
\begin{aligned}
&- 1.52572E-06 \cdot T \cdot LHSV + 6.67038E-07 \cdot T \cdot ECP_1 + 4.88297E-07 \cdot T \cdot ECP_2 \\
&- 2.29458E-07 \cdot P \cdot LHSV - 9.63116E-08 \cdot P \cdot ECP_1 + 2.20153E-07 \cdot P \cdot ECP_2 \\
&- 8.58897E-07 \cdot LHSV \cdot ECP_1 - 8.08159E-07 \cdot LHSV \cdot ECP_2 \\
&+ 5.91898E-07 \cdot ECP_1 \cdot ECP_2 + 1.02236E-06 \cdot T \cdot T - 1.41063E-07 \cdot P \cdot P \\
&+ 2.24722E-06 \cdot LHSV \cdot LHSV - 1.38162E-05 \cdot ECP_1 \cdot ECP_1 \\
&- 1.01272E-05 \cdot ECP_2 \cdot ECP_2 \qquad \text{(B.3d)}
\end{aligned}
$$

$$
\begin{aligned}
Yield_{NPH} = &+ 0.11777 + 0.021445 \cdot T - 1.28947E-04 \cdot P - 0.067381 \cdot LHSV \\
&+ 1.97129E-04 \cdot ECP_1 - 3.27788E-04 \cdot ECP_2 + 3.10209E-04 \cdot T \cdot P \\
&+ 0.022373 \cdot T \cdot LHSV + 1.07914E-04 \cdot T \cdot ECP_1 + 2.98032E-05 \cdot T \cdot ECP_2 \\
&+ 1.40234E-03 \cdot P \cdot LHSV - 3.86118E-04 \cdot P \cdot ECP_1 - 4.53019E-04 \cdot P \cdot ECP_2 \\
&- 3.43755E-05 \cdot LHSV \cdot ECP_1 + 5.13883E-04 \cdot LHSV \cdot ECP_2 \\
&- 6.47313E-04 \cdot ECP_1 \cdot ECP_2 - 9.70043E-03 \cdot T \cdot T - 5.22198E-04 \cdot P \cdot P \\
&+ 0.021160 \cdot LHSV \cdot LHSV - 3.21635E-04 \cdot ECP_1 \cdot ECP_1 \\
&+ 4.05702E-04 \cdot ECP_2 \cdot ECP_2 \qquad \text{(B.3e)}
\end{aligned}
$$

$$
\begin{aligned}
Nitrogen_{LGO} = &+ 3167.36248 + 966.95393 \cdot T - 222.24454 \cdot P - 1765.64686 \cdot LHSV + 19.10654 \cdot ECP_2 \\
&+ 129.39707 \cdot ECP_3 + 130.16295 \cdot T \cdot P - 575.79654 \cdot T \cdot LHSV + 120.69455 \cdot T \cdot ECP_2 \\
&- 50.50055 \cdot T \cdot ECP_3 + 306.69573 \cdot P \cdot LHSV + 28.33706 \cdot P \cdot ECP_2 \\
&+ 134.39392 \cdot P \cdot ECP_3 + 18.81081 \cdot LHSV \cdot ECP_2 - 125.96863 \cdot LHSV \cdot ECP_3 \\
&+ 39.92547 \cdot ECP_2 \cdot ECP_3 + 463.74811 \cdot T \cdot T + 24.44352 \cdot P \cdot P \\
&+ 802.08556 \cdot LHSV \cdot LHSV - 1.06322 \cdot ECP_2 \cdot ECP_2 + 73.50016 \cdot ECP_3 \cdot ECP_3 \qquad \text{(B.3f)}
\end{aligned}
$$

$$
\begin{aligned}
Sulfur_{LGO} = &+ 0.41063 + 0.032678 \cdot T - 0.069094 \cdot P + 0.15122 \cdot LHSV - 2.51931E-03 \cdot ECP_2 \\
&+ 0.035220 \cdot ECP_3 + 0.042902 \cdot T \cdot P - 0.19831 \cdot T \cdot LHSV + 0.038598 \cdot T \cdot ECP_2 \\
&- 0.015138 \cdot T \cdot ECP_3 + 0.081554 \cdot P \cdot LHSV + 0.017462 \cdot P \cdot ECP_2 + 0.033751 \cdot P \cdot ECP_3 \\
&+ 0.013190 \cdot LHSV \cdot ECP_2 - 0.035162 \cdot LHSV \cdot ECP_3 + 0.011618 \cdot ECP_2 \cdot ECP_3 \\
&+ 0.14777 \cdot T \cdot T + 0.018187 \cdot P \cdot P - 0.039419 \cdot LHSV \cdot LHSV \\
&+ 4.44425E-03 \cdot ECP_2 \cdot ECP_2 + 0.022925 \cdot ECP_3 \cdot ECP_3 \qquad \text{(B.3g)}
\end{aligned}
$$

$$
\begin{aligned}
Mhu_{LGO} = &+ 3.65865 - 9.49532E-06 \cdot T - 1.44527E-05 \cdot P + 1.04932E-05 \cdot LHSV \\
&+ 9.58153E-04 \cdot ECP_2 + 3.07835E-04 \cdot ECP_3 - 8.64477E-09 \cdot T \cdot P \\
&- 4.69822E-05 \cdot T \cdot LHSV + 5.45373E-05 \cdot T \cdot ECP_2 - 5.19681E-06 \cdot T \cdot ECP_3 \\
&+ 1.70518E-05 \cdot P \cdot LHSV + 3.49412E-06 \cdot P \cdot ECP_2 - 8.11921E-08 \cdot P \cdot ECP_3 \\
&- 8.13329E-05 \cdot LHSV \cdot ECP_2 - 8.85966E-06 \cdot LHSV \cdot ECP_3
\end{aligned}
$$

$$
\begin{aligned}
&+ 6.61154E-06 \cdot ECP_2 \cdot ECP_3 + 1.86287E-05 \cdot T \cdot T - 1.01915E-06 \cdot P \cdot P \\
&+ 2.72862E-05 \cdot LHSV \cdot LHSV - 6.20927E-04 \cdot ECP_2 \cdot ECP_2 \\
&- 1.98719E-04 \cdot ECP_3 \cdot ECP_3 \qquad \text{(B.3h)} \\
SG_{LGO} = &+ 0.87765 - 8.82460E-08 \cdot T - 1.48344E-07 \cdot P + 6.58251E-08 \cdot LHSV \\
&+ 9.80475E-06 \cdot ECP_2 + 3.09982E-06 \cdot ECP_3 - 1.66885E-09 \cdot T \cdot P \\
&- 4.80794E-07 \cdot T \cdot LHSV + 5.63031E-07 \cdot T \cdot ECP_2 - 6.03971E-08 \cdot T \cdot ECP_3 \\
&+ 1.78507E-07 \cdot P \cdot LHSV + 3.60836E-08 \cdot P \cdot ECP_2 - 1.01823E-09 \cdot P \cdot ECP_3 \\
&- 8.43907E-07 \cdot LHSV \cdot ECP_2 - 8.99008E-08 \cdot LHSV \cdot ECP_3 \\
&+ 7.22447E-08 \cdot ECP_2 \cdot ECP_3 + 1.79635E-07 \cdot T \cdot T - 9.48794E-09 \cdot P \cdot P \\
&+ 2.99735E-07 \cdot LHSV \cdot LHSV - 6.65705E-06 \cdot ECP_2 \cdot ECP_2 \\
&- 1.99214E-06 \cdot ECP_3 \cdot ECP_3 \qquad \text{(B.3i)} \\
Yield_{LGO} = &+ 0.46674 + 0.066242 \cdot T + 3.75962E-03 \cdot P - 0.25769 \cdot LHSV \\
&+ 2.86661E-03 \cdot ECP_2 + 4.15940E-03 \cdot ECP_3 - 3.10249E-03 \cdot T \cdot P \\
&+ 0.10063 \cdot T \cdot LHSV - 5.38294E-04 \cdot T \cdot ECP_2 - 1.69813E-03 \cdot T \cdot ECP_3 \\
&+ 9.41468E-04 \cdot P \cdot LHSV - 4.68033E-04 \cdot P \cdot ECP_2 + 1.79257E-03 \cdot P \cdot ECP_3 \\
&- 4.59509E-03 \cdot LHSV \cdot ECP_2 - 5.64333E-03 \cdot LHSV \cdot ECP_3 \\
&+ 1.33593E-03 \cdot ECP_2 \cdot ECP_3 - 0.040983 \cdot T \cdot T - 1.20684E-03 \cdot P \cdot P \\
&+ 0.083729 \cdot LHSV \cdot LHSV + 2.02456E-03 \cdot ECP_2 \cdot ECP_2 \\
&+ 1.28804E-03 \cdot ECP_3 \cdot ECP_3 \qquad \text{(B.3j)} \\
Nitrogen_{HGO} = &+ 7268.17072 + 1303.56042 \cdot T + 44.07329 \cdot P - 3314.53700 \cdot LHSV - 58.87150 \cdot ECP_3 \\
&+ 65.09952 \cdot ECP_4 - 20.32531 \cdot T \cdot P + 246.77068 \cdot T \cdot LHSV + 41.56060 \cdot T \cdot ECP_3 \\
&- 59.01644 \cdot T \cdot ECP_4 - 23.26028 \cdot P \cdot LHSV - 18.42330 \cdot P \cdot ECP_3 - 34.03890 \cdot P \cdot ECP_4 \\
&+ 35.34010 \cdot LHSV \cdot ECP_3 - 99.04020 \cdot LHSV \cdot ECP_4 - 22.97694 \cdot ECP_3 \cdot ECP_4 \\
&- 180.36058 \cdot T \cdot T + 36.68995 \cdot P \cdot P + 1295.57970 \cdot LHSV \cdot LHSV \\
&+ 6.88741 \cdot ECP_3 \cdot ECP_3 - 33.52652 \cdot ECP_4 \cdot ECP_4 \qquad \text{(B.3k)} \\
Sulfur_{HGO} = &+ 1.05856 - 0.10396 \cdot T - 0.015836 \cdot P + 0.27752 \cdot LHSV - 0.026894 \cdot ECP_3 \\
&+ 7.51131E-03 \cdot ECP_4 - 3.35266E-03 \cdot T \cdot P - 0.056983 \cdot T \cdot LHSV \\
&+ 0.013423 \cdot T \cdot ECP_3 - 0.024971 \cdot T \cdot ECP_4 + 5.40647E-03 \cdot P \cdot LHSV \\
&- 2.01790E-03 \cdot P \cdot ECP_3 - 0.013200 \cdot P \cdot ECP_4 + 0.028471 \cdot LHSV \cdot ECP_3 \\
&- 5.81032E-04 \cdot LHSV \cdot ECP_4 - 8.22142E-03 \cdot ECP_3 \cdot ECP_4 + 0.010617 \cdot T \cdot T \\
&+ 4.57408E-03 \cdot P \cdot P - 0.070819 \cdot LHSV \cdot LHSV - 3.51422E-05 \cdot ECP_3 \cdot ECP_3 \\
&- 3.07582E-03 \cdot ECP_4 \cdot ECP_4 \qquad \text{(B.3l)}
\end{aligned}
$$

$$
\begin{aligned}
Mhu_{HGO} = &+ 117.55272 + 0.14602 \cdot T + 0.33294 \cdot P - 9.94748 \cdot LHSV + 0.081572 \cdot ECP_3 \\
&+ 1.05279 \cdot ECP_4 - 0.23869 \cdot T \cdot P - 0.37189 \cdot T \cdot LHSV + 0.11297 \cdot T \cdot ECP_3 \\
&+ 0.11099 \cdot T \cdot ECP_4 - 0.50196 \cdot P \cdot LHSV - 0.18944 \cdot P \cdot ECP_3 + 0.16522 \cdot P \cdot ECP_4 \\
&- 0.058885 \cdot LHSV \cdot ECP_3 - 0.67274 \cdot LHSV \cdot ECP_4 - 0.019799 \cdot ECP_3 \cdot ECP_4 \\
&- 0.30085 \cdot T \cdot T - 0.22270 \cdot P \cdot P + 7.54237 \cdot LHSV \cdot LHSV + 0.28398 \cdot ECP_3 \cdot ECP_3 \\
&+ 0.54671 \cdot ECP_4 \cdot ECP_4 \qquad \text{(B.3m)} \\
SG_{HGO} = &+ 0.97062 - 9.01114E-07 \cdot T + 4.76308E-07 \cdot P + 3.94463E-06 \cdot LHSV \\
&+ 1.00091E-05 \cdot ECP_3 + 9.26941E-07 \cdot ECP_4 - 3.45808E-07 \cdot T \cdot P \\
&- 1.65386E-06 \cdot T \cdot LHSV + 2.88458E-06 \cdot T \cdot ECP_3 - 5.64434E-08 \cdot T \cdot ECP_4 \\
&- 7.48300E-07 \cdot P \cdot LHSV - 2.40854E-07 \cdot P \cdot ECP_3 + 2.93950E-07 \cdot P \cdot ECP_4 \\
&- 3.92804E-06 \cdot LHSV \cdot ECP_3 + 8.50085E-07 \cdot LHSV \cdot ECP_4 \\
&+ 4.06377E-07 \cdot ECP_3 \cdot ECP_4 + 7.53210E-07 \cdot T \cdot T - 9.92663E-07 \cdot P \cdot P \\
&- 1.25808E-06 \cdot LHSV \cdot LHSV - 5.16411E-06 \cdot ECP_3 \cdot ECP_3 \\
&- 5.13526E-07 \cdot ECP_4 \cdot ECP_4 \qquad \text{(B.3n)} \\
Yield_{HGO} = &+ 0.22751 - 0.027942 \cdot T - 1.55459E-03 \cdot P + 0.014683 \cdot LHSV \\
&- 3.22375E-04 \cdot ECP_3 - 2.39003E-03 \cdot ECP_4 - 4.82315E-03 \cdot T \cdot P \\
&+ 0.045397 \cdot T \cdot LHSV - 7.83962E-04 \cdot T \cdot ECP_3 - 1.42722E-04 \cdot T \cdot ECP_4 \\
&+ 4.62728E-03 \cdot P \cdot LHSV + 1.19579E-03 \cdot P \cdot ECP_3 - 1.91786E-04 \cdot P \cdot ECP_4 \\
&+ 1.89660E-03 \cdot LHSV \cdot ECP_3 + 4.79569E-03 \cdot LHSV \cdot ECP_4 \\
&- 1.14340E-03 \cdot ECP_3 \cdot ECP_4 - 0.019561 \cdot T \cdot T + 1.86774E-06 \cdot P \cdot P \\
&- 0.011247 \cdot LHSV \cdot LHSV + 3.75757E-04 \cdot ECP_3 \cdot ECP_3 \\
&+ 1.14776E-03 \cdot ECP_4 \cdot ECP_4 \qquad \text{(B.3o)} \\
Q_{HGO} = &(-3.39517E+05 + 1.14393E+06 \cdot T + 3.12490E+05 \cdot F + 6.42882E+05 \cdot T \cdot F \\
&+ 1.72245E+06 \cdot T \cdot T - 54584.71611 \cdot F \cdot F)/1000 \qquad \text{(B.3p)} \\
W_{HGO} = &+ 494.11312 + 141.06849 \cdot P + 330.71955 \cdot F + 94.38573 \cdot P \cdot F \qquad \text{(B.3q)} \\
H_{HGO} = &+ 170.13415 - 159.48710 \cdot T + 18.07227 \cdot P + 2756.40939 \cdot LHSV \\
&+ 1128.88291 \cdot T \cdot LHSV - 169.30304 \cdot T \cdot T - 598.49850 \cdot LHSV \cdot LHSV \qquad \text{(B.3r)}
\end{aligned}
$$

Hydrotreaters:

$$
\begin{aligned}
\Delta Nitrogen_{NPH} = &+ 60.77707 + 41.66915 \cdot T - 14.37791 \cdot LHSV \\
&- 6.26008 \cdot T \cdot LHSV + 5.94631 \cdot T \cdot T \qquad \text{(B.4a)} \\
\Delta Sulfur_{NPH} = &+ 73.21807 + 43.07642 \cdot T - 15.77011 \cdot LHSV \qquad \text{(B.4b)} \\
\Delta Mhu_{NPH} = &1 - (+0.43601 - 4.06361E-03 \cdot T
\end{aligned}
$$

$$+ 1.51180E-03_{NPH} \cdot LHSV)/0.450139213 \tag{B.4c}$$

$$\Delta SG_{NPH} = + 0.032580 + 6.34514E-03 \cdot T - 2.35756E-03 \cdot LHSV \tag{B.4d}$$

$$Yield_{NPH} = + 1.00737 - 3.50701E-04 \cdot T + 1.33269E-04 \cdot LHSV \tag{B.4e}$$

$$\begin{aligned} Q_{NPH} =&(+6.08362E+06 + 9.86426E+05 \cdot T + 2.02593E+06 \cdot F \\ &+ 3.32985E+05 \cdot T \cdot F)/1000 \end{aligned} \tag{B.4f}$$

$$W_{NPH} = + 19.19399 + 4.80090 \cdot P + 6.39800 \cdot F + 1.60030 \cdot P \cdot F \tag{B.4g}$$

$$H_{NPH} = + 79.27962 + 26.42654 \cdot F \tag{B.4h}$$

$$\begin{aligned} \Delta Sulfur_{LGO} =&97.82 + 2.62 \cdot T - 0.87 \cdot P - 2.46 \cdot LHSV - 1.76 \cdot T \cdot T \\ &- 2.79 \cdot LHSV \cdot LHSV + 1.53 \cdot T \cdot LHSV \end{aligned} \tag{B.4i}$$

$$\begin{aligned} \Delta Nitrogen_{LGO} =&97.63 + 4.45 \cdot T + 0.95 \cdot P - 5.87 \cdot LHSV - 4.57 \cdot T \cdot T - 2.08 \cdot P \cdot P \\ &- 4.44 \cdot LHSV \cdot LHSV + 4.68 \cdot T \cdot LHSV \end{aligned} \tag{B.4j}$$

$$\begin{aligned} \Delta Mhu_{LGO} =&1 - (+2.67053 + 0.014100 \cdot T + 2.67768E-03 \cdot P - 0.092056 \cdot LHSV \\ &- 0.022893 \cdot T \cdot LHSV + 0.018423 \cdot T \cdot T + 3.33457E-03 \cdot P \cdot P \\ &+ 0.044867 \cdot LHSV \cdot LHSV)/4.099412038 \end{aligned} \tag{B.4k}$$

$$\begin{aligned} \Delta SG_{LGO} =& + 0.049251 - 5.41131E-04 \cdot T - 1.89403E-04 \cdot P \\ &+ 4.49671E-03 \cdot LHSV + 9.85380E-04 \cdot T \cdot LHSV - 8.23986E-04 \cdot T \cdot T \\ &- 7.67398E-05 \cdot P \cdot P - 2.16191E-03 \cdot LHSV \cdot LHSV \end{aligned} \tag{B.4l}$$

$$\begin{aligned} Yield_{LGO} =& + 1.00186 + 6.12256E-04 \cdot T + 1.47213E-04 \cdot P \\ &- 4.37508E-03 \cdot LHSV - 1.03479E-03 \cdot T \cdot LHSV + 8.48566E-04 \cdot T \cdot T \\ &+ 1.29708E-04 \cdot P \cdot P + 2.12058E-03 \cdot LHSV \cdot LHSV \end{aligned} \tag{B.4m}$$

$$\begin{aligned} Q_{LGO} =&(+4.02898E+07 + 5.04764E+06 \cdot T + 2.41741E+07 \cdot F \\ &+ 3.02862E+06 \cdot T \cdot F)/1000 \end{aligned} \tag{B.4n}$$

$$W_{LGO} = + 306.25656 + 80.61929 \cdot P + 183.75577 \cdot F + 48.37206 \cdot P \cdot F \tag{B.4o}$$

$$H_{LGO} = + 944.44848 + 566.67476 \cdot F \tag{B.4p}$$

$$\begin{aligned} \Delta Sulfur_{HGO} =& + 110.97149 + 3.14614 \cdot T - 31.04071 \cdot LHSV - 3.09076 \cdot P + 9.41569 \cdot T \cdot LHSV \\ &+ 0.69886 \cdot T \cdot P + 3.15327 \cdot LHSV \cdot P - 2.86939 \cdot T \cdot T + 8.00992 \cdot LHSV \cdot LHSV \\ &+ 3.77024 \cdot P \cdot P \end{aligned} \tag{B.4q}$$

$$\begin{aligned} \Delta Nitrogen_{HGO} =& + 124.13675 + 37.04429 \cdot T - 95.96074 \cdot LHSV + 3.01747 \cdot P - 6.13035 \cdot T \cdot LHSV \\ &+ 6.25095 \cdot T \cdot P + 4.77172 \cdot LHSV \cdot P + 3.08388 \cdot T \cdot T + 26.05143 \cdot LHSV \cdot LHSV \\ &+ 2.54806 \cdot P \cdot P \end{aligned} \tag{B.4r}$$

$$\begin{aligned} \Delta Mhu_{HGO} =&1 - (+92.12549 - 6.89087 \cdot T + 3.49695 \cdot P + 58.33384 \cdot LHSV - 15.18849 \cdot T \cdot LHSV \\ &- 5.45676 \cdot P \cdot LHSV + 5.68455 \cdot T \cdot T - 5.91243 \cdot P \cdot P \end{aligned}$$

$$- 14.49135 \cdot LHSV \cdot LHSV)/310.315054 \tag{B.4s}$$

$$\begin{aligned}\Delta SG_{HGO} = &+ 0.066817 + 8.64371E-04 \cdot T - 3.93170E-04 \cdot P - 5.40953E-03 \cdot LHSV \\ &+ 1.69116E-04 \cdot T \cdot P + 1.23313E-03 \cdot T \cdot LHSV + 4.91936E-04 \cdot P \cdot LHSV \\ &- 3.61730E-04 \cdot T \cdot T + 5.51660E-04 \cdot P \cdot P + 1.41079E-03 \cdot LHSV \cdot LHSV\end{aligned} \tag{B.4t}$$

$$\begin{aligned}Yield_{HGO} = &+ 0.98036 - 2.33689E-03 \cdot T + 8.23424E-04 \cdot P + 0.012987 \cdot LHSV \\ &- 4.45198E-04 \cdot T \cdot P - 2.62276E-03 \cdot T \cdot LHSV - 1.13332E-03 \cdot P \cdot LHSV \\ &+ 7.53868E-04 \cdot T \cdot T - 1.23712E-03 \cdot P \cdot P - 3.39929E-03 \cdot LHSV \cdot LHSV\end{aligned} \tag{B.4u}$$

$$\begin{aligned}Q_{HGO} = &(+1.95583E+07 + 8.62127E+06 \cdot T + 1.17351E+07 \cdot F \\ &+ 5.17281E+06 \cdot T \cdot F)/1000\end{aligned} \tag{B.4v}$$

$$W_{HGO} = + 295.50004 + 74.36190 \cdot P + 177.30180 \cdot F + 44.61758 \cdot P \cdot F \tag{B.4w}$$

$$H_{HGO} = + 1423.42951 + 854.06624 \cdot F \tag{B.4x}$$

Notice that for hydrotreaters, the outlet stream properties (e.g., $Nitrogen_{out}$) are calculated using the above correlations and inlet stream properties (e.g., $Nitrogen_{in}$) as following:

$$Nitrogen_{out} = Nitrogen_{in} \cdot (100 - \Delta Nitrogen)/100 \tag{B.5a}$$

$$Sulfur_{out} = Sulfur_{in} \cdot (100 - \Delta Sulfur)/100 \tag{B.5b}$$

$$Mhu_{out} = Mhu_{in} \cdot (1 - \Delta Mhu) \tag{B.5c}$$

$$SG_{out} = SG_{in} - \Delta SG \tag{B.5d}$$

Appendix C

The Counterpart Derivations for Chapter 5

In this part, derivations of objective function and constraints for the stochastic programming model under the linear decision rule are explained.

Counterpart of objective function 5.43a

First term: $\mathbb{E}\left[\sum_{t\in T}\sum_{p\in MP}\frac{{}^{UC_1}/_{\rho_p}}{(1+r)^t}\cdot\widetilde{\gamma}_t^{SCO}(\xi)\cdot M_{p,t}^{HTout}(\xi)\right]$

1. Apply LDR, factor $\xi_{[t-1]}$, and use truncate matrices of P_t^{ξ} and P_t^{SCO}, $\mathbb{E}\left[\sum_{t\in T}\sum_{p\in MP}\frac{{}^{UC_1}/_{\rho_p}}{(1+r)^t}\cdot(A_t^{SCO}\cdot P_t^{SCO}\cdot\xi+B_t^{SCO})\cdot M_{p,t}^{HTout}\cdot P_t^{\xi}\cdot\xi\right]$

2. Apply expectation operator on decision variables and uncertain parameter,
$\sum_{t\in T}\sum_{p\in MP}\frac{{}^{UC_1}/_{\rho_p}}{(1+r)^t}\cdot\mathbb{E}\left[(A_t^{SCO}\cdot P_t^{SCO}\cdot\xi+B_t^{SCO})\cdot M_{p,t}^{HTout}\cdot P_t^{\xi}\cdot\xi\right]=$
$\sum_{t\in T}\sum_{p\in MP}\frac{{}^{UC_1}/_{\rho_p}}{(1+r)^t}\cdot\mathbb{E}\left[A_t^{SCO}\cdot P_t^{SCO}\cdot\xi\cdot M_{p,t}^{HTout}\cdot P_t^{\xi}\cdot\xi+B_t^{SCO}\cdot M_{p,t}^{HTout}\cdot P_t^{\xi}\cdot\xi\right]$

3. Switch the $[A_t^{SCO}\cdot P_t^{SCO}\cdot\xi]$ term with its equivalent where all its elements are transposed; $[\xi^T\cdot(P_t^{SCO})^T\cdot(A_t^{SCO})^T]$,
$\sum_{t\in T}\sum_{p\in MP}\frac{{}^{UC_1}/_{\rho_p}}{(1+r)^t}\cdot\mathbb{E}\left[\xi^T\cdot(P_t^{SCO})^T\cdot(A_t^{SCO})^T\cdot M_{p,t}^{HTout}\cdot P_t^{\xi}\cdot\xi+B_t^{SCO}\cdot M_{p,t}^{HTout}\cdot P_t^{\xi}\cdot\xi\right]$

4. Knowing that $\mathbb{E}[X'\cdot A\cdot X]=tr(A\cdot\mathbb{E}[X\cdot X'])$,
$\sum_{t\in T}\sum_{p\in MP}\frac{{}^{UC_1}/_{\rho_p}}{(1+r)^t}\cdot\left[tr\left((P_t^{SCO})^T\cdot(A_t^{SCO})^T\cdot M_{p,t}^{HTout}\cdot P_t^{\xi}\cdot\mathbb{E}[\xi\cdot\xi^T]\right)+B_t^{SCO}\cdot M_{p,t}^{HTout}\cdot P_t^{\xi}\cdot\mathbb{E}[\xi]\right]=$
$\sum_{t\in T}\sum_{p\in MP}\frac{{}^{UC_1}/_{\rho_p}}{(1+r)^t}\cdot\left[tr\left((P_t^{SCO})^T\cdot(A_t^{SCO})^T\cdot M_{p,t}^{HTout}\cdot P_t^{\xi}\cdot\mathbb{E}_{\xi\in\Xi}[\xi\cdot\xi^T]\right)+B_t^{SCO}\cdot M_{p,t}^{HTout}\cdot P_t^{\xi}\cdot\mathbb{E}_{\xi\in\Xi}[\xi]\right]$

Second term: $\mathbb{E}\left[-\sum_{t\in T}\frac{C_t^{CAPEX}(\xi)}{(1+r)^t}\right]$

1. Apply LDR, factor $\xi_{[t-1]}$, and use the P_t^{ξ} truncate matrix, $\mathbb{E}\left[-\sum_{t\in T}\frac{C_t^{CAPEX}\cdot P_t^{\xi}\cdot\xi}{(1+r)^t}\right]$

2. Apply expectation operator on decision variables, $-\sum_{t\in T}\left[\frac{C_t^{CAPEX}}{(1+r)^t}\cdot P_t^{\xi}\cdot\mathbb{E}_{\xi\in\Xi}[\xi]\right]$

Third term: $\mathbb{E}\left[-\sum_{t\in T}\frac{OT/_{UC_2}}{(1+r)^t}\cdot\left(\sum_u\gamma_u^E\cdot E_{u,t}(\xi)+\sum_{p\in MP}\gamma^{H_2}\cdot M_{p,t}^{H2}(\xi)\right)\right]$

1. Apply LDR, factor $\xi_{[t-1]}$, and use the P_t^{ξ} truncate matrix,
$\mathbb{E}\left[-\sum_{t\in T}\frac{OT/_{UC_2}}{(1+r)^t}\cdot\left(\sum_u\gamma_u^E\cdot E_{u,t}\cdot P_t^{\xi}\cdot\xi+\sum_{p\in MP}\gamma^{H_2}\cdot M_{p,t}^{H2}\cdot P_t^{\xi}\cdot\xi\right)\right]$

2. Apply expectation operator on decision variables,
$-\sum_{t\in T}\frac{OT/_{UC_2}}{(1+r)^t}\cdot\left(\sum_u\gamma_u^E\cdot E_{u,t}+\sum_{p\in MP}\gamma^{H_2}\cdot M_{p,t}^{H2}\right)\cdot P_t^{\xi}\cdot\mathbb{E}_{\xi\in\Xi}[\xi]$

Fourth term: $\mathbb{E}\left[-\sum_{t\in T}\frac{\gamma^{MAINEX}}{(1+r)^t}\cdot\sum_{t'=1}^{t}C_{t'}^{CAPEX}(\xi)\right]$

1. Apply LDR, factor $\xi_{[t-1]}$, and use the P_t^{ξ} truncate matrix, $\mathbb{E}\left[-\sum_{t\in T}\frac{\gamma^{MAINEX}}{(1+r)^t}\cdot\sum_{t'=1}^{t}C_{t'}^{CAPEX}\cdot P_{t'}^{\xi}\cdot\xi\right]$

2. Apply expectation operator on decision variables, $-\sum_{t\in T}\frac{\gamma^{MAINEX}}{(1+r)^t}\cdot\sum_{t'=1}^{t}C_{t'}^{CAPEX}\cdot P_{t'}^{\xi}\cdot\mathbb{E}_{\xi\in\Xi}[\xi]$

Fifth term: $\mathbb{E}\left[-\sum_{t\in T}\frac{OT/_{UC_2}}{(1+r)^t}\cdot\widetilde{\gamma}_t^{CO_2}(\xi)\cdot\left(\sum_u\delta_u^E\cdot E_{u,t}(\xi)+\sum_{p\in MP}\delta^{H_2}\cdot M_{p,t}^{H2}(\xi)+\delta^{SCO}\cdot M_t^{SCO}(\xi)\right)\right]$

1. Apply LDR, factor $\xi_{[t-1]}$, and use the truncate matrices of $P_t^{CO_2}$ and P_t^{ξ},
$\mathbb{E}\left[-\sum_{t\in T}\frac{OT/_{UC_2}}{(1+r)^t}\cdot\gamma^{CO_2}\cdot(1+P_t^{CO_2}\cdot\xi)\cdot\left(\sum_u\delta_u^E\cdot E_{u,t}\cdot P_t^{\xi}\cdot\xi+\sum_{p\in MP}\delta^{H_2}\cdot M_{p,t}^{H2}\cdot P_t^{\xi}\cdot\xi+\delta^{SCO}\cdot M_t^{SCO}\cdot P_t^{\xi}\cdot\xi\right)\right]$

2. Apply expectation operator on decision variables and uncertain parameter,
$-\sum_{t\in T}\frac{OT/_{UC_2}}{(1+r)^t}\cdot\gamma^{CO_2}\cdot\mathbb{E}\left[(1+P_t^{CO_2}\cdot\xi)\cdot\left(\sum_u\delta_u^E\cdot E_{u,t}+\sum_{p\in MP}\delta^{H_2}\cdot M_{p,t}^{H2}+\delta^{SCO}\cdot M_t^{SCO}\right)\cdot P_t^{\xi}\cdot\xi\right]=$
$-\sum_{t\in T}\frac{OT/_{UC_2}}{(1+r)^t}\cdot\gamma^{CO_2}\cdot\mathbb{E}\left[F\cdot P_t^{\xi}\cdot\xi+P_t^{CO_2}\cdot\xi\cdot F\cdot P_t^{\xi}\cdot\xi\right]$
where $F=\left(\sum_u\delta_u^E\cdot E_{u,t}+\sum_{p\in MP}\delta^{H_2}\cdot M_{p,t}^{H2}+\delta^{SCO}\cdot M_t^{SCO}\right)$

3. Switch the $[P_t^{CO_2}\cdot\xi]$ term with its equivalent where all its elements are transposed; $[\xi^T\cdot(P_t^{CO_2})^T]$,
$-\sum_{t\in T}\frac{OT/_{UC_2}}{(1+r)^t}\cdot\gamma^{CO_2}\cdot\mathbb{E}\left[F\cdot P_t^{\xi}\cdot\xi+\xi^T\cdot(P_t^{CO_2})^T\cdot F\cdot P_t^{\xi}\cdot\xi\right]$

4. Knowing that $\mathbb{E}[X'\cdot A\cdot X]=tr(A\cdot\mathbb{E}[X\cdot X'])$,
$-\sum_{t\in T}\frac{OT/_{UC_2}}{(1+r)^t}\cdot\gamma^{CO_2}\cdot\left[F\cdot P_t^{\xi}\cdot\mathbb{E}[\xi]+tr\left((P_t^{CO_2})^T\cdot F\cdot P_t^{\xi}\cdot\mathbb{E}[\xi\cdot\xi^T]\right)\right]=$
$-\sum_{t\in T}\frac{OT/_{UC_2}}{(1+r)^t}\cdot\gamma^{CO_2}\cdot\left[F\cdot P_t^{\xi}\cdot\mathbb{E}_{\xi\in\Xi}[\xi]+tr\left((P_t^{CO_2})^T\cdot F\cdot P_t^{\xi}\cdot\mathbb{E}_{\xi\in\Xi}[\xi\cdot\xi^T]\right)\right]$

5. Plug in the F back,

$$-\sum_{t\in T}\frac{{}^{OT}/_{UC_2}}{(1+r)^t}\cdot\gamma^{CO_2}\cdot\left[\left(\sum_u\delta^E_u\cdot E_{u,t}+\sum_{p\in MP}\delta^{H_2}\cdot M^{H2}_{p,t}+\delta^{SCO}\cdot M^{SCO}_t\right)\cdot P^\xi_t\cdot\mathbb{E}_{\xi\in\Xi}[\xi]+tr\Bigg((P^{CO_2}_t)^T\cdot\left(\sum_u\delta^E_u\cdot E_{u,t}+\sum_{p\in MP}\delta^{H_2}\cdot M^{H2}_{p,t}+\delta^{SCO}\cdot M^{SCO}_t\right)\cdot P^\xi_t\cdot\mathbb{E}_{\xi\in\Xi}[\xi\cdot\xi^T]\Bigg)\right]$$

Sixth term: $\mathbb{E}\left[-\sum_{t\in T}\frac{{}^{UC_1}/_{\rho_{DR}}\cdot\gamma^{Bitumen}}{(1+r)^t}\cdot M^{in}_{DR,t}(\xi)\right]$

1. Apply LDR, factor $\xi_{[t-1]}$, and use the P^ξ_t truncate matrix, $\mathbb{E}\left[-\sum_{t\in T}\frac{{}^{UC_1}/_{\rho_{DR}}\cdot\gamma^{Bitumen}}{(1+r)^t}\cdot M^{in}_{DR,t}\cdot P^\xi_t\cdot\xi\right]$
2. Apply expectation operator on decision variables, $-\sum_{t\in T}\frac{{}^{UC_1}/_{\rho_{DR}}\cdot\gamma^{Bitumen}}{(1+r)^t}\cdot M^{in}_{DR,t}\cdot P^\xi_t\cdot\mathbb{E}_{\xi\in\Xi}[\xi]$

Counterpart of constraint 5.43c

$M^{out}_{p,c,t}(\xi)=\alpha^{yield}_{p,c}\cdot M^{in}_{p,t}(\xi)\quad\forall p\in SP,c\in C,t\in T,\xi\in\Xi$

1. Apply LDR and factor $\xi_{[t-1]}$, $M^{out}_{p,c,t}\cdot\xi_{[t-1]}=\alpha^{yield}_{p,c}\cdot M^{in}_{p,t}\cdot\xi_{[t-1]}\quad\forall p\in SP,c\in C,t\in T,\xi\in\Xi$
2. Cancel $\xi_{[t-1]}$, $M^{out}_{p,c,t}=\alpha^{yield}_{p,c}\cdot M^{in}_{p,t}\quad\forall p\in SP,c\in C,t\in T$

Counterpart of constraint 5.43d

$M^{in}_{TC,t}(\xi)=(1-\sum_c\alpha^{yield}_{DR,c})\cdot M^{in}_{DR,t}(\xi)\quad\forall t\in T,\xi\in\Xi$

1. Apply LDR and factor $\xi_{[t-1]}$, $M^{in}_{TC,t}\cdot\xi_{[t-1]}=(1-\sum_c\alpha^{yield}_{DR,c})\cdot M^{in}_{DR,t}\cdot\xi_{[t-1]}\quad\forall t\in T,\xi\in\Xi$
2. Cancel $\xi_{[t-1]}$, $M^{in}_{TC,t}=(1-\sum_c\alpha^{yield}_{DR,c})\cdot M^{in}_{DR,t}\quad\forall t\in T$

Counterpart of constraint 5.43e

$\sum_{p'\in SP}M^{out}_{p',c,t}(\xi)=M^{in}_{p,t}(\xi)\quad\forall(p,c)\in PC,t\in T,\xi\in\Xi$

1. Apply LDR and factor $\xi_{[t-1]}$, $\sum_{p'\in SP}M^{out}_{p',c,t}\cdot\xi_{[t-1]}=M^{in}_{p,t}\cdot\xi_{[t-1]}\quad\forall(p,c)\in PC,t\in T,\xi\in\Xi$
2. Cancel $\xi_{[t-1]}$, $\sum_{p'\in SP}M^{out}_{p',c,t}=M^{in}_{p,t}\quad\forall(p,c)\in PC,t\in T$

Counterpart of constraint 5.43f

$M^{HTout}_{p,t}(\xi)=\alpha^{HT}_p\cdot\left(M^{in}_{p,t}(\xi)+M^{H2}_{p,t}(\xi)\right)\quad\forall p\in MP,t\in T,\xi\in\Xi$

1. Apply LDR and factor $\xi_{[t-1]}$, $M^{HTout}_{p,t}\cdot\xi_{[t-1]}=\alpha^{HT}_p\cdot\left(M^{in}_{p,t}+M^{H2}_{p,t}\right)\cdot\xi_{[t-1]}\quad\forall p\in MP,t\in T,\xi\in\Xi$
2. Cancel $\xi_{[t-1]}$, $M^{HTout}_{p,t}=\alpha^{HT}_p\cdot\left(M^{in}_{p,t}+M^{H2}_{p,t}\right)\quad\forall p\in MP,t\in T$

Counterpart of constraint 5.43g

$M^{H2}_{p,t}(\xi)=\frac{\alpha^{H_2}_p\cdot M^{in}_{p,t}(\xi)}{\rho_p}\quad\forall p\in MP,t\in T,\xi\in\Xi$

1. Apply LDR and factor $\xi_{[t-1]}$, $M^{H2}_{p,t}\cdot\xi_{[t-1]}=\frac{\alpha^{H_2}_p\cdot M^{in}_{p,t}}{\rho_p}\cdot\xi_{[t-1]}\quad\forall p\in MP,t\in T,\xi\in\Xi$
2. Cancel $\xi_{[t-1]}$, $M^{H2}_{p,t}=\frac{\alpha^{H_2}_p\cdot M^{in}_{p,t}}{\rho_p}\quad\forall p\in MP,t\in T$

Counterpart of constraint 5.43h

$M_t^{SCO}(\xi) = \sum_{p \in MP} M_{p,t}^{HTout}(\xi) \quad \forall t \in T, \xi \in \Xi$

1. Apply LDR and factor $\xi_{[t-1]}$, $M_t^{SCO} \cdot \xi_{[t-1]} = \sum_{p \in MP} M_{p,t}^{HTout} \cdot \xi_{[t-1]} \quad \forall t \in T, \xi \in \Xi$ 2. Cancel $\xi_{[t-1]}$, $M_t^{SCO} = \sum_{p \in MP} M_{p,t}^{HTout} \quad \forall t \in T$

Counterpart of constraint 5.43i

$\underline{\Omega}_p^{Spec} \leq \dfrac{M_{p,t}^{HTout}(\xi)}{M_t^{SCO}(\xi)} \quad \forall p \in MP, t \in T, \xi \in \Xi$

1. Arrange the uncertain variable in left–hand–side, $\underline{\Omega}_p^{Spec} \cdot M_t^{SCO}(\xi) - M_{p,t}^{HTout}(\xi) \leq 0 \quad \forall p \in MP, t \in T, \xi \in \Xi$

2. Apply LDR and factor $\xi_{[t-1]}$, $\left(\underline{\Omega}_p^{Spec} \cdot M_t^{SCO} - M_{p,t}^{HTout}\right) \cdot \xi_{[t-1]} \leq 0 \quad \forall p \in MP, t \in T, \xi \in \Xi$

3. Derive the robust counterpart and introduce the truncate operator P_t^{ξ}, $\left\{ \max_{\xi \in \Xi} \quad \left(\underline{\Omega}_p^{Spec} \cdot M_t^{SCO} - M_{p,t}^{HTout}\right) \cdot P_t^{\xi} \cdot \xi \right\} \leq 0 \quad \forall p \in MP, t \in T, \xi \in \Xi$

4. Define the uncertain set,

$$\left\{ \begin{array}{c} \max \quad \left(\underline{\Omega}_p^{Spec} \cdot M_t^{SCO} - M_{p,t}^{HTout}\right) \cdot P_t^{\xi} \cdot \xi \\ s.t. \quad -W \cdot \xi \leq -h \end{array} \right\} \leq 0 \quad \forall p \in MP, t \in T$$

5. Introduce dual variable $\Lambda_{p,t}^i$ and apply duality to the inner LP problem,

$$\left\{ \begin{array}{c} \min \quad -h^T \cdot \Lambda_{p,t}^i \\ s.t. \quad -W^T \cdot \Lambda_{p,t}^i = \left(\left[\underline{\Omega}_p^{Spec} \cdot M_t^{SCO} - M_{p,t}^{HTout} \right] \cdot P_t^{\xi} \right)^T \\ \Lambda_{p,t}^i \geq 0 \end{array} \right\} \leq 0 \quad \forall p \in MP, t \in T$$

6. Drop the min operator,

$$\left\{ \begin{array}{l} -h^T \cdot \Lambda_{p,t}^i \leq 0 \quad \forall p \in MP, t \in T \\ -W^T \cdot \Lambda_{p,t}^i = \left(\left[\underline{\Omega}_p^{Spec} \cdot M_t^{SCO} - M_{p,t}^{HTout} \right] \cdot P_t^{\xi} \right)^T \quad \forall p \in MP, t \in T \\ \Lambda_{p,t}^i \geq 0 \quad \forall p \in MP, t \in T \end{array} \right.$$

Counterpart of constraint 5.43j

Part one:

$\underline{\Omega}_p^X \cdot Y_{p,t} \leq X_{p,t}(\xi) \quad \forall p \in P, t \in T, \xi \in \Xi$

1. Arrange the uncertain variable in left–hand–side, $-X_{p,t}(\xi) \leq -\underline{\Omega}_p^X \cdot Y_{p,t} \quad \forall p \in P, t \in T, \xi \in \Xi$

2. Apply LDR and factor $\xi_{[t-1]}$, $-X_{p,t} \cdot \xi_{[t-1]} \leq -\underline{\Omega}_p^X \cdot Y_{p,t} \quad \forall p \in P, t \in T, \xi \in \Xi$

3. Derive the robust counterpart and introduce the truncate operator P_t^{ξ}, $\left\{ \max_{\xi \in \Xi} \quad -(X_{p,t} \cdot P_t^{\xi}) \cdot \xi \right\} \leq -\underline{\Omega}_p^X \cdot Y_{p,t} \quad \forall p \in P, t \in T, \xi \in \Xi$

4. Define the uncertain set,

$$\left\{ \begin{array}{ll} \max & -(X_{p,t} \cdot P_t^{\xi}) \cdot \xi \\ s.t. & -W \cdot \xi \leq -h \end{array} \right\} \leq -\underline{\Omega}_p^X \cdot Y_{p,t} \quad \forall p \in P, t \in T$$

5. Introduce dual variable $\Lambda_{p,t}^{j_1}$ and apply duality to the inner LP problem,

$$\left\{ \begin{array}{ll} & \min \quad -h^T \cdot \Lambda_{p,t}^{j_1} \\ s.t. & -W^T \cdot \Lambda_{p,t}^{j_1} = \left(-X_{p,t} \cdot P_t^{\xi}\right)^T \\ & \Lambda_{p,t}^{j_1} \geq 0 \end{array} \right\} \leq -\underline{\Omega}_p^X \cdot Y_{p,t} \quad \forall p \in P, t \in T$$

6. Drop the min operator,

$$\left\{ \begin{array}{l} -h^T \cdot \Lambda_{p,t}^{j_1} \leq -\underline{\Omega}_p^X \cdot Y_{p,t} \quad \forall p \in P, t \in T \\ -W^T \cdot \Lambda_{p,t}^{j_1} = \left(-X_{p,t} \cdot P_t^{\xi}\right)^T \quad \forall p \in P, t \in T \\ \Lambda_{p,t}^{j_1} \geq 0 \quad \forall p \in P, t \in T \end{array} \right.$$

Part two:

$X_{p,t}(\xi) \leq \bar{\Omega}_p^X \cdot Y_{p,t} \quad \forall p \in P, t \in T, \xi \in \Xi$

1. Arrange the uncertain variable in left–hand–side, $X_{p,t}(\xi) \leq \bar{\Omega}_p^X \cdot Y_{p,t} \quad \forall p \in P, t \in T, \xi \in \Xi$

2. Apply LDR and factor $\xi_{[t-1]}$, $X_{p,t} \cdot \xi_{[t-1]} \leq \bar{\Omega}_p^X \cdot Y_{p,t} \quad \forall p \in P, t \in T, \xi \in \Xi$

3. Derive the robust counterpart and introduce the truncate operator P_t^{ξ}, $\left\{ \max_{\xi \in \Xi} \quad (X_{p,t} \cdot P_t^{\xi}) \cdot \xi \right\} \leq \bar{\Omega}_p^X \cdot Y_{p,t} \quad \forall p \in P, t \in T, \xi \in \Xi$

4. Define the uncertain set,

$$\left\{ \begin{array}{ll} \max & (X_{p,t} \cdot P_t^{\xi}) \cdot \xi \\ s.t. & -W \cdot \xi \leq -h \end{array} \right\} \leq \bar{\Omega}_p^X \cdot Y_{p,t} \quad \forall p \in P, t \in T$$

5. Introduce dual variable $\Lambda_{p,t}^{j_2}$ and apply duality to the inner LP problem,

$$\left\{ \begin{array}{ll} & \min \quad -h^T \cdot \Lambda_{p,t}^{j_2} \\ s.t. & -W^T \cdot \Lambda_{p,t}^{j_2} = \left(X_{p,t} \cdot P_t^{\xi}\right)^T \\ & \Lambda_{p,t}^{j_2} \geq 0 \end{array} \right\} \leq \bar{\Omega}_p^X \cdot Y_{p,t} \quad \forall p \in P, t \in T$$

6. Drop the min operator,

$$\left\{ \begin{array}{l} -h^T \cdot \Lambda_{p,t}^{j_2} \leq \bar{\Omega}_p^X \cdot Y_{p,t} \quad \forall p \in P, t \in T \\ -W^T \cdot \Lambda_{p,t}^{j_2} = \left(X_{p,t} \cdot P_t^{\xi}\right)^T \quad \forall p \in P, t \in T \\ \Lambda_{p,t}^{j_2} \geq 0 \quad \forall p \in P, t \in T \end{array} \right.$$

Counterpart of constraint 5.43k

$Q_{p,t}(\xi) = Q_{p,t-1}(\xi) + X_{p,t}(\xi) \quad \forall p \in P, t \in T_{-1}, \xi \in \Xi$

1. Apply LDR and factor $\xi_{[t-1]}$, $Q_{p,t} \cdot \xi_{[t-1]} = Q_{p,t-1} \cdot \xi_{[t-1]} + X_{p,t} \cdot \xi_{[t-1]} \quad \forall p \in P, t \in T_{-1}, \xi \in \Xi$

2. Cancel $\xi_{[t-1]}$, $Q_{p,t} = Q_{p,t-1} + X_{p,t} \quad \forall p \in P, t \in T_{-1}$

Counterpart of constraint 5.43l

Part one:

$\underline{\Omega}_p^Q \cdot Q_{p,t}(\xi) \leq \dfrac{UC_1 \cdot M_{p,t}^{in}(\xi)}{\rho_p} \quad \forall p \in P, t \in T, \xi \in \Xi$

1. Arrange the uncertain variable in left–hand–side, $\underline{\Omega}_p^Q \cdot Q_{p,t}(\xi) - \dfrac{UC_1 \cdot M_{p,t}^{in}(\xi)}{\rho_p} \leq 0 \quad \forall p \in P, t \in T, \xi \in \Xi$

2. Apply LDR and factor $\xi_{[t-1]}$, $\left(\underline{\Omega}_p^Q \cdot Q_{p,t} - \dfrac{UC_1 \cdot M_{p,t}^{in}}{\rho_p}\right) \cdot \xi_{[t-1]} \leq 0 \quad \forall p \in P, t \in T, \xi \in \Xi$

3. Derive the robust counterpart and introduce the truncate operator P_t^{ξ}, $\left\{ \max_{\xi \in \Xi} \quad \left(\underline{\Omega}_p^Q \cdot Q_{p,t} - \dfrac{UC_1 \cdot M_{p,t}^{in}}{\rho_p}\right) \cdot P_t^{\xi} \cdot \xi \right\} \leq 0 \quad \forall p \in P, t \in T, \xi \in \Xi$

4. Define the uncertain set,

$$\left\{ \begin{array}{l} \max \quad \left(\underline{\Omega}_p^Q \cdot Q_{p,t} - \dfrac{UC_1 \cdot M_{p,t}^{in}}{\rho_p}\right) \cdot P_t^{\xi} \cdot \xi \\ s.t. \quad -W \cdot \xi \leq -h \end{array} \right\} \leq 0 \quad \forall p \in P, t \in T$$

5. Introduce dual variable $\Lambda_{p,t}^{l_1}$ and apply duality to the inner LP problem,

$$\left\{ \begin{array}{l} \min \quad -h^T \cdot \Lambda_{p,t}^{l_1} \\ s.t. \quad -W^T \cdot \Lambda_{p,t}^{l_1} = \left(\left[\underline{\Omega}_p^Q \cdot Q_{p,t} - \dfrac{UC_1 \cdot M_{p,t}^{in}}{\rho_p} \right] \cdot P_t^{\xi} \right)^T \\ \Lambda_{p,t}^{l_1} \geq 0 \end{array} \right\} \leq 0 \quad \forall p \in P, t \in T$$

6. Drop the min operator,

$$\left\{ \begin{array}{l} -h^T \cdot \Lambda_{p,t}^{l_1} \leq 0 \quad \forall p \in P, t \in T \\ -W^T \cdot \Lambda_{p,t}^{l_1} = \left(\left[\underline{\Omega}_p^Q \cdot Q_{p,t} - \dfrac{UC_1 \cdot M_{p,t}^{in}}{\rho_p} \right] \cdot P_t^{\xi} \right)^T \quad \forall p \in P, t \in T \\ \Lambda_{p,t}^{l_1} \geq 0 \quad \forall p \in P, t \in T \end{array} \right.$$

Part two:

$\dfrac{UC_1 \cdot M_{p,t}^{in}(\xi)}{\rho_p} \leq Q_{p,t}(\xi) \quad \forall p \in P, t \in T, \xi \in \Xi$

1. Arrange the uncertain variable in left–hand–side, $\dfrac{UC_1 \cdot M_{p,t}^{in}(\xi)}{\rho_p} - Q_{p,t}(\xi) \leq 0 \quad \forall p \in P, t \in T, \xi \in \Xi$

2. Apply LDR and factor $\xi_{[t-1]}$, $\left(\dfrac{UC_1 \cdot M_{p,t}^{in}}{\rho_p} - Q_{p,t}\right) \cdot \xi_{[t-1]} \leq 0 \quad \forall p \in P, t \in T, \xi \in \Xi$

3. Derive the robust counterpart and introduce the truncate operator P_t^{ξ}, $\left\{ \max_{\xi \in \Xi} \quad \left(\dfrac{UC_1 \cdot M_{p,t}^{in}}{\rho_p} - Q_{p,t}\right) \cdot P_t^{\xi} \cdot \xi \right\} \leq 0 \quad \forall p \in P, t \in T, \xi \in \Xi$

4. Define the uncertain set,

$$\left\{ \begin{array}{l} \max \quad \left(\dfrac{UC_1 \cdot M_{p,t}^{in}}{\rho_p} - Q_{p,t}\right) \cdot P_t^{\xi} \cdot \xi \\ s.t. \quad -W \cdot \xi \leq -h \end{array} \right\} \leq 0 \quad \forall p \in P, t \in T$$

5. Introduce dual variable $\Lambda_{p,t}^{l_2}$ and apply duality to the inner LP problem,

$$\left\{ \begin{array}{cc} & \min \quad -h^T \cdot \Lambda_{p,t}^{l_2} \\ s.t. & -W^T \cdot \Lambda_{p,t}^{l_2} = \left(\left[\dfrac{UC_1 \cdot M_{p,t}^{in}}{\rho_p} - Q_{p,t} \right] \cdot P_t^{\xi} \right)^T \\ & \Lambda_{p,t}^{l_2} \geq 0 \end{array} \right\} \leq 0 \quad \forall p \in P, t \in T$$

6. Drop the min operator,

$$\left\{ \begin{array}{l} -h^T \cdot \Lambda_{p,t}^{l_2} \leq 0 \quad \forall p \in P, t \in T \\ -W^T \cdot \Lambda_{p,t}^{l_2} = \left(\left[\dfrac{UC_1 \cdot M_{p,t}^{in}}{\rho_p} - Q_{p,t} \right] \cdot P_t^{\xi} \right)^T \quad \forall p \in P, t \in T \\ \Lambda_{p,t}^{l_2} \geq 0 \quad \forall p \in P, t \in T \end{array} \right.$$

Counterpart of constraint 5.43m

$E_{u,t}(\xi) = \sum_p \beta_{p,u} \cdot M_{p,t}^{in}(\xi) \quad \forall u \in U, t \in T, \xi \in \Xi$

1. Apply LDR and factor $\xi_{[t-1]}$, $E_{u,t} \cdot \xi_{[t-1]} = \sum_p \beta_{p,u} \cdot M_{p,t}^{in} \cdot \xi_{[t-1]} \quad \forall u \in U, t \in T, \xi \in \Xi$

2. Cancel $\xi_{[t-1]}$, $E_{u,t} = \sum_p \beta_{p,u} \cdot M_{p,t}^{in} \quad \forall u \in U, t \in T$

Counterpart of constraint 5.43n

$C_t^{CAPEX}(\xi) = \sum_p (a_p \cdot Q_{p,t}(\xi) + b_p) \quad \forall t = 1, \xi \in \Xi$

1. Introduce an auxiliary parameter B_p as $b_p = B_p \cdot \xi_{[t-1]}$, Apply LDR, and factor $\xi_{[t-1]}$, $C_t^{CAPEX} \cdot \xi_{[t-1]} = \sum_p (a_p \cdot Q_{p,t} + B_p) \cdot \xi_{[t-1]} \quad \forall t = 1, \xi \in \Xi$

2. Cancel $\xi_{[t-1]}$, $C_t^{CAPEX} = \sum_p (a_p \cdot Q_{p,t} + B_p) \quad \forall t = 1$

Counterpart of constraint 5.43o

$C_t^{CAPEX}(\xi) = \sum_p (a_p \cdot X_{p,t}(\xi) + b_p \cdot Y_{p,t}) \quad \forall t \in T_{-1}, \xi \in \Xi$

1. Introduce an auxiliary parameter B_p as $b_p = B_p \cdot \xi_{[t-1]}$, Apply LDR, and factor $\xi_{[t-1]}$, $C_t^{CAPEX} \cdot \xi_{[t-1]} = \sum_p (a_p \cdot X_{p,t} + B_p \cdot Y_{p,t}) \cdot \xi_{[t-1]} \quad \forall t \in T_{-1}, \xi \in \Xi$

Note that, we can write the $[B_p \cdot \xi_{[t-1]} \cdot Y_{p,t}]$ term as $[B_p \cdot Y_{p,t} \cdot \xi_{[t-1]}]$ since the $Y_{p,t}$ is a scalar.

2. Cancel $\xi_{[t-1]}$, $C_t^{CAPEX} = \sum_p (a_p \cdot X_{p,t} + B_p \cdot Y_{p,t}) \quad \forall t \in T_{-1}$

Counterpart of constraint 5.43p

$C_t^{CAPEX}(\xi) \leq \bar{\Omega}_t^{Investment} \quad \forall t \in T, \xi \in \Xi$

1. Apply LDR and factor $\xi_{[t-1]}$, $(C_t^{CAPEX}) \cdot \xi_{[t-1]} \leq \bar{\Omega}_t^{Investment} \quad \forall t \in T, \xi \in \Xi$

2. Derive the robust counterpart and introduce the truncate operator P_t^{ξ}, $\left\{ \max_{\xi \in \Xi} \quad (C_t^{CAPEX} \cdot P_t^{\xi}) \cdot \xi \right\} \leq \bar{\Omega}_t^{Investment} \quad \forall t \in T, \xi \in \Xi$

3. Define the uncertain set,

$$\left\{ \begin{array}{cc} \max & (C_t^{CAPEX} \cdot P_t^{\xi}) \cdot \xi \\ s.t. & -W \cdot \xi \leq -h \end{array} \right\} \leq \bar{\Omega}_t^{Investment} \quad \forall t \in T$$

4. Introduce dual variable Λ_t^p and apply duality to the inner LP problem,

$$\left\{ \begin{array}{c} \min \quad -h^T \cdot \Lambda_t^p \\ s.t. \quad -W^T \cdot \Lambda_t^p = (C_t^{CAPEX} \cdot P_t^{\xi})^T \\ \Lambda_t^p \geq 0 \end{array} \right\} \leq \bar{\Omega}_t^{Investment} \quad \forall t \in T$$

5. Drop the min operator,

$$\left\{ \begin{array}{l} -h^T \cdot \Lambda_t^p \leq \bar{\Omega}_t^{Investment} \quad \forall t \in T \\ -W^T \cdot \Lambda_t^p = (C_t^{CAPEX} \cdot P_t^{\xi})^T \quad \forall t \in T \\ \Lambda_t^p \geq 0 \quad \forall t \in T \end{array} \right.$$

Counterpart of constraint 5.43q

$0 \leq M_{p,t}^{in}(\xi) \quad \forall t \in T, p \in P, \xi \in \Xi$

1. Arrange the uncertain variable in left–hand–side, $-M_{p,t}^{in}(\xi) \leq 0 \quad \forall t \in T, p \in P, \xi \in \Xi$
2. Apply LDR and factor $\xi_{[t-1]}$, $(-M_{p,t}^{in}) \cdot \xi_{[t-1]} \leq 0 \quad \forall t \in T, p \in P, \xi \in \Xi$
3. Derive the robust counterpart and introduce the truncate operator P_t^{ξ}, $\left\{ \max_{\xi \in \Xi} \quad (-M_{p,t}^{in} \cdot P_t^{\xi}) \cdot \xi \right\} \leq 0 \quad \forall t \in T, p \in P, \xi \in \Xi$
4. Define the uncertain set,

$$\left\{ \begin{array}{c} \max \quad (-M_{p,t}^{in} \cdot P_t^{\xi}) \cdot \xi \\ s.t. \quad -W \cdot \xi \leq -h \end{array} \right\} \leq 0 \quad \forall t \in T, p \in P$$

5. Introduce dual variable $\Lambda_{t,p}^q$ and apply duality to the inner LP problem,

$$\left\{ \begin{array}{c} \min \quad -h^T \cdot \Lambda_{t,p}^q \\ s.t. \quad -W^T \cdot \Lambda_{t,p}^q = (-M_{p,t}^{in} \cdot P_t^{\xi})^T \\ \Lambda_{t,p}^q \geq 0 \end{array} \right\} \leq 0 \quad \forall t \in T, p \in P$$

6. Drop the min operator,

$$\left\{ \begin{array}{l} -h^T \cdot \Lambda_{t,p}^q \leq 0 \quad \forall t \in T, p \in P \\ -W^T \cdot \Lambda_{t,p}^q = (-M_{p,t}^{in} \cdot P_t^{\xi})^T \quad \forall t \in T, p \in P \\ \Lambda_{t,p}^q \geq 0 \quad \forall t \in T, p \in P \end{array} \right.$$

Appendix D

The Counterpart Derivations for Chapter 6

D.1 Deriving the robust counterpart for H1

In this part, robust counterpart derivations of constraints for the MSP model are explained.

Counterpart of constraint 6.3d

1. Introduce appropriate truncate matrices to generalize the uncertainties as ξ, $\sum_{i\in I}\bar{\beta}_i\cdot(1+P^{\beta_i}\cdot\xi)\cdot C_i\leq\bar{\gamma}\cdot(1+P^{\gamma}\cdot\xi)$

2. Arrange the uncertain variables in left–hand–side and derive the robust counterpart, $\left\{\max_{\xi\in\Xi}\quad\left[\sum_{i\in I}\bar{\beta}_i\cdot P^{\beta_i}\cdot C_i-\bar{\gamma}\cdot P^{\gamma}\right]\cdot\xi\right\}\leq\left[\bar{\gamma}-\sum_{i\in I}\bar{\beta}_i\cdot C_i\right]$

3. Define the uncertain set,

$$\left\{\begin{array}{ll}\max & \left[\sum_{i\in I}\bar{\beta}_i\cdot P^{\beta_i}\cdot C_i-\bar{\gamma}\cdot P^{\gamma}\right]\cdot\xi\\ s.t. & -W\cdot\xi\leq -h\end{array}\right\}\leq\left[\bar{\gamma}-\sum_{i\in I}\bar{\beta}_i\cdot C_i\right]$$

4. Introduce dual variable Λ^d and apply duality to the inner LP problem,

$$\left\{\begin{array}{ll}\min & -h^T\cdot\Lambda^d\\ s.t. & -W^T\cdot\Lambda^d=\left[\sum_{i\in I}\bar{\beta}_i\cdot P^{\beta_i}\cdot C_i-\bar{\gamma}\cdot P^{\gamma}\right]^T\\ & 0\leq\Lambda^d\end{array}\right\}\leq\left[\bar{\gamma}-\sum_{i\in I}\bar{\beta}_i\cdot C_i\right]$$

5. Drop the min operator,

$$\left\{\begin{array}{l}-h^T\cdot\Lambda^d\leq\left[\bar{\gamma}-\sum_{i\in I}\bar{\beta}_i\cdot C_i\right]\\ -W^T\cdot\Lambda^d=\left[\sum_{i\in I}\bar{\beta}_i\cdot P^{\beta_i}\cdot C_i-\bar{\gamma}\cdot P^{\gamma}\right]^T\\ 0\leq\Lambda^d\end{array}\right.$$

Counterpart of constraint 6.3e

1. Introduce appropriate truncate matrices to generalize the uncertainties as ξ, $\sum_{i\in I}\bar{\beta}_i\cdot(1+P^{\beta_i}\cdot\xi)\cdot X_{i,s}\leq\bar{\gamma}\cdot(1+P^{\gamma}\cdot\xi)\quad\forall s\in S_{-1}$

2. Arrange the uncertain variables in left–hand–side and derive the robust counterpart, $\left\{\max_{\xi\in\Xi}\quad\left[\sum_{i\in I}\bar{\beta}_i\cdot P^{\beta_i}\cdot X_{i,s}-\bar{\gamma}\cdot P^{\gamma}\right]\cdot\xi\right\}\leq\left[\bar{\gamma}-\sum_{i\in I}\bar{\beta}_i\cdot X_{i,s}\right]\quad\forall s\in S_{-1}$

3. Define the uncertain set,

$$\left\{\begin{array}{c}\max\quad\left[\sum_{i\in I}\bar{\beta}_i\cdot P^{\beta_i}\cdot X_{i,s}-\bar{\gamma}\cdot P^{\gamma}\right]\cdot\xi\\ s.t.\quad -W\cdot\xi\leq -h\end{array}\right\}\leq\left[\bar{\gamma}-\sum_{i\in I}\bar{\beta}_i\cdot X_{i,s}\right]\quad\forall s\in S_{-1}$$

4. Introduce dual variable Λ_s^e and apply duality to the inner LP problem,

$$\left\{\begin{array}{c}\min\quad -h^T\cdot\Lambda_s^e\\ s.t.\quad -W^T\cdot\Lambda_s^e=\left[\sum_{i\in I}\bar{\beta}_i\cdot P^{\beta_i}\cdot X_{i,s}-\bar{\gamma}\cdot P^{\gamma}\right]^T\\ 0\leq\Lambda_s^e\end{array}\right\}\leq\left[\bar{\gamma}-\sum_{i\in I}\bar{\beta}_i\cdot X_{i,s}\right]\quad\forall s\in S_{-1}$$

5. Drop the min operator,

$$\left\{\begin{array}{l}-h^T\cdot\Lambda_s^e\leq\left[\bar{\gamma}-\sum_{i\in I}\bar{\beta}_i\cdot X_{i,s}\right]\quad\forall s\in S_{-1}\\ -W^T\cdot\Lambda_s^e=\left[\sum_{i\in I}\bar{\beta}_i\cdot P^{\beta_i}\cdot X_{i,s}-\bar{\gamma}\cdot P^{\gamma}\right]^T\quad\forall s\in S_{-1}\\ 0\leq\Lambda_s^e\quad\forall s\in S_{-1}\end{array}\right.$$

Counterpart of constraint 6.3f

1. Introduce appropriate truncate matrices to generalize the uncertainties as ξ, $\Phi\cdot\sum_{i\in I}(C_i+\sum_{s'\in P(s)}X_{i,s'})\leq\sum_{i\in I}\bar{\phi}_i\cdot(1+P^{\phi_i}\cdot\xi)\cdot(C_i+\sum_{s'\in P(s)}X_{i,s'})\quad\forall s\in L$

2. Arrange the uncertain variables in left–hand–side and derive the robust counterpart, $\left\{\max_{\xi\in\Xi}\quad\left[-\sum_{i\in I}\bar{\phi}_i\cdot P^{\phi_i}\cdot(C_i+\sum_{s'\in P(s)}X_{i,s'})\right]\cdot\xi\right\}\leq\left[\sum_{i\in I}\left(\bar{\phi}_i\cdot(C_i+\sum_{s'\in P(s)}X_{i,s'})-\Phi\cdot(C_i+\sum_{s'\in P(s)}X_{i,s'})\right)\right]\quad\forall s\in L$

3. Define the uncertain set,

$$\left\{\begin{array}{c}\max\quad\left[-\sum_{i\in I}\bar{\phi}_i\cdot P^{\phi_i}\cdot(C_i+\sum_{s'\in P(s)}X_{i,s'})\right]\cdot\xi\\ s.t.\quad -W\cdot\xi\leq -h\end{array}\right\}\leq\begin{array}{c}\left[\sum_{i\in I}\left(\bar{\phi}_i\cdot(C_i+\sum_{s'\in P(s)}X_{i,s'})\right.\right.\\ \left.\left.-\Phi\cdot(C_i+\sum_{s'\in P(s)}X_{i,s'})\right)\right]\end{array}\quad\forall s\in L$$

4. Introduce dual variable Λ_s^f and apply duality to the inner LP problem,

$$\left\{\begin{array}{c}\min\quad -h^T\cdot\Lambda_s^f\\ s.t.\ -W^T\cdot\Lambda_s^f=\left[-\sum_{i\in I}\bar{\phi}_i\cdot P^{\phi_i}\cdot(C_i+\sum_{s'\in P(s)}X_{i,s'})\right]^T\\ 0\leq\Lambda_s^f\end{array}\right\}\leq\begin{array}{c}\left[\sum_{i\in I}\left(\bar{\phi}_i\cdot(C_i+\sum_{s'\in P(s)}X_{i,s'})\right.\right.\\ \left.\left.-\Phi\cdot(C_i+\sum_{s'\in P(s)}X_{i,s'})\right)\right]\end{array}\quad\forall s\in L$$

5. Drop the min operator,

$$\begin{cases} -h^T \cdot \Lambda_s^f \leq \left[\sum_{i \in I} \left(\bar{\phi}_i \cdot (C_i + \sum_{s' \in P(s)} X_{i,s'}) - \Phi \cdot (C_i + \sum_{s' \in P(s)} X_{i,s'}) \right) \right] & \forall s \in L \\ -W^T \cdot \Lambda_s^f = \left[- \sum_{i \in I} \bar{\phi}_i \cdot P^{\phi_i} \cdot (C_i + \sum_{s' \in P(s)} X_{i,s'}) \right]^T & \forall s \in L \\ 0 \leq \Lambda_s^f & \forall s \in L \end{cases}$$

D.2 Deriving the robust counterpart for H2

In this part, robust counterpart derivations of constraints for the MSP model are explained.

Counterpart of constraint 6.6b

1. Introduce appropriate truncate matrices to generalize the uncertainties as ξ, $P_t^\nu \cdot \xi \leq \sum_i O_{i,t} \cdot P_t \cdot \xi \quad \forall t \in T, \xi \in \Xi$

2. Arrange the uncertain variables in left–hand–side and derive the robust counterpart, $\left\{ \max_{\xi \in \Xi} \quad (P_t^\nu - \sum_i O_{i,t} \cdot P_t) \cdot \xi \right\} \leq 0 \quad \forall t \in T$

3. Define the uncertain set,

$$\left\{ \begin{array}{c} \max \quad \left[P_t^\nu - \sum_i O_{i,t} \cdot P_t \right] \cdot \xi \\ s.t. \quad -M \cdot \xi \leq -l \end{array} \right\} \leq 0 \quad \forall t \in T$$

4. Introduce dual variable Π_t^b and apply duality to the inner LP problem,

$$\left\{ \begin{array}{cc} \min & -l^T \cdot \Pi_t^b \\ s.t. & -M^T \cdot \Pi_t^b = \left[P_t^\nu - \sum_i O_{i,t} \cdot P_t \right]^T \\ & 0 \leq \Pi_t^d \end{array} \right\} \leq 0 \quad \forall t \in T$$

5. Drop the min operator,

$$\begin{cases} -l^T \cdot \Pi_t^b \leq 0 & \forall t \in T \\ -M^T \cdot \Pi_t^b = \left[P_t^\nu - \sum_i O_{i,t} \cdot P_t \right]^T & \forall t \in T \\ 0 \leq \Pi_t^b & \forall t \in T \end{cases}$$

Counterpart of constraint 6.6c

Part one:

1. Introduce appropriate truncate matrices to generalize the uncertainties as ξ, $0.75 \cdot (C_i + \sum_{t' \leq t-1} X_{i,t'} \cdot P_{t'} \cdot \xi) \leq O_{i,t} \cdot P_t \cdot \xi \qquad \forall i \in I, t \in T, \xi \in \Xi$

2. Arrange the uncertain variables in left–hand–side and derive the robust counterpart, $\left\{ \max_{\xi \in \Xi} \quad \left[0.75 \cdot \right. \right.$

$\sum_{t' \le t-1}(X_{i,t'} \cdot P_{t'}) - O_{i,t} \cdot P_t \Big] \cdot \xi \Big\} \le -0.75 \cdot C_i \quad \forall i \in I, t \in T$

3. Define the uncertain set,

$$\left\{ \begin{array}{c} \max \quad \Big[0.75 \cdot \sum_{t' \le t-1}(X_{i,t'} \cdot P_{t'}) - O_{i,t} \cdot P_t\Big] \cdot \xi \\ s.t. \quad -M \cdot \xi \le -l \end{array} \right\} \le -0.75 \cdot C_i \quad \forall i \in I, t \in T$$

4. Introduce dual variable $\Pi_{i,t}^{c_1}$ and apply duality to the inner LP problem,

$$\left\{ \begin{array}{c} \min \quad -l^T \cdot \Pi_{i,t}^{c_1} \\ s.t. \quad -M^T \cdot \Pi_{i,t}^{c_1} = \Big[0.75 \cdot \sum_{t' \le t-1}(X_{i,t'} \cdot P_{t'}) - O_{i,t} \cdot P_t\Big]^T \\ 0 \le \Pi_{i,t}^{c_1} \end{array} \right\} \le -0.75 \cdot C_i \quad \forall i \in I, t \in T$$

5. Drop the min operator,

$$\left\{ \begin{array}{l} -l^T \cdot \Pi_{i,t}^{c_1} \le -0.75 \cdot C_i \quad \forall i \in I, t \in T \\ -M^T \cdot \Pi_{i,t}^{c_1} = \Big[0.75 \cdot \sum_{t' \le t-1}(X_{i,t'} \cdot P_{t'}) - O_{i,t} \cdot P_t\Big]^T \quad \forall i \in I, t \in T \\ 0 \le \Pi_{i,t}^{c_1} \quad \forall i \in I, t \in T \end{array} \right.$$

Part two:

1. Introduce appropriate truncate matrices to generalize the uncertainties as ξ, $O_{i,t} \cdot P_t \cdot \xi \le C_i + \sum_{t' \le t-1} X_{i,t'} \cdot P_{t'} \cdot \xi \qquad \forall i \in I, t \in T, \xi \in \Xi$

2. Arrange the uncertain variables in left–hand–side and derive the robust counterpart, $\Big\{ \max_{\xi \in \Xi} \quad \Big[O_{i,t} \cdot P_t - \sum_{t' \le t-1} X_{i,t'} \cdot P_{t'}\Big] \cdot \xi \Big\} \le C_i \quad \forall i \in I, t \in T$

3. Define the uncertain set,

$$\left\{ \begin{array}{c} \max \quad \Big[O_{i,t} \cdot P_t - \sum_{t' \le t-1} X_{i,t'} \cdot P_{t'}\Big] \cdot \xi \\ s.t. \quad -M \cdot \xi \le -l \end{array} \right\} \le C_i \quad \forall i \in I, t \in T$$

4. Introduce dual variable $\Pi_{i,t}^{c_2}$ and apply duality to the inner LP problem,

$$\left\{ \begin{array}{c} \min \quad -l^T \cdot \Pi_{i,t}^{c_2} \\ s.t. \quad -M^T \cdot \Pi_{i,t}^{c_2} = \Big[O_{i,t} \cdot P_t - \sum_{t' \le t-1} X_{i,t'} \cdot P_{t'}\Big]^T \\ 0 \le \Pi_{i,t}^{c_2} \end{array} \right\} \le C_i \quad \forall i \in I, t \in T$$

5. Drop the min operator,

$$\left\{ \begin{array}{l} -l^T \cdot \Pi_{i,t}^{c_2} \le C_i \quad \forall i \in I, t \in T \\ -M^T \cdot \Pi_{i,t}^{c_2} = \Big[O_{i,t} \cdot P_t - \sum_{t' \le t-1} X_{i,t'} \cdot P_{t'}\Big]^T \quad \forall i \in I, t \in T \\ 0 \le \Pi_{i,t}^{c_2} \quad \forall i \in I, t \in T \end{array} \right.$$

Counterpart of constraint 6.6e

1. Introduce appropriate truncate matrices to generalize the uncertainties as ξ, $\sum_{i\in I}\beta_{i,k}\cdot X_{i,t}\cdot P_t\cdot\xi \leq \gamma_k \quad \forall k\in K, t\in T, \xi\in\Xi$

2. Arrange the uncertain variables in left–hand–side and derive the robust counterpart, $\left\{\max_{\xi\in\Xi} \quad \left[\sum_{i\in I}\beta_{i,k}\cdot X_{i,t}\cdot P_t\right]\cdot\xi\right\} \leq \gamma_k \quad \forall k\in K, t\in T, \xi\in\Xi$

3. Define the uncertain set,

$$\left\{\begin{array}{ll}\max & \left[\sum_{i\in I}\beta_{i,k}\cdot X_{i,t}\cdot P_t)\right]\cdot\xi \\ s.t. & -M\cdot\xi\leq -l\end{array}\right\} \leq \gamma_k \quad \forall k\in K, t\in T$$

4. Introduce dual variable $\Pi^e_{k,t}$ and apply duality to the inner LP problem,

$$\left\{\begin{array}{c}\min \quad -l^T\cdot\Pi^e_{k,t} \\ s.t. \quad -M^T\cdot\Pi^e_{k,t}=\left[\sum_{i\in I}\beta_{i,k}\cdot X_{i,t}\cdot P_t\right]^T \\ 0\leq\Pi^e_{k,t}\end{array}\right\} \leq \gamma_k \quad \forall k\in K, t\in T$$

5. Drop the min operator,

$$\left\{\begin{array}{ll}-l^T\cdot\Pi^e_{k,t}\leq\gamma_k & \forall k\in K, t\in T \\ -M^T\cdot\Pi^e_{k,t}=\left[\sum_{i\in I}\beta_{i,k}\cdot X_{i,t}\cdot P_t\right]^T & \forall t\in T \\ 0\leq\Pi^e_{k,t} & \forall k\in K, t\in T\end{array}\right.$$

Counterpart of constraint 6.6f

1. Introduce appropriate truncate matrices to generalize the uncertainties as ξ, $\Phi \leq \sum_{i\in I}\phi_{i,k}\cdot(C_i+\sum_{t\in T}X_{i,t}\cdot P_t\cdot\xi)\ /\sum_{i\in I}(C_i+\sum_{t\in T}X_{i,t}\cdot P_t\cdot\xi) \quad \forall k\in K, \xi\in\Xi$

2. Arrange the uncertain variables in left–hand–side and derive the robust counterpart, $\left\{\max_{\xi\in\Xi} \quad \left[\Phi\cdot\sum_{i\in I}\sum_{t\in T}X_{i,t}\cdot P_t-\sum_{i\in I}\phi_{i,k}\cdot\sum_{t\in T}X_{i,t}\cdot P_t\right]\cdot\xi\right\} \leq \sum_{i\in I}\phi_{i,k}\cdot C_i-\Phi\cdot\sum_{i\in I}C_i \quad \forall k\in K, \xi\in\Xi$

3. Define the uncertain set,

$$\left\{\begin{array}{ll}\max & \left[\Phi\cdot\sum_{i\in I}\sum_{t\in T}X_{i,t}\cdot P_t\right. \\ & \left.-\sum_{i\in I}\phi_{i,k}\cdot\sum_{t\in T}X_{i,t}\cdot P_t\right]\cdot\xi \\ s.t. & -M\cdot\xi\leq -l\end{array}\right\} \leq \sum_{i\in I}\phi_{i,k}\cdot C_i-\Phi\cdot\sum_{i\in I}C_i \quad \forall k\in K$$

4. Introduce dual variable Π^f_k and apply duality to the inner LP problem,

$$\left\{\begin{array}{c}\min \quad -l^T\cdot\Pi^f_k \\ s.t. \ -M^T\cdot\Pi^f_k=\left[\Phi\cdot\sum_{i\in I}\sum_{t\in T}X_{i,t}\cdot P_t\right. \\ \left.-\sum_{i\in I}\phi_{i,k}\cdot\sum_{t\in T}X_{i,t}\cdot P_t\right]^T \\ 0\leq\Pi^f_k\end{array}\right\} \leq \sum_{i\in I}\phi_{i,k}\cdot C_i-\Phi\cdot\sum_{i\in I}C_i \quad \forall k\in K$$

5. Drop the min operator,

$$\begin{cases} -l^T \cdot \Pi_k^f \leq \sum_{i \in I} \phi_{i,k} \cdot C_i - \Phi \cdot \sum_{i \in I} C_i \quad \forall k \in K \\ -M^T \cdot \Pi_k^f = \left[\Phi \cdot \sum_{i \in I} \sum_{t \in T} X_{i,t} \cdot P_t - \sum_{i \in I} \phi_{i,k} \cdot \sum_{t \in T} X_{i,t} \cdot P_t \right]^T \quad \forall k \in K \\ 0 \leq \Pi_k^f \quad \forall k \in K \end{cases}$$

Counterpart of constraint 6.6h

Part one:

1. Introduce appropriate truncate matrices to generalize the uncertainties as ξ, $\underline{\Omega} \cdot Y_{i,t}^X \leq X_{i,t} \cdot P_t \cdot \xi \quad \forall i \in I, t \in T, \xi \in \Xi$

2. Arrange the uncertain variables in left–hand–side and derive the robust counterpart, $\left\{ \max_{\xi \in \Xi} \quad \left[-X_{i,t} \cdot P_t \right] \cdot \xi \right\} \leq -\underline{\Omega} \cdot Y_{i,t}^X \quad \forall i \in I, t \in T$

3. Define the uncertain set,

$$\left\{ \begin{array}{cc} \max & \left[-X_{i,t} \cdot P_t \right] \cdot \xi \\ s.t. & -M \cdot \xi \leq -l \end{array} \right\} \leq -\underline{\Omega} \cdot Y_{i,t}^X \quad \forall i \in I, t \in T$$

4. Introduce dual variable $\Pi_{i,t}^{h_1}$ and apply duality to the inner LP problem,

$$\left\{ \begin{array}{cc} \min & -l^T \cdot \Pi_{i,t}^{h_1} \\ s.t. & -M^T \cdot \Pi_{i,t}^{h_1} = \left[-X_{i,t} \cdot P_t \right]^T \\ & 0 \leq \Pi_{i,t}^{h_1} \end{array} \right\} \leq -\underline{\Omega} \cdot Y_{i,t}^X \quad \forall i \in I, t \in T$$

5. Drop the min operator,

$$\begin{cases} -l^T \cdot \Pi_{i,t}^{h_1} \leq -\underline{\Omega} \cdot Y_{i,t}^X \quad \forall i \in I, t \in T \\ -M^T \cdot \Pi_{i,t}^{h_1} = \left[-X_{i,t} \cdot P_t \right]^T \quad \forall i \in I, t \in T \\ 0 \leq \Pi_{i,t}^{h_1} \quad \forall i \in I, t \in T \end{cases}$$

Part two:

1. Introduce appropriate truncate matrices to generalize the uncertainties as ξ, $X_{i,t} \cdot P_t \cdot \xi \leq \bar{\Omega} \cdot Y_{i,t}^X \quad \forall i \in I, t \in T, \xi \in \Xi$

2. Arrange the uncertain variables in left–hand–side and derive the robust counterpart, $\left\{ \max_{\xi \in \Xi} \quad \left[X_{i,t} \cdot P_t \right] \cdot \xi \right\} \leq \bar{\Omega} \cdot Y_{i,t}^X \quad \forall i \in I, t \in T$

3. Define the uncertain set,

$$\left\{ \begin{array}{cc} \max & \left[X_{i,t} \cdot P_t \right] \cdot \xi \\ s.t. & -M \cdot \xi \leq -l \end{array} \right\} \leq \bar{\Omega} \cdot Y_{i,t}^X \quad \forall i \in I, t \in T$$

4. Introduce dual variable $\Pi_{i,t}^{h_2}$ and apply duality to the inner LP problem,

$$\left\{ \begin{array}{cc} & \min \quad -l^T \cdot \Pi_{i,t}^{h_2} \\ s.t. & -M^T \cdot \Pi_{i,t}^{h_2} = \left[X_{i,t} \cdot P_t \right]^T \\ & 0 \leq \Pi_{i,t}^{h_2} \end{array} \right\} \leq \bar{\Omega} \cdot Y_{i,t}^X \quad \forall i \in I, t \in T$$

5. Drop the min operator,

$$\left\{ \begin{array}{l} -l^T \cdot \Pi_{i,t}^{h_2} \leq \bar{\Omega} \cdot Y_{i,t}^X \quad \forall i \in I, t \in T \\ -M^T \cdot \Pi_{i,t}^{h_2} = \left[X_{i,t} \cdot P_t \right]^T \quad \forall i \in I, t \in T \\ 0 \leq \Pi_{i,t}^{h_2} \quad \forall i \in I, t \in T \end{array} \right.$$